AD-A072 309 NAVAL RESEARCH LAB WASHINGTON DC F/G 20/1

ACOUSTIC FLUCTUATION WORKSHOP, HELD AT NAVAL RESEARCH LABORATOR--ETC(U)

JUL 78 S HANISH, C R ROLLINS, J CYBULSKI

UNCLASSIFIED NRL-MR-3884-VOL-1 NL

1 OF 3

AD
A072309

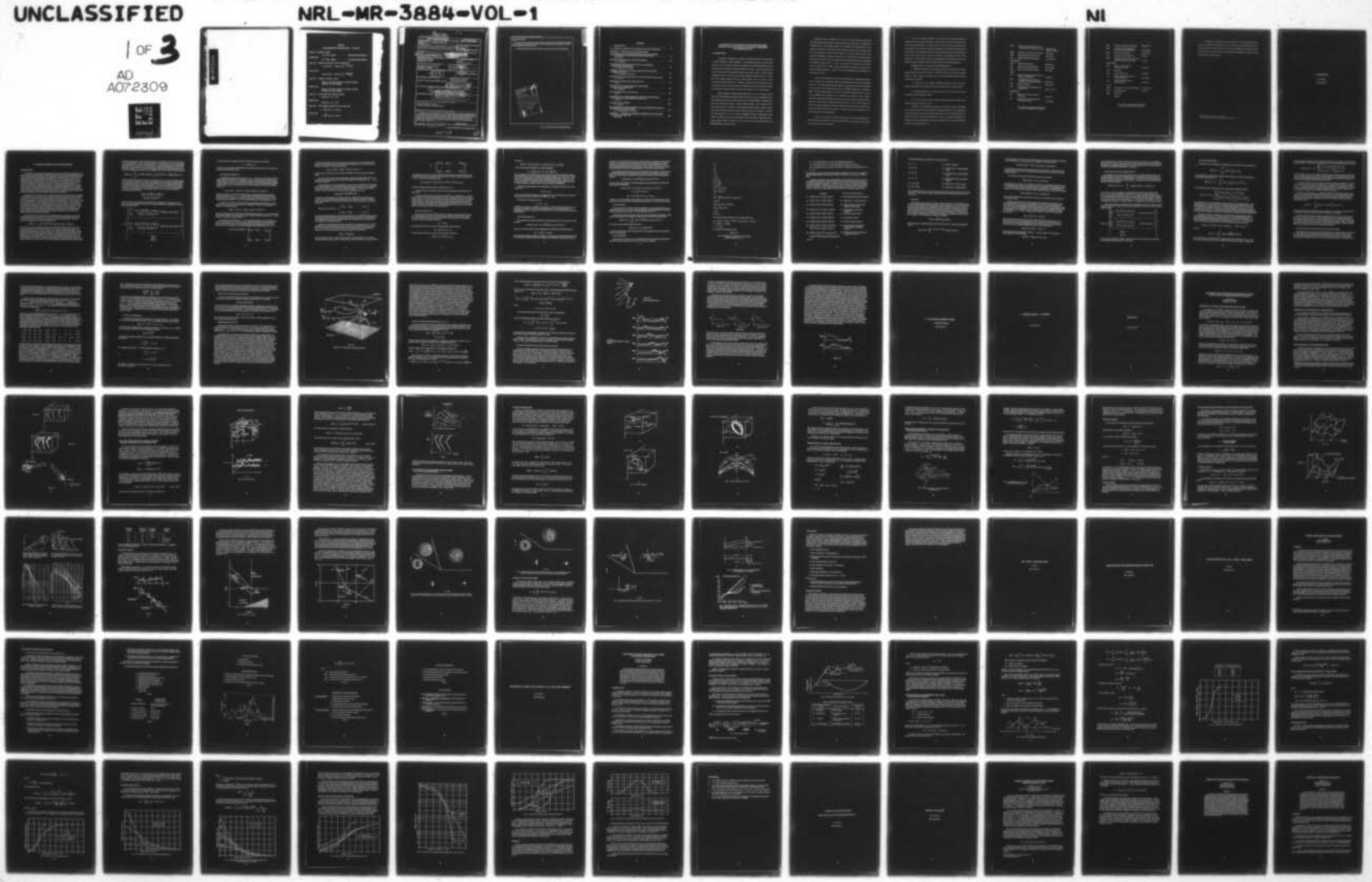

SIFIED

1 OF 3

AD
A072309

ERRATA

NRL MEMORANDUM REPORT 3884 — VOLUME 1

Page 85 — Reference 6 reads:

R. J. Urick, "Signal . . . . Fluctuating Sonal Signals in

Should read:

R. J. Urick, "Signal . . . . Fluctuating Sonar Signals in

Page 153 — Equation second from bottom of page reads:

$$< p(1)\ p^*(2) > = p^*_0(2) \exp \left[- \begin{matrix} D(1,2) \\ 2 \end{matrix} \right]$$

Should read:

$$< p(1)\ p^*(2) > = p^*_0(2) \exp \left[- \frac{D(1,2)}{2} \right]$$

Page 154 — Caption for Figure 7 reads:

Sketch of 4th Order Moment (or Mutual Integrity)
Calculated by Path Integrals

Should read:

Sketch of 4th Order Moment (or Mutual Intensity)
Calculated by Path Integrals

Page 177 — Lower right side of Figure 26 reads:

WITH $C_n^E = 6.3 \times 10^{-9}$

Should read:

WITH $C_n^2 = 6.3 \times 10^{-9}$

Page 186 — First centered equation at top of page reads:

$$\Lambda = \frac{25}{\sigma}; \text{ HZ, } L_y = 240 \text{ M}$$

Should read:

$$\Lambda = \frac{25}{\sigma} \text{ HZ; } L_y = 240 \text{ M}$$

(14) NRL-MR-

SECURITY CLASSIFICATION OF THIS PAGE (When Data Entered)

REPORT DOCUMENTATION PAGE		READ INSTRUCTIONS BEFORE COMPLETING FORM
1. REPORT NUMBER NRL Memorandum Report 3884-VOL-1 Volume 1	2. GOVT ACCESSION NO.	3. RECIPIENT'S CATALOG NUMBER
4. TITLE (and Subtitle) (6) ACOUSTIC FLUCTUATION WORKSHOP, Feb. 22-23,,1978 Technical Review, Editorial Summary, Synopsis and Papers		5. TYPE OF REPORT & PERIOD COVERED (9) Final Report,
		6. PERFORMING ORG. REPORT NUMBER
7. AUTHOR(s) (10) S. Hanish, C. R. Rollins [redacted] J. Cybulski	~~held [redacted] 22-23 1978 Naval Research Laboratory, Washington, DC.~~	8. CONTRACT OR GRANT NUMBER(s)
9. PERFORMING ORGANIZATION NAME AND ADDRESS Naval Research Laboratory Washington, D.C. 20375		10. PROGRAM ELEMENT, PROJECT, TASK AREA & WORK UNIT NUMBERS 81S01-91 62711N XF11-121-200
11. CONTROLLING OFFICE NAME AND ADDRESS Naval Electronic Systems Command Washington, D.C. 20360	(11) 2	12. REPORT DATE July [redacted] 1979
		13. NUMBER OF PAGES 195
14. MONITORING AGENCY NAME & ADDRESS(if different from Controlling Office) (12) 197p.		15. SECURITY CLASS. (of this report) UNCLASSIFIED
		15a. DECLASSIFICATION/DOWNGRADING SCHEDULE

16. DISTRIBUTION STATEMENT (of this Report)

Approved for public release; distribution unlimited.

(16) F11121

(17) XF11121200

17. DISTRIBUTION STATEMENT (of the abstract entered in Block 20, if different from Report)

(6) Acoustic Fluctuation Workshop, held at on February 22-23 1978, Naval Research Laboratory, Washington, DC. Volume 1. Technical Review, Editorial Summary, Synopsis and Papers.

18. SUPPLEMENTARY NOTES

19. KEY WORDS (Continue on reverse side if necessary and identify by block number)

Acoustics Fluctuations in the Ocean
Workshop Proceedings on Acoustic Fluctuations

20. ABSTRACT (Continue on reverse side if necessary and identify by block number)

A Workshop on Acoustic Fluctuations in the Ocean, sponsored by NAVELEX 320 was held at the Naval Research Laboratory, Washington, D.C., on Feb. 22-23, 1978. The theme was ~~(1)~~ to highlight the relation between requirements of system performance models (APSURV, PSEUDO, APAIR, etc.) and current research on acoustic fluctuations conducted by Industry and the Navy, ~~(2)~~ to find ways to establish closer cooperation between Researchers working in the field, and Users of research results, and ~~(3)~~ to recommend programs. → next page

(Abstract Continues)

DD FORM 1 JAN 73 1473 EDITION OF 1 NOV 65 IS OBSOLETE
S/N 0102-014-6601

SECURITY CLASSIFICATION OF THIS PAGE (When Data Entered)

251950

HB

20. Abstract Continued

This memorandum summarizes the agenda and key technical issues of the Workshop, and contains all papers presented. It also gives a brief histroy or previous Workshops on this subject, and a technical review of acoustic fluctuations in general.

Recommendations for programs are scheduled to be made available in a separate publication.

CONTENTS

ACOUSTICS FLUCTUATIONS: GUIDELINES FOR R&D BASED ON THE ACOUSTIC FLUCTUATION WORKSHOP 22-23 FEBRUARY 1978

I. INTRODUCTION

The detection, localization and tracking of submarines by underwater acoustic signals are greatly disturbed by signal fluctuations. These originate primarily in source/receiver motion, but also are caused by acoustic rays reflected from wind-roughened surface, and by scattering from inhomogeneities randomly dispersed in the ocean. In past years such fluctuations have been spatially and temporally averaged to mean values. However, random variations of signals about mean values have recently taken on significant meaning because they strongly affect target detection methods which use statistical decision, such as is found in receiver operating characteristic (ROC) curves. In addition, a higher order statistical analyses of acoustic fluctuations provides a means to evaluate the reliability of experimental data and can lead to the construction of confidence limits to the mean values currently used in ASW operations.

Research progress in acoustic fluctuations has been reviewed and evaluated in several recently held conferences and workshops. Since 1974 there have been four distinctive but related workshops of this nature, one review panel, and an Acoustical Society of America (ASA) session held which bear somewhat on acoustic signal fluctuations. On 27-28 March 1974 a fluctuation workshop was conducted at Naval Research Laboratory (NRL) hosted by Acoustic Environmental Support Detachment (AESD) and a summary (Ref. 1) is available. An International Workshop (Ref. 2) on Low Frequency Propagation and Noise was sponsored by CNO (OP-95) and supported by Chief of Naval Research (CNR) and held at Woods Hole Oceanographic Institute (WHOI) in October 1974. The David Taylor Naval Ship Research and

Manuscript submitted September 28, 1978.

Development Center (DTNSRDC) was the host for an Operations Research Models of Fluctuations Affecting Sonar Detection Workshop during 19-21 March 1975. Proceedings were published (Ref. 3) in two classified volumes. On 1-2 October 1975 a workshop (Ref. 4) under auspices of Underwater Sound Advisory Group (USAG) was held on Acoustic Signal Coherence at Naval Underwater Systems Center (NUSC). Next, under direction of chief of Naval Operations (CNO:OP95) a technical review panel for a coordinated Ocean Acoustics Program Plan met 8-10 November 1977 at Naval Ocean Research and Development Acitivity (NORDA) and produced a summary (Ref. 5). Lastly, at the December 1977 meeting of the Acoustical Society of America (ASA) at Miami a session on Underwater Acoustics was devoted to Fluctuations and Signal processing. A review of several of the significant papers presented at that session appears in Ref. 6.

Each of the preceding efforts did not completely address the signal fluctuation problems. For instance the one hosted by AESD was specifically directed to satisfy potential SASS contractors. The International Workshop at WHOI was unclassified and many system applications were omitted. The Operations Research effort at DTNSRDC neglected the environmental effects. The one on Signal Coherence at NUSC was constrained in subject material. The scope of the coordinated plan at NORDA (Ref. 5) examined the contributions of Navy research, exploratory and advanced development programs to the four ocean acoustic subjects of bottom interaction, signal fluctuation, coherence and directional noise. Each of these subjects was divided into segments dealing with modeling, measurement systems and data acquisition programs. Of necessity these elements received a very broad treatment and generally were of a non-technical nature and lacked specificity.

Lastly, the ASA session was instructive but again because of its unclassified nature a proper discussion and exposition of the efforts being made by the exploratory and advanced development workers could not be made.

c Current Navy sponsored programs in data acquisition and analytical modeling of fluctuations of received acoustic signals show a great diversity of approach, data collection, signal processing and final display. The ultimate use of the results of research to improve undersea surveillance often falls short of expectations because of a mismatch between the user's understanding of his requirements and the investigator's interpretation of those requirements. There is and has been a need to clarify both the user's and investigator's concept of their requirements. To this end the Chief of Naval Development with the assistance of the Naval Electronic Systems Command sponsored a classified workshop on Acoustic Fluctuations.

The objectives of the Acoustic Fluctuations Workshop were to:

a. Delineate the problem areas associated with modeling of fluctuations of acoustic signals and noise as caused by the medium, its boundaries and motion of the source or receiver platforms. Assess the impact of these fluctuations on system performance models as translated into model input parameters.

b. Examine the current programs addressing underwater acoustic fluctuations. Present program goals, technical approaches to meet the goals, and work currently underway.

c. Recommend adjustments to program goals to meet the input needs of users of acoustic environmental fluctuation models.

On 22-23 Feb. 1978 on Acoustic Fluctuation Workshop was held at NRL and the Agenda was essentially as per Figs. 1 and 2.

Attendance at the Workshop was limited to the principal investigators and managers from the involved sectors of the Navy, industry and academic community. Over 50 participated in the presentations that were made and discussions that were held. An editorial summary was made for those papers which were supplied by the authors. A synopsis was prepared for all unwritten papers and combined with a comprehensive technical review on Ocean Science Fluctuations into a separate report (Ref. 6).

0830	Welcome, Workshop Objectives, Navy Unified Program, Prologue, and Filters	Spalding, Miller, Winokur, Cybulski
0900	Key Issues in Fluctuations & Coherence	Sam Hanish
0945	APSURV Model (& Fluctuations)	Ron Larsen
1015	PSEUDO Model (& Fluctuations)	Lyman Fretwell
Movable Break		
1100	APETC (& Fluctuations)	Robert Flum
1130	Beam Noise Fluctuation Models	Ray Cavanagh
1200	Signal Processor (& Fluctuations)	Don Grace
Lunch		
1330	Effects of Fluctuating Signals & Noise on Detection Performance	John Heine
1400	A Working Fluctuation Model with Application to Performance Prediction	Robert Urick
1430	Signals Fluctuations	Ken Flowers
1500	A Model of Acoustic Propagation Thru Internal Waves	Harry De Ferrari
Movable Break		
1545	Single Path — Phase & Amplitude Fluctuations	Terry Ewart
1615	Fluctuations From a Communication Engineering Viewpoint	A. Ellinthorpe

Fig. 1. Agenda — Acoustic Fluctuation Workshop
22 Feb. 1978, NRL, Bldg. No. 43, Rm. 205

0800	Prediction of Detection Performance	Magnus Moll
0820	Acoustic Fluctuation Modeling for System Performance Estimation	Ray Cavanagh
0845	Beam Output Fluctuations	Andy Fabula
0915	Fluctuations Due to Range Rate	Ira Dyer
0945	Importance of Source Motion, Receiver Motion and Ocean Environment	W. Jobst
Movable Break		
1030	Impact of Source Motional Fluctuations on IAP	Al Gerlach
1100	Discussion	
1115	Acoustic Fluctuations	R. Spindel
1145	Range Independent Fluctuations — Pattern Recognition	Fred Fisher
1215	Omni Noise Field Statistics — Depth & Clutter	J. Schooter
Lunch		
1330	Characterization of Acoustic Propagation	Harry De Ferrari
1345	Measurement tools	Dave Keir
1400	Open Forum	
	Adjourn	

Fig. 2. Agenda — Acoustic Fluctuation Workshop
23 Feb. 1978, NRL, Bldg. No. 43, Rm. 205

Subsequently, a working group* was charged with the task of formulating objectives, approaches and specific tasks which could serve to assist in structuring R&D programs on acoustic fluctuations. This document is the result of those efforts and has undergone several revisions one as a result of consultation and convening of a special panel** where Navy laboratories and industry were represented.

* Dr. Sam Hanish, C.R. Rollins, J. Cybulski of NRL.
** Dr. P. Cable (NUSC), Dr. J. Stewart (NOSC), Mr. C. Spofford (SAI).

II. BACKGROUND

C. R. Rollins

(See Volume 2)

III. TECHNICAL REVIEW OF FLUCTUATION PHYSICS

INTRODUCTION

Fluctuations of acoustic signals propagating in the ocean is a subject of considerable complexity. This is caused primarily by random inhomogeneities along the propagation path coupled to the comparable size wavelengths of these signals. Its two key elements of environment and acoustics have been studied separately and together, and a copious literature exists. In this regard the physics of that part of the ocean environment which is thought to be the cause of fluctuations is still receiving attention. It could be used as the basis of the review to be made below. An alternate and complementary basis is to consider the propagating medium as a "channel" along which a communication signal is being transferred from a source to a distant receiver. Such a communications approach offers a considerable advantage in that it permits a large overview of the theoretical and experimental aspects of fluctuations to be formulated in a simple abstract way which makes visible the otherwise very complicated subject matter of the study. We shall adopt the communications approach in all that follows.

We begin then with a distant source of sound and assume there is a distribution of radiators (or transmitting antenna) which generate a spatial and temporal distribution of sound $Q(\vec{r}_s, t_s)$, a portion Q_m of which is injected into the channel, thus constituting the channel input. The channel then propagates the sound along a particular path, transforming it in the process, according to an operation T_m, so that it arrives at a receiver in the state $T_m Q_m$. At the receiver the received signal is then combined with other signals in the receiver antenna which transforms it according to an operator T_R, and delivers the total acoustic pressure $p = T_R T_m Q_m$. During transfer, as well as during reception, the channel is corrupted by noise so that both T_m and T_R contain random parts. The signal reported by the receiving antenna will therefore be a random variable, both because the medium is changing in a random way, and because the medium and the receiving antenna are noisy.

In general, there will be more than one propagation path connecting source to receiver. We call each distinct path a channel. Let there be a total of M channels between the center of the source $\vec{r}_s$ and the i^{th} element of an N-element receiver, located at $\vec{r}_R^{\,(i)}$. Thus the total received signal at the i^{th} element hydrophone is,

$$p(\vec{r}_R^{\,(i)}, t_E, t_s) = \sum_m T_m(t_s | \vec{E}(\vec{r}_s, \vec{r}_R^{\,(i)}, t_E)\, Q_m^{(s)}\ (t_s | \vec{r}_s\,(\theta, \varphi) + N(r_R^{(i)}, t_N)$$

Here the source radiation injected into the m^{th} channel is labeled $Q_m^{(s)}$, and is a function of the "source time" t_s, and source coordinates $\vec{r}_s\,(\theta, \varphi)$, where θ, φ are spherical angles. The transmission operator is T_m which is conceived to be a function of the source time t_s, and an environment matrix $\vec{E}$ which contains all the aspects of the environment which govern the propagation of sound, both deterministic and random. In particular $\vec{E}$ is a function of the "environment time" t_E, distinguished from t_s by its (generally) different scale, and a function of source and receiver location. The number of components in matrix $\vec{E}$ depends on which transmission problem is to be solved, and may include such effects as randomly rough ocean surfaces,

internal waves, eddies, currents, volume scattering, etc. The symbol N is the local noise at the i^{th} receiver hydrophone. It is a function of receiver location $\vec{r}_R^{(i)}$ and of a time t_N, which again generally differs from t_s and t_E by its different scale. Actually N represents an acoustic signal generated by a noise source $Q^{(N)}$ at location $\vec{r}_N(\theta, \varphi)$ and propagated along one or more channels to the receiver. Thus, the total received pressure field at the i^{th} hydrophone may be represented in a different way by the sum of multipaths, each of which may be corrupted by noise,

$$p(\vec{r}_R^{(i)}, t_E, t_s) = \sum_{m=1}^{M} T_m \left(t_s \,|\, \vec{E}(\vec{r}_s, \vec{r}_N, \vec{r}_R^{(i)}, t_E)\right) \left\{ Q_m^{(s)}(t_s \,|\, \vec{r}_s(\theta, \varphi)) + Q_m^{(N)}(t_N \,|\, \vec{r}_N(\theta, \varphi) \right\}$$

This formulation allows the m^{th} channel to carry signals, or noise, or both. When the receiver is an L element array designed for steering, the pressure in the i^{th} hydrophone is multiplied by a steering operator $A(r_R^{(i)}, t)$. The result is cross-multiplied with the received signal plus noise in all other hydrophones at different time delays τ_d to form products which in turn are time averaged to form hydrophone cross-correlation in space and time. Each such cross-correlation is normalized with respect to the time averaged power of the i^{th} and the j^{th} hydrophone, thus delivering a typical term,

$$\frac{A(r_R^{(i)}, \tau_d)\, R_p(\vec{r}_R^{(ij)}, \tau_d)\, A(\vec{r}_R^{(j)}, \tau_d)}{[R_p(r_p^{(i)}, o)\, R_p(r_R^{(i)}, o)]^{1/2}} .$$

The ratio of sum of all these terms when signal only is considered, to the sum when noise only is considered, divided by the same ratio in a single hydrophone as averaged over the array constitutes the array gain:

$$AG = \left\{ \frac{\left[\dfrac{\sum_{i,j}^{L} \dfrac{A(r^{(i)}, \tau_d)\, R_p^{(s)}(\vec{r}_R^{(i,j)}, \tau_d)\, A(r_R^{(i)}, \tau_d)}{[R_p^{(s)}(r_R^{(i)}, o)\, R_p^{(s)}(r_R^{(j)}, o)]^{1/2}} \; [R_p^{(s)}(\vec{r}_R^{(i)}, o)\, R_p^{(s)}(r_R^{(j)}, o)]^{1/2}}{\sum_{i,j}^{L} \dfrac{A(r_R^{(i)}, \tau_d)\, R_p^{(N)}(r_R^{(i,j)}, \tau_d)\, A(r_R^{(j)}, \tau_d)}{[R_p^{(N)}(r_R^{(i)}, o)\, R_p^{(N)}(r_R^{(j)}, o)]^{1/2}} \; [R_p^{(N)}(r_R^{(i)}, o)\, R_p^{(N)}(r_R^{(j)}, o)]^{1/2}} \right]}{\dfrac{R_p^{(s)}(o)}{R_p^{(N)}(o)}} \right\}$$

In actual practice the steering operators are random functions of time and space,

$$A \to A(r_R^{(i)}, \tau_d\ t_A)$$

in which t_A is an array time, distinguished from all other times by its scale. We return to the statistics of steering matrices later.

The Environmental Matrix $\vec{E}$

In general $\vec{E}$ is a matrix whose elements $E_1, E_2 \ldots$ describe the various random environmental processes which affect the propagation of sound. Each element is a random function of space ($\vec{r}_s, \vec{r}_R$) and time (t_E). A transmission channel can be characterized as time-varying, or space-varying, or both. To begin, let the m^{th} channel be a time-varying channel randomly perturbed by $E_m(t_E)$ and assume it has an ensemble of realizations. Then the autovariance of $E_m(t_E)$ is,

$$K_{Em}(t_E, t_E') = \langle (E_m(t_E) - \langle E_m(t_E)\rangle)(E_m(t_E') - \langle E_m(t_E')\rangle)\rangle$$

in which the symbol $\langle\rangle$ represents ensemble-average. In real physical events this function effectively vanishes then $t_E - t_E' \cong L_t$, which then defines the *correlation time* for the E_m perturbation of the environment. If the channel $E_m(t_E)$ is nonstationary then $L_t = L_t(t_E)$. Only for stationary channels is L_t function of time difference $t_E - t_E'$, independent of t_E.

Next let the m^{th} channel be space-varying channel randomly perturbed by $E_m(z)$ and assume it has an ensemble of realizations in the z-direction (= depth). The autovariance in spatial z is the ensemble average

$$K(Z,Z') = \langle (E_m(Z) - \langle E_m(Z)\rangle)(E_m(Z') - \langle E_m(Z')\rangle)\rangle$$

Again, for real physical events this function effectively vanishes then $Z - Z' \cong L_Z$ which defines the correlation length of the perturbation $E_m(Z)$. If $E_m(Z)$ is nonstationary then $L_Z = L_Z(Z)$, namely the correlation length depends on z.

Now assume all J elements $E_1, E_2 \ldots E_g$ of matrix $\vec{E}$ participate in the propagation of sound. This might mean, for example, that the transmission channel experiences effects of surface scattering (call this E_1), volume scattering (E_2), internal waves (E_3), eddies (E_4), tides (E_5), etc. One can then form a covariance matrix of all perturbations E_m, m = 1, 2 . . .,

$$K(t_E, t_E', \vec{r}_s, \vec{r}_s{}', \vec{r}_R, \vec{r}_R{}') = \begin{bmatrix} K_{E_1E_1} & K_{E_1E_2} & \ldots & K_{E_1E_J} \\ \vdots & \vdots & & \vdots \\ \vdots & \vdots & \ldots & \vdots \\ \vdots & \vdots & & \vdots \\ K_{E_JE_1} & K_{E_JE_2} & & K_{E_JE_J} \end{bmatrix}$$

in which the diagonal elements are autovariances, already defined, and the off-diagonal elements are cross-variances, either time-varying or space-varying, or both. Their form is illustrated by an example of a time-varying channel.

$$K_{E_iE_j} = \langle (E_i(t_E) - \langle E_i(t_E) \rangle)(E_j(t_E') - \langle E_j(t_E') \rangle) \rangle$$

For each element in this matrix one can define correlation times and length, as illustrated earlier.

From this it is seen that a complete description of the randomizing effects of the environment requires the construction of the covariance matrix of *all* elements $E_1, E_2 \dots$ of the environment matrix $\vec{E}$.

In most practical cases of the propagation of sound only one realization of $\vec{E}$ is available, rather than an ensemble. If this sample is long enough (in time or space) it can be applied by means of the *ergodic hypothesis* to form correlation averages, R. Thus for a time-varying channel, in place of $K_{E_iE_j}$ the time average over a single realization is used,

$$R_{E_iE_j}(t_E, t_E') = \overline{E_i(t_E)\, E_j(t_E + t_E')}$$

in which the overbar indicates an average over time t_E. Again, if the process $Ei(t_E)$ is stationary, the auto-correlation $R_{E_iE_j}$ is independent of t_E. When all J elements of $\vec{E}$ participate in the propagation of sound one can describe the environmental effects by a *coherence matrix*, $R_{\vec{E}}$

$$R_{\vec{E}}\,(t_E, t_E', \vec{r}_s, \vec{r}_s\,', \vec{r}_R, \vec{r}_R\,') = \begin{bmatrix} R_{E_1E_1} & R_{E_1E_2} & \cdots\cdots & R_{E_1E_J} \\ \vdots & \vdots & & \\ R_{E_jE_1} & R_{E_JE_2} & \cdots\cdots & R_{E_JE_J} \end{bmatrix}$$

in which the diagonal elements are the autocorrelations, and the off-diagonal elements are the cross-correlations, all elements being general functions of space and time. Correlation times and correlation lengths can then be deduced from each correlation function in the manner noted earlier for the covariance matrix.

The effects of the environment need not be confined to real space and time. It is often advantageous to transform the matrices $R_{\vec{E}}$ and $K_{\vec{E}}$ into wavenumber space and frequency space. The results are spectral density matrices whose elements $\mathscr{W}_{E_iE_j}$ are obtainable by application of Fourier transformation through the Wiener-Kinchine theorem,

$$\mathscr{W}_{E_iE_j} = 2F\left\{K_{E_iE_j}\right\}$$

Here the transform coordinate pair fixes which space is being transformed. The matrix of spectral and across-spectral densities corresponding to various perturbations E_m then becomes,

$$\vec{\mathscr{W}} = \begin{bmatrix} \mathscr{W}_{E_1E_1} & \mathscr{W}_{E_1E_2} & \cdots & \mathscr{W}_{E_1E_j} \\ \vdots & \vdots & & \vdots \\ \mathscr{W}_{E_jE_1} & \mathscr{W}_{E_jE_2} & & \mathscr{W}_{E_jE_j} \end{bmatrix}$$

To illustrate, let E_j be the component of $\vec{E}$ which deals with the propagation effects of the temporal fluctuations in sound-speed profile, that is $E_j \rightarrow \delta\, C(t_E)$. Let the Fourier pair be $t_E \leftrightarrow \Phi_E$. Then, for non-stationary $\delta\, C(t_E)$,

$$\mathscr{W}_{\delta C}(\Phi_E, \Phi_E') = 2 \int_{-\infty}^{\infty} K_{\delta C}(t_E, t_E')\, e^{-i[\Phi_E t_E - \Phi_E' t_E']}\, d(t_E, t_E')$$

Only for a stationary process does $\mathscr{W}_{\delta C}$ depend on $\Phi_E - \Phi_E'$.

A further discussion of frequency space, and wavenumber space will be taken up in a later section.

The time coordinate of the environmental matrix $\vec{E}$ has been designated t_E. A second time coordinate may be introduced whenever the space coordinates $\vec{r}_s$, $\vec{r}_R$ themselves become functions of time. This occurs when source, or receiver, or both are in motion. One writes $\vec{r}_s(t_{SM})$, $\vec{r}_R(t_{RM})$, in which t_{SM}, t_{RM} mean source time and receiver time associated with motion. Motion of source and receiver thus associates a temporal significance to a purely spatial description of the medium. By Fourier transformation of t_{SM}, t_{RM}, source receiver motion can be studied *in frequency* (or doppler) space.

The Channel Operator T_m

While the environmental matrix $\vec{E}$ describes the effects of a randomizing environment on the propagation of sound, the channel transmission itself is described by the operator T_m which transfers the sound from source to receiver. Thus for the m^{th} channel which contains source Q_m the delivered pressure is,

$$p_m = T_m\, Q_m$$

To elucidate the nature of T_m let Q_m be delta-function is space and time,

$$Q_m = \delta(\vec{r}_s - \vec{r}_{so})\ \delta(t - t_o)$$

It is known that the acoustic pressure is then the Green's function G:

$$p_m(\vec{r}_R, t) = G_m(\vec{r}_R, \vec{r}_{so} \mid t_s, t_{so})$$

If we write

$$p_m(\vec{r}_R, t) = \iint G_m(\vec{r}_R, \vec{r}_s' \mid t_s, t_s')\, \delta(\vec{r}_g' - \vec{r}_{so})\, \delta(t_s' - t_{so})\, d^3\vec{r}_s'\, dt_s'$$

it is then seen that the transmission is an integral operator,

$$T_m \rightarrow \iint G_m(\vec{r}_R, \vec{r}_s' \mid t_s, t_s') \left\{ \quad \right\} d^3\vec{r}_s' dt_s'$$

Thus in general T_m is a *weighted integral* over space and time of the sources of the pressure field, whether these sources are true sources supplying energy to the channel, or fictitious sources redirecting energy (by scattering) during channel transmission. In the former case the space of integration is the small volume surrounding the true source, while in the latter case it is the space of the fictitious sources of the channel, such as channel area in the case of surface scattering, or channel volume in the case of volume scattering, etc.

Additional characterization of the transmission T_m is obtained by study of the inverse operator T_m^{-1},

$$T_m^{-1}\, p_m = Q_m$$

This is the partial differential equation of propagation of an acoustic pressure in the presence of sources Q_m. When Q_m is fictitious it is written $Q_m \propto a p_m$.

The equation of propagation is then

$$T_m^{-1}\, p_m = -a\, p_m$$

in which a is a function of coordinates, or is constant. Actual forms of this equation in common use are the parabolic equation, the Helmholtz equation, the eikonal equation, etc. A great literature exists on the subject of the operator's T_m, T_m^{-1}, and the solutions of the equations they obey.

The Acoustic Pressure p_m

The contribution of acoustic pressure from a single channel to the i^{th} hydrophone of the receiver is,

$$p_m(r_R^{(i)}, t_s, t_E) = T_m(t_s \mid E(\vec{r}_s, \vec{r}_R^{(i)}, t_E)\, Q_m(t_s \mid \vec{r}_s(\theta, \varphi))$$

Since p_m is a random variable it can be separated into a mean part and a fluctuation part,

$$p_m = \langle T_m Q_m \rangle + \delta\, T_m Q_m$$

In nonstationary fields the mean part is a function of space and time while the fluctuation part is a function of coordinates, rather than differences of coordinates. The properties of p_m are

summed up in its probability density P_{p_m} (or distribution) and its statistics (or probability moments). The statistics most often used fall into the category of single-point in which moments are calculated for one point in space or time, or both; and two-point in which moments are determined with two points in space or time, or both. Three-point and higher order of statistics are used when special properties of the acoustic field are needed.

The probability description of p_m is often extended from real space to transform space by Fourier transformation. In particular, the source time t_s is transformed to source frequency f_s whenever narrow (frequency) band sources are present. Then the field pressure becomes,

$$p_m(f_s, \vec{r}_R, t_E) = T_m \left(f_s \mid \vec{E}\,(\vec{r}_s, \vec{r}_R, t_E\right) Q_m \left(f_s \mid \vec{r}_s\,(\theta, \varphi)\right)$$

which at short enough ranges, or for weak scattering, can be represented by a phasor with explicit amplitude and phase,

$$\begin{aligned} p_m\,(f_s, r_R, t_E) &= \left|\, p_m\,(f_s, \vec{r}_R, t_E) \right| \exp\left\{ i\,\phi_m\,(f_s, \vec{r}_R, t_E)\right\} \\ &= p_{o_m}\,(f_s, \vec{r}_R)\, \exp\,(X_m) \end{aligned}$$

$$X_m = X_m\,(f_s, \vec{r}_R, t_E) = X_{m(1)} + i\, X_{m(2)}$$

in which p_o is the deterministic acoustic pressure at the receiver in the absence of any fluctuations, and exp X is the effect of fluctuations, as described by a complex random variable.

One-Point Statistics

The received acoustic pressure, whether expressed in real space or transform space, or mixed space, allows one to construct a list of *observables*, which are defined as real physical events at single points in space-time: (See following sheet, Fig. III.1.)

Observables at single points such as these cover only single channel transmission. Multichannel transmission from M channels to single points are described by the expression,

$$p(r_R^{(i)}, t_s, t_E) = \sum_{m=1}^{M} T_m^{(i)} \left(t_s \mid \vec{E}(\vec{r}_s, \vec{r}_R^{(i)}, t_E\right) Q_m \left(t_s \mid \vec{r}_s\,(\theta, \varphi)\right)$$

In the case of narrow band sources this becomes,

$$p(r_R^{(i)}, f_s, t_E) = p_o\,(f_s, r_R^{(i)}) \exp\,(X)$$

A new list of observables can be constructed from these quantities by removal of subscript m from the previous list.

Two-Point Statistics

We return now to the case of one or several single channel receptions and consider two space-time acoustic pressures received under the following conditions:

p

$\langle p \rangle$

p^2

$|p|$

$|p|^2$

$\phi,\ X_2$

$\langle \phi \rangle,\ \langle X_2 \rangle$

$\langle \phi^2 \rangle,\ \langle X_2^2 \rangle$

$\ln\ |p|^2 = 1$

$\langle I^2 \rangle = \langle (\ln\ |p|^2)^2 \rangle$

$\langle \phi I \rangle = 2\ \langle X_1 X_2 \rangle$

X_1

$\langle p_1^2 \rangle = \frac{po^2}{4}\ [\exp\ 2(\langle X^2 \rangle) + \exp\ 2(\langle X^2 \rangle)]$

$\ln\ |\langle p \rangle|^2$

$\langle X_{\frac{1}{2}}^2 \rangle = \frac{1}{2}(\langle |X|^2 \rangle \pm \mathrm{Re}\langle X^2 \rangle)$

$\langle X_1 X_2 \rangle = \frac{1}{2} I_m\ \langle X^2 \rangle$

$\ln\ \langle p^2 \rangle$

$TQ\ \cos\ \phi$

Note the following definitions of the channel pressure p_{mi}

$p_m = T_m Q_m = \langle T_m Q_m \rangle + \delta QM = |p_m| \exp\ i\phi_m = p_o\ \exp\ X_m$

$p = \Sigma T_m Q_m = p_o\ \exp\ X$

$X = X_1 + iX_2$

m = channel or multipath number

Figure III.1

List of Observables at Real Points in Space-time
(Symbols defined in text)

(1) Two single channels to two space points $\vec{r}_R^{(i)}$, $r_R^{(j)}$ at fixed time.

(2) One single channel at one space point $\vec{r}_R^{(i)}$ at two different times t_E, t_E'.

(3) One single channel at one space point $\vec{r}_R^{(i)}$ at two different source frequencies, f_s, f_s'.

(4) etc.

The symbol etc. means a further listing of whatever combination of two events in real space-time or transform space-time where "time" means a choice of t_E, t_S, t_{SM}, t_{RM}, as defined above.

The random pressures (or one random pressure and its conjugate) are used to form two-point statistics in space-time. These are elements of a covariance matrix K, if ensembles of the random pressures are available, or coherence matrix R, if only one realization is available. Consider the latter since they are most common, and to begin with, construct cross correlations of two channels. A list of these follows in which m, n denote the m^th channel and n^th channel, i, j denote two receiver space points $r_R^{(i)}$, $r_R^{(j)}$, and t, t′ denotes two time points,

Correlation	*Name of Correlation Function*
(1) $R[f_s^{(i)}(m), f_s^{(j)'}(n) \mid t_E^{(i)}(m), t_E^{(j)'}(n)]$	(1) Signal frequency-environmental time
(2) $R[t_s^{(i)}(n), t_s^{(j)'}(n) \mid t_E^{(i)}(m), t_E^{(j)}(n)]$	(2) Signal range — environmental time
(3) $R[f_s^{(i)}(n), f_s^{(j)}(n) \mid \Phi_E^{(i)}(m), \Phi_E^{(j)}(n)]$	(3) Signal frequency-environmental frequency (bifrequency)
(4) $R[t_s^{(i)}(m), t_s'^{(j)}(n) \mid \Phi_E^{(i)}(m), \Phi_E^{(j)'}(n)]$	(4) Range-doppler, or temporal scattering
(5) $R[f_s^{(i)}(m), f_s^{(j)}(n) \mid k_R^{(i)}(m), k_R^{(j)'}(n)]$	(5) Frequency-angle of arrival
(6) $R[t_s^{(i)}(m), t_s^{(j)'}(n) \mid k_R^{(i)}(m), k_R^{(j)'}(n)]$	(6) Range-angle of arrival
(7) $R[k_s^{(i)}(m), k_s^{(j)},(n) \mid k_R^{(i)}(m), k_R^{(j)'}(n)]$	(7) Spatial (or angle) scattering
(8) $R[t_s^{(i)}(m), t_s^{(i)'}(m) \mid \Phi_E^{(i)}(m), \Phi_E^{(i)'}(m) \mid \vec{k}_s^{(i)}(m), \vec{k}_s^{(i)}(m) \mid k_R^{(i)}(m), k_R^{(i)}(m)]$	(8) Range-doppler-angle of arrival autocorrelation or ambiguity function.
(9) $R[t_s^{(i)}(m), t_s'^{(i)}(m) \mid \vec{k}_s^{(i)}(\Phi_{SM}(m)), k_s^{(i)'}(\Phi_{SM}(m)) \mid \vec{k}_R^{(i)}(\Phi_{RM}(m), \vec{k}_R^{(i)}(\Phi_{RM}(m))]$	(9) Range-doppler autocorrelation due to motion of receiver.
(10) etc.	

The real and transform coordinates in these correlations are:

(1) $t_s \leftrightarrow f_s$	(1) Range → frequency
(2) $\vec{r}_s \leftrightarrow \vec{k}_s$	(2) Location vector → angle of arrival vector
(3) $\vec{r}_R \leftrightarrow \vec{k}_R$	(3) Location vector → angle of arrival vector
(4) $t_E \leftrightarrow \Phi_E$	(4) Environment time → environment doppler
(5) $t_{SM} \leftrightarrow \Phi_{SM}$	(5) Motion time → motion doppler
(6) $t_{RM} \leftrightarrow \Phi_{RM}$	(6) Motion time → motion doppler

These correlations, and many more of the same type, are functions of space and time and thus correspond to nonstationary processes. Since stationarity is important, we discuss it in the next section.

Stationarity

Each element in the matrix $\vec{E}$ is a random process in space-time. The transmission channel and the arrived signal are thus also random. Because in general the ocean is nonstationary, and because the construction of nonstationary statistics to difficult at best, it has been customary to consider the transmission process as *locally stationary*. To define this concept it will be sufficient to take one of the random variables, say the environmental matrix $\vec{E}$, and focus attention on one of its coordinates, say the environmental time t_E. We will then consider conditions for stationarity in this selected coordinate. For simplicity we take only the m^{th} component of $\vec{E}$ and represent it as a Fourier transform,

$$E_m(t_E) = \int_{-\infty}^{\infty} \exp\left[i\Phi_E t_E\right] Z(dt_E)$$

in which $Z(d\Phi_E)$ is a random amplitude with mean value of zero. Now the autocorrelation of E_m is,

$$R_{E_m}(t_E, t_E') = \iint_{-\infty}^{\infty} e^{i[\Phi_E t_E - \Phi_E' t_E']} \langle Z(d\Phi_E) Z^*(d\Phi'_E)\rangle$$

In order for E_m to be stationary in the coordinate t_E it is required that correlation R depend only on difference $t_E - t_E'$ and not on t_E, t_E' separately. Thus one must set,

$$\langle Z(d\Phi_E)\, Z^*(d\Phi_E') \rangle = \delta(\Phi_E - \Phi_E')\, \mathscr{W}(\Phi_E - \Phi_E')\, d\Phi_E\, d\Phi_E'$$

in which $\mathscr{W}(\Phi_E)$ is the frequency power spectrum of the random E_m. This means that the random spectral amplitudes are uncorrelated at different frequencies Φ_E if E_m is to be stationary in time t_E.

In a similar way stationarity of $E_m(\Phi_E)$ in frequency requires that

$$\langle Z(dt_s)\, Z^*(dt_s') \rangle = \delta(t_s - t_s')\, F(dt, dt_s')$$

so that $R(\Phi_E, \Phi_E') = R(\Phi_E - \Phi_E')$. This is the condition of *uncorrelated* scattering in which the scattering of that portion of the signal at time t_s is uncorrelated to the scattering at time t_s'. Stationarity of $E_m(\vec{r}_s, \vec{r}_R)$ in space is defined in the same way. For example, the stationarity in z-coordinate requires that the random amplitudes $Z(dk_z)$, $Z'(dk_z)$ be uncorrelated,

$$\langle Z(dk_z)\, Z^*(dk'_z) \rangle = \delta(k_z - k'_z)\, F(dk_z, dk'_z)$$

This means that different ray paths arriving at a point are uncorrelated in the z-component of the angle of arrival.

Propagation channels which obey stationarity in the limited sense describe here, and which have constant mean values in the transmission of a field are wide-sense stationary. Few channels of ocean propagation which are long enough in space-time are stationary. However, over a "short enough interval" in space-time the *increment* in the random ocean process may be stationary. For example, let E_m be a random process with nonstationary mean in the coordinate time t_E. Choose a "small-enough" increment in time, call it T_E, and form the increment

$$\Delta E_m = E_m(t_E + T_E) - E_m(t_E)$$

If the low frequency swings in $E_m(t_E)$ occur so slowly that the increment ΔE_m is unaffected by them then the nonstationary function $E_m(t_E)$ is defined to be stationary in its first increments. The second order statistics of ΔE_m are then described by the *structure function*, which is the ensemble average of the square of its zero-mean part:

$$D_{Em}(T_E) = \langle (\Delta E_m - \langle \Delta E_m \rangle)^2 \rangle$$

The properties of D are self evident: (1) $D(0) = 0$ (2) $D(\infty)$ is finite (3) if $E_m(t_E)$ is a random process with zero-mean then

$$D_{Em}(T_E) = 2\,[R_{Em}(0) - R_{Em}(T_E)]$$

From the definition of the concept of structure function it is seen that it can be applied to each coordinate of space, or time, or both, and to each random process of ocean propagation, particularly the acoustic processes itself. Thus structure functions of received pressure are in use wherever nonstationity is tentatively accounted for.

Antenna Function and Total Received Pressure

The pressure received by the i^{th} hydrophone in an L element hydrophone array is customarily modified by an antenna steering function A which shades the received amplitude and introduces a time delay, τ_d. In actual practice, A is a random process of space and time, with the coordinate of randomness in time being t_A. Summation over all hydrophones then gives the total received pressure,

$$p(\vec{r}_R\,(\theta,\varphi), t_E, t_s, t_A) = \sum_{i=1}^{L} A(\vec{r}_R\,(\theta,\varphi) \,|\, r_R^{(i)}, \tau_d, t_A)\, p(r_R^{(i)}, t_E, t_s)$$

in which $\vec{r}_R\,(\theta,\varphi)$ is the coordinate of spatial distribution of the received pressure and $p(r^{(i)}, t_E, t_s)$ is a sum of multipaths. A plot of $|p|$ vs θ, φ gives the beam pattern of the received pressure, which because of both $p^{(i)}$ and A, is a random variable. The random aspects of A can be studied in the same way as for the environmental matrix $\vec{E}$, namely by formation of a covariance matrix in the time coordinate t_A, or in the space coordinate $\vec{r}_R^{(i)}$, or in both. Alternatively one can form a coherence matrix R of correlations of A in the same coordinates.

The coherence matrix in correlations of the total pressure allows one to obtain the array gain AG as a function of steering τ_d and random perturbation τ_A in S/N power in the manner suggested earlier:

$$AG(\tau_d, t_A) = \left\{ \frac{\left[\dfrac{\displaystyle\sum_{i,j}^{L} \dfrac{A(i, t_A)\, R^{(s)}(i,j,\tau_d)\, A(j, t_A)}{[R^{(s)}(i,o)\, R^{(s)}(j,o)]^{1/2}}}{\displaystyle\sum_{i,j}^{L} \dfrac{A(i, t_A)\, R^{N}(i,j,\tau_d)\, A(j, t_A)}{[R^{(N)}(i,o)\, R^{(N)}(j,o)]^{1/2}}} \qquad \dfrac{[R^{s}(i,o)\, R^{(s)}(j,o)]^{1/2}}{[R^{N}(i,o)\, R(j,o)]^{1/2}} \right]}{\dfrac{R^{(s)}(o)}{R^{N}\,(o)}} \right\}$$

in an obvious shortening of notation. Once again, since the A's are random we noted that the array gain is a random function of space-time.

Coherence and Fluctuations

The temporal cross correlation of two signals, $p(\vec{x}_1, t)$ and $p(\vec{x}_2, t)$ over time duration T is,

$$R(\vec{x}_1, \vec{x}_2, \tau) = \int_{-T/2}^{T/2} p(\vec{x}_1, t_s)\, p(\vec{x}_2, t_s + \tau) dt_s$$

If the signal at $\vec{X}_2$ simultaneously undergoes a shift in phase, $\omega_d t$, the cross correlation features an additional parameter ω_d,

$$R(\vec{x}_1, \vec{x}_2, \tau, \omega_d) = \int_{-T/2}^{T/2} p(\vec{x}_1, t_s)\, p^*(\vec{x}_2, t_s + \tau)\, e^{-j\omega_d t_s}\, dt_s$$

The normalized absolute value squared of this quantity is the ambiguity function,

$$N_{\vec{x}_1 \vec{x}_2}(\tau, \omega_d)|^2 = \frac{\left| \int_{-T/2}^{T/2} p(\vec{x}_1, t_s)\, p^*(\vec{x}_2, t_s + \tau)\, e^{-j\omega_d t_s}\, dt_s \right|^2}{\left[\int_{-T/2}^{T/2} \left| p(\vec{x}_1, t_s) \right|^2 dt_s \right] \left[\int_{-T/2}^{T/2} \left| p(\vec{x}_2, t_s) \right|^2 dt_s \right]}$$

If the signal at $\vec{X}_1$ is the transmitted signal, and that at $\vec{X}_2$ is the same signal delayed τ units and phase shifted $\omega_d t$ units, this function measures the mean square departure of the transmitted signal from its original waveform. A three-dimensional plot of $|\chi(\tau, \omega_d)|^2$ vs τ and ω_d is used in sonar detection and localization because it exhibits a peak at the supposed location where there is a target. However, the peak is usually broad, and is generally accompanied by other peaks, indicating the uncertainty of the presence of a target in the midst of false alarms.

The search for target by integration over the time domain is advantageously replaced in many instances by a search in the frequency domain. The method of constructing the appropriate mathematical surface in which peaks are to be found is briefly as follows. Let a record of pressure p(t) be represented by N values $p(m\Delta t)$, n = 0, 1, 2 . . . N. The discrete Fourier transform of these N points into N points in frequency yields the sequence,

$$\left\{ G(m\Delta\omega) \right\} = \left\{ G(o) + G(\Delta\omega) + G(2\Delta\omega) + ... + G((N-1)\Delta\omega) \right\}$$

in which

$$G(m\Delta\omega) = \sum_{m=0}^{N-1} g(m\Delta t) \exp\left[\frac{2\pi j}{N} mn\Delta\omega\Delta t \right]$$

Each G is thus a sum of N exponentials or phasors for each value of frequency $m\Delta\omega$. In this way signals at space points $\vec{X}_1, \vec{X}_2$ can be represented in the frequency plane. Similarly the

cross correlation of signals in the time domain has its analog in the crosspower spectrum in the frequency domain. In particular, the ambiguity function at a *single frequency* ($m\Delta\omega$) becomes,

$$S_{\vec{x}_1\vec{x}_2}(m\Delta\omega, \tau, \omega_d) = \frac{\left|\sum_{l=1}^{N} e^{-jl\omega_d}\, G_{x_1}(m\Delta\omega)\, G^*_{\vec{x}_2}(m\Delta\omega, \tau)\right|^2}{\sum^{N} \left| G_{\vec{x}_1}(m\Delta\omega)\right|^2 \ \sum^{N}\left| G(m\Delta\omega, \tau)\right|^2}$$

A plot of $S_{\vec{x}_1\vec{x}_1}$ vs τ and ω_d is a topological surface of the cross-power spectrum between signals at X_1 and X_2 calculated on the basis of a single frequency. The highest peaks of all peaks of this surface identifies possible targets, but with ambiguity caused by the broadness of the peaks and by the presence of false alarms (smaller peaks).

The locations $\vec{X}_1, \vec{X}_2$ can refer to several points of measurement of signals: $\vec{X}_1$ can be the source location and X_2 the point of reception; or, X_1, X_2 can be the location of two hydrophones in an array, or two arrays in a multi-array receiving system. In all cases plots of $S_{\vec{x}1,\vec{x}2}$ vs τ and ω_d are labeled *coherence surfaces of signals at* X_1, X_2, τ is called the range, or the time difference of arrival, and ω_d is called the differential Doppler.

The factor $\exp(-jl\omega_d)$ in $S_{x1,x2}$ is significant. Since ℓ (or discrete time) and ω_d are a Fourier pair, it is seen that increasing the limit of ℓ from N to some higher integer simultaneously decreases the width of ω_d, that is, it increases the *resolution in Doppler*. One says that increase in the integration time(meaning the sum over ℓ)increases the resolution in ω_d. Similarly in the form,

$$G(m\Delta\omega, \tau) = \sum_{m-1}^{N-1} g(m(\Delta t + \tau)) \exp\left(\frac{-2\pi j}{N} mn\Delta\omega(\Delta t + \tau)\right)$$

if one increases the limiting value of m which is equivalent to increasing the bandwidth of the processing, the resolution in differential time of arrival τ is also increased.

The mathematical content of coherence surfaces $|\chi_{\vec{x}1,\vec{x}2}|^2$ and $S_{\vec{x}1,\vec{x}2}$ so far have not accounted for ocean fluctuations. In actual measurements in the ocean these surfaces have been found to fluctuate as functions of environmental time t_E and multichannel interferences ΣT_m caused by relative motion of source and target, whether opening or closing. The study of coherence surfaces may thus be distinct from the study of fluctuations. The latter is essentially a study in statistics, the former is essentially deterministic.

Modeling Fluctuations in Signal Excess in Sonar Detection Models

Each term SE_i in the equation of signal excess represents a random variable in space-time. For a fixed point in space the stochastic process $SE_i(t)$ can be modeled in several ways in accordance with the requirements of the underlying physical process. In most applications the mean $SE_i(t)$ although the function of time, is considered deterministic. Attention is then

focused on the fluctuating part X(t). Given the great diversity of causes of ocean randomness it would seem that the construction of a single model of X(t) is not feasible. However, if the underlying physical process leads to a normal probability distribution of X(t) and an auto-correlation which is exponential in time, and if a plot of X(t) vs. t looks like a random walk with discrete steps of relatively small size, one could usefully adopt a random walk model for X(t).

Fig. III.2 shows two realizations of a random function Y(t) pictured as a random walk: the abscissa is Y(t), quantized into distinct excursion steps, or states, Y_2, Y_1, Y_0, Y_1, Y_2 ...., while the ordinate is quantized in time, 0, τ_E, $2\tau_E$, ... Realization 1 consists of the walk $Y_1, Y_0, Y_{-1}, Y_0, Y_{-1}, Y_{-2}, Y_{-1}$ while Realization 2 describes another walk $Y_{-1}, Y_{-2}, Y_{-1}, Y_0, Y_{-1}, Y_0, Y_1$. The probability of the occurrence of Realization 1 is modeled as a Markov chain,

$$P\{1\} = a_1\, p_{1,0}\, p_{0,-1}\, p_{-1,0}\, p_{0,-1}\, p_{-1,-2}\, p_{-2,-1}$$

in which a_1 is the initial probability that Y(t) is in state Y_1; $p_{1,0}$ is the conditional (or transition) probability of going from state Y_1 to state Y_0; $p_{0,1}$ is the transition or probability of going from state Y_0 to state Y_1, etc. The probability of occurrence of Realization 2 ($P\{2\}$), is similarly constructed. In numerical work one must assign probability distributions to a_i, and p_{ij}, depending on the physics. Since these choices are critical a variety of them have been proposed to fit measurements. Suppose the chain of a + 1 states exhibits a tendency to cluster about a central state Y_c, and that the movement from a high number state toward the central state is always more likely to happen than away from it. The matrix of transition probabilities is then modeled as,

$$\begin{bmatrix} p_{00} & p_{01} & p_{02} & p_{03} \cdots & p_{0a} \\ p_{10} & p_{11} & p_{12} & p_{13} \cdots & p_{1a} \\ p_{20} & p_{21} & p_{22} & p_{23} \cdots & p_{2a} \\ p_{a0} & p_{a1} & p_{a2} & p_{a3} \cdots & p_{aa} \end{bmatrix} = \begin{bmatrix} 0 & 1 & 0 & 0 \ldots\ldots & 00 \\ a^{-1} & 0 & 1\text{-}a^{-1} & 0 \ldots\ldots & 00 \\ 0 & 2a^{-1} & 0 & 1\text{-}2a^{-1} & 00 \\ \vdots & \vdots & \vdots & \vdots & \vdots \\ 0 & 0 & 0 & 0 \ldots\ldots & 10 \end{bmatrix}$$

A Markov chain of Y(t) that features these transition probabilities is an Ehrenfest random walk. The entries mean the following: if Y(t) is initially in state Y_0 it has zero probability of remaining there, $p_{00} = 0$. In contrast it moves to state Y_1 with certainty, $p_{01} = 1$. If Y(t) is in state Y_1 it has zero probability of remaining there, $p_{11} = 0$. It either moves to state Y_0 with probability a^{-1}, or to state Y_2 with probability $1\text{-}a^{-1}$. It has zero probability of moving to any other state than the one immediately to the left or to the right. Since a is usually large the movement favors Y_2. If Y(t) is in state Y_2 it again has zero probability of remaining there. Instead it moves to state Y_1 with probability $2a^{-1}$, and to Y_3 with probability $1\text{-}2a^{-1}$. Once again Y_3 is more likely. Now suppose Y(t) is in state Y_j, $j > a/2$. Then the movements Y_{j-1} has probability j/a, which is greater than 1/2, and to Y_{j+1} with probability 1-j/a which is less than 1/2. The movement back to a lower state is therefore most likely. Thus Y(t) in this model is a diffusion

with a central force. The random walk pictured by $Y(t)$ clusters around a mean value a/4, with a standard deviation of $\sqrt{a/4}$. In order to model the fluctuation $X(t)$ it must have the mean value removed. When this is done one can form the ratios,

$$\frac{SE - \overline{SE}}{\sigma_{SE}} = \frac{X}{\sigma_{SE}} = \frac{Y - a/4}{\sqrt{a/4}}$$

in which σ_{SE} is the standard deviation of the signal excess (an experimentally determined quantity). Now the probability distribution of $Y(mt_E)$, $m = 0, 1, 2 \ldots$ is known to be binomial with mean a/4, and variance a/4 (see Feller). By choosing the number $a+1$ of states of Y Y one can construct a random number generator from which realizations of sequences $Y_0, Y_1 \ldots Y_a$ can be obtained, modeled as Ehrenfest random walks, with mean a/4 and variance a/4. From these sequences one can obtain realizations $X_0, X_1, \ldots X_a$ by multiplication with σ_{SE}. Thus any sequence $\{X_i\}$ can be generated as a Monte Carlo trial beginning with the state Y_i, which itself is selected according to some probability distribution (usually normal).

Time Interval of Stepping, τ_E

A random walk in time requires specification of a stepping interval τ_E. Now if $X(t)$ is taken as a general Gauss-Markov process its normalized correlation-function is exponential,

$$\rho_X(t_2 - t_1) = e^{-\frac{\Delta t}{\tau_R}} ; \quad \Delta t = | t_2 - t_1 |$$

in which τ_R is the "relaxation time", or that time interval $t_2 - t_1$ when $\rho_X = e^{-1}$. In contrast the autocorrelation function for the Ehrenfest random walk is

$$\rho_E(s) = \left(\frac{a-2}{a}\right)^S$$

in which S is the number of steps of $Y(t)$ to be used in forming ρ_E. If $Y(t)$ is to model $X(t)$ one requires,

$$\left(\frac{a-2}{a}\right)^S = e^{-\Delta t/\tau_R}$$

For a single step one sets S = 1. This then defines the interval $\tau_E = \Delta t$.

$$\frac{a-2}{a} = e^{-\tau_E/\tau_R}$$

or

$$\tau_E = -\tau_R \ln\left(\frac{a-2}{a}\right)$$

*W. Feller, "An Introduction to Probability Theory and Its Applications", Vol. I. Wiley, New York (1943).

Thus the stepping interval in time ($=\tau_E$) is determinable as soon as the relaxation time τ_R of the underlying Gauss-Markov physical process is known, and a number a + 1 of states is specified. Random realizations of $Y(m\tau_E)$ are then supplied by the random number generator in the form of steps of the Ehrenfest random walk, from which various $X(m\tau_E)$ are determined.

Environment, Target and Sensor Fluctuations

In more refined models of detections of sonar the total fluctuation X(t) is taken to be a sum of fluctuations of terms in the equation for signal excess $SE = \overline{SE} + X(t)$. Typically,

$$X(t)=X_E(t)+X_t(t)+X_S\,(t)$$

in which environment (or transmission loss), target, and sensor (hydrophone or array) are represented. Each X_i can be modeled as a statistically independent random walk with measured standard deviation $\sigma_{X(i)}$, measured relaxation $\tau_{R(i)}$, and selected stepping interval $\tau_{E(i)}$ as determined from $\tau_{R(i)}$ and the selected number of states $(a+1)_{(i)}$. The variance of the total X(t) is then,

$$\sigma_{SE}{}^2 = \sigma_E{}^2 + \sigma_R{}^2 + \sigma_S{}^2$$

The variations of X_i with time t make it sensitive to frequency. Thus the assignment of $\sigma_{x(i)}$ and $\tau_{R(i)}$ will vary with frequency.

SYSTEM SIMULATION (SS)

Underwater surveillance systems are visualized in Fig. III.2. The key features are: (1) number and location of signal sources S_n, m = 1, 2...; (2) number and location of noise sources N_m, m = 1,2...; (3) spectrum of the signal source, or noise source; (4) number of sensors, $A_H{}^{(i)}$, i = 1,2...; $A_V{}^{(i)}$, i = 1,2...; (5) number and character of transmission channels.

This visualization in its entirety is *simulated* (not duplicated in a physical sense) in its dynamic operations (detection, localization, tracking) by the computer program SS. The simulation is on a very large scale: it handles a large number of separate sources of signal and noise, several frequency lines per received target, and a large number of sensors. Simulation begins with a sonar equation for each source-channel-receiver to determine signal-to-noise ratio. Since each term in the equation is a random variable there is a need to specify its probability distribution and statistics. The mean value of each term is obtained by interpolation from a table of mean values previously stored in the memory of the computer from accumulated field data. Its value is stationary with time. The fluctuating component of each term is modeled as a Gauss-Markov process (or chain), meaning that in successive realizations of time record of length O to T, the probability between immediately adjoining points is Markov. Since the sonar equation is in logarithmic units the probability distribution of the Gauss-Markov chain is taken as lognormal with a variance (or standard deviation) to be supplied to SS as drawn from field data. The second order characterization of the Gauss-Markov simulation is the temporal autocorrelation of a single realization. Since this correlation is assumed exponential with a characteristic relaxation time τ_R field data must again be used to furnish this to SS as an input. Other acoustic inputs to SS are listed in the proceedings paper by Fretwell.

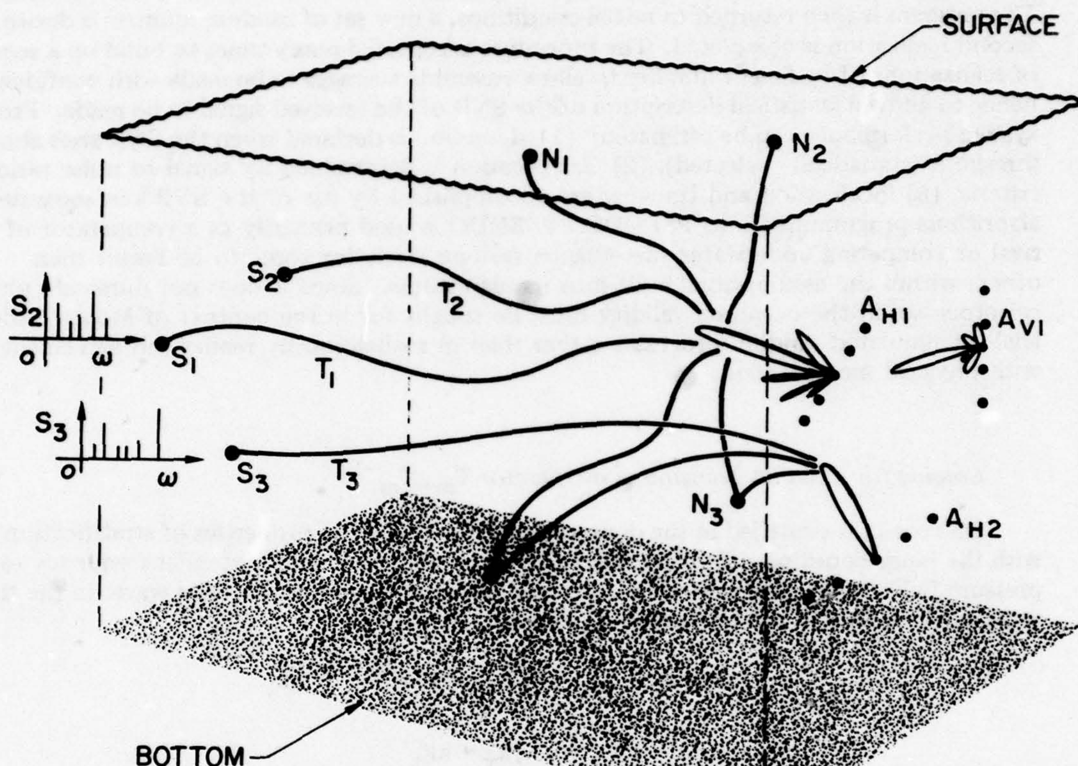

Fig. III.2

Schematic of Underwater Surveillance Systems

When all the acoustic input to PSEUDO is completed the computer program selects from a random number generator based on Gauss-Markov statistics and from the input field data a set of random numbers to represent realizations of fluctuation processes in target strength, transmission loss, ambient noise, beam noise and signal gain. Mean values of these same quantities are obtained from an interior stored table by simple look-up guided by the acoustic input. PSEUDO then completes one run, delivering a single realization of received acoustic pressure versus time. The program is then returned to initial conditions, a new set of random number is drawn, and a second realization is completed. The procedure is repeated many times to build up a sequence of realizations of sufficient number to allow ensemble averages to be made with confidence, and hence to allow a statistical description of the SNR of the received signal to be made. From this system performance can be estimated: (1) detection is declared when the SNR rises above a threshold (statistically selected), (2) classification is determined by signal to noise ratio criteria, (3) localization and tracking are accomplished by use of the SNR's in separate algorithms programmed into PSEUDO. PSEUDO is used primarily as a comparator of rival or competing underwater surveillance systems declaring some to be better than others within the assumptions built into its algorithms. Since it does not duplicate physical processes in the ocean its validity must be sought for in the context of Monte Carlo trial on simulated random processes rather than in realization by realization agreement with physical measurement.

Solving for Channel Transmission Operator T_m, T_m^{-1}

The ocean is stratified in the depth coordinate z, and the properties of stratification vary with the range coordinate X. At a point $\vec{r}$ in the medium and at a particular frequency ω the pressure field can be represented by an angular (spatial) spectrum of plane waves in the transverse wavenumber $\vec{k}_t$ and transverse coordinate $\vec{\rho} = \hat{j}y + \hat{k}z$

$$p(\vec{r}, \omega) = \iint_{-\infty}^{\infty} F(\vec{k}_t, \omega; x)\, e^{i\vec{k}_t \cdot \vec{\rho}}\, d\vec{k}_t$$

$$\vec{k}_t = \hat{j}k_y + \hat{k}k_z$$

The plane wave amplitudes F are generally not expressible in closed form. However, for slow medium variations F may be approximated by the WKB representation,

$$F(\vec{k}_t, \omega; x) = A(k_t, \omega; x) \exp\left\{ i \int^{x} k_x (\vec{k}_t, \omega; \xi)\, d\xi \right\}$$

Thus the angular spectrum representation of the pressure field becomes,

$$p(\vec{r}, t) = \int_{-\infty}^{\infty} e^{-i\omega t}\, d\omega \iint_{-\infty}^{\infty} A(\vec{k}_t, \omega; x) \exp\left\{ i \left[\vec{k}_t \cdot \vec{\rho} + \int^{x} k_x (\vec{k}_t, \omega; \xi)\, d\xi \right] \right\} d\vec{k}_t$$

Here the source of the field is not explicitly represented. If a point source in space is present, $Q = \delta(\vec{\rho} - \vec{\rho}\,')\,\delta(x - x')$, the amplitudes F are the longitudinal Green's functions G, which in the WKB approximation, become

$$F = G(\vec{k}_t, \omega; x, x') = A(\vec{k}_t, \omega; x, x') \exp\left\{ i \int^{x'} \int^{x} \left[k_x (\vec{k}_t, \omega; \xi) - k_x (k_t, \omega; \xi') \right] \right\} d\xi\, d\xi'$$

The four-dimensional space time Green's function is then constructible in the form,

$$G(\vec{r}, \vec{r}; t, t') = \iiint G(\vec{k}_t, \omega; x, x')\, e^{i\vec{k}_t(\vec{\rho} - \vec{\rho}\,')}\, e^{-i\omega(t-t')} \frac{d\vec{k}_t\, d\omega}{(2\pi)^3}$$

When the source is distributed in space/time, $Q(\vec{r}_s, t_s)$, the resultant pressure field at a specific frequency ω is

$$p(\vec{r}_R, \omega) = \int_{vol} G(\vec{r}_R, \vec{r}_S \mid \omega)\, Q(\vec{r}_s \mid \omega)\, d\vec{r}_s$$

or

$$p(\vec{r}_R, \omega) = \int_{vol} \iint_{-\infty}^{\infty} A(\vec{k}_t, \omega; x_R, x_s) \exp\left\{ i \int_{x_s}^{x_R} k_x\, (\vec{k}_t, \omega; \xi)\, d\xi \right\} e^{i\vec{k}_t \cdot (\vec{\rho}_R - \vec{\rho}_s)} \times Q(\vec{r}_s \mid \omega)\, d\vec{k}_t\, d\vec{r}_s$$

where

$$\vec{r}_s = \hat{i}\, x_s + \hat{j}\, y_s + \hat{k} z_s = \hat{i}\, x_s + \vec{\rho}_s$$

The relation of these forms to the operator T_m is seen in the definition,

$$p_m = T_m Q_m$$

Thus, in the WKB approximation, the channel operator T_m becomes,

$$T_m \rightarrow \int_{vol} \iint_{-\infty}^{\infty} A(\vec{k}_t, \omega; x, x_s) \exp\ i \left\{ \int_{x_s}^{x_R} k_x\, (\vec{k}_t, \omega; \xi)\, d\xi \right. \times e^{i\vec{k}_t{}' (\vec{\rho}_R - \vec{\rho}_s)} \left\{ \quad \right\} d\vec{k}_t\, d\vec{r}_s$$

A principal feature of this operator is integration over the range (X) component of the propagation vector to give the WKB approximation to phase.

This form of T_m is deterministic. However, in ocean propagation the pressure at $\vec{r}_R$ is a random variable. To represent this condition the amplitudes A are made random variables. Thus T_m for the general transmission channel is a random variable.

The Basic Tracking Problem in System Performance Modeling

A submarine radiating specific sounds follows a prescribed underwater track in a selected area of the ocean (Fig. III.3). Several listening receivers (A through F) are required to track the path of the submarine. The received signals and noise at these arrays form time series (Fig. III.4). These exhibit random behavior about some mean. At several times in each record there are sudden drop-outs, where occurrences are random. At other times the signals fade out completely. Let a threshold TH be set for each time record, and assume that when SNR is above TH the submarine is detected. Because of the random nature of these records several probability statements on detection are required to be formulated. Two examples are:

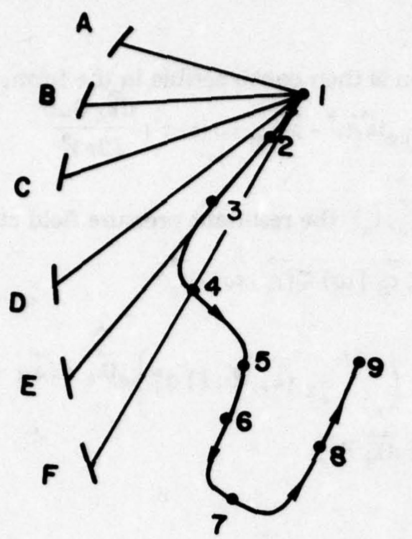

Figure III.3
Basic Tracking Problem

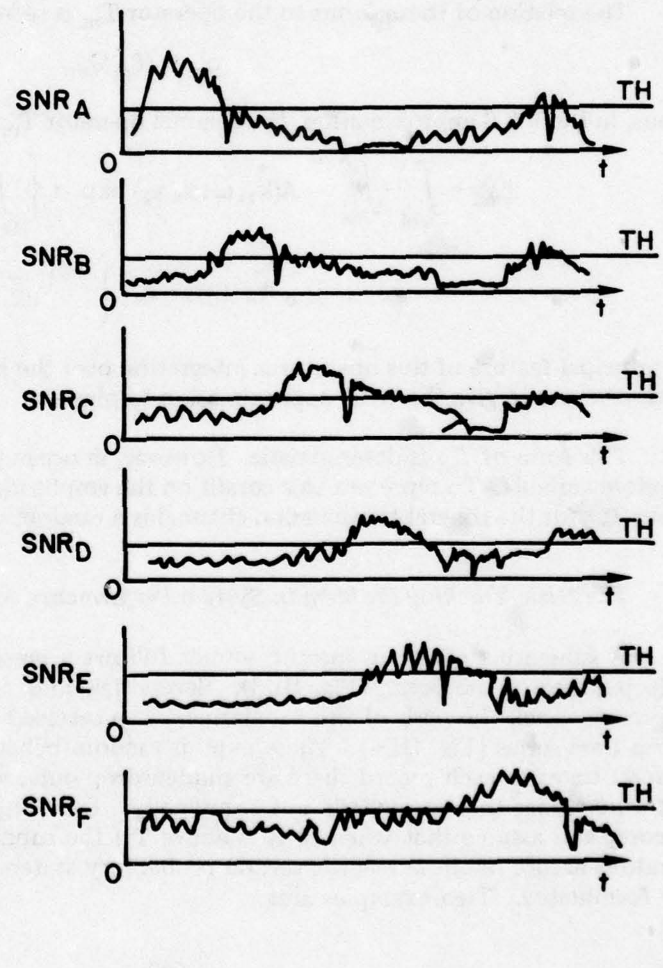

Fig. III.4
Received SNR's of Basic Tracking Problem

(1) What is the probability distribution that a specific array will track the target at least X minutes? (2) What is the joint probability that two (three, four, etc.) arrays will track the same target at least X minutes. The answers to these questions and others in existing systems are of course obtained by trial. However, proposed new systems and proposed improvements on old systems must be critically evaluated between competing candidates, making system performance prediction mandatory. The construction of prediction algorithms becomes thus a basic problem.

A first approach to system performance modeling is to duplicate the underlying physics directly by mathematical formulas and numerical analysis. In this procedure the acoustic pressure arriving at arrays A through F by multipath channels through a randomizing ocean is obtained by physical analysis. This yields a spatial distribution of mean value, which is locally a function of time, and spatial and temporal auto-and cross-correlations (or mutual coherence) of the fluctuating component of the field. Correlation lengths correlation times, power spectra, etc., are predicted from a knowledge of the environment. This approach is shown in Fig. III.5

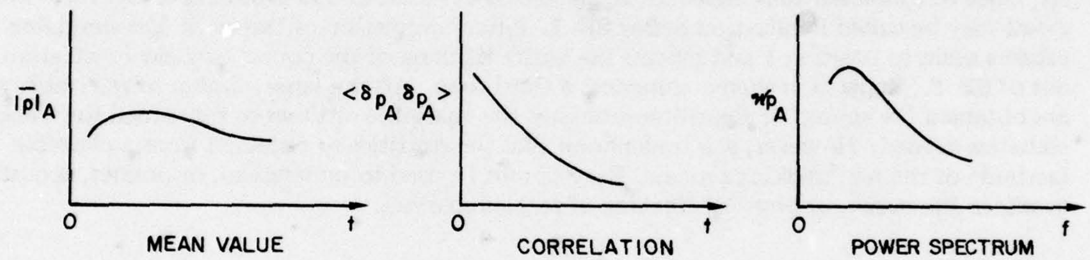

Figure III.5

Using this model one computes acoustic intensity and thus one obtains transmission loss. Other components of the sonar equation are similarly treated e.g., analysis of underlying physics is made for ambient noise, and a model constructed. Also, by means of statistical antenna theory one constructs a mathematical model of the array gain, beamwidth, etc. which includes spatial and temporal fluctuations.

All these analytic models of sonar equation components contribute to the SNR at each array. Since each SNR is a random process it will have a predicted probability distribution, from which all the statistical moments can be drawn. Thus the statistics of SNR at each array can be predicted for each position of the submarine along the track. Furthermore, the models also contain algorithms for predicting the spatial and temporal cross correlation of total SNR between arrays. This gives estimates of SNR interarray mutual coherence, SNR correlation time and correlation length, which in turn can be used to calculate the real physical tracking statistics of real systems, and hence can be used for system performance prediction.

A second approach to system performance modeling is to devise a *simulation* algorithm which models the tracking problem as a random process, chosen for convenience as plausible, but not specifically addressed to the underlying physics. For each track position the acoustic intensity (or transmission loss) from submarine to arrays A through F is simulated as the sum of a deterministic mean value and a random (fluctuating) value. The mean value at each array is obtained from entries in a previously prepared table which are based on past experience and past modeling, in similar ocean areas at similar ranges between source and receiver. The fluctuating part of received acoustic intensity at each array is modeled as a plausible temporal random process. Currently, the popular choice is a Gauss-Markov process equivalent to a random walk, implemented in the form of a random number generator. Each number delivered by this generator is a step of random amplitude to be added to the mean value of transmission loss already obtained for the specific track position and specific listening array, the total being a realization of random transmission loss. At the same track position, other components of the sonar equation are similarly realized, and hence a single realization of signal excess is obtained for each array. Upon moving to the next position, and eventually to all positions, a final sequence of *simulated* time series for signal excess at all the arrays is obtained, Fig. III.6. The result may be called Realization Set of SE 1. After completion of the track, the simulator returns again to position 1 and repeats the entire tracking of the course to yield Realization Set of SE 2. Repetition then commences a third time. After a large number of realizations are obtained the simulator algorithm processes the ensemble of them to furnish all the tracking statistics needed. However, it is understood that the statistics so obtained form a plausible facsimile of the real tracking process. They cannot be used to understand, or predict, acoustic events in the ocean, or physical tracking of real submarines.

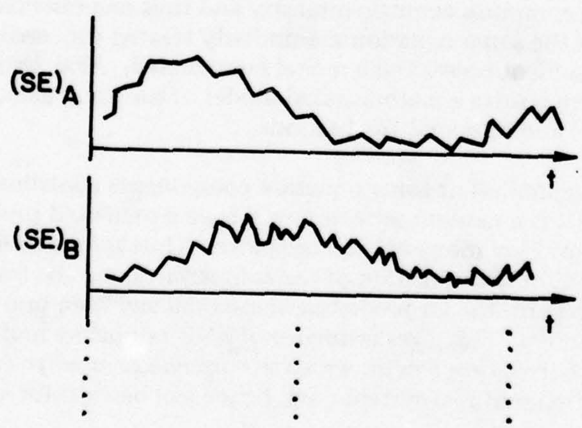

Figure III.6

IV. FLUCTUATION WORKSHOP PAPERS:

An Editorial Summary

(See Volume 2)

V. RESEARCH RESULTS -- A SUMMARY

(See Volume 2)

REFERENCES

(See Volume 2)

KEY ISSUES IN THE APPLICATION OF STATISTICS OF ACOUSTIC FLUCTUATIONS TO SYSTEM PERFORMANCE MODELING

Sam Hanish
Naval Research Laboratory
Washington, D.C. 20375

PERFORMANCE CRITERIA AND STOCHASTIC SIGNAL EXCESS

The performance of underseas surveillance systems in their task of detecting, classifying and tracking hostile submarines is modeled on several criteria. Two of these currently in use are *cumulative probability of detection* and *mean time to hold contact*. A simple model of each is to write it as the sum of a deterministic part and a random part, both being functions of time. For example, a parameter of these criteria, signal excess $S(t)$, is written,

$$(1)\ S(t) = M(t) + \xi(t) \qquad (2)\ M = SL - TL - (NL - DI + DT)$$

in which $M(t)$ is deterministic, based on prior knowledge of source level SL, transmission loss TL, noise level NL, directivity index DI, and detection threshold DT; and $\xi(t)$ is random, representing the effects of random changes in ocean environment, target characteristics, sonar equipment, operator efficiency, etc. The calculation of $M(t)$ can be done in the conventional manner. The stochastic term is more elusive in that it requires a probabilistic statement tailored to the mode of operation (whether active or passive). For example, during passive detection one requires an estimate of the probability that signal excess is greater than zero during some time interval:

$$P_r\{S(t) > 0,\ 0 \leqslant t \leqslant T\}.$$

Likewise, during tracking by a number m of sensors each of which can hold the target only part of the time, the operator needs an estimate of the probability that some j sensors of the total m, during some interval T, will exhibit a signal excess,

$$P_r\{S_j(t) > 0,\ 1 \leqslant j \leqslant m,\ 0 \leqslant t \leqslant T\}.$$

Naturally, a prediction model of these probabilities would be of great importance. An oft-quoted one (now mainly historical) is called the λ, σ model. In it the stochastic signal excess $S(t)$ is taken to be normally distributed with zero mean and standard deviation σ. The probability that a signal excess will occur in an interval x is written $\Phi(x)$. Since not all intervals will generate favorable detection levels, their occurrence is assumed to be a Poisson, or shot, process. The model for probability of detection is then written as

$$P_d(t) = 1 - [1 - \Phi(\sigma)]\, e^{-\lambda \Phi(x) t}$$

in which λ is the rate of favorable arrivals. It predicts that when signal excess is negative the probability of detection is not zero, even in short observation times. Indeed the model predicts that for signal excess of $-\sigma$ dB the probability at the end of 6.2 relaxation times $T(T = 1/\lambda)$ is nearly 0.7, a large value.

In the years 1969-1972 an effort was made by NSRDC in conjunction with Commander Submarine Development Two to use data of at-sea-exercises to estimate λ, σ. The results are somewhat unsatisfactory, the fundamental difficulty being the lack of consistency from one exercise to the next.* Thus, while the problem of modeling cumulative detection probability for stochastic processes has been current for a decade, it still continues. Part of the continuing problem is that in all models the stochastic variable of signal excess cannot be calculated from a simple enough algorithm in such a way to be both accurate and practical at the same time. It is a focal issue of this workshop to assess current ability to provide such an algorithm, tailored to the needs of the system performance modeler.

COMPONENTS OF THE PROBLEM OF DESCRIBING $\xi(t)$

The stochastic part of signal excess is an effect of ocean environment, and source-receiver characteristics. The components are pictured as shown in Figs. 1(a) through 1(c).

Figure 1(a) shows a background, or equilibrium ocean, having surface and bottom with a distribution of sound speed profiles. Figure 1(b) shows a perturbed ocean in which the profiles undergo random variations in space and time. Figure 1(c) shows volume distributed sources and receivers in horizontal and vertical motion. The general problem of describing the random part of signal part of signal excess $\xi(t)$ consists in assembling all three pieces, Figs. 1(a), 1(b), and 1(c), constructing a model of the propagation of an acoustic signal in the assembly, and predicting the statistical characteristics of the received signal. This signal is then inserted in the sonar equation, a threshold set, a signal excess calculated, and from it the cumulative probability of detection is predicted.

To keep within reasonable bounds we restrict attention hereafter to the acoustic problem alone, which concentrates on finding the statistical characteristics of the received signal as a function of the components shown in Figs. 1(a), 1(b), and 1(c) and of the frequency content of the acoustic signal. We now address the first issue.

THE BACKGROUND, OR EQUILIBRIUM, OCEAN

To begin the problem of modeling (that is, understanding) fluctuations in the ocean, we must inquire, which ocean? The acoustician's ocean is contained in dynamic relations between seven variables; 3 components of convection velocity, u, v, w; mass density ρ, total pressure p, salinity S, and temperature T. Seven equations are need to show the interrelations of these variables. The first is an equation of state relating p, ρ, S, T. The second is an equation of continuity which accounts for temporal changes in mass density. The third is an equation of diffusion of salinity S. The fourth, fifth and sixth are three dynamic equations of motion in u, v, w. Finally, the seventh is the equation of heat flux.

*During the same time more elaborate models were constructed by Navy laboratories and Navy contractors, the chief being APSURV, PSEUDO, APAIR, etc. These will be discussed by other speakers. They contain to this day several difficulties which make their predictions uncertain, and which this workshop will seek to resolve.

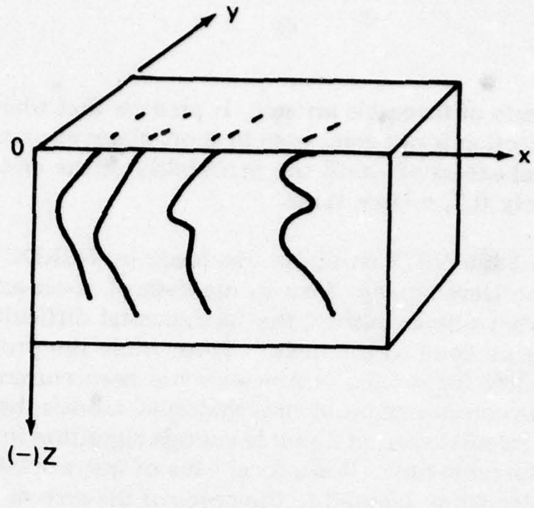

Figure 1(a)

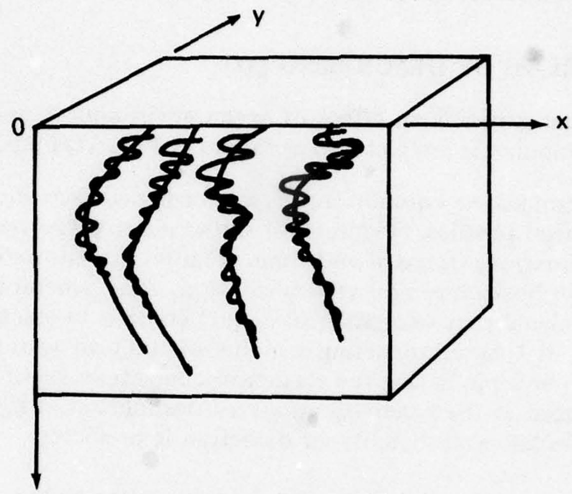

Figure 1(b)

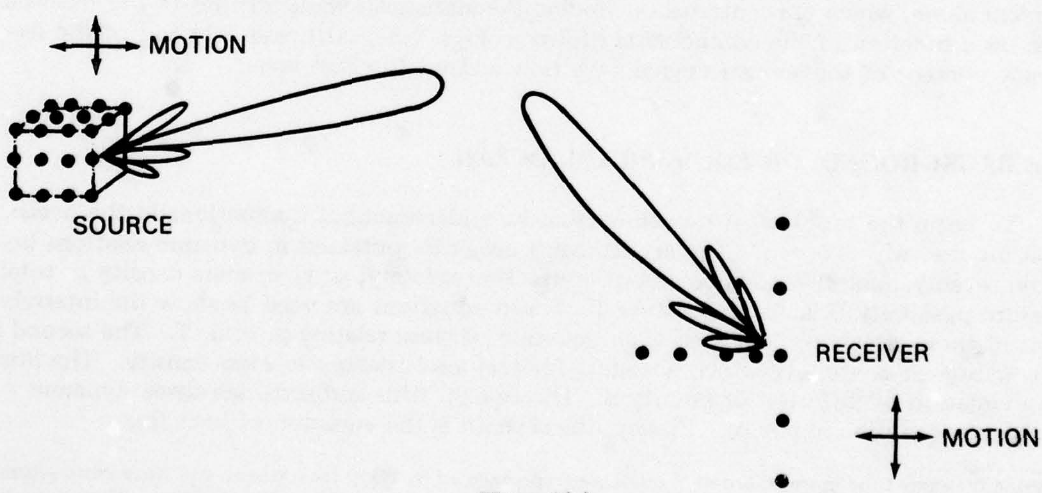

Figure 1(c)

Naturally we would prefer constructing models on the most realistic description. However, the ocean description in this case leads to very cumbersome, perhaps intractable, mathematics. But there are minimum statements. An irreducible minimum choice is that the ocean is channeled, inhomogeneous and anisotropic. Secondary but important statements are that the ocean surface is in random motion, and the ocean bottom is randomly rough. Other choices may be that the ocean is isohaline and adiabatic (meaning no diffusion of salinity, and no heat transfer). However, no matter what choices are made the crucial issue in describing the background ocean is not only fidelity to reality, but one other thing, namely the internal consistency among all assumptions. Clearly the choice of a background ocean which is an assemblage of desired properties not necessarily consistent, will lend an air of arbitrariness to all subsequent calculations of signal excess.

Of equal importance are the boundary conditions associated with the seven equations. These occur at (1) discontinuities of surface and bottom, (2) discontinuities in the volume of velocity, salinity, temperature, pressure of mass density. Such conditions determine in great measure the specific form solutions of the equations, as they apply to the ocean, and in particular the sound speed profiles.

OCEAN PERTURBATIONS DUE TO DRIFTING INHOMOGENITIES AND THEIR SPACE AND TIME SCALES

A second problem is the proper description of ocean perturbations. Since there are several causes, the question is, which perturbations? Let us consider here perturbations inside a volume V caused by inhomogenities, Fig. 2(a). Choose one variable of the seven of the background ocean, or choose some scalar quantity, say sound speed, which is a combination of them. Let $h(x, t)$ represent the choice of parameter. A measurement of h actually made at sea may show it to be a random variable, Fig. 2(b). We ask: from this record can we determine the *characteristic sizes or space scales* of h? One answer might be, try Fourier decomposition, viz, at time t_1,

$$h(\vec{x}, t_1) = \int \frac{d^3K}{(2\pi)^3} H(\vec{K}, t_1) e^{i\vec{K}\cdot\vec{x}}$$

$$\vec{H}(K, t_1) = \int d^3\vec{x}\, h(\vec{x}, t_1) e^{-i\vec{K}\cdot\vec{x}} .$$

Each sinusoidal component has a spectral weight $H(\vec{K}, t_1)\, d^3\vec{K}$. This could be a characteristic scale. More conveniently, the ocean volume V can be pictured as a sample member of a periodic train. Then $H(K, t_1)$ is a line spectrum, which could also be considered a scale. Other mathematical measures of characteristic size are in vogue. But it is more physical to use second-order, or energy-related, statistics. Thus to obtain spatial scales one forms the autocorrelation,

$$\Upsilon(\Delta\vec{x}, t_1) = \frac{1}{V} \int h(\vec{x}, t_1) h(\vec{x} + \Delta\vec{x}, t_1)\, d^3\vec{x} \qquad \text{(units: field}^2\text{)}$$

from which the correlation function (or coefficient) is defined to be

OCEAN PERTURBATIONS

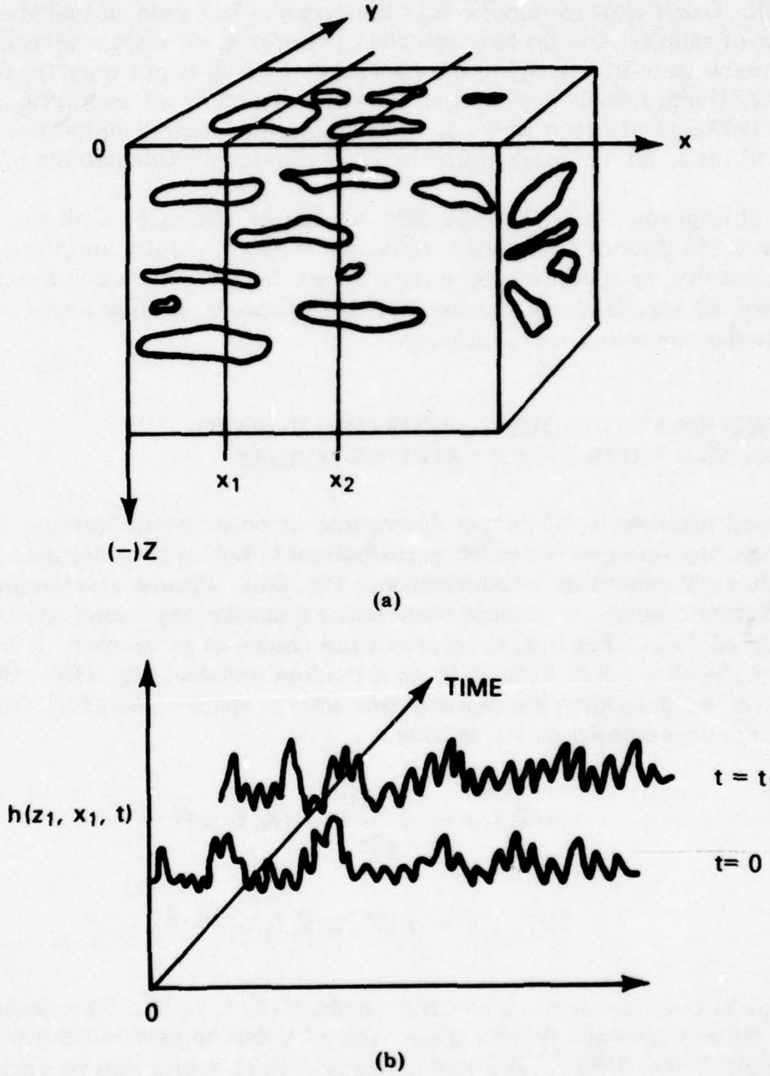

Fig. 2—Ocean perturbations

$$\rho(\Delta\vec{x}, t_1) = \frac{\Upsilon(\Delta\vec{x})}{\Upsilon(0)}.$$

Several characteristic sizes are based on the functional dependence of ρ: for example, the value of separation $\Delta\vec{x}$ where $\rho = e^{-1}$ is taken to be the correlation length of random process h; or the integral $J = \int \rho(\Delta\vec{x}, t_1)\, d^3\Delta\vec{x}$ (units: m^3) is taken to be the integral scale of h. Other measures of characteristic sizes are obtained by Fourier inversion of the autocorrelation, which is the "power spectrum" of the random spatial process h:

$$W(\vec{k}, t_1) = \int \Upsilon(\Delta\vec{x}, t_1) e^{-i\vec{K}\cdot\Delta\vec{x}}\, d^3\Delta\vec{x}. \qquad \text{(units: field}^2 \text{x m}^3\text{)}$$

The power spectrum in space-time is similarly obtained,

$$W(\vec{k}, \omega) = \int \Upsilon(\Delta\vec{x}, \tau) \exp(-i\vec{K}\cdot\Delta\vec{x} + i\omega\tau)\, d^3\Delta\vec{x}\, d\tau.$$

The spectral energy over a range of wave numbers from $\vec{K}_1$ to $\vec{K}_2$ is

$$\mathcal{E}(\vec{K}_1\vec{K}_2, t_1) = \int_{\vec{K}_1}^{\vec{K}_2} W(\vec{K}, t_1)\, d^3\vec{K}. \qquad \text{(units: field}^2\text{)}$$

The magnitude of this number tells how much energy is associated with the Fourier-derived wavelengths in the range $K_1^{-1}2\pi$ and $K_2^{-1}2\pi$. Significance of power spectra will be taken up after a discussion of the temporal power spectrum.

We consider time scales by fixing point X_1 and allowing time to vary. The entire discussion is repeated using period $\underset{\sim}{\mathfrak{T}}$ as analog of volume V, τ as analog of $\Delta\vec{x}$, and ω as analog of $\vec{K}$. One thus obtains the temporal power spectrum at X_1, $W(\vec{X}_1, \omega)$ (units: $\text{field}^2 \text{x S}$), the correlation $\Upsilon(\vec{x}_1, \tau)$, and the correlation length L_t.

Space and time separation can be taken together, and a space-time power spectrum $W(\vec{K}, \omega)$ of the perturbation process h constructed. Figure 3 shows a one-dimensional spectrum of this type. The significance of this plot can be understood if we take the perturbation parameter to be in the sound speed and the cause to be the vertical displacements $\zeta(z)$ of internal waves. An integration of the spectrum over frequency range ω_1 to ω_2 and spatial wavenumber range K_1, K_2 of internal waves then generates the random variable $\langle\zeta^2(z)\rangle$. Several models of the power spectra of displacement and of fluctuations in sound speed profiles are in current use, mostly constructed by Garrett and Munk. They are random functions of depth z and range R. From them one can construct the variation of mean values of displacement with depth and range which is the basic component in calculating the rms value of the random change in sound speed profile. These models predict coherence lengths L_V of $\delta c/c$ in the vertical, and L_H in the horizontal. Figure 4 is a pictorial statement of such type perturbations of ocean sound speed profile. It shows schematically a coherence length in depth which is much smaller than the coherence length in range. The complexity of this sketch invites efforts at simple modeling. Here we see the background modeled by a bilinear profile, and the perturbations of these profiles as functions of range. One can add additional perturbations as functions of time.

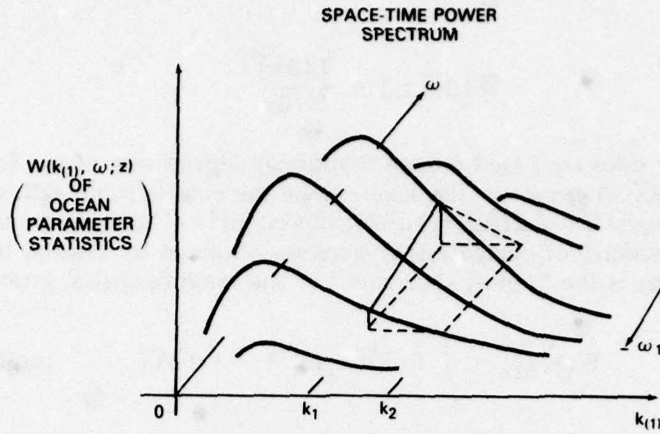

Fig. 3—Space-time power spectrum

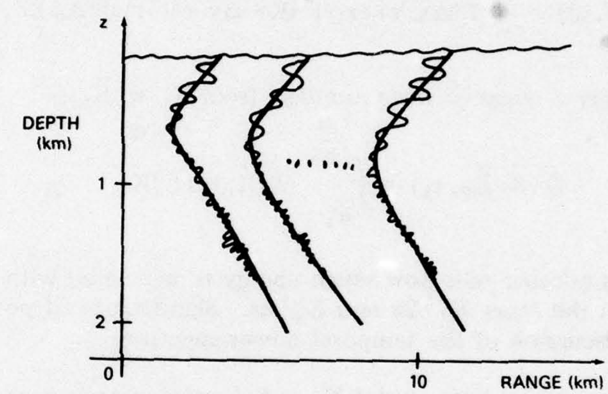

Figure 4

Another important ocean parameter perturbation is random surface waves. Here we see approximate amplitude spectra of these waves for which a useful model is that of Pierson-Moskowitz.

FLUCTUATIONS IN SOUND SPEED PROFILES CAUSED BY SOURCE-RECEIVER MOTION

On selected time scales an ocean of inhomogeneities may appear frozen. A sound wave generated by a fixed source arrives at a fixed receiver with a determinate phase. Suppose, however, the source-receiver combination are in relative motion. Then since the perturbation in sound speed is random in space, although frozen in time, the effect on the receiver sensor is the same as if it were fixed and the frozen ocean convected past it at the speed of the relative motion. The sensor is effectively scanning the random scalar field can be constructed. An additional effect is the change in the random path over which acoustic signals are propagated. This is discussed later.

ACOUSTIC PROPAGATION

When a source-receiver pair is inserted in the random ocean the propagation of the acoustic signal becomes randomized. Several decades of effort have been spent in investigating propagation, and many models are currently in use. Let us choose a ray-trace model for this review. Evidently, the effect of random inhomogenities depends on the selected ray, but a first question is, *which ray*? In addition, in a realistic ocean model a second question is how many rays must be considered to contribute to the field at a point? Consider a point source of sound fixed in the volume V, and radiating a CW signal. The resultant acoustic field is governed by the elliptical equation of Helmholtz in the scalar acoustic pressure,

$$[\nabla^2 + k^2(\vec{x}, t)]\, p(\vec{x}, t) = V(\vec{x}, t) p(\vec{x}, t)\,, \qquad k(\vec{x}) = \omega / c(\vec{x}, t)$$

in which $V(\vec{x}, t)$ is the perturbation in the propagation wave number $k(\vec{x})$, which in turn is the perturbation in the sound speed. Neglecting for a moment temporal effects caused by the changes of the environment we find the appropriate Green's function, or response at vector location $\vec{y}$ due to a unit delta function source at $\vec{x}$,

$$[\nabla^2 + k^2(\vec{x})]\, G(\vec{x}|\vec{y}) = \delta^3(\vec{x} - \vec{y})\,.$$

This is a deterministic statement of rays propagating in space. It shows that one or several of them reach y, depending on the nature of $k(\vec{x})$. Suppose $k(\vec{x}) = k =$ constant. Then only one ray from the point source reaches from $\vec{x}$ to $\vec{y}$ along the path of a straight line, Fig. 5(a). Since the medium is here assumed isotropic and homogeneous the Green's function is $G = e^{ik|\vec{x}-\vec{y}|}/4\pi|\vec{x} - \vec{y}|$. If, however, k depends on location vector then several rays originating a source vector $\vec{x}$ may reach location vector $\vec{y}$, Fig. 5(b). In this case the field at y is the sum of n rays,

$$G(\vec{y}|\vec{x}) = \sum_{i}^{n} G_i(\vec{y}|\vec{x})\,.$$

We recognize this to be a statement of a sound channel. The deterministic rays 1, 2, 3, etc., can be calculated to sufficient approximation by geometric optics. If the source is at the origin, this means each ray has the form,

$$G_i(\vec{y}|\vec{0}) = K(\vec{y}|\vec{0}) \exp \left\{ i \int_{\vec{0}}^{\vec{y}} ds\, k[\vec{x}(s)] \right\}\,.$$

Consider next that the perturbation $V(\vec{x}, t)$ of the medium is random so that each ray executes a sort of random walk filling a tube, Fig. 5(c). The acoustic field pressure at $\vec{y}$ is now a sum of contributions of those rays along zig-zag tracks within tubes which connect $\vec{x}$ to $\vec{y}$.

$$p(y) = \sum_{i} p_i(\vec{y})\,.$$

An enlarged view of a ray-tube is shown in Fig. 5(d). Along cross-section a - a each ray is identified by two symbols, q, y, that is, $p_i(q;y)$. When q = y, $p_i(y;y)$ means the unperturbed ray. Outside the tube $p_i(q,y)$ vanishes.

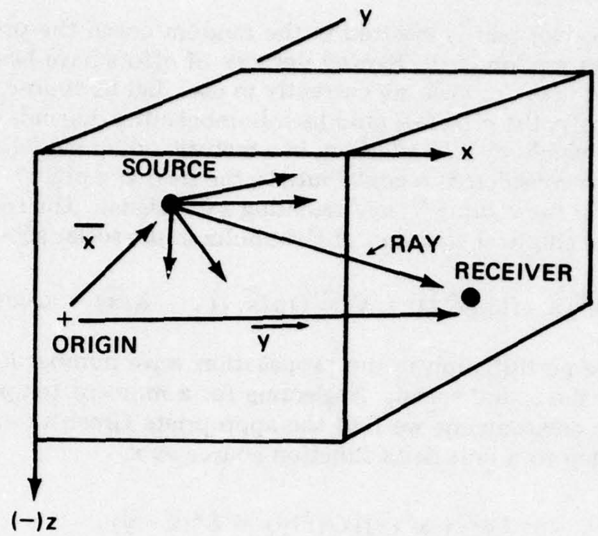

(a)

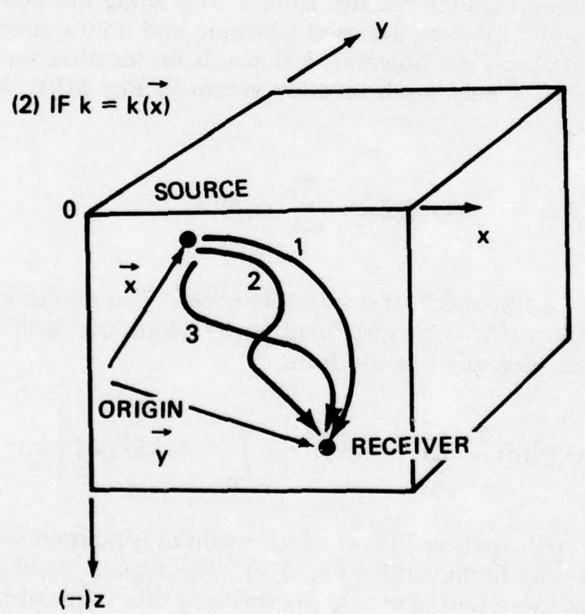

(b)

Fig. 5—Acoustic propagation

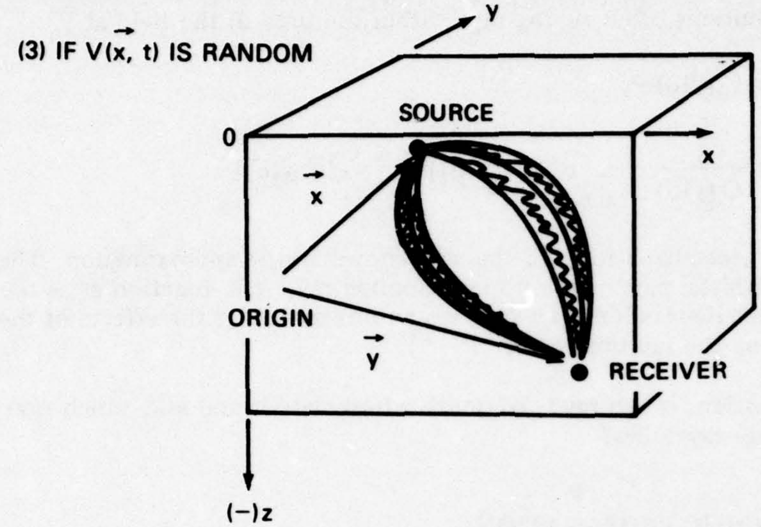

(c)

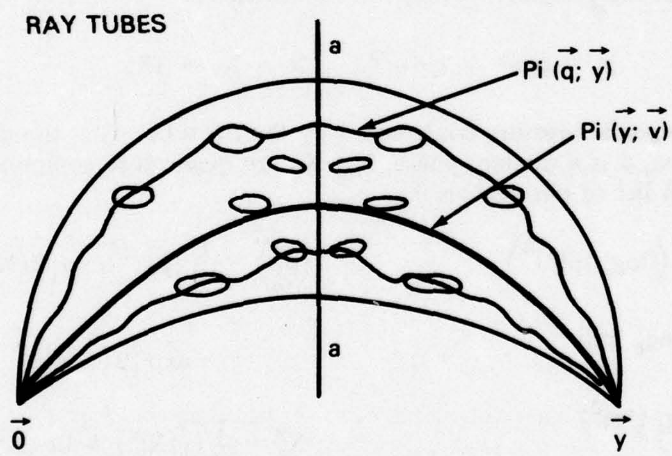

(d)

Fig. 5—Acoustic propagation (continued)

A Green's function associated with each ray inside the tube is written $G_i(\vec{q};\vec{y}|\vec{o})$, in which the source of the rays is at the origin. The field at $\vec{q}$ couples with the perturbation of sound speed $V(\vec{q})$, and the scattered field is propagated from $\vec{q}$ to $\vec{y}$ by $G(\vec{y}|\vec{q})$. Thus, each ray tube contributes the geometric optics ray multiplied by a complex phase factor which sums up the contributions of all zig-zag rays within the tube to the field at $\vec{y}$,

$$p_i(\vec{y}) = G_i(\vec{y}|\vec{o})e^{X}$$

$$X = \frac{1}{G_i(\vec{y}|\vec{o})} \int_{i \text{ tube ray}} d^3\vec{q}\, G(\vec{y}|\vec{q})\,[V(\vec{q})G_i(\vec{q},\vec{y}|\vec{o})]\,.$$

This important result is a generalized form of the well-known Rytov approximation. The field $G_i(\vec{y}|\vec{o})$ is the deterministic part of the *i*th contributing ray. The function e^X is the random part. One sees that the random part requires an integration of the effects of the random phase changes along the ray-tube paths.

Returning to our question, which ray? We must reformulate it and ask, which ray-tube? Secondly, how many ray tubes?

OBSERVABLES IN ACOUSTIC PROPAGATION

Let us accept the generalized Rytov form for the ray-tube. For each ray-tube we ask the question, what observables in the field measurement are useful in categorizing the nature of the field at the receiver? Write, for convenience,

$$p_i = p_0 e^X = |p|\, e^{i\phi}, \qquad X = X_1 + iX_2$$

in which p_i is the acoustic pressure contributed by the *i*th tube, p_0 is the deterministic ray-tube contribution, ϕ is a random phase, X_1, X_2 are quadrature components of the integral factor X. A list of observables is:

$$\langle I^2 \rangle = \left\langle \left(\log_e |p|^2\right)^2 \right\rangle$$

$$\langle I \rangle = \log_e |p_0^2|$$

$$\bar{I} = \log_e \langle |p|^2 \rangle$$

$$\ell n \left(\langle p \rangle\right)^2$$

$$\langle \phi^2 \rangle = \langle X_2^2 \rangle, \quad \langle \phi I \rangle = 2\langle X_1 X_2 \rangle$$

$$\phi, \quad |p|$$

$$\left\langle p_{\frac{1}{2}}^2 \right\rangle = \frac{1}{4}|p_0|^2 \left[\exp\left(2\langle X^2 \rangle\right) + \exp\left(2\langle X^{*2} \rangle\right)\right]$$

$$X_{\frac{1}{2}}^2 = \frac{1}{2}\left(\langle |X|^2 \rangle \pm \mathrm{Re}\langle X^2 \rangle\right)$$

$$X_1 X_2 = \frac{1}{2}\,\mathrm{Im}\,\langle X^2 \rangle\,.$$

Of particular interest in modeling are $\langle X \rangle$, and $\langle e^x \rangle$. Some modelers assume the δc fluctuations to be Gaussian distributed in space and time. This they take $\langle X \rangle = 0$ and $\langle e^x \rangle$ to be $e^{[(1/2)\langle x^2 \rangle]}$. Attention is then focused on finding a model for $\langle X(\vec{y})^2 \rangle$. In addition, focus is made on p^2 as defined above, hence $\langle |X|^2 \rangle$. Other modelers create an entire theory on the observable,

$$\langle I^2 \rangle - \langle I \rangle^2 = 2\left(\langle |X|^2 \rangle + \mathrm{Re}\langle X^2 \rangle\right).$$

This entity takes a prominent part in the determining regimes of fluctuations, now to be discussed.

DIFFRACTION PARAMETER Λ, STRENGTH PARAMETER Φ^2 FOR STRAIGHT-LINE RAYS

We noted earlier that the deviation $\delta c/c$ of sound speed is a random function of space and time, and that by use of autocorrelations or power spectra we can define three correlation lengths: vertical L_V, horizontal L_H, transverse L_y; and one correlation time L_τ. These specify the spatial and temporal characteristic sizes of $\delta c/c$.

A CW sound wave of wavelength λ passing through a field of $\delta c/c$ is diffracted by the inhomogenities. A question arises: how important is diffraction? One can try to decide by calculating a diffraction parameter which is the square of the ratio of the radius of the first Fresnel zone R_F of a point source at range R to a selected coherence length, L, Fig. 6. In a homogeneous ocean, where propagation is along straight lines, the ratio Λ is a function of range. The average Λ is,

$$\Lambda_{AV} = \frac{1}{R}\int_0^R \left(\frac{R_F(x)}{L}\right)^2 \frac{dx}{2\pi} = \frac{R}{6L^2 k}.$$

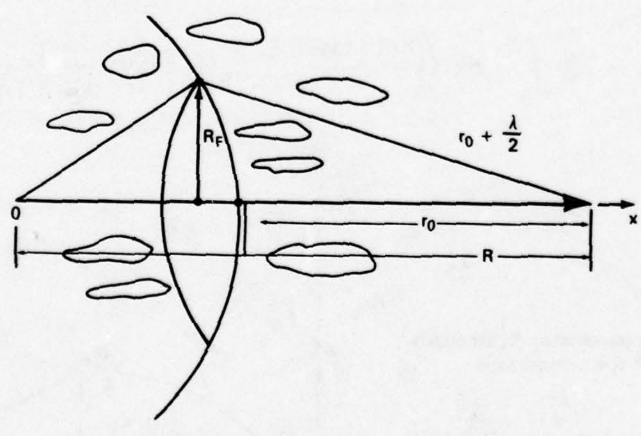

Fig. 6—Diffraction parameter Λ, strength parameter Φ^2 for straight-line rays

Similarly, an acoustic wave passing through a field of $\delta c/c$ experiences a random change of phase. Again the question arises, how strong is the phase change? A convenient measure is the ensemble average Φ^2 of the square of the integrated phase along a ray, Φ^2 is called the strength parameter. In a homogeneous medium.

$$\Phi^2 \equiv \left\langle \left\{ k \int_0^R \frac{\delta c(x)}{c} \, dx \right\}^2 \right\rangle = k^2 \int_0^R \int_0^R dx\, dx' \rho(|x - x'|)$$

$$\approx k^2 \left\langle \left(\frac{\delta c}{c}\right)^2 \right\rangle LR \, .$$

The product $\Phi^2\Lambda$ is a measure of the combined effects of diffraction and random phase change.

In a realistic description of the ocean acoustic rays travel in curved paths. The correlation vector length L has a component L_p along the ray path. We wish to calculate Φ^2 and Λ. A typical case is shown in Fig. 7. Ray 1 is deterministic from the origin to $\vec{y}$. Ray 2 reaches a point 3, distance a from Ray 1, and instead of continuing to point C is deflected at angle θ to pass on to y along path 4. The difference ΔS in path length between paths 2, 4 and path 1 is a geometric construct. In 3-space

$$[\Delta S] = [A] \frac{a^2}{2}$$

in which [A] is a matrix. In one dimension $A(x) = d\theta/da$.

Using these definitions one finds that in the case of a deterministic sound channel, an integration along the ray path is needed to find Φ^2, and Λ:

$$\Phi^2 = k_0^2 \int_0^R dx \left\langle \left(\frac{\delta c(z \text{ ray})}{c}\right)^2 \right\rangle L_p(\theta, z \text{ ray})$$

$$\Phi^2\Lambda = k_0^2 \int_0^R dx \left\langle \left(\frac{\delta c(z \text{ ray})}{c}\right)^2 \right\rangle L_p(\theta, z \text{ ray}) \frac{1}{k_0 |A| L_V^2} \, .$$

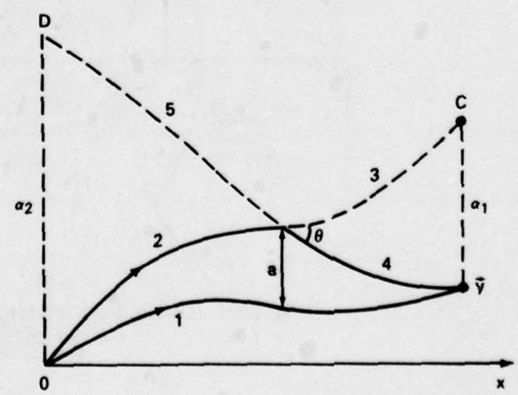

Fig. 7—Diffraction parameter Λ, strength parameter Φ^2 for curved rays

This says that at each increment in range, the segment at depth z-ray experiences a contribution to Φ given by the integrand shown. The important point to notice is that $\Phi^2\Lambda$ is just the quantity $\langle I^2 \rangle - \langle I \rangle^2$. It's significance will appear later. Generally, however, the integration must be done by numerical means. The parameters $\Phi^2\Lambda$ are crucial in establishing regimes of signal statistics.

SIGNAL STATISTICS

In the presence of a determinate channeled ocean the received signal is

$$p(\vec{x}, \omega, t) = p_0(\vec{x}, \omega)e^{-i\omega t}.$$

When fluctuations are included the signal is

$$p(\vec{x}, \omega, t) = p(\vec{x}, \omega, t)e^{-i\omega t}.$$

It is convenient to define a reduced wave function,

$$\psi(x, \omega, t) = \frac{p(x, \omega, t)}{p_0(\vec{x}, \omega)}.$$

As before, several *real* functions of ψ are observables. To list them one writes,

$$\psi = |p|e^{i\phi} \qquad \ln \psi = \ln |p| + i\phi$$

$$I = |\psi|^2 = |p|^2 = e^{\ln I}.$$

The list is

(1) I (3) $\ln |p|$ (5) $\mathrm{Re}\,\psi$

(2) $\ln I$ (4) ϕ (6) $\mathrm{Im}\,\psi$.

Let us picture ψ as a m-multi-dimensional plot of space, time and frequency, Fig. 8(a). In general there are 3 space coordinates; 1 frequency coordinate; 1 time coordinate; and perhaps 1 range coordinate. At point 1, $\psi = \psi(z_1, t_1, \omega_1)$, and at point 2, $\psi(z_2, t_2, \omega_2)$ A similar chart for the three variables, angle of arrival, doppler shift, and pulse time, (which are Fourier conjugates of Fig. 8(a)) is shown in Fig. 8(b). The important idea is that ψ is a random variable, so that a complete description of the m-dimensional field requires all n-point correlations. n = 1, 2, ..., ∞. It is customary to use one-point and two-point correlations of signal statistics. A list follows:

One-Point Statistics

These are statistics constructed on measurements at a single point, say X_1, along the time axis in the m-multi-dimensional plot. For example, measurements of $\psi = \psi(x_1, t, \omega_1)$ are used to construct the random intensity I, $\ln$ I, $\ln |p|$, ϕ, etc., as time progresses. An important application of one-point functions in detection is that of Urick, which is now discussed.

Urick's Phenomenological Model Based on Intensity Statistics at One Spatial Point

Fluctuations of received signal are caused by multipath propagation of an initially CW signal in an inhomogeneous moving medium. No matter what the cause the direct path component decreases with range, and the scattered or diffracted components increase with range.

A useful theoretical model is the probability distribution of the envelope of a sine wave plus narrow band Gaussian random noise, or the probability distribution of a constant vector, summed with a random vector whose x; y components are Gaussian distributed time-functions (Fig. 8(c)). Here

$$X(t) = P \cos \Psi + x(t)$$

$$Y(t) = P \sin \Psi + y(t) .$$

The solution of this problem is well-known to be the Rician distribution, Fig. 8(d). Here P is the magnitude of the constant victor, and T is the fractional relative power of the random component,

$$T = \frac{\text{RAYLEIGH POWER}}{\text{TOTAL POWER}}$$

in which Rayleigh power corresponds to zero constant vector, and V is the vector sum,

$$V = \sqrt{X(t)^2 + Y^2(t)} .$$

Cumulative distributions, obtained by integration over a specific Rician distribution curve from $-\infty$ to V, expressed in units of $V^2/\overline{V}^2$, where $\overline{V}$ is the mean value of $\overline{V}$ over the distribution, is shown in Fig. 8(e). A similar presentation with logarithmic horizontal scale is shown in Fig. 8(f). A great number of measurements made at sea have been assembled and compared with these theoretical predictions. One can gauge from this the popularity of intensity statistics at one spatial point.

Two-Point Functions

Measurements are made at 2 points in m-space. They are separated in space (Δz, Δy), in time $\Delta t = t_2 - t_1$, or in frequency $\Delta\omega$. One measures, for example,

$$\psi(z_1, t_1, \omega) , \quad \psi(z_1 + \Delta z_1, t + \Delta t, \omega_1 + \Delta\omega) .$$

Cross-correlation, or covariance, of ψ is written as an average over space, time and frequency

$$\left\langle \psi_1(z_1, t_1, \omega_1)\psi_2^*(z_1 + \Delta z_1, t_1 + \Delta t_1, \omega_1 + \Delta\omega_1)\right\rangle .$$

As noted earlier, for each separation variable Δz, Δt, $\Delta\omega$, etc., a plot of $\langle \psi_1, \psi_2^* \rangle$ vs separation can be used to define a coherence scale. Similarly, by Fourier transformation one finds the cross-power-spectrum for the conjugate variable, and from it obtains a characteristic scale of this conjugate. A table of conjugate variables is:

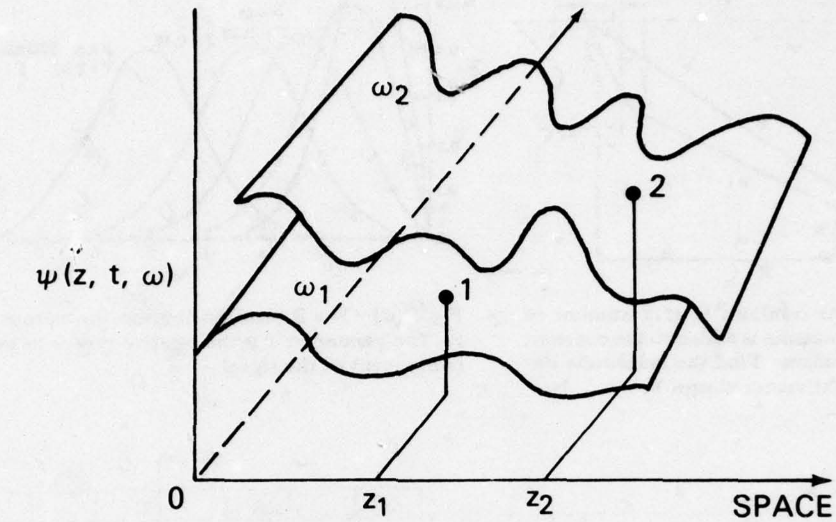

Figure 8(a)

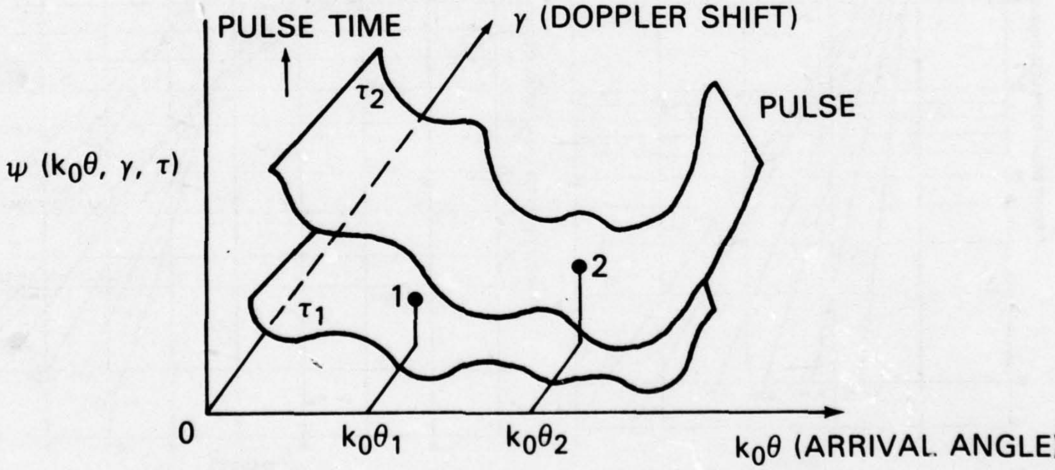

Figure 8(b)

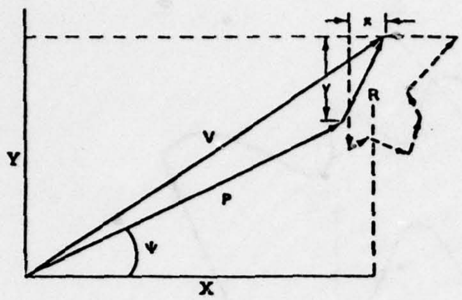

Fig. 8(c)—The resultant R of a number of random components is added to the constant vector P. Problem: Find the amplitude distribution of the vectorial sum V.

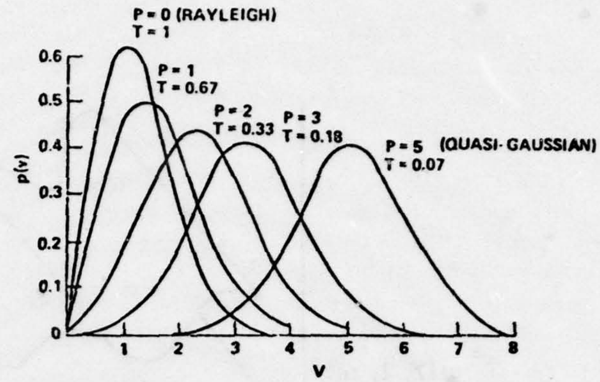

Fig. 8(d)—The Rician distribution for various values of P. The parameter T is the relative power in the random component of the signal

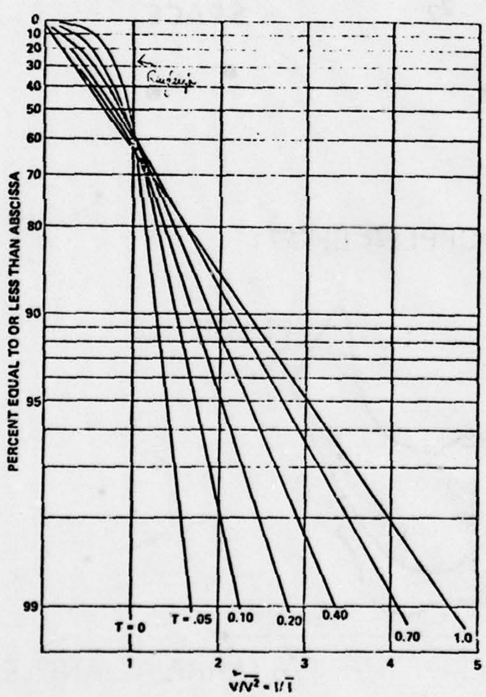

Fig. 8(e)—Rician curves with T as parameter on semi-log coordinates

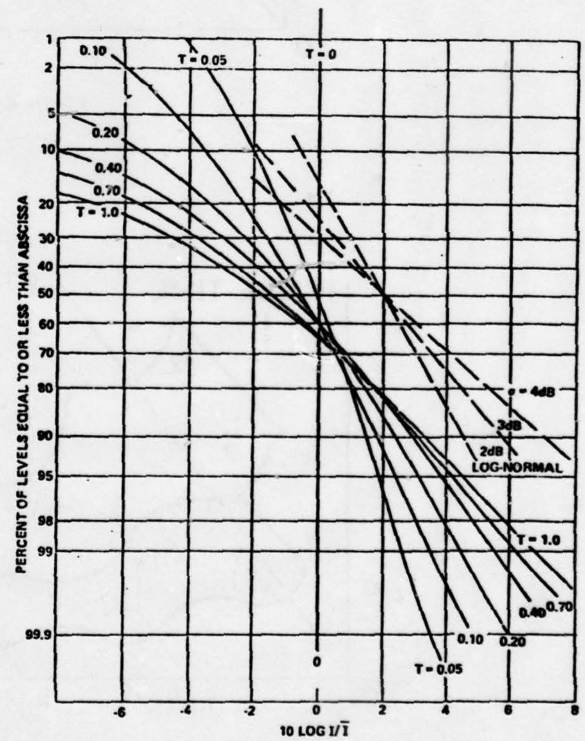

Fig. 8(f)—Ricain curves with T as parameter on probability coordinates and a logarithmic horizontal scale

Separation Scale		Separation Variable	Conjugate Variable		Conjugate Scale
L_V	$\leftarrow$	Δz	$k_0\theta_V$	$\rightarrow$	θ_V
L_H	$\leftarrow$	Δy	$k_0\theta_H$	$\rightarrow$	θ_H
L_t	$\leftarrow$	Δt	γ	$\rightarrow$	doppler shift
$L_{\Delta\omega}$	$\leftarrow$	$\Delta\omega$	τ	$\rightarrow$	pulse time

Thus the conjugate of separation in depth is vertical angle of arrival, etc. Conjugates are very useful in applied work.

Three-Point Functions

A cross-power spectrum constructed on 2-points may be a function of time. For example, take the time separation correlation $\langle \psi_1(t_1)\psi_2^*(t_1 + \Delta t)\rangle$ and its cross-power spectrum of doppler shift $W(\gamma)$. Measured over a given duration, T. Break T into several smaller durations, or integration times, and construct $W(\gamma)$ for each of these. Plots of $W_1(\gamma)$, $W_2(\gamma)$, etc., show different *spread* of W among them, and show the central doppler shift wandering, Fig. 9. A description of *spread* and *wander* can be obtained by use of three-point functions.

Signal statistics contained in 1-, 2- and 3-point functions form the basis for calculating the coherence scales or their conjugates as they vary along ray paths. Thus path lengths of disturbed rays become functions of Λ, Φ.

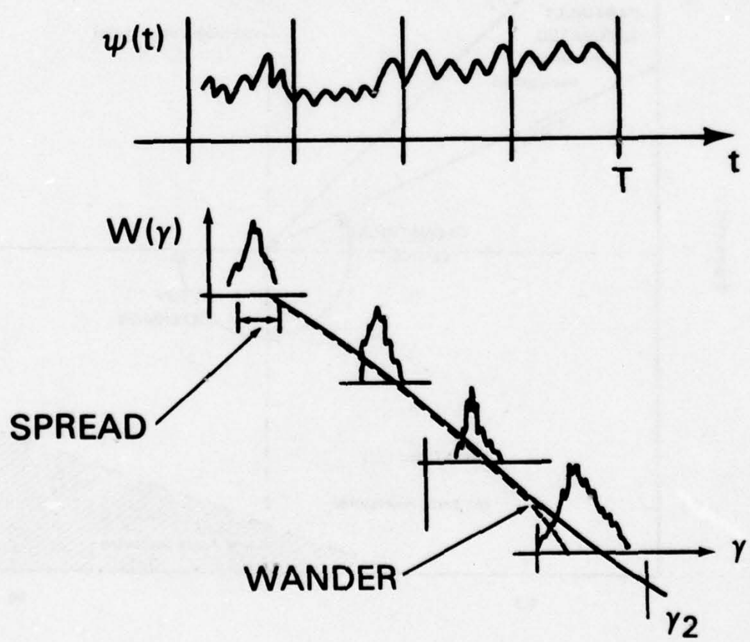

Figure 9

Earlier it was stated that when the medium was fluctuating the sound propagates in ray tubes rather than rays. Each tube contains a number of separate rays which start at the source and end at the receiver. They are *micro multipaths*. Ray tubes themselves that meet at a receiver are multipaths proper. The question arises: what is the spread of the micromultipaths compared to correlation lengths? Figure 10 shows comparisons.

Take the case of vertical separation, Δz, and calculate its 2-point correlations, its cross-power spectrum and thus, its vertical correlation length, L_V. Also calculate the strength parameter Φ and the diffraction parameter Λ. It is found that when $\Lambda\Phi \geq 1$ the micromultipaths are spread over a region larger than L_V and are thus uncorrelated. The regime is called fully saturated. When $\Lambda\Phi^2 > 1$ the micromultipaths are spread over a region smaller than L_V and are correlated. The regime is called partially saturated. When $\Phi < 1$ there are no extra micropaths. The regime is called unsaturated. In this regime calculation of ray statistics can be accomplished by small modifications of geometric optics.

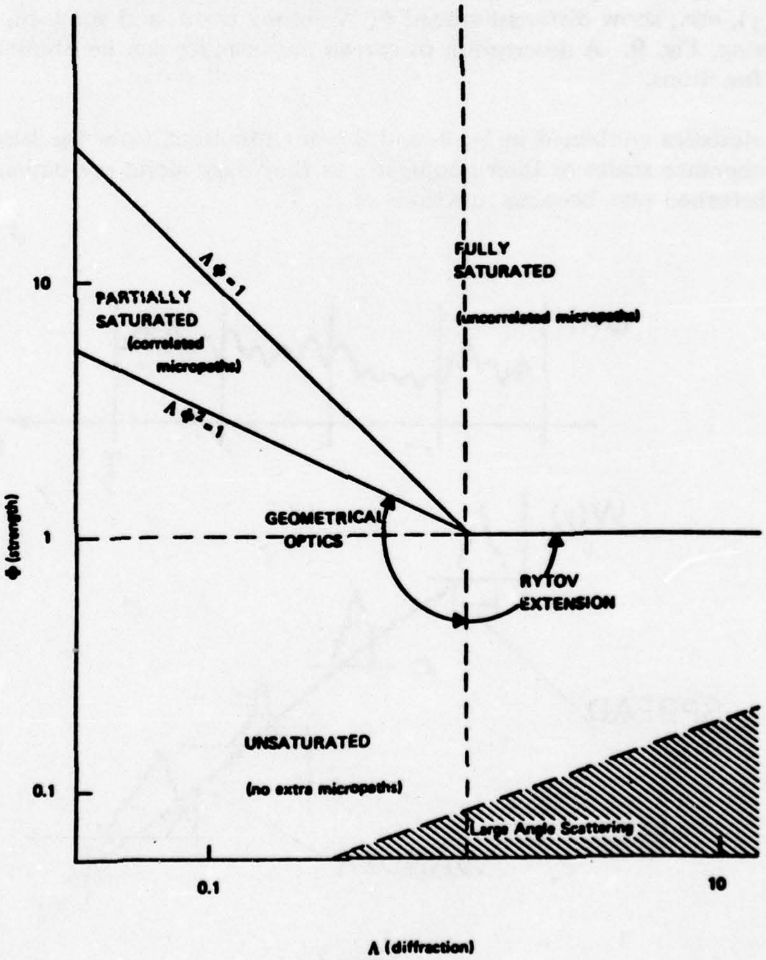

Fig. 10—Regions in $\Lambda - \Phi$ space

This diagram can be useful in finding the regime in which a particular sound-transmission experiment is operating. Choose a specific unperturbed ray, then calculate Φ, Λ by integrating amplitude and phase accumulation along the ray path caused by random fluctuations in the medium. Then convert the information into a frequency range plot of the type shown in Fig. 11.

The usefulness of Λ - Φ space is illustrated for three cases: (1) time separation, Fig. 12, in which the tip of the signal phase shows a temporal history of different type depending on Λ, Φ for a chosen ray; (2) space separation, Fig. 13, in which the ocean is frozen, and 2-point statistics are determined for each separation, and the signal phase executes a dance as the spatial separation is increased; (3) pulse time wherein a delta pulse emitted at the source arrives at the receiver with a different spread in time, depending on Λ, Φ, Fig. 14.

Actually the JASON theory presented here has strong analogs in the theory of FM modulation. Standard references, say Taub and Schilling "Principles of Communications Systems" describe phasor diagrams of wide band and narrow band FM signals (Fig. 15(b). Here two sidebands consituting a modulation of a carrier form a resultant R. The properties of this modulation, as discussed in this text, parallel concepts shown in Figs. 11, 12, and 13.

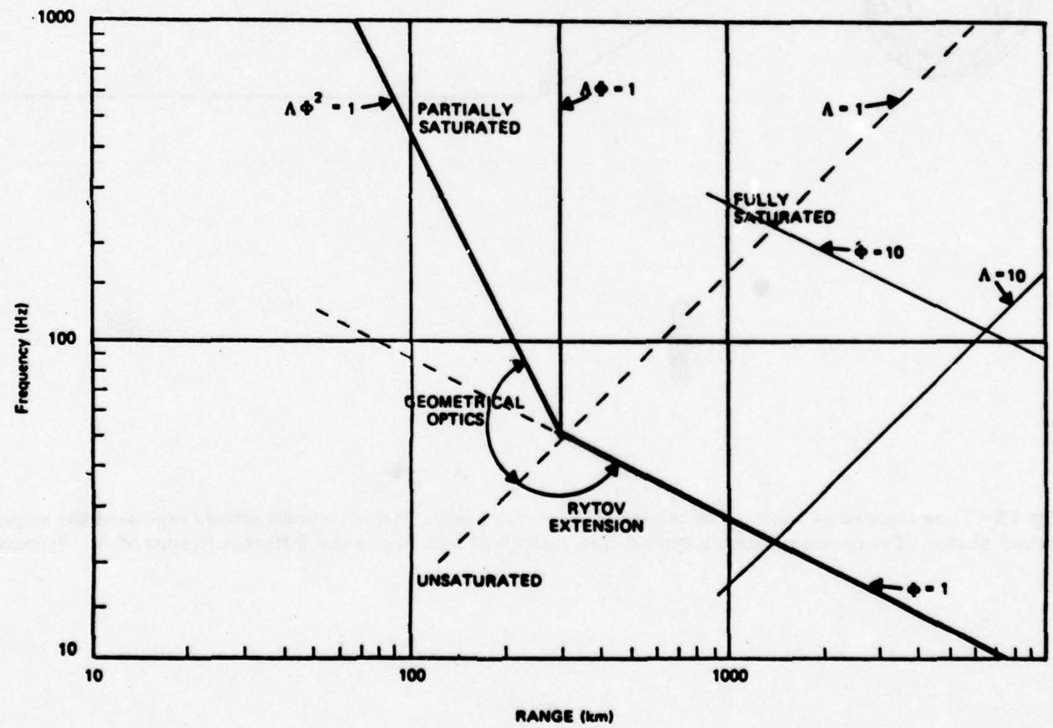

Figure 11

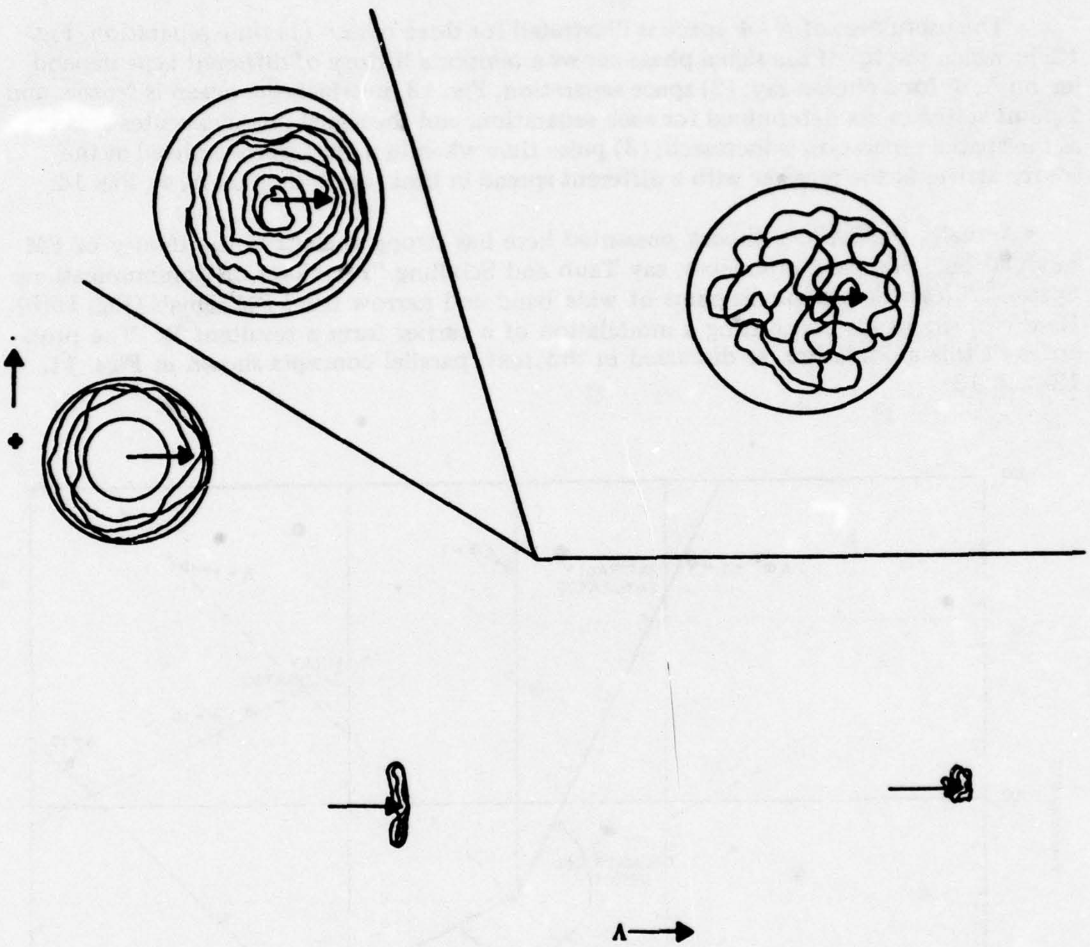

Fig. 12—Time-separation behavior of the wave-function phasor. The horizontal arrows represent the unperturbed phasor. The curves indicate a typical time history of a phasor in the different regions of $\Lambda - \Phi$ space.

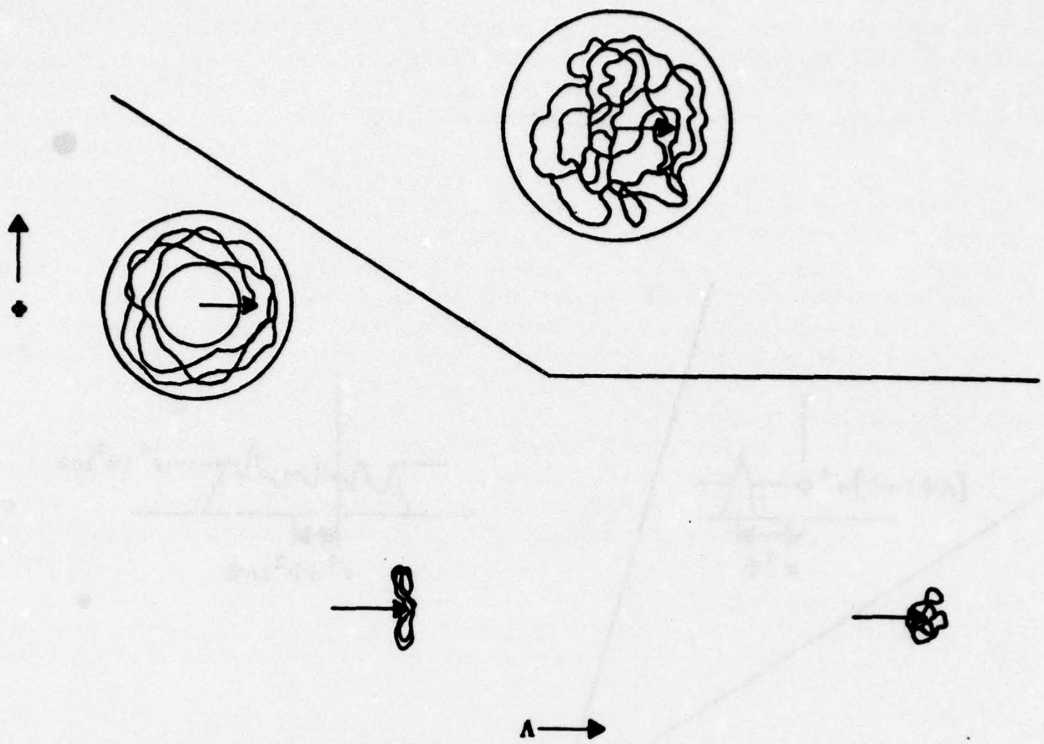

Fig. 13—Space-separation behavior of the wave-function phasor. The curves indicate a typical behavior of the phasor, where the parameter along the curve is spatial separation.

ANTENNAS AND FLUCTUATIONS

Inhomogeneous medium impose limits on the achievable directive gain. Consider the case of a wave front which is initially plane, then transverses an inhomogeneous medium resulting in random distortions of phase and amplitude. An antenna length L receives the random phase signal. The mean directive gain is written.

$$\bar{G} = \frac{G_0}{4} \iint_{-1}^{+1} \left\langle e^{j[\phi(x)-\phi(x_1)]} \right\rangle dx\, dx_1$$

in which G_0 is the determinate gain in the absence of fluctuations, $x = 2z/L$, and ϕ is a random phase, mean zero, variance α and correlation distance ρ. The question is posed, is there a practical limit to the mean directive gain as the length L increases? The answer depends on α, ρ, L. There is a wide literature on the subject, contributed by radar and underwater surveillance research. NRL has worked on this problem over several years. A specific answer of radar, tailored to atmospheric inhomogeneities is shown in Fig. 16. Other characteristics of statistical antenna are mean beam width, mean side-lobe levels, mean directivity, etc.; variance and correlations in directive gain; beam width direction of the principal maximum, etc. All these similarly depend on α, ρ, L.

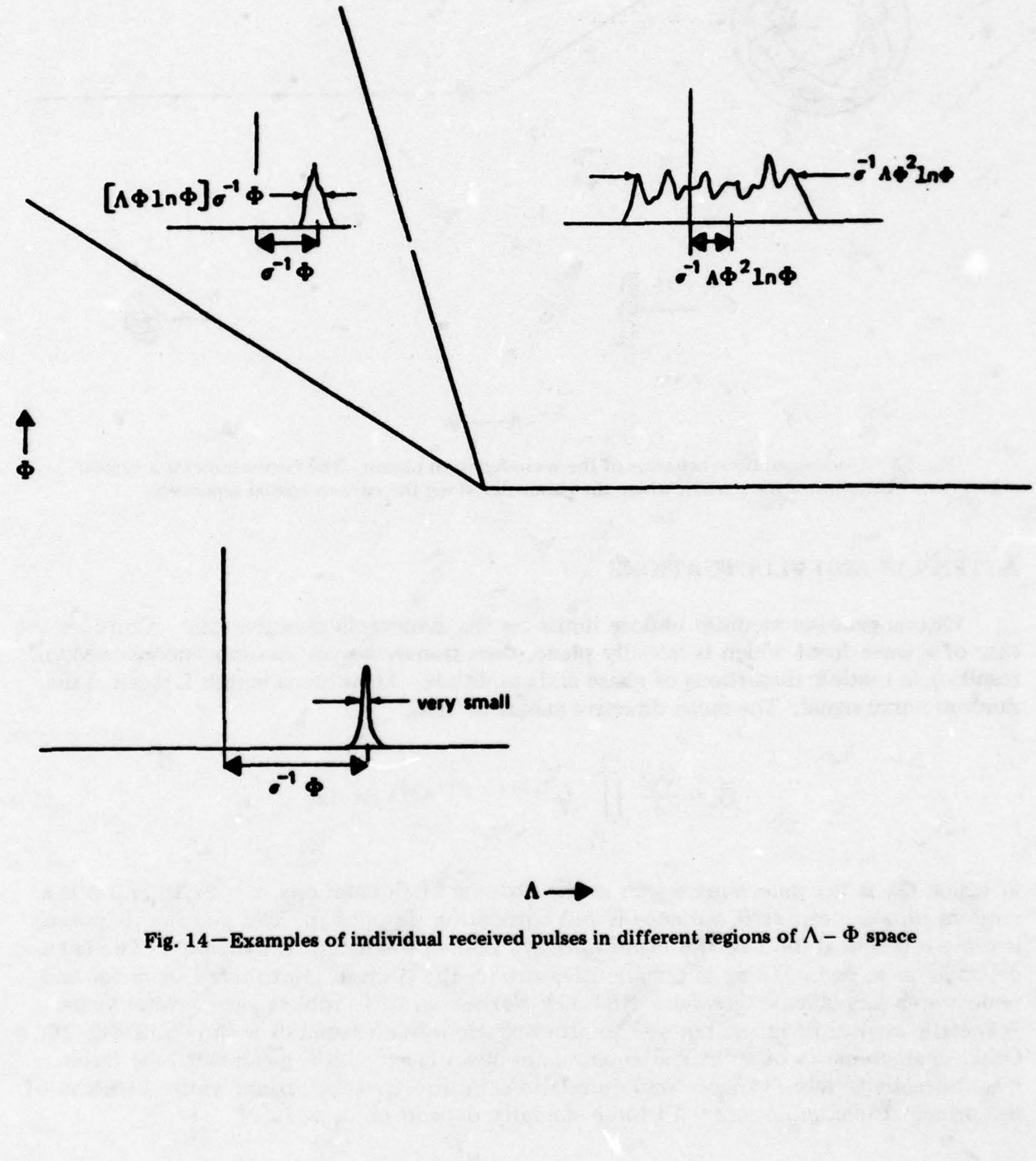

Fig. 14—Examples of individual received pulses in different regions of $\Lambda - \Phi$ space

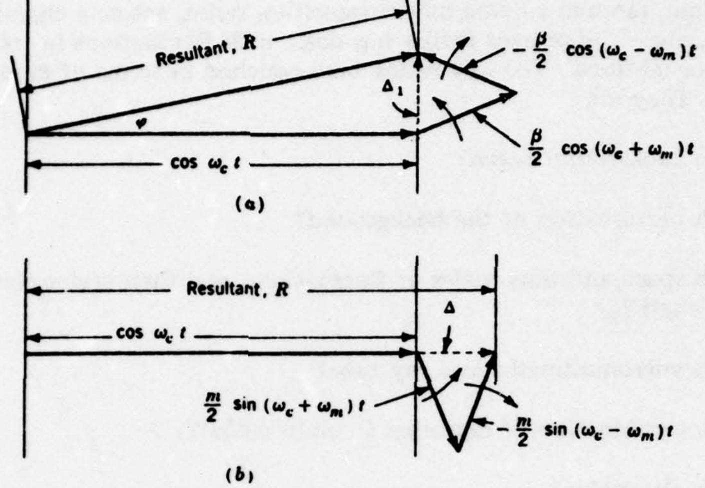

Fig. 15—(a) Phasor diagram for a narrowband FM signal.
(b) Phasor diagram for an AM signal.

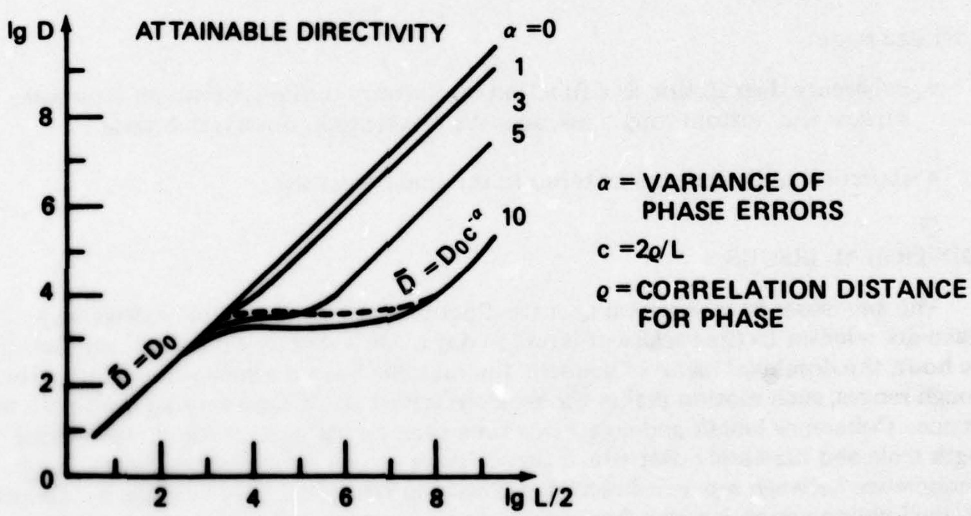

Fig. 16—Mean directive gain as a function of antenna length at 3 cm wavelength for ρ = 50 m (full curves) and ρ = 100 meters (broken curve). (Ref. Y.S. Shifrim "Statistical Antenna Theory").

CONCLUSION

Performance criteria of underwater surveillance systems in current use are cumulative probability of detection and mean time to hold contact. Both are calculated from a knowledge of signal excess. In a fluctuating medium where source-receiver may be in motion, signal excess is a random variable caused by perturbations in ray paths due to surface, bottom, random volume inhomogeneities, noise, antenna characteristics, operator performance, etc. The present review has dealt with fluctuations in transmission loss and source-receiver motions. The key issues were couched in terms of modeling the fluctuation effects. They are:

- which background ocean?
- which perturbation of the background?
- which space and time scales of fluctuations, and their scales compared to acoustic wavelength?
- which micromultipaths in a ray tube?
- which combination of ray-tubes (= multi paths)?
- which observable?
- which signal processing of which observable?
- which signal statistical regimes of the $\Lambda - \Phi$ chart?

Other issues are:

- coherence degradation as a function of platform motion, multipath structure, surface and bottom roughness, acoustic wavelength, observation time.
- statistical independence of terms in the sonar equation.

ADDITIONAL ISSUES

The key issues in research on acoustic fluctuations caused volume scattering just discussed are relevant to time scales of hours to days. On a shorter time scale, say less than one hour, the dominant cause of acoustic fluctuations is source/receiver motion. Over long enough ranges, such motion makes the received signals show time-varying multipath interference. Coherence length and coherence time become parameters for characterizing the length scale and time scale over which these signals can be effectively averaged. Degradation of coherence between separated receiving sensors as range and time increase is a frequently observed phenomenon for high frequencies, but more rarely observed for very low frequencies in deep ocean paths. Thus, a key issue in acoustic fluctuation research is coherence degradation as a function of platform velocity, multipath structure, surface and bottom roughness, acoustic wavelength, and duration of observation.

The results of research on acoustic fluctuations in the ocean have accumulated in the last decade in various scientific journals, government laboratory reports and personal notes. Only a portion of these has reached potential users in systems applications. The unused portion is large and clearly needs to be applied to practical problems in submarine detection. However, even if *all* of it were used there would still be unresolved issues requiring further research. In this connection, a key problem remaining is the statistical interdependence of terms in the sonar equation for signal excess. For example, the mutual coupling of ambient noise and directivity is recognized to be significant. Further analysis and measurement are needed to fix magnitudes of this coupling, and other coupling of terms in the power equation, and to evaluate their importance in detection algorithms.

THE APSURV DETECTION MODEL

R. Larsen

(See Volume 2)

PSEUDO-SURVEILLANCE SYSTEM PERFORMANCE SIMULATOR

L. Fretwell

(See Volume 2)

FLUCTUATIONS FOR THE APAIR, APSURF, APSUB MODELS

R. Flum

(See Volume 2)

REVIEW OF BEAM-NOISE FLUCTUATION MODELS

R. C. Cavanagh
Science Applications, Inc.
McLean, Virginia 22101

SUMMARY

For system performance estimation and the interpretation of measured data, there is a need to predict and simulate the statistical properties of the response of a horizontally-directive acoustic array to ambient noise. In current use in the Navy there are a number of such "beam-noise" models which predict the properties of noise caused by the dominant, prevailing source at low frequencies: surface shipping. A study was performed, with objective: to review these models in some detail and then to recommend, for specific applications, approaches which utilize the best features of each model.

Nine Navy-sponsored models were thus investigated, and all were found to be based on the fundamental hypothesis that the beam noise is the convolution of the array beam pattern with the sum of intensities from the individual ship sources. The models are then distinguishable by their treatments of the ship sources, the transmission loss (TL), and the array's response. Two categories were natural: *Analytical* models which calculate the statistical properties of noise directly from those of the components (source level, TL, etc.); and *Brute-Force* models which use simulation or Monte Carlo techniques. The ability to calculate statistics over all possible values of a parameter (e.g., ship locations for a given density, all possible source levels), or over values which might occur in a short time period (say 24 hours) led to a second type of classification: "grand" and "short-term" ensembles.

The nine models have been reviewed and are described in a final report* in terms of approach, treatment of ships and TL, receiver submodel, implementation, advantages, and shortcomings. Tables are given to summarize these findings.

For various applications of beam-noise models, the statistical quantities and types of ensembling required have been proposed (e.g., first-order statistics with full ensembles, or multi-array statistics), and the most promising models and techniques are identified for each. General recommendations for an advanced-development approach are given.

The work was supported by the Long Range Acoustic Propagation Project (NORDA Code 600).

*Review of Models of Beam-Noise Statistics," Final Report to LRAPP, SAI-78-696-WA; Ocean Science Division, Science Applications, Inc., McLean, VA; November 1977.

EXPLANATORY NOTES AND THE FIGURES

1. Nine beam-noise fluctuation models were reviewed, Fig. 1.

2. In general, the models concentrate on certain fluctuation mechanisms, as shown, Fig. 2. No model explicitly treats all of these, but the list gives the ones most often treated in rough order. Although wind-related noise can be very important, all of the models concentrate on the surface-ship component. Take note of the time scales.

3. Before discussing how the models predict, consider what they predict, Fig. 3. For each application, as shown, specific beam-noise statistics are required. In defining such statistics, care must be taken to specify a time scale. There can be a substantial difference between temporal statistics assembled over a day and over a week or season.

4. To illustrate the last point, histograms of modeled-beam noise are shown, Fig. 4. Each corresponds to a 12-hour sample, but the three are taken over one week's period of time. The histogram corresponding to one week's ensemble is the average of the individual histograms, and here would be much broader than any of the short-term components. The suggestion is that it would be a mistake to use a long-term (or "grand") ensemble distribution of noise in a model to predict such a Measure of Effectiveness (MOE) as the 24-hour cumulative detection probabilities.

5. Consider next how the models calculate noise fluctuations: Formula (1-1), Fig. 5, is common to all of the models reviewed. If each variable were known and deterministic, then a standard "point" model such as RANDI would result. The form of the equation should not suggest that the factors are uncoupled—for in most treatments at least the array given depends on transmission angles. No model actually uses the time dependence of SL nor performs the sum in phase.

Models are thus distinguished by their treatment of the ship source field and by the method of calculating the statistics of Noise (N).

6. To help differentiate model types, two approaches are defined, Fig. 6. The term "Brute-Force" is not meant to suggest that the approach is unsophisticated or mathematically trivial, nor is "Analytic" meant to convey more than the notion that the calculation is performed without direct realizations of the random variables.

The first four models of Fig. 1 are Analytic, the others Brute Force.

7. Consider next some statistical quantities, Fig. 7, and how they might best be predicted by the models reviewed.

- First order statistics, with long-term ensembling, can be most efficiently predicted by an Analytic model.
- Statistics for limited-time ensembles are difficult to generate with Analytic models, but are natural for the Brute-Force models.
- Of the Analytic models, only the BTL model is capable of predicting the autocovariance function for the general case. Certain of the Brute-Force models routinely predict it.

- For higher order temporal statistics (such as level-crossing properties) and/or limited-time ensembling, the Analytic approaches can seldom be applied. Hence, a Brute-Force model is indicated.

- Multi-beam and multi-site statistics (e.g., cross-correlations) are predicted by several Brute-Force models, but only by one Analytic approach (BTL).

In summary, no single model will satisfy all requirements; a carefully combination of the best of each type seems the best approach.

8. Selected problem areas for a beam-noise prediction capability are noted, Fig. 8.

A – USI Model (Underwater Systems, Inc.)
B – BTL Model (Bell Laboratories)
C – BBN Model (Bolt, Beranek and Newman, Inc.)
D – WAGNER Model (Wagner Associates)
E – NABTAM Model (ORI, USI, NORDA, et al)
F – DSBN Model (Science Applications, Inc.)
G – BEAMPL (NORDA)
H – SIAM I (NRL)
I – SIAM II (NRL)

Figure 1

Mechanism	Typical Time for a Significant Change
• Ships on and off beams	Minutes for Nearby Ships, Hours to Days for Distant Ships
• Average TL variations	Hours
• Detailed TL fluctuations	Minutes to Hours
• Array response variations	Minutes to Hours
• Ship source level variations	Hours to Days
• Wind noise variations	Hours to Days

Figure 2

TYPICAL APPLICATIONS

- Instantaneous P_D
- CP_D over hours or a day
- Distribution of Holding Times over a Day

BEAM-NOISE STATISTICS

- Distribution of Beam-Noise Level (over a Short Time Period and Small Ocean Region)
- Statistical Dependence of Noise at Two Points in Time
- Distribution of Beam-Free Times
- Distribution of Time Intervals for Which Noise is Below a Threshold

Figure 3

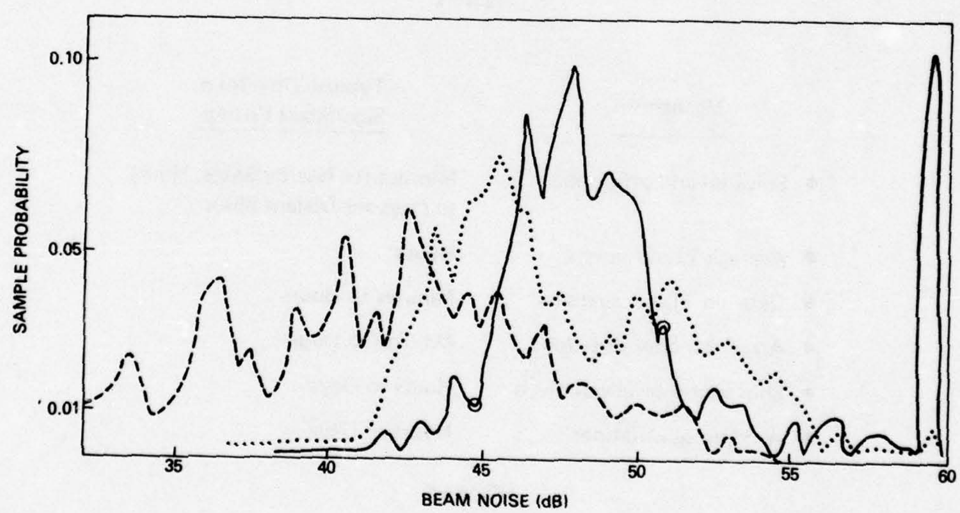

Figure 4

$$N(t) = \sum_{J=1}^{J(t)} SL_j(t) \cdot T_j(t) \cdot AG_j(t),$$

where

$J(t)$	is the number of ships at time t,
$SK_j(t)$	is the source intensity of the j-th ship at time t,
$T_j(t)$	is the transmission ratio for ship j at time t (i.e., $TL = -10 \log (T_j)$),
$AG_j(t)$	is the array response for the arrivals from ship j at time t.

Figure 5

BEAM-NOISE FLUCTUATION MODELING

- Analytic Approach:
  - treats variables as well-defined random processes
  - calculates statistical properties "directly"
  - typically employs convolutions
  - can yield efficient model for predicting selected noise statistics
  - is difficult to set up and to do higher-order statistics
- Brute Force Approach:
  - evaluation of statistics is numerical, using realizations of ship tracks, etc.
  - can be used to estimate just about any statistic
  - can use all available information
  - is often very expensive and requires special analysis routines

Figure 6

STATISTICAL QUANTITIES

- One-Dimensional Density Functions and Moments, Grand Ensemble
- One-Dimensional Density Functions and Moments, Limited-Time Ensemble
- Basic Temporal Statistics, Grand Ensemble
- Higher-Order Temporal Statistics
- Multi-Beam and Multi-Array Statistics

Figure 7

SOME PROBLEMS

- Inputs for Detection Simulations: Need approach to predict signal-plus-noise in one "Bin" and noise in another
- Statistics for Time-Dependent Array Response: None of the models treat a moving array.
- Ship Information: In spite of some recent progress, still lack information on source levels and locations
- Model Evaluation: Convincing evaluations of models for mean noise are scarce.
- Wind-Dependent Noise: Array system response to wind-generated noise is not understood.

Figure 8

THE EFFECT OF ACOUSTIC FLUCTUATIONS IN THE OCEAN UPON COHERENCE

O. D. Grace

(See Volume 2)

THE EFFECTS OF FLUCTUATING SIGNALS AND NOISE ON DETECTION PERFORMANCE

J. C. Heine and J. R. Nitsche
Bolt Beranek and Newman Inc.
Arlington, Virginia 22209

ABSTRACT

Receiver operator characteristics derived for post detection integration receivers are significantly perturbed if the signal power fluctuates with a characteristic time roughly two or more times the receiver integration time. In this paper, the effects on detection performance of slow fluctuations in both signal power and in noise power, such as occur in the 10–200 Hz region due to merchant shipping, are explicitly considered and are compared to results for signal fluctuations alone. Furthermore, degradation in detection performance in the region of $P_D > 0.5$ is shown to occur and the sensitivity of the degradation to the statistics of the noise power fluctuations is demonstrated. The effects of the noise statistics on experimental determination of sonar system performance is discussed.

INTRODUCTION

For discussion purposes, the system will consist of an ideal single channel quadratic detector which is preceded by a narrow band filter and followed by an ideal integrator. The input to this temporal processor is the output from a single beam of an underwater acoustic array.

One measure of the detection performance for such a system is obtained from the system's receiver operator characteristic (ROC) curve. Classically, the system's ROC curves are obtained in terms of ideal inputs; namely, stable sinusoidal signals in white Gaussian noise.

It is well known that the real ocean environment is not characterized as white Gaussian noise. Moreover, because of multipath propagation primarily, the signals are not received as stable sinusoids.

In this paper, we examine the impact of fluctuating signals and noise (in short, fluctuating output signal to noise ratios) on system performance prediction.

In particular, we are herein concerned with the effects of signal and noise fluctuations which have characteristic times on the order of two or three times the receiver integration time.

In the body of the paper, we first identify the sources of fluctuating output signal to noise ratios (SNR's) and estimate their characteristic times.

The transition curve, which is here defined to be a plot of detection probability (P_D) vs SNR for a given false alarm probability (P_{FA}) and integration time (T), is one means

for assessing system performance. In order to establish a basis for comparison, we next review the development of the ROC or transition curve for the constant signal case.

Our method of approach, in the manner of A. D. Whalen [1]* is to then consider the SNR as a random variable so that P_D is a function of a random variable. Given the probability density function of SNR, namely p (SNR), we can determine a set of modified transition curves which will be average P_D (i.e., $E[P_D]$) vs E [SNR]. The principal task then is to determine the forms of p (SNR).

Finally, we interpret the resulting set of transition curves in the context of system performance prediction.

RECEIVER OUTPUT FLUCTUATIONS

We shall consider a single channel NB filter-square-law detector-integrator as our temporal processor or receiver as sketched in Fig. 1. To determine whether a signal is present, the output of the integrator is compared to a threshold V_T. The level of the threshold is established on the basis of a desired false alarm probability (P_{FA}) constraint.

The receiver input r(t) will be assumed to be obtained from a single beam of an underwater acoustic array. For now, assume that r(t) is ocean ambient noise and that we are interested in the general spectral range of 10 to 200 Hz.

The receiver output Z(t) plotted as a function of time would typically appear as sketched in Fig. 2. As indicated in Fig. 2, several noise power fluctuation time scales are often observable. These characteristic times are identified as:

τ_S = a short-term fluctuation associated with the response of the receiver (controlled by the input filter bandwidth)

τ_M = a medium-term fluctuation associated with the motion of a specific ship population in the ocean space sampled by the spatial processor

τ_L = a long-term fluctuation associated with the rate of passage of ships in the area.

These characteristic times are listed in Table 1.

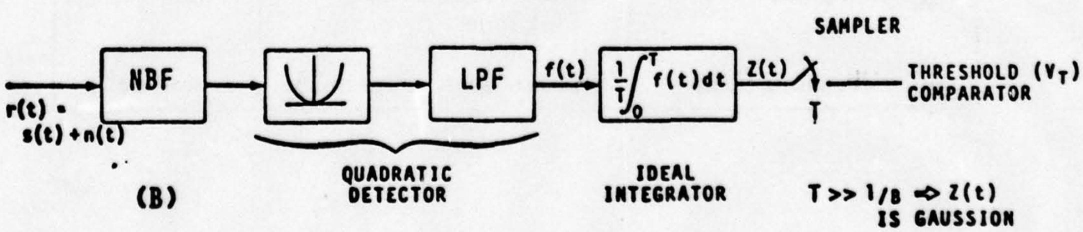

Fig. 1—Single channel receiver

*References are identified at the end of the paper.

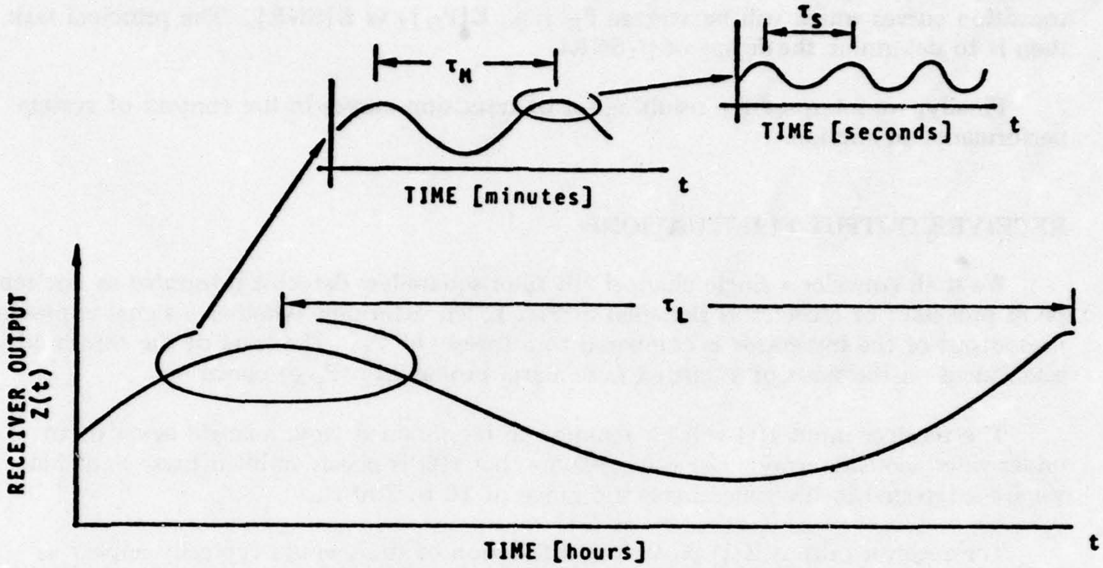

Fig. 2—Characteristic fluctuation times of receiver output

Table 1—Characteristic Fluctuation Times

Characteristic Fluctuation Times		Source of Fluctuation	Typical Times (sec)
τ_S	Short [S]	Filter response	1-10
τ_M	Medium [M]	Moving ships (e.g., TL and $\dot{R}$)	10^2-10^3
τ_L	Long [L]	Different ships at different look times	10^4-10^5
τ_{UL}	Ultra long [UL]	Seasonal fluctuations in TL	Seasonal

The latter three noise processes are random processes. The ones of particular interest are τ_M and τ_L and especially τ_M because it is on the order of the receiver integration time. It has been shown [2] that

$$\tau_M \sim \delta/\dot{R}$$

where

δ = correlation length of the transmission loss condition

$\dot{R}$ = range rate of passing ship relative to the spatial sensor.

Heine [3] has estimated the probability density function for Z(t) (see Fig. 1) for such an M-term noise process and we shall use it shortly.

With regard to the signal, if a sine wave of constant amplitude is transmitted to the underwater acoustic sensor especially over the appreciable ranges of interest, the received signal amplitude will not usually be constant. The random amplitude variations at the receiver input are primarily due to multipath acoustic propagation. If the number of paths is sufficiently large, the received signals will look very much like a sample function of a narrow-band Gaussian noise process [4]. The envelope of such a process has a Rayleigh probability density function (pdf) and the signal is termed a Rayleigh fading signal.

RECEIVER OUTPUT CHARACTERISTIC (ROC) CURVE FOR STATIONARY SIGNALS

The ROC curve (or alternatively, the transition curve) is one of the more useful ways of estimating receiver detection performance. Because it is used to define the recognition differential (N_{RD}) and because it will serve as the basis for comparison, we will briefly review the development of the ROC for the case of detecting a stable sinusoidal signal in the presence of additive stationary white Gaussian noise. For this case, the input to the receiver is given as

$$r(t) = A \cos(\omega_0 t + \theta) + n(t)$$

A = constant amplitude

ω_0 = constant carrier frequency

$$p_{(A)}(\theta) = \frac{1}{2\pi}; \quad 0 \leqslant \theta \leqslant 2\pi.$$

The noise is white Gaussian (with a power density spectrum $S_n(f) = N_0/2; -\infty < f < \infty$) and it can be represented in quadrature form [5] as

$$n(t) = x(t) \cos \omega_0 t + y(t) \sin \omega_0 t.$$

A detection decision is made every T-seconds at the output of the integrator. The integrator output at the sample time is

$$Z_0(T) = \frac{1}{2T} \int_0^T [A^2 + 2Ax(t)]\, dt + \frac{1}{2T} \int_0^T [x^2(t) + y^2(t)]\, dt\,.$$

With regard to the decision process, there are two hypotheses:

H_0 noise alone is present

H_1 signal plus noise are present.

When $Z_0 t$ exceeds the threshold V_T, we decide that signal is present; when V_T is not exceeded, we decide that signal is absent.

Since the time-bandwidth product of the receiver is large, we assume that $Z_0(T)$ is Gaussian by the Central Limit Theorem. We can then express two probability density functions of the output, depending upon the hypotheses.

$$p_{H_0}(Z) = \frac{1}{\sqrt{2\pi}\,\sigma_0} \exp\left[-\frac{Z^2}{2\sigma_0^2}\right]$$

$$p_{H_1}(Z) = \frac{1}{\sqrt{2\pi}\,\sigma_1} \exp\left[-\frac{Z-(\Delta m)^2}{2\sigma_1^2}\right],$$

where

- We made a change of variables $Z(t) = Z_0(t) - R_x(0)$ for convenience where $R_x(0) \approx$ total noise power
- $p_{H_0}(Z)$ and $p_{H_1}(Z)$ are termed likelihood functions
- Δm is the difference in the means of these two pdf's.

The receiver output pdf's as defined above are depicted in Fig. 3. The probabilities of detection and false alarm are obtained by suitably integrating the respective likelihood functions.

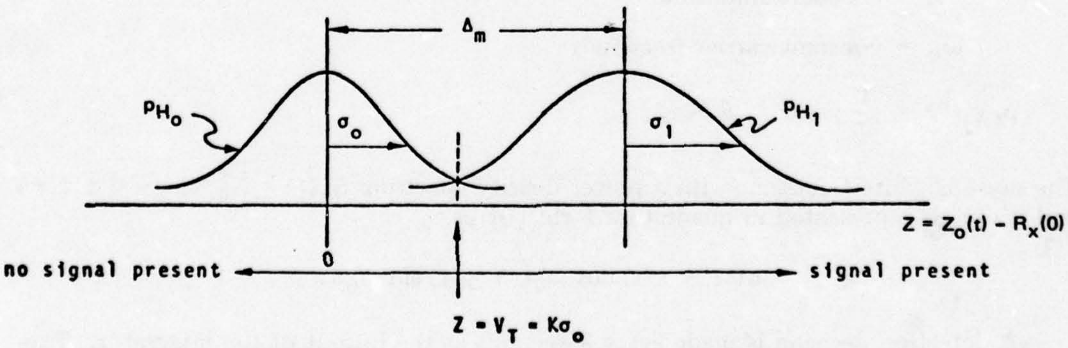

Fig. 3—Receiver output probability density functions

$$P_{FA} = \int_{K\sigma_0}^{\infty} p_{H_0}(Z)\,dZ = \int_{K\sigma_0}^{\infty} \frac{1}{\sqrt{2\pi}\,\sigma_0} \exp\left[-\frac{Z^2}{\sigma_0^2}\right] dZ$$

$$P_D = \int_{K\sigma_1}^{\infty} p_{H_1}(Z)\,dZ = \int_{K\sigma_1}^{\infty} \frac{1}{\sqrt{2\pi}\,\sigma_1} \exp\left[-\frac{(Z-\Delta m)^2}{\sigma_1^2}\right] dZ .$$

It may be shown that

$$\Delta m = S = A^2/2 = \text{average signal power}$$

$$\sigma_0^2 = \frac{N_0^2 B}{T} = \text{var}\,[Z(T)/H_0]$$

$$\sigma_1^2 = \frac{2SN_0}{T} + \frac{N_0^2 B}{T} .$$

By making the change of variables

$$t_1^2 = \frac{(Z-S)^2}{2\sigma_1^2} \quad \text{and} \quad t_2^2 = \frac{Z^2}{2\sigma_0^2}$$

we may obtain the forms

$$P_{FA} = \frac{1}{2}\,\text{erfc}\left[\frac{K}{\sqrt{2}}\right]$$

$$P_D = \frac{1}{2}\,\text{erfc}\left[\frac{K\sigma_0 - S}{\sqrt{2}\,\sigma_1}\right].$$

We can further express P_D in terms of the output SNR where we define

$$R = \frac{S}{N_0} \equiv \frac{S}{N} = \frac{\text{average signal power}}{\text{noise power per unit bandwidth}}$$

$$P_D = \frac{1}{2}\,\text{erfc}\left[\frac{\sqrt{K}\ B - \sqrt{T}\ R}{\sqrt{4R + 2B}}\right].$$

A plot of P_D vs R is termed a transition curve. Such a curve for the receiver of interest is shown in Fig. 4 for the nonfluctuating signal case. The parameter K is chosen on the basis of a specified acceptable P_{FA}. As an aside, it is pointed out that K is not a very strong function of P_{FA} as noted in the following table.

Desired P_{FA}	Threshold Factor K
10^{-2}	2.33
10^{-3}	3.10
10^{-4}	3.71
10^{-5}	4.27

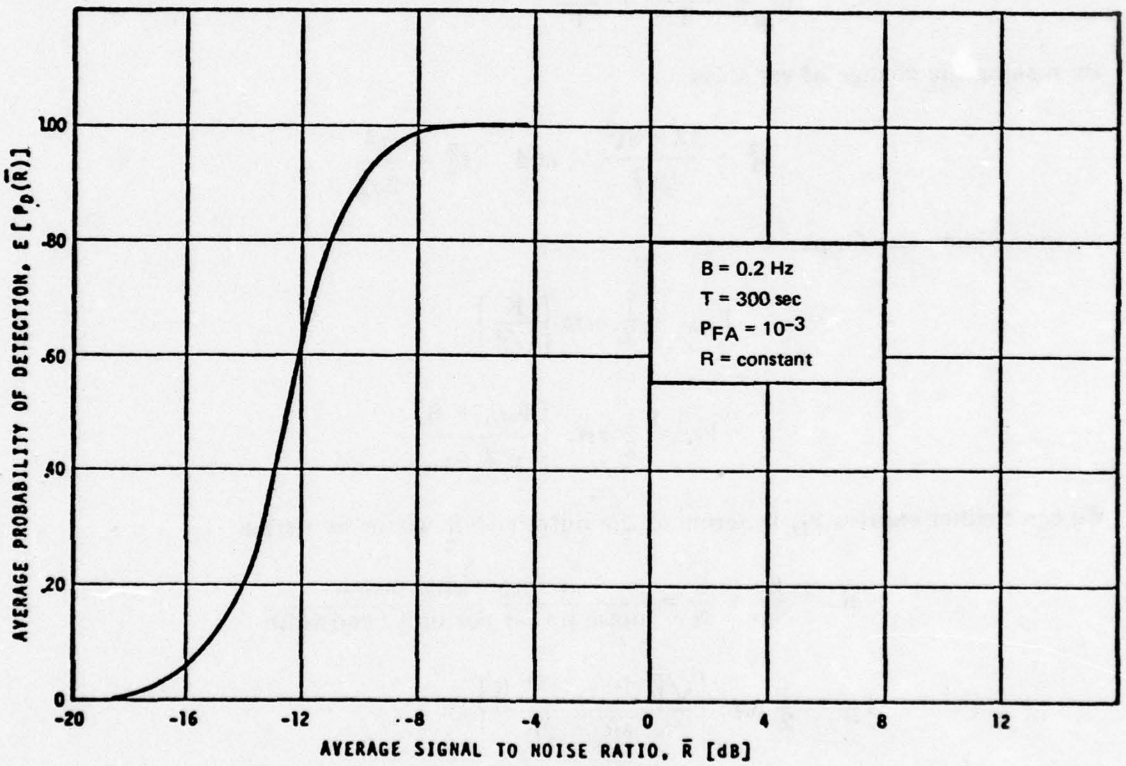

Fig. 4—Transition curve for the nonfluctuating signal case

Figure 4 is labeled as average P_D vs average R in anticipation of the fluctuating R cases to be considered next. For the constant signal (thus constant R) case, of course no averaging was done.

Finally, before we leave this case, it is well to point out that the $P_D[R]$ that was derived is not restricted to the small signal or low R case. The forms are slightly different as noted below

$$P_D[R] = \frac{1}{2} \operatorname{erfc} \left[\frac{K\sqrt{B} - \sqrt{T}\,R}{\sqrt{2B}}\right]; \quad \text{small R case}.$$

ROC CURVES FOR FLUCTUATING SIGNAL TO NOISE RATIOS

In what follows we shall consider the receiver output signal to noise ratio to be a random variable. Consequently $P_D[R]$ will be a function of a random variable and the expected or average P_D will be

$$E[P_D(R)] = \int_{-\infty}^{\infty} P_D(R)\,p(R)\,dR\,,$$

where

$E[\ ]$ = the statistical expectation operator

$$P_D(R) = \frac{1}{2} \operatorname{erfc} \left[\frac{K\sqrt{B} - \sqrt{T}\,R}{\sqrt{4R} + 2B}\right]$$

$p(R)$ = the probability density function of R.

Thus, the transition curves for the fluctuating R case will be the standard transition curve for nonfluctuating R averaged over all R or smoothed by $p(R)$. The problem is then to determine the appropriate analytic forms for $p(R)$.

We are herein concerned with medium term (see Table 1) fluctuations in R. That is, fluctuations in R that are such that R can be considered to be constant over any T-second interval, but varying from interval to interval. The fluctuations in R can be due to fluctuating signal only or to a combination of fluctuating signals and fluctuating noise. We shall compare the effects of both.

Fluctuating Signal Only

The case of a slowly fluctuating signal has been considered by a number of investigators [1,4,6]. The amplitude A of a Rayleigh fading signal has a probability density function (pdf) given by

$$p(A) = \frac{A}{S} \exp\left[-\frac{A^2}{2S}\right]; \quad 0 \leq A < \infty ,$$

where

$$S = E\left[\frac{A^2}{2}\right] = \text{average signal power.}$$

The average P_D is thus

$$E[P_D(A)] = \int_0^{\infty} \frac{1}{2} \operatorname{erfc}\left[\frac{K\sigma_0 - \frac{A^2}{2}}{\sqrt{2}\,\sigma_1}\right] \cdot \frac{A}{S} \exp\left[-\frac{A^2}{2S}\right] dA ,$$

and in terms of the average signal to noise ratio ($R = A^2/2N$), we have

$$E[P_D(\bar{R})] = \int_{-\infty}^{\infty} \frac{1}{2} \operatorname{erfc}\left[\frac{K\sqrt{B} - \sqrt{T}\,R}{\sqrt{4R + 2B}}\right] \frac{1}{R} e^{-R/\bar{R}} dR ,$$

where $\bar{R} = E[R]$.

The average P_D vs average R is plotted in Fig. 5 and the standard transition curve is shown also for comparison. We can interpret the new transition curve as a smoothing of

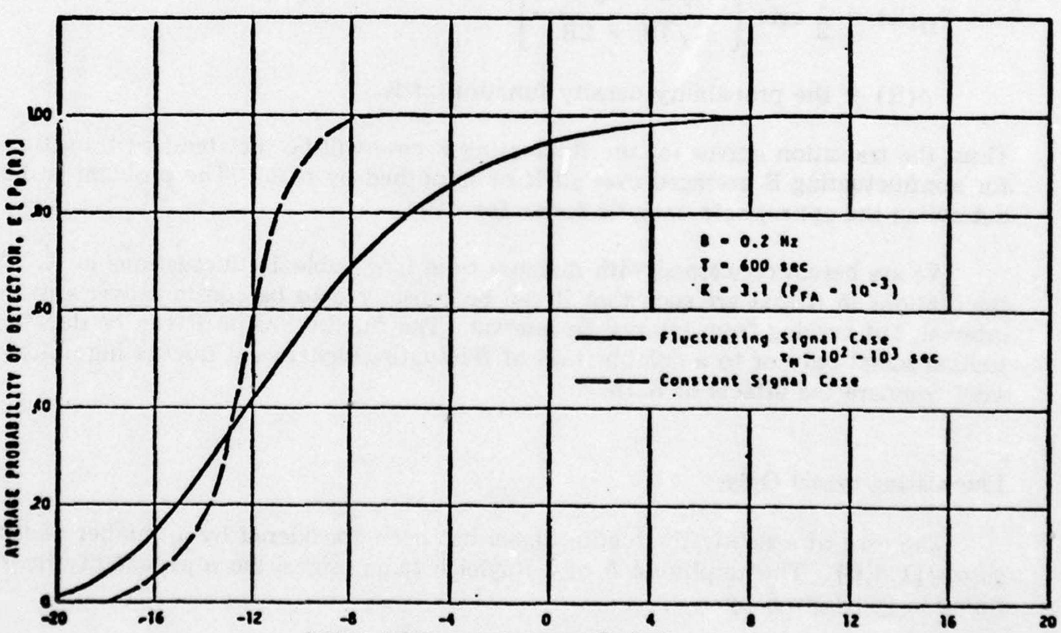

Fig. 5—Transition curve for fluctuating signal case

the standard curve by p(R). In this case p(R) is an exponential pdf and is shown plotted in Fig. 6 for various values of $\bar{R}$. Whereas the standard transition curve shows a rather abrupt "transition" from low to high probabilities of detection (i.e., over a $\Delta\bar{R} \simeq 3$ dB), the smoothed curve shows the same transition (i.e., from $P_D = 0.2$ to 0.8) occurring over a considerably greater range of SNR, namely $\Delta\bar{R} \simeq 9.5$ dB.

Fluctuating Signal and Noise

We now extend the previous development by considering a random signal to noise ratio due to fluctuations in both signal and noise. Again we restrict our attention to the characteristic fluctuation time $\tau_M \sim 10^2 - 10^3$ seconds.

The signal power fluctuations will again be assumed to be exponential. The noise power fluctuations have been hypothesized as being gamma distributed [3] with

$$p(N) = \frac{\lambda_n}{\Gamma[r]} (\lambda_n N)^{r-1} \exp[-\lambda_n N] \text{ ,}$$

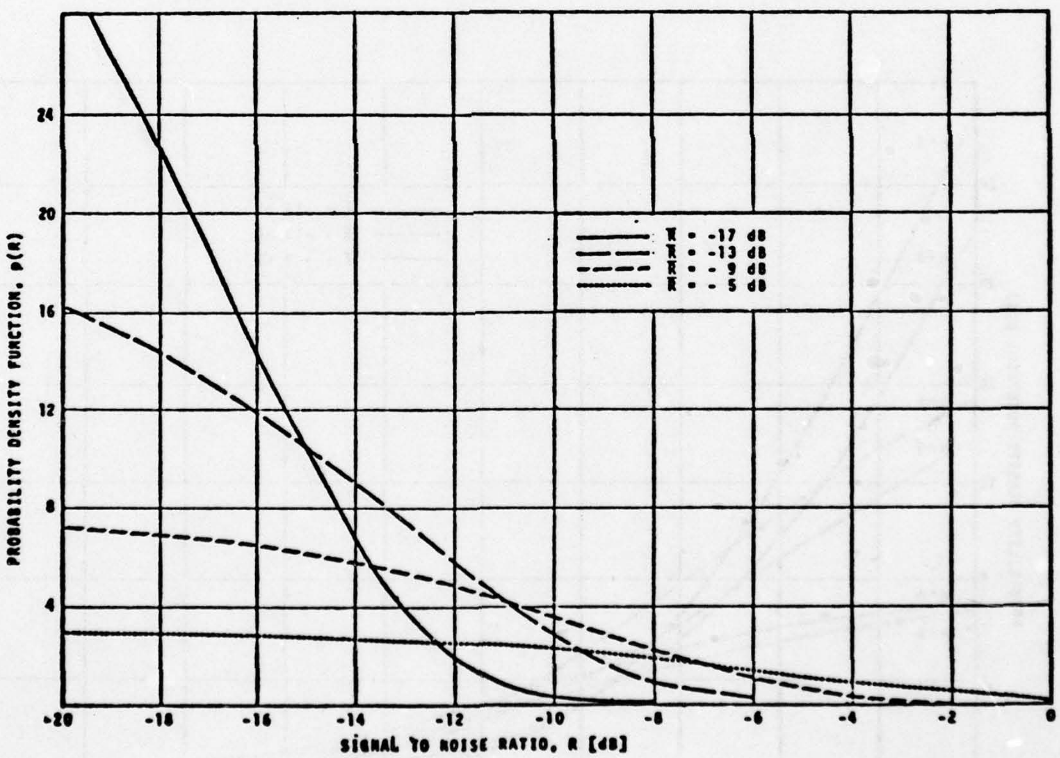

Fig. 6—Probability density function of R for fluctuating signal only

where

$$r = E^2[N]/\mathrm{var}[N] = \text{half the number of degrees of freedom}$$

$$\lambda_n = r/E[N].$$

The signal to noise ratio $R = A^2/2N$ can be obtained by a direct transformation since we have $p(A)$ and $p(N)$ and they are assumed to be independent. Also since R is the ratio of two Chi-squared pdf's, R will have an F-pdf.

$$p(R) = \frac{1}{\bar{R}\left[1 + \frac{R}{r\bar{R}}\right]^{r+1}} .$$

A family of these pdf's is shown in Fig. 7. They are plotted parametrically for various mean signal to noise ratios ($\bar{R}$) and for 2 and 6 degrees of freedom. The average P_D for the case of fluctuating signals and noise is thus

$$E[P_D(\bar{R})] = \int_{-\infty}^{\infty} \frac{1}{2}\,\mathrm{erfc}\left[\frac{K\sqrt{B} - \sqrt{T}\,R}{4R + 2B}\right] \frac{dR}{\bar{R}\left[1 + \frac{R}{r\bar{R}}\right]^{r+1}} .$$

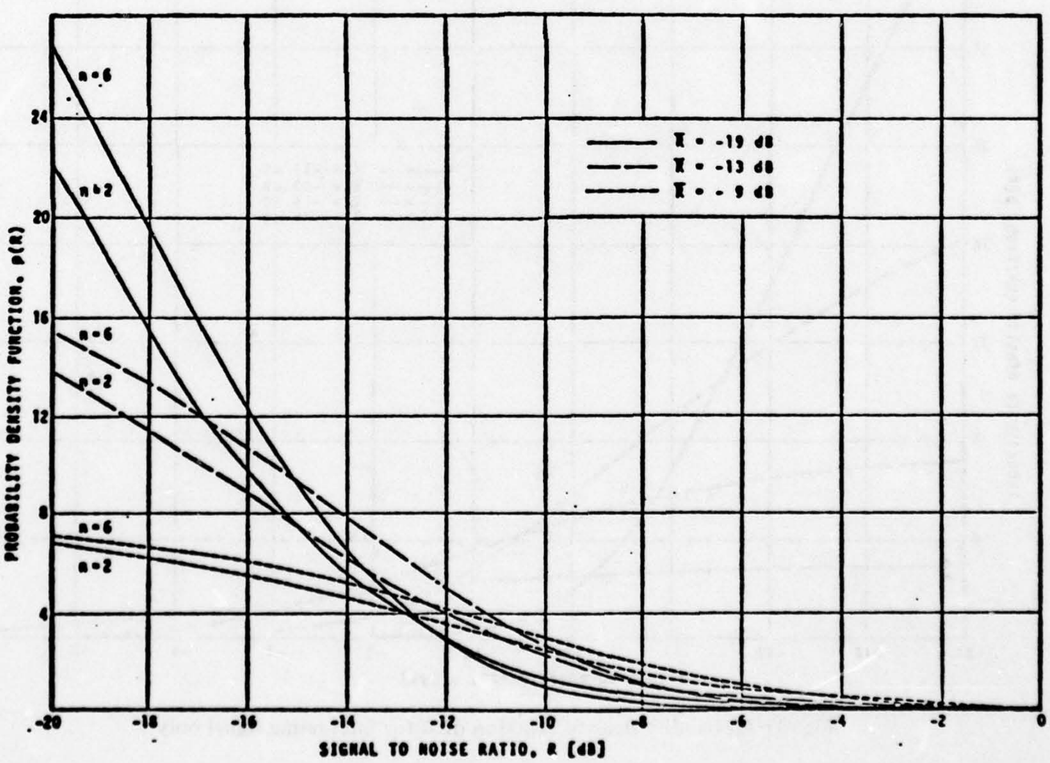

Fig. 7—Probability density functions of R for fluctuating signals and noise for various $\bar{R}$ and degrees of freedom

A set of transition curves (for 2, 6, and 10 degrees of freedom) for the case of fluctuating signals and noise is shown in Fig. 8. The standard curve is shown for comparison. As was true for the fluctuating signal alone case, we can interpret these new transition curves as smoothed or averaged versions of the constant version.

Observe that as the number of degrees of freedom n increases, the fluctuating signal and noise curves approach the fluctuating signal alone curve. This asymptotic behavior for large n can be understood by recalling that p(N) was assumed to be gamma and that its variance decreases as N increases. In the limit N large, the density p(R) becomes exponential; as is p(S) for signal fluctuations alone. Figure 9 compares the exponential pdf (appropriate to fluctuating signal alone) with the F-density with two degrees of freedom (appropriate to the extreme case of signal and noise fluctuations).

IMPLICATIONS ON PERFORMANCE PREDICTION

We have observed that the transition curves for the fluctuating signal and noise case are smoothed versions of the constant amplitude case. The amount of smoothing was seen to be a function of the numbers of degrees of freedom of p(R). To demonstrate the possible impact that such smoothing could have on system performance prediction, consider Fig. 10.

A pair of dashed and solid curves were calculated for two different spatial sensors; one spatial sensor provided a theoretical 5 dB improvement in average signal to noise ratio, $\bar{R}$. Assume this improvement was due solely to the fact that the acoustic aperture of one array was three times the aperture of the other. One curve in a pair assumes constant R; the other assumes a fluctuating R due to fluctuating signal and noise.

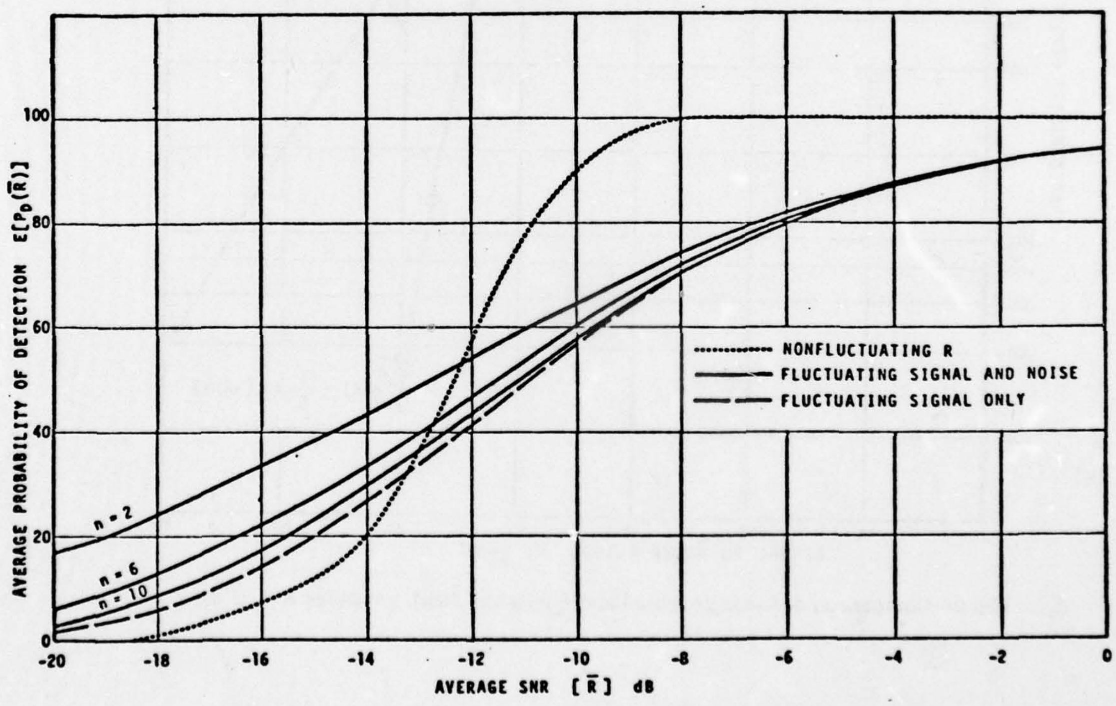

Fig. 8—Transition curves for the fluctuating signal and noise case

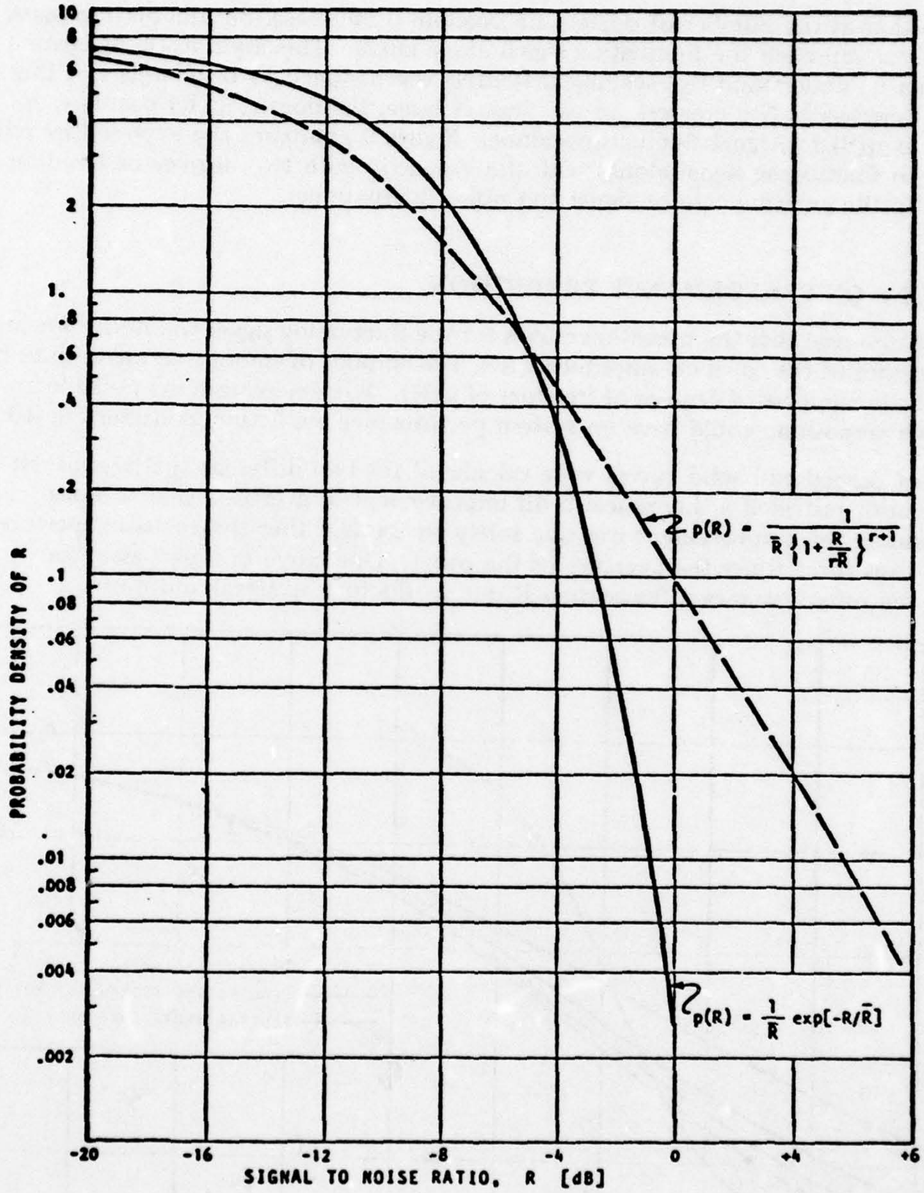

Fig. 9—Comparison of the exponential and F-densities (with n = 2) for $\bar{R} = -9$ dB

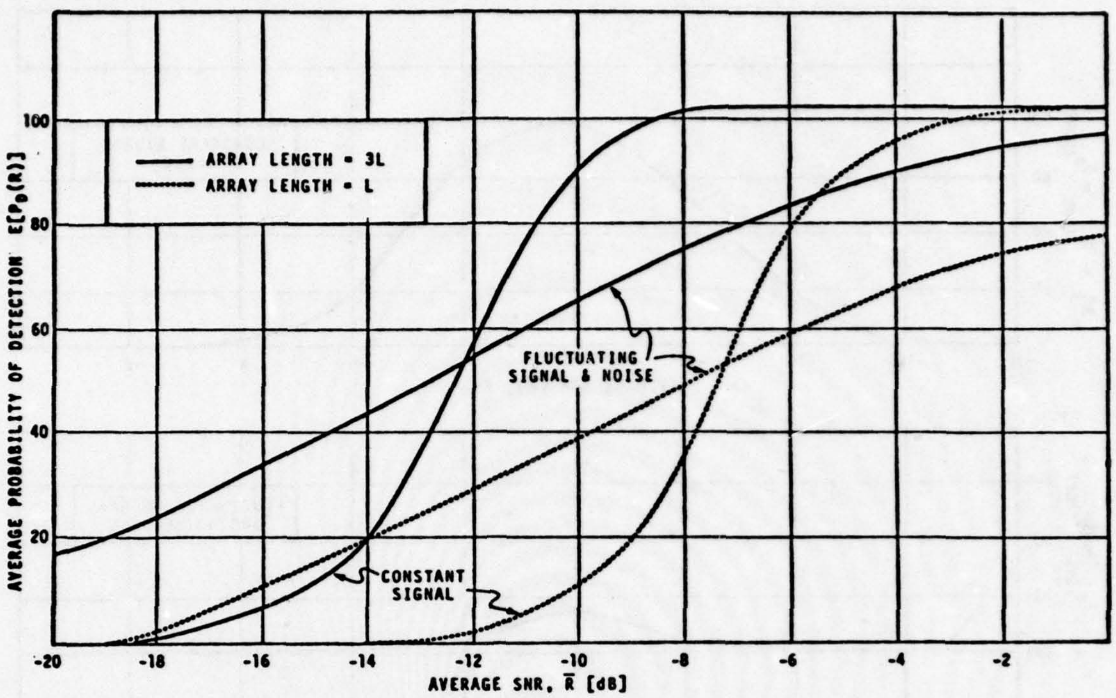

Fig. 10—Comparison of transition curves for increased array length

Consider the predicted improvement in detection performance as would be calculated under the constant-R assumption. This is shown in the upper half of Fig. 11. Note that at $\bar{R} \sim -10$ dB, the P_D for the long array is the P_D for the short array plus 80%; a significant improvement in detection performance. Furthermore, an improvement of about 40 percentage points is obtained over the range $-12.5 \text{ dB} \lesssim \bar{R} \lesssim -7.5$ dB.

Now consider the predicted improvement for the fluctuating R case. The results are shown in the lower half of Fig. 11. For this case, an improvement is seen for all $\bar{R}$, but the improvement is an almost constant 20 percentage points. It is not immediately clear that such an improvement is significant, especially when viewed in terms of the overall costs of increasing the array length by a factor of three.

SUMMARY

We have discussed the effects of fluctuating output signal to noise ratios (R) on system performance and performance prediction. The effects due to fluctuating signal alone were compared to those due to fluctuating signal and noise. The fluctuations considered were assumed to have characteristic times on the order of two or more receiver integration times and we confined our attention to the 10–200 Hz spectral range. The p(R) for fluctuating signal alone was exponential and the p(R) for fluctuating signal and noise was F-type.

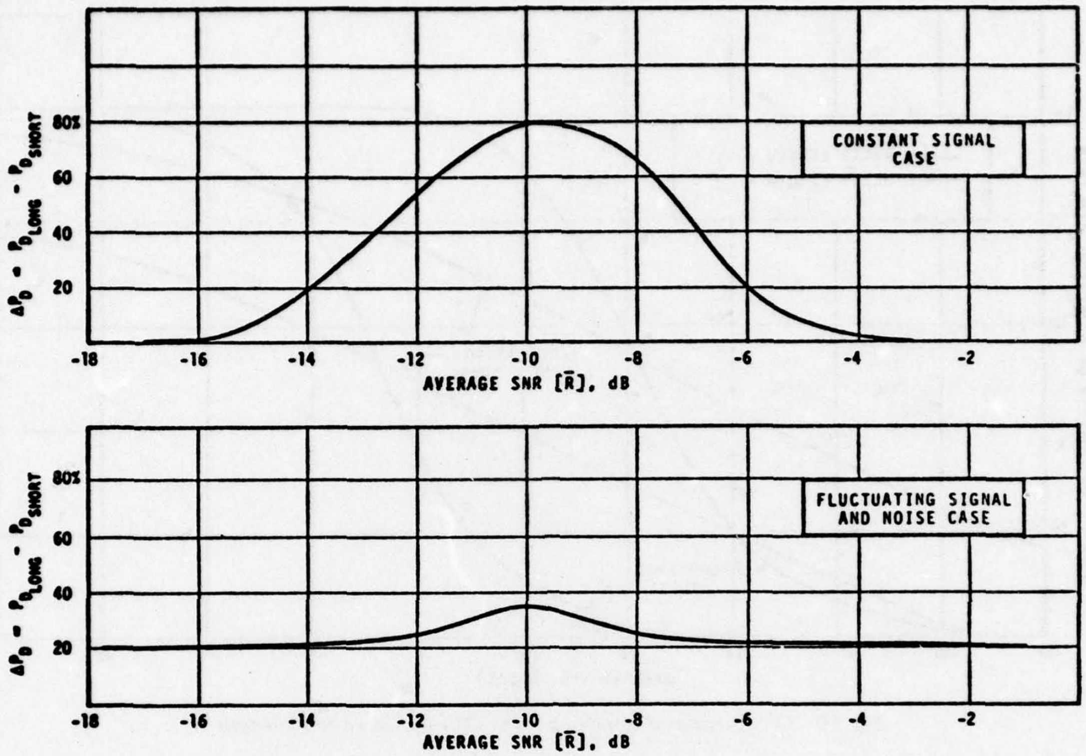

Fig. 11—Comparison of improvements in detection probability with increase in array length

The following summary statements are made in the context of the stated assumptions.

- Under the assumptions of constant signal in white Gaussian noise, the transition curve is very sharp; i.e., $0.2 \leqslant P_D \leqslant 0.8$ for a $\Delta R \simeq 3$ dB. Hence this would indicate a strong emphasis on accurate measurements of mean values. Actual transition curves are considerably more smooth, implying a need for measuring the statistics of R.

- The fluctuating R, regardless of the source of fluctuations, results in an improved detection performance at low $\bar{R}$ (i.e., long ranges) and decreased performance at shorter ranges. Stated in other terms, the $\bar{R}$ required at a given range for the fluctuating R is on the order of 5 dB more than that required for nonfluctuating R at a $P_D \simeq 0.8$.

- The fact that the fluctuating signal and noise case approaches the fluctuating signal alone case as the number of degrees of freedom increases implies that less emphasis need be placed on obtaining noise statistics or conversely more emphasis should be placed on signal statistics. This comment is more appropriate for short range detections, less appropriate for long range detections (especially with high resolution spatial sensors).

- Predicted performance improvements based on nonfluctuating R can lead to gross over estimates.

REFERENCES

1. A. D. Whalen, *Detection of Signals in Noise*, Academic Press, New York, 1971.
2. P. W. Smith, personal communication.
3. J. C. Heine, "Recommendations for Modified Statistical Analysis of Ambient Noise Data," Bolt Beranek and Newman Inc. Tech Memo No. 385, November 1977.
4. I. Dyer, "Statistics of Distant Shipping Noise," *J. Acous. Soc. Amer.* 53, 2, 564-570.
5. W. B. Davenport and W. L. Root, *An Introduction to the Theory of Random Signals and Noise*, McGraw-Hill, New York, 1958.
6. R. J. Urick, "Signal Excess and Detection Probability of Fluctuating Sonal Signals in Noise," *USN J. Underwater Acoustics* 27, 3, 569-585.

WORKING FLUCTUATION MODELS

WITH APPLICATION TO DETECTION PREDICTION

R. J. Urick

(See Volume 2)

SIGNAL FLUCTUATIONS

K. D. Flowers

(See Volume 2)

NUMERICAL MODELS OF ACOUSTIC PROPAGATION THROUGH INTERNAL WAVES

H. A. DeFerrari and R. Leung
University of Miami
Rosenthal School of Marine and Atmospheric Science
Miami, Florida 33149

A theory of propagation through a fluctuating ocean (FDMZ 1977)* predicts statistics of acoustic variability in regions of $\Lambda - \Phi$ space, where Λ and Φ are the diffraction and strength parameters. Statistics for a single path or for large numbers of micro- or deterministic multipaths are derived. Applications to ocean propagation usually employ the Garrett-Munk internal wave model (GM72)† to predict the sound-speed fluctuations which are, in turn, used as input to the propagation model. Once the internal wave statistics are specified, $\Lambda - \Phi$ parameters are computed by integration along the path of propagation which requires a detailed ray analysis.

We have developed general numerical methods for the computation of Λ and Φ. For arbitrary depth dependence of sound-speed C and buoyancy frequency N, a numerical model computes internal wave modes subject to the boundary condition of vanishing vertical velocity at the surface and bottom. The approximate forms of the wave functions used in GM72 give good approximation in the interior, away from the boundaries, and for the lower and more energetic frequencies of the internal wave spectrum. Our numerically computed wave functions, dispersion relationships and spectra are valid near the surface and for the higher frequencies of the internal wave spectrum, although they are considerably more complicated to compute. Thus we anticipate better approximation for ray paths which have turning points near the surface.

Ray paths are determined with conventional ray tracing equations by fitting the sound-speed profile with a large number of linear segments. The ray model is used to approximate the path of propagation only, and therefore, errors are not introduced by the discontinuous derivatives at the interception of the linear segments. With the sound-speed fluctuations determined from the internal wave model and the ray path known, Φ is determined by numerically evaluating the integral.

$$\Phi^2 = q_0^2 \int dx \int dx' \rho [z(x), z(x')] \;.$$

Computations of Λ are tedious, requiring the determination of R_f the Fresnel zone radius along the propagation path. For the calculation of R_f we have used the ray tube method (FDMZ 1977). To employ the method, it was necessary to solve the differential equation.

*Flatte, Dashen, Munk, Zachariasen Model 1977
†Garrett Munk Model 1972.

$$\partial_{xx}\xi(x) + U_0''[z_{ray}(x)]\,\xi(x) = 0$$

where, $\xi(x)$ is a small displacement from the unperturbed ray and $U_0 = (c^2 - c_0^2)/2c^2$.

Measured values of $U_0(z)$ are fit with a cubic spline, which insures unique and continuous second derivatives at every depth. Finite difference methods are used to solve the equation for any specified ray path. Λ is then computed by numerical evaluation of the integral.

$$\Lambda = \sigma^{-2} q_0^2 \int dx \int dx' \, \rho\,[z(x), z(x')]\,(g_0 A L_v^2)^{-1}$$

where L_v is the vertical coherence length.

The models described have recently been completed and we have begun to systematically examine the effects of source-receiver geometry, sound-speed profile, and Brunt-Väisälä profile. Initial results indicate that Λ parameter is very sensitive to ray geometry. The Fresnel zone radius changes greatly along the propagation path, having large contributions to the Λ integral near convergences and caustics, and little near the turning point. Source-receiver depth can result in order of magnitude changes even at the same source-receiver range. Rays having turning points near the surface incur significantly less Φ variation than predicted with (GM72). Examples are presented to illustrate these points.

Our objectives are to extend results for the single-ray case to the special cases of two and four paths, which are typical in long-range deep-ocean propagation and result from combinations of up-going and down-going rays. Such paths very often have nearly identical travel times and cannot be separated by temporal processing. Direct observation of statistics of the combined paths is easily accomplished in ocean experiments, whereas, isolation of a single path is often impossible for frequencies below 500 Hz at ranges in excess of 100 km.

SINGLE PATH—PHASE AND AMPLITUDE FLUCTUATIONS

Terry E. Ewart
Applied Physics Laboratory
University of Washington
Seattle, Washington 98195

ABSTRACT

A discussion of this signal processing techniques and the results from two acoustics transmission experiments will be presented (the range of acoustic frequencies is 2 to 16 KHz). The focus of these experiments is to measure the stochastic behavior of the phase and amplitude of a single Fermat path, to measure the index of refraction fluctuations in time and space over the transmission path and compare the results with theoretical predictions of acoustic scattering based on the index of refraction fluctuation measurements. We have concentrated on the range of time and space scales appropriate to the tides, internal waves and fire structure. We show that the signal processing technique used to separate single paths from a multipath environment work to the limit of one wave length path separation (which is the limit of distinct Format path separation). Acoustic frequency dependent effects are observed in the amplitude fluctuations. These effects and others are discussed in the context of the environmental observations. The results from the second experiment, MATE (Mid-Ocean Acoustic Transmission Experiment), are preliminary, but serve to indicate the focus of the research effort.

PREDICTION OF DETECTION PERFORMANCE

Magnus Moll
Bolt Beranek and Newman Inc.
1701 North Fort Myer Drive
Arlington, Virginia 22209

ABSTRACT

Statistical methods of systems analysis are employed to predict the performance of a passive sonar receiver operating in environments with fluctuating signals and noise. The receiver analog employed is a multichannel processor that produces for each channel a decision threshold that is determined by the outputs of other channels. The receiver inputs are assumed to be a compound random process exhibiting characteristics observed in experimental studies of ambient noise. The parameters of these processes including their relaxation times can be selected to suit a particular set of environmental conditions. The principal objective is to achieve realistic predictions of the probability of detection by single observations. Results obtained to show that receiver performance depends on both the time scale of the fluctuation and its extent. The effort is supported by the Naval Analysis Programs, Code 431, Office of Naval Research.

SUMMARY

Statistical methods of systems analysis are employed to predict the performance of a passive sonar receiver operating in environments with fluctuating acoustic inputs. The use of this approach requires an analog of the sonar receiver and statistical characterization of acoustic signals and noise.

A multi-channel analog was employed to represent either a multi-beam receiver and recording display or a frequency analysis device. Each channel includes a rectifier and an integrator. For detection decisions, the output of each integrator is compared to a threshold value that is a linear combination of the outputs of the integrators of other channels. These thresholds therefore adjust to variations in noise background level.

The random process model employed has characteristics that conform to the findings of several experimental studies of underwater ambient noise:

1. Estimates of first-order probability measures from short data segments supported, more often than not, the hypothesis that the amplitude of noise is normally distributed.

2. However, the number of departures from first-order normality increased with sample length.

3. In one set of experiments, about 28% of the estimates of kurtosis fell outside the 95% confidence limits for a Gaussian variate, and almost all of these were on the high side.

AD-A072 309 NAVAL RESEARCH LAB WASHINGTON DC F/G 20/1

ACOUSTIC FLUCTUATION WORKSHOP, HELD AT NAVAL RESEARCH LABORATOR--ETC(U)

JUL 78 S HANISH, C R ROLLINS, J CYBULSKI

UNCLASSIFIED NRL-MR-3884-VOL-1 NL

2 OF 3

AD A072309

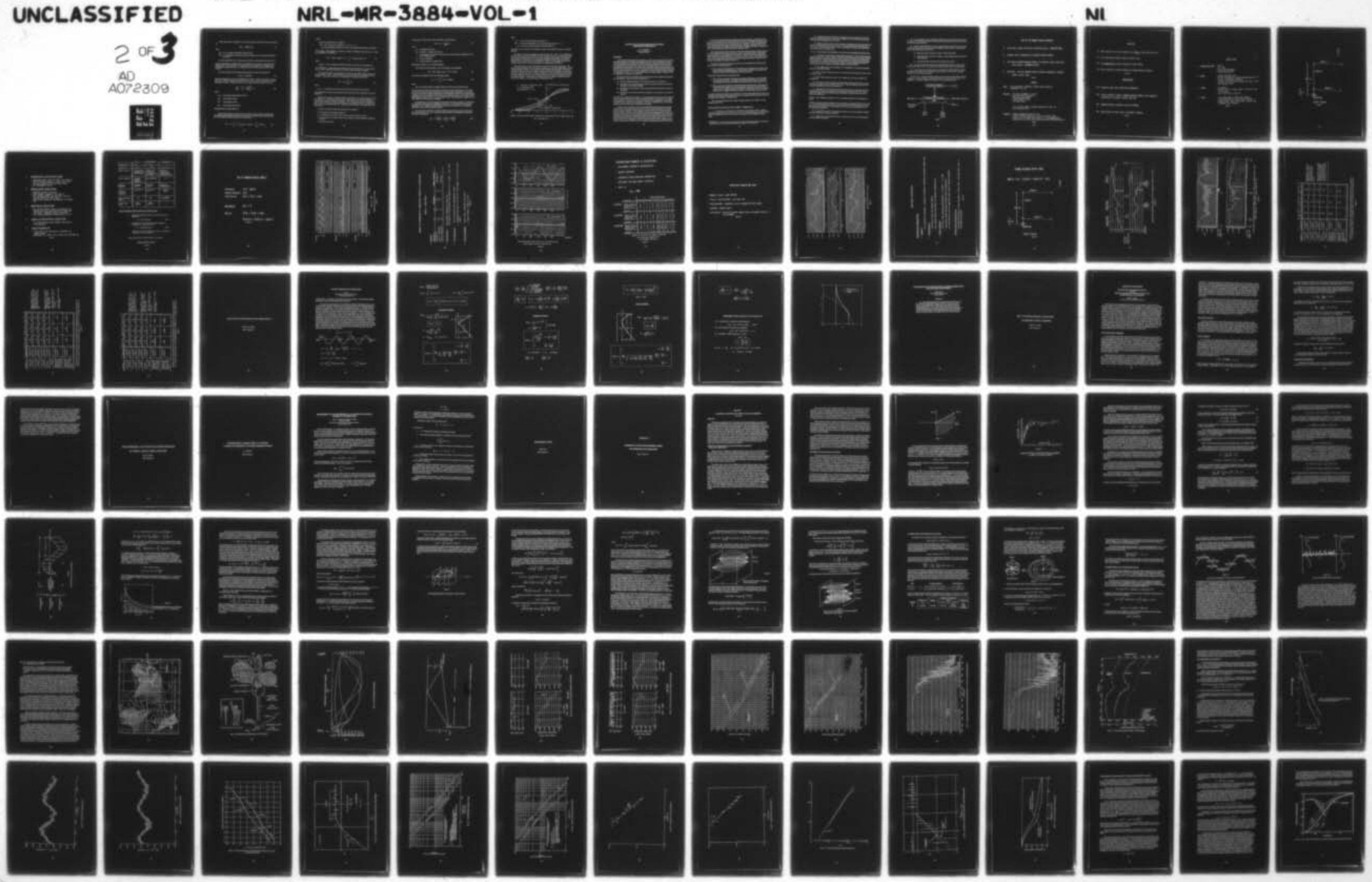

SIFIED

2 OF 3

AD
A072309

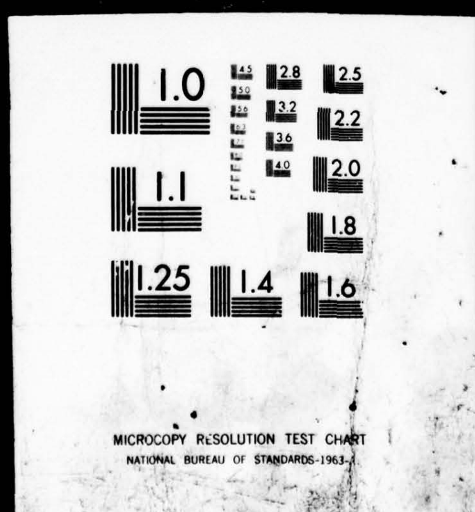

These traits would be exhibited by a class of compound random processes represented by

$$N(t) = \sqrt{P(t)}\, G(t) \tag{1}$$

where

P(t) is a non-negative stationary random process

G(t) is a zero-mean unit-variance stationary Gaussian process, statistically independent of P(t).

It is also assumed that the relaxation time of P(t) is much greater than that of G(t).

If the last assumption is satisfied, then the bandwidth of the process is essentially determined by G(t). It is clear from (1) that given P(t), the process N(t) is conditionally a nonstationary Gaussian process. It is easily shown that all odd-order moments of N(t) are zero.

Since each channel of the receiver analog squares its input, the properties of

$$N^2(t) = P(t)G^2(t) \tag{2}$$

affect the performance of the post-rectification smoother. Analysis shows that the relaxation time of $N^2(t)$ is effectively determined by P(t), which can be considered as a fluctuating power envelope. Starting with (2), it can be shown that the kurtosis of N(t) is

$$\frac{\mu_{4N}}{\sigma_N^4} = 3\left[1 + \left(\frac{\sigma_P}{m_P}\right)^2\right] \geqslant 3 \tag{3}$$

where

μ_{4N} is the fourth central moment of N(t)

σ_N^2 is the variance of N(t)

σ_P^2 is the variance of P(t)

m_P is the average value of P(t).

The kurtosis for a normal variate is 3.

For the receiver channel of interest, the test statistic that provides the basis for detection decisions is the difference between the output of its integrator and the threshold function. For channel 0, the test statistic can be expressed as

$$Z_0 = T^{-1} \int_0^T du \left\{ [S_0(u) + N_0(u)]^2 - \sum_{i=1}^{n} c_{0_i} N_i^2(u) \right\} \tag{4}$$

where

$S_0(t)$ is the signal input to channel 0

$N_i(t)$ is the noise input to channel i, i = 0, 1, 2, ..., n

c_{0_i} is the weighting coefficient for channel i in forming the threshold for channel 0.

If the output of the integrator of channel 0 exceeds its threshold value, then $Z_0 > 0$. Thus the probability of detection is

$$P_{D_0} = P[Z_0 > 0 | S_0(t) > 0] = \int_0^{\infty} dz f_{Z_0}[z_0 | S_0(t) > 0] \tag{5}$$

where

$f_{Z_0}(z_0|)$ is the conditional probability density function for the test statistic Z_0.

The coefficients c_{0_i} were selected to maximize detection performance in isotropic noise and to achieve a specified probability of detection when the noise is Gaussian.

The principal burden of the analysis is to derive the probability density function for the test statistic. This is a difficult problem in that the inputs to the averagers are non-Gaussian. The approach chosen was to approximate the required density by

$$h(x) = g(x) \sum_{i=0}^{m} a_i x^i \tag{6}$$

where

$g(x)$ is a probability density function selected as the basis of the expansion.

The coefficients a_i are selected so that the first m moments of $h(x)$ match those of the test statistic Z_0.

The use of the method therefore requires the derivation of low-order moments of the test statistic Z_0. Obtaining the first moment is trivial, the second moment interesting, and the third moment extremely burdensome. The analysis show that the calculation of a given order of moment requires knowledge of the corresponding order of moment functions of the power envelope processes. Expressions for moments one through three have been derived.

A special case with the following features will be discussed:

- All channels have identical parameters.
- All channels have the same power envelope function $P_N(t)$ for noise.
- A large number of averager outputs are combined to form the detection threshold function.
- The signal is Gaussian.

For this case, the mean value of the test statistic is approximately

$$m_Z \simeq p_S - \frac{\gamma}{\sqrt{WT}} p_N \tag{7}$$

where

p_S is average signal power

$p_N = E[P_N(t)] =$ average noise power

γ is a parameter whose value is determined by the false alarm probability for the case of Gaussian noise

W is input bandwidth

T is post-rectification averaging time.

When signal is absent, m_Z is obviously negative.

For the same case, the variance of the test statistic is approximately

$$\sigma_Z^2 = (WT)^{-1}\left[(p_S + p_N)^2 + \sigma_P^2(1 + \gamma^2 I_P)\right] \tag{8}$$

where σ_P^2 is the variance of the noise envelope process

$$I_P = T^{-1} \int_{-T}^{T} dt\,(1 - |t|) k_P(t) \tag{9}$$

where

$k_P(t)$ is the autocovariance coefficient function for the power envelope process.

The second term of (8) shows the effects of the power envelope fluctuation. The contribution is proportional to the variance of the envelope process. Expression (9) shows that the variance of the test statistic is affected by the relationship between the post-rectification averaging time and the relaxation time of the power envelope process. If the latter is much larger than the former, then $I_p \rightarrow 1$, the maximum value. This assumption is implicit in the usual analysis of the effects of fluctuation.

An expression for the third moment has also been derived, and all three moments will be employed to determine the coefficients of (6) for m = 3. That result in turn will be employed in (5) to examine the dependence of detection performance on the statistical parameters of the power fluctuation envelope.

For some cases of interest, a normal probability density function can be used as the basis function g(x) in (6). For a third-order approximation, the probability of detection can then be expressed as

$$P_{D_0} \simeq P\left(\frac{m_Z}{\sigma_Z}\right) + \frac{1}{6}\frac{\mu_{3Z}}{\sigma_Z^3} Z^{(2)}\left(\frac{m_Z}{\sigma_Z}\right) \tag{10}$$

where

$P(\ )$ is the normal distribution function (0, 1)

$Z^{(2)}(\ )$ is the second derivative of the normal density function (0, 1)

μ_{3Z} is the third central moment of the test statistic Z_0.

The form (10) is convenient in that tables of both of the required functions are readily available.

The result (10) has been applied to a case in which $(\sigma_P \div m_P)^2 = 1/2$. Substitution of that value in (3) yields a kurtosis of 4.5 for the noise process. It was further assumed that the autocovariance function for the power envelope is exponential. The results of the calculation are plotted as a set of detection transition curves, which show that the spread of the curves increase with the ratio D/T, where D is the relaxation time of the envelope process, and T is the post-rectification averaging time (See Fig. 1).

Mean and variance of the test statistic are given by (7) and (8) respectively. The former requires the mean value of the power envelope, and the latter additionally requires its autocovariance function. Such data have been acquired experimentally. Calculation of the third moment of the test statistic requires a third moment function for the power envelope, a function that is not commonly estimated. We are investigating the possibility of approximating this function on the basis of the third moment and autocovariance of the power envelope. If that effort is successful, then more realistic performance predictions can be based on a modest amount of experimental data.

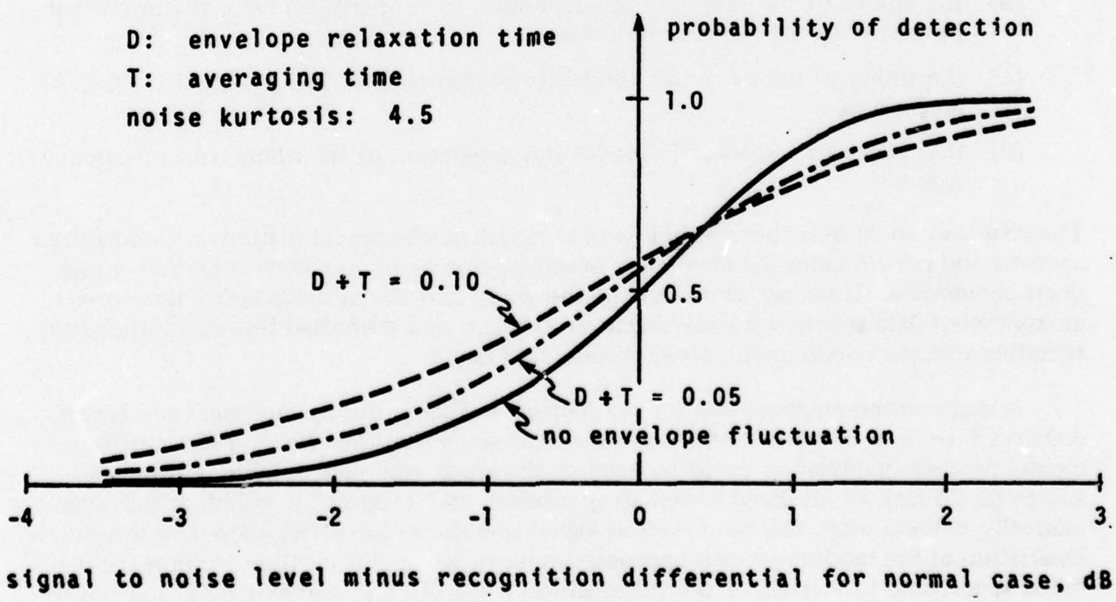

Fig. 1—Transition curves

ACOUSTIC FLUCTUATION MODELING FOR SYSTEM PERFORMANCE ESTIMATION

R. C. Cavanagh
Service Applications, Inc.
McLean, Virginia

SUMMARY

A critical part of the analysis and estimation of sonar system performance is the characterization of the acoustic signal and background noise. Current techniques in performance and engagement modeling employ random processes to simulate the long and short-term variations of these parameters in time. The usual justification is that the complex mechanisms govering the generation, transmission, reception, and processor response of signals and noise are sufficiently "random" to be modeled by stochastic processes determined by a few input parameters. Since such an approach is much more efficient than measuring or modeling the details of the acoustic environment, it is widely utilized. However, it has not undergone a comprehensive evaluation.

SAI has performed an investigation into several aspects of the validity of the random-process approach. Among the topics considered are:

(a) the basic statistical properties of acoustic signal and noise fluctuations

(b) the ability of the random-process models to properly simulate the important properties of the acoustic variables

(c) the ability of the stochastic models to accurately predict measures of system effectiveness

(d) the choice of a stochastic model and estimation of its inputs, for a particular scenario.

The ideal way to address these would be to compare stochastic simulations with measured acoustic and performance data for many ocean environments, sonar systems, and engagement geometries. However, the scope of the study and the availability of appropriate measurement data required the investigation to focus on a simplified test case for a representative acoustic environment, sonar system, and target.

A single ocean environment (in the Northeast Pacific during Summer) and target scenario have been selected for the test case. To ensure that the effects of the environmental acoustic parameters could be gauged, the study assumed a stable narrowband source (at 25 Hz), an idealized towed array receiver, and a processing system which automatically detects when the beam-output signal-to-noise ratio (SNR) exceeds a threshold. Evaluation of the random-process approach under these conditions then requires the detailed space/time properties of the transmission loss (TL) and ambient noise. A novel aspect of the present investigation is the use of state-of-the-art acoustic propagation and ambient-noise models to fabricate such a controlled, representative acoustic environment.

For the test scenario and target conditions, there is good reason to attribute fluctuations in TL to relative receiver movement through the source's multipath interference field (assuming little influence from ocean dynamics). The acoustic TL "data" were generated from models which fully account for this mechanism. Similarly, a special ambient noise model was developed to simulate the dominant noise fluctuation mechanism: movement of many contributing surface ships through the interference field.

Once signal and noise time series were constructed with the acoustic models, several of the more popular random-process models were used to simulate the series. Input parameters (the trend in TL, the variance and decorrelation scales of TL and noise) were determined directly from the acoustic data. Comparisons were then made of the statistical properties of the acoustically and stochastically modeled signal and noise, as well as of the detection properties of the signal-to-noise ratio.

The principal conclusion of the study, subject to the limitations in the test environment and data, is stated generally as:

- Given proper input parameters, the stochastic-process approach can produce adequate simulations of signal and noise. The accuracy is sufficient to provide useful estimates of detection probabilities and detection histories.

This result is tempered by the observations that:

- The accuracy and utility of the approach are greatly dependent on the availability of accurate input data (e.g., the variance of beam-noise fluctuations). Such data may be difficult to obtain, and without them the predictions will usually be poor.

- The accuracy also depends on the particular random process used. This study concentrated on the popular ones, and the agreement with acoustic data was just adequate. However, significant improvements can be realized when the basic statistical properties (e.g., marginal density) are tailored to the variable and case at hand.

A report* presents the details of the comparisons on which these judgements are based, and discusses the estimation of input data, the choice of a particular random-process model, and the prediction of measures of effectiveness.

The work was supported by the Naval Analysis Program of the Office of Naval Research (ONR 431).

EXPLANATORY NOTES FOR THE FIGURES, 1 THROUGH 24

1. Concentrate on the fluctuation submodel of a performance model. Usually a structured, random-process model depending on 2 or 3 input parameters, it provides a time series of fluctuations which in turn is added to the signal or noise or signal-excess time series.

*Cananagh, R.C., "Acoustic Fluctuation Modeling and System Performance Estimation," Final Report, Contract N00014-76-C-0753, Science Applications, Inc.; McLean, VA, January 1978.

2. A proper test of the random-process approach involves comparison of acoustic data with stochastic simulations. Agreement is gauged in terms of detection-related properties (e.g., level-crossings) of the time series.

3. Ideally, the test would involve comparisons of measured data with simulated data for many environments, sensors and conditions. The approach taken in the study was to focus on one environment and system. Also, state-of-the-art acoustic-model predictions were used in place of measured data.

4. & 5. Four questions were addressed in the study, and four general conclusions drawn.

6. A data base of acoustically modeled data was generated. Note that the Parabolic Equation model and a coherent version of the FACT model were used to construct complex pressure fields for waterborne and bottom-bounce paths respectively; the two fields were summed in phase. A detailed simulation of shipping noise was constructed with the DSBN noise model. In each case, the ocean medium is static, so that all fluctuations are due to source/receiver motion through the detailed multipath interference field.

7. Three target tracks were considered, two "tangential" to the array's broadside beam and one radially closing.

8. The "acoustic" data base is shown. It serves as the control data for the test of the "stochastic" data.

9. Three random-process models were considered, and their properties are summarized.

10. The random-process models provide an additive, dB fluctuator X(t) for the variable Z(t), be it signal or noise or signal-to-noise ratio. Note that signal fluctuations are derived from transmission loss (TL) and range rate.

11. Although the picture does not have proper resolution, the acoustically-modeled TL fluctuations in range are compared for various scales of trend removal. The "trend" might be thought of as the deterministic part, presumably a quantity which can be predicted with confidence.

12.&13. Some statistical properties of the acoustically-modeled TL fluctuations are shown.

14.&15. Compare properties inherent to the random-process models with those of 13. and 14. Notable discrepancies include the symmetry properties of the distributions of TL and the form of the autocovariance. Best agreement was for the Jump process added to the 2-nm intensity-averaged TL.

16. Acoustically modeled, omnidirectional ambient noise had properties consistent with those inherent to the random processes.

17. Beam noise, on the other hand, can be a complicated function of steering angle and beam width, as illustrated.

18. Some properties of the acoustically modeled beam-noise fluctuations are shown. Comparison with stochastic data showed reasonable good agreement when the Jump model was used with accurate inputs.

19. Finally, consider SNR and a detector which detects when SNR exceeds a threshold (the case when there is much incoherent averaging of filter outputs). For the special case at hand, fluctuations are driven by:

(a) Signal fluctuations caused by changes in target range (R(t))

(b) Signal fluctuation caused by changes in target bearing ($\phi(t)$) which affect array signal gain

(c) Noise fluctuations caused by ship movements in R and ϕ.

20. Acoustically simulated SNR for the tangential target (Track 1) as seen on two neighboring beams is shown. The variations are dominated by noise and the signal gain.

21. For the same noise sources as 20, the acoustically modeled SNR for the radial target (track 3) is shown for both short and long range cases. In the former, the rapid bottom-bounce variations are apparent.

22., 23. & 24. Detection-related statistics for the acoustic and stochastic data are compared. The best stochastic models and perfectly accurate inputs were used. The judgement of "adequate" agreement is based on such comparisons as these.

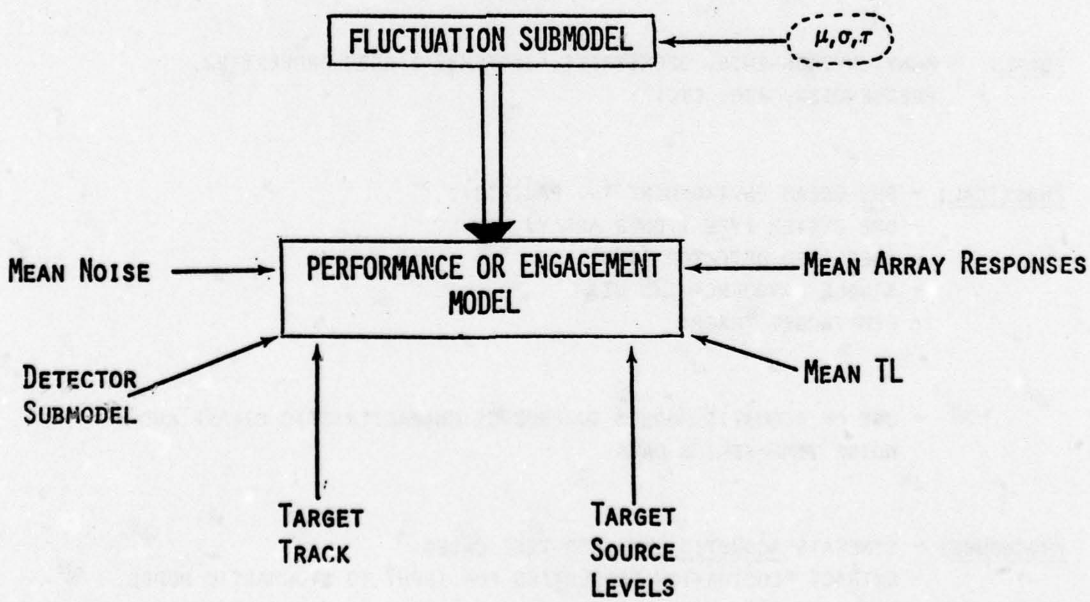

Figure 1

TEST OF THE RANDOM-PROCESS APPROACH

- GIVEN REAL SIGNAL AND NOISE FLUCTUATION DATA: ACOUSTIC DATA

- EXTRACT INPUT PARAMETERS FOR RANDOM-PROCESS MODELS

- USE POPULAR RANDOM-PROCESS MODELS TO SIMULATE SIGNAL AND NOISE TIME SERIES: STOCHASTIC DATA

- QUESTION: CAN THE RANDOM-PROCESS APPROACH ADEQUATELY SIMULATE SIGNAL, NOISE, SNR?

Figure 2

APPROACH

IDEAL: - MANY ENVIRONMENTS, GEOMETRIES, SYSTEMS, TARGET PROPERTIES, FREQUENCIES, ETC, ETC.

PRACTICAL: - ONE OCEAN ENVIRONMENT (N. PACIFIC)
- ONE SYSTEM TYPE (TOWED ARRAY)
- IDEALIZED DETECTOR (SNR)
- SINGLE FREQUENCY (25 Hz)
- FEW TARGET TRACKS

- USE OF ACOUSTIC MODELS TO PRODUCE CHARACTERISTIC SIGNAL AND NOISE TIME-SERIES DATA

PROCEDURE: - GENERATE ACOUSTIC DATA FOR TEST CASES
- EXTRACT FLUCTUATION PROPERTIES FOR INPUT TO STOCHASTIC MODEL
- SIMULATE DATA WITH RANDOM-PROCESS MODELS TO YIELD STOCHASTIC DATA
- COMPARE BASIC STATISTICS, LEVEL-CORSSING PROPERTIES, DETECTION HISTORIES

Figure 3

QUESTIONS

(1) WHAT ARE BASIC STATISTICAL PROPERTIES OF ACOUSTIC SIGNAL AND NOISE DATA?

(2) CAN RANDOM-PROCESS MODELS SIMULATE ACOUSTIC DATA?

(3) CAN RANDOM-PROCESS APPROACH ADEQUATELY PREDICT MOE'S?

(4) HOW CAN PREDICTIVE ACOUSTIC MODELING AID RANDOM-PROCESS APPROACH?

Figure 4

CONCLUSIONS

(1) ACOUSTIC DATA HAVE EXPECTED PROPERTIES.

(2) GIVEN ACCURATE INPUTS, RANDOM-PROCESS MODELS GIVE ADEQUATE SIMULATION OF SIGNAL, NOISE, AND SNR.

(3) RANDOM-PROCESS APPROACH CAN BE IMPROVED.

(4) PREDICTION OF INPUT DATA IS BIGGEST PROBLEM.

Figure 5

ACOUSTIC DATA

- TRANSMISSION LOSS:
  - TL(R)
  - PE + CFACT
  - SIMPLIFIED ENVIRONMENT
  - 1/6 NM SAMPLING RATE
- ARRAY:
  - SHADED, HORIZONTAL LINE
  - 8° AND 4° BEAMWIDTHS, STEERED NEAR BROADSIDE AT 0° T
  - 30 AND ∞ DB SIDELOBE SUPPRESSION
  - PERFECTLY STRAIGHT AND STATIONARY WITH IDEAL, PLANE-WAVE RESPONSE, $AG(\phi)$
- SIGNAL:
  - SL CONSTANT
  - CONSTANT VELOCITY TARGET TRACKS: $(R(\tau),\phi(\tau))$ WITH 5 KNOT SPEED
  - $S(\tau) = SL-TL(R(\tau)) + AG(\phi(\tau))$
- NOISE:
  - LIKE SIGNAL MODEL, BUT MANY SHIP SOURCES
  - SHIPS DISTRIBUTED ON LANES ROUGHLY EAST-WEST
  - RANDOM COURSE, SPEED, SOURCE LEVEL, ARRIVAL TIMES
  - INCOHERENT SUM OF SOURCES

Figure 6

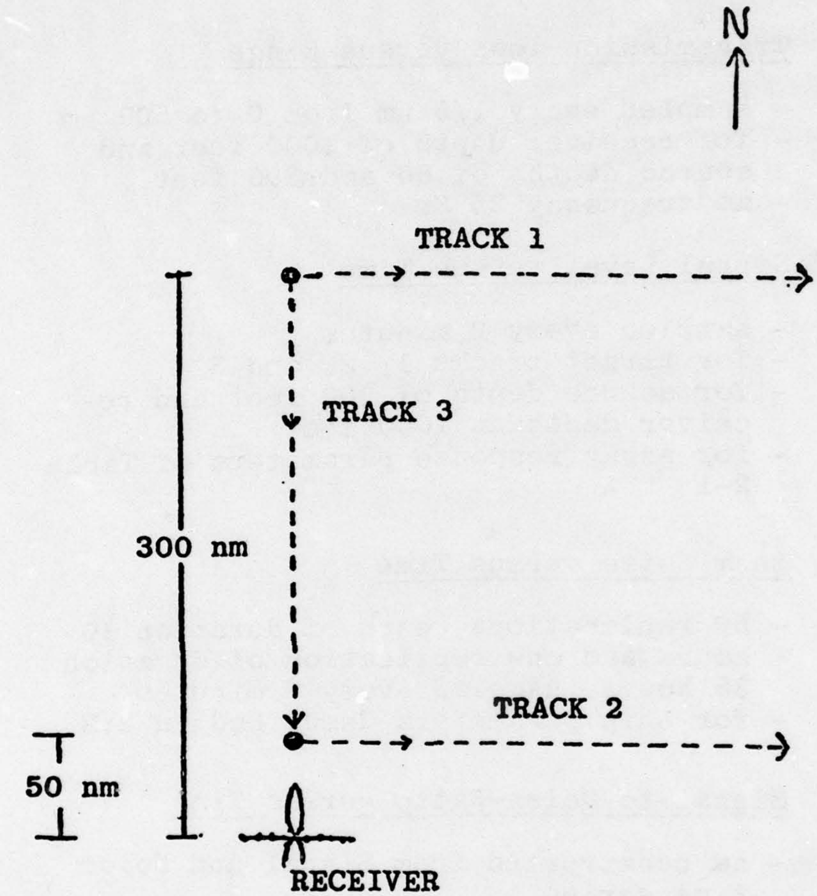

TARGET TRACKS

Figure 7

- **Transmission loss versus Range**
  - sampled every 1/6 nm from 0 to 500 nm
  - for receiver depth of 1000 feet and source depths of 60 and 300 feet.
  - at frequency 25 Hz

- **Signal Level versus Time**
  - sampled every 2 minutes
  - for target tracks 1, 2, and 3
  - for source depth of 300 feet and receiver depth at 1000 feet
  - for array response parameters of Table 2-1

- **Beam Noise versus Time**
  - 50 replications, each of duration 10 hours and one replication of duration 35 hours, sampled every 2 minutes
  - for ship parameters described in 2.2

- **Signal-to-Noise-Ratio versus Time**
  - as constructed from Signal and Noise time series

- **Range-Averaged TL**
  - 2 nm and 5 nm intensity averages for above cases
  - A+BlogR fit (LMS) over 0-100 and 100-500 nm

Figure 8

	GM	Gauss-Jump	Ehrenfest
Parameters	μ,σ,λ	μ,σ,λ	n
Index Set	$t\varepsilon[0,T]$	$t\varepsilon[0,T]$	$k = 0,1,2,\ldots$
Sample Paths	continuous, nowhere differentiable	piece-wise constant, discontinuous at jumps	discrete (paths constructed by interpolation)
Joint Density	2-dimensional Gaussian	Not Gaussian	—
Marginal Density	Gaussian (μ,σ^2)	Gaussian (μ,σ^2)	Binomial (normalized)
Autocovariance Function	$\sigma^2 e^{-\lambda\|t\|}$	$\sigma^2 e^{-\lambda\|t\|}$	$(\frac{n-2}{n})^k$
Decorrelation Time	$1/\lambda$	$1/\lambda$	$-1/\ln(\frac{n-2}{n})$
Power Spectrum	$\frac{2\sigma^2}{\omega^2+\lambda^2}$	$\frac{2\sigma^2}{\omega^2+\lambda^2}$	—

Level-Crossing Properties for the Gauss-Jump:

- Expected Waiting Time for Jump Process to Exceed L

$$= (1/\lambda)(1-P_D)/P_D \qquad (3\text{-}1)$$

- Probability that Jump Process Exceeds L Sometime in Interval [0,T]

$$= 1-(1-P_D)\exp(-P_D T/\lambda) \qquad (3\text{-}2)$$

where P_D is the probability that a Gaussian variable (μ,σ^2) exceeds L.

Some Properties of Stochastic Processes

RANDOM-PROCESS MODELS

Figure 9

USE OF RANDOM-PROCESS MODELS

VARIABLE: $Z(\tau)$ (dB's)

RANDOM PROCESS: $X(\tau)$

SIMULATION: $\hat{Z}(\tau) = \bar{Z}(\tau) + X(\tau)$

<u>FOR NOISE</u>: $\bar{Z}(\tau) = \bar{Z}$

<u>FOR TL</u>: $\hat{TL}(R) = \bar{TL}(R) + X(R)$

$$\hat{TL}(R(\tau)) = \bar{TL}(R(\tau)) + X(R(\tau))$$

Figure 10

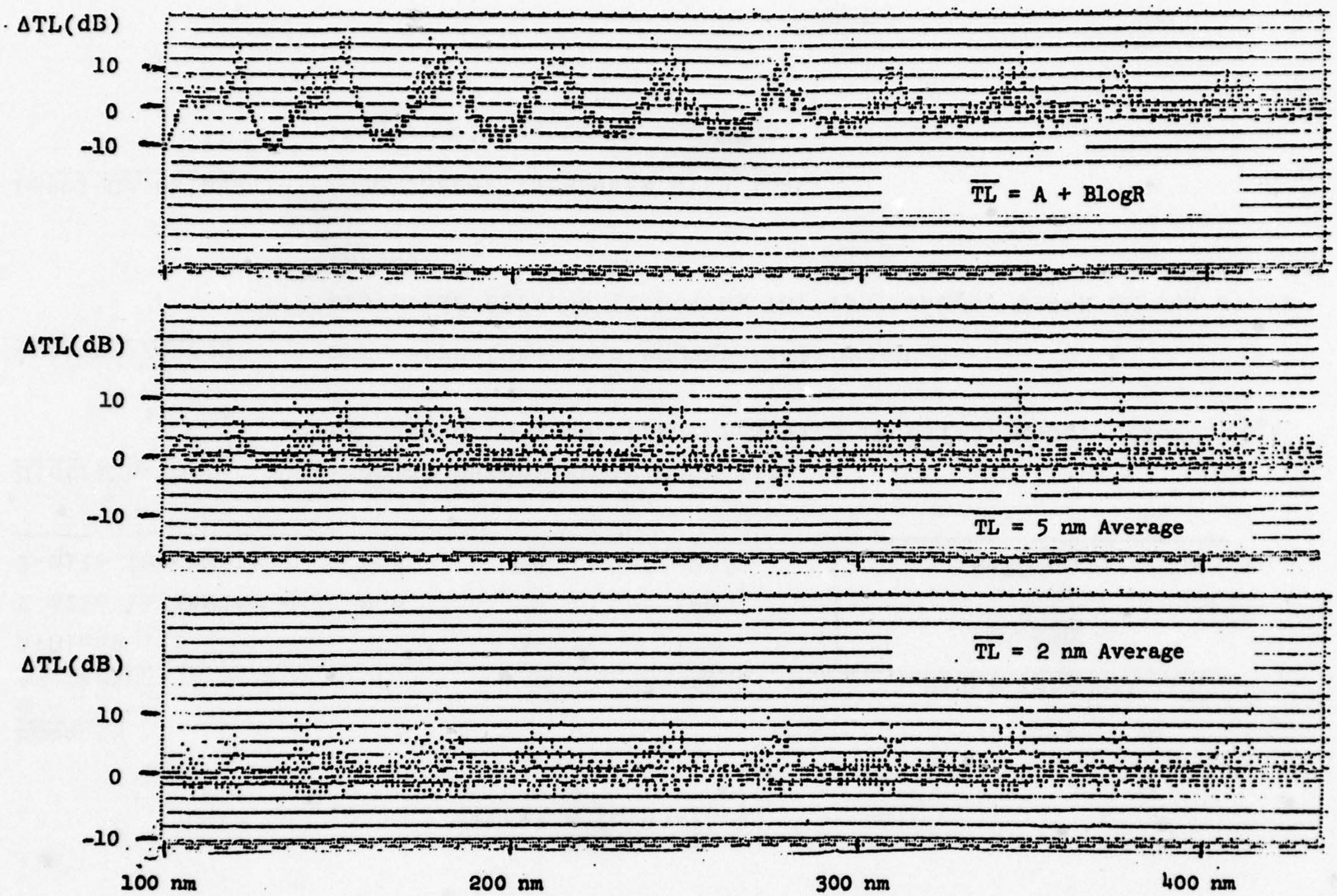

$\Delta TL = TL - \overline{TL}$

Fluctuation of TL with Range

Figure 11

SUMMARY OF PROPERTIES OF ACOUSTICALLY MODELED TL FLUCTUATIONS

$$\Delta TL(R) = TL(R) - \overline{TL}(R)$$

- **Moments**

Averaging	μ	σ	skewness	Range Interval
A+BlogR fit	0	5-7	1-2	100-500 nm
2-mile intensity	0.6	2	1-2	100-500 nm
2-mile intensity	1.5	4	2	2-75 nm

- **Distribution**: log-normal intensity is poor fit
  chi-square or non-central chi-square (2 d.f.), good. (for $-\Delta TL$)

- **Autocovariance**: - more structure than exponential decay
  - preferred periods (1.5-4 nm for long range, 0.5-2 nm for short range)

- **Level-Crossings**: - more longer intervals with TL>L
  - longer waiting times for TL<L

Figure 12

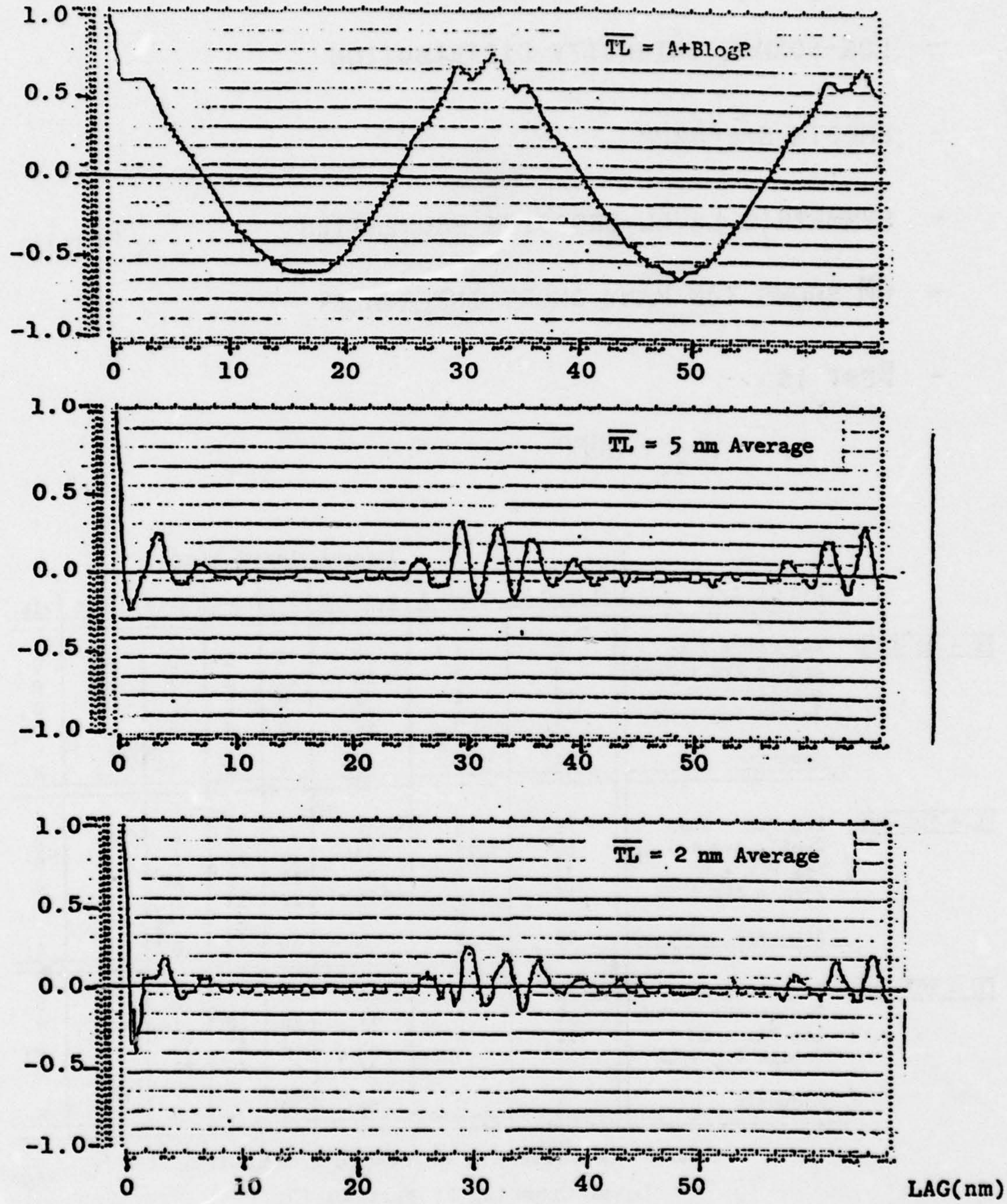

Autocovariance Functions for TL Fluctuations
Over Range Interval 100-500 nm

Figure 13

STOCHASTICALLY MODELED TL FLUCTUATIONS

- LOG-NORMAL INTENSITY DISTRIBUTION
- SMOOTH SPECTRUM
- SYMMETRIC LEVEL-CROSSING PROPERTIES
- GM SHOWS TOO MANY SHORT INTERVALS
- BEST IS

$\overline{TL}_2$ + JUMP

Figure 14

		Interval Length k(nm)							
	Simulation	0.16-0.2	0.2-0.5	0.5-1.0	1-2	2-4	4-10	10-16	>16
L = 99 dB	Log Fit + Jump	1	1	0	1	1	0	3	0
	2-mile Avg + Jump	9	7	12	11	5	2	0	0
	Log Fit + GM	18	8	8	9	2	1	0	0
	2-mile Avg + GM	34	6	12	6	3	3	0	0
	Acoustic	2	1	9	6	4	3	0	0
L = 103 dB	Log Fit + Jump	1	0	1	2	2	6	6	2
	2-mile Avg + Jump	15	15	23	15	11	6	3	0
	Log Fit + GM	33	7	24	11	9	6	7	0
	2-mile Avg + GM	18	26	35	26	11	6	3	0
	Acoustic	12	3	30	30	7	0	2	4
L = 107 dB	Log Fit + Jump	0	1	0	0	2	3	4	8
	2-mile Avg + Jump	12	10	12	16	10	11	2	7
	Log Fit + GM	26	4	10	21	10	10	4	4
	2-mile Avg + GM	47	17	17	22	10	12	7	3
	Acoustic	1	3	24	20	7	6	1	8

Number of Intervals of Length k with TL<L

Level-Crossing Properties TL:

Over Ranges 100-500 *nm*

Figure 15

ACOUSTICALLY MODELED OMNI NOISE

- NUMBER OF SHIPS: ABOUT 150-160
- TYPICAL σ OVER 10 HOURS: LESS THAN 3 dB
- AUTOCOVARIANCE: EXPONENTIAL, WITH τ BETWEEN 0.5 AND 2 HOURS
- SKEWNESS: GREATER THAN 1
- DISTRIBUTION: WHEN NOT TOO MANY NEARBY SHIPS, CHI-SQUARE (HIGH D.F.) OR LOG-NORMAL

Figure 16

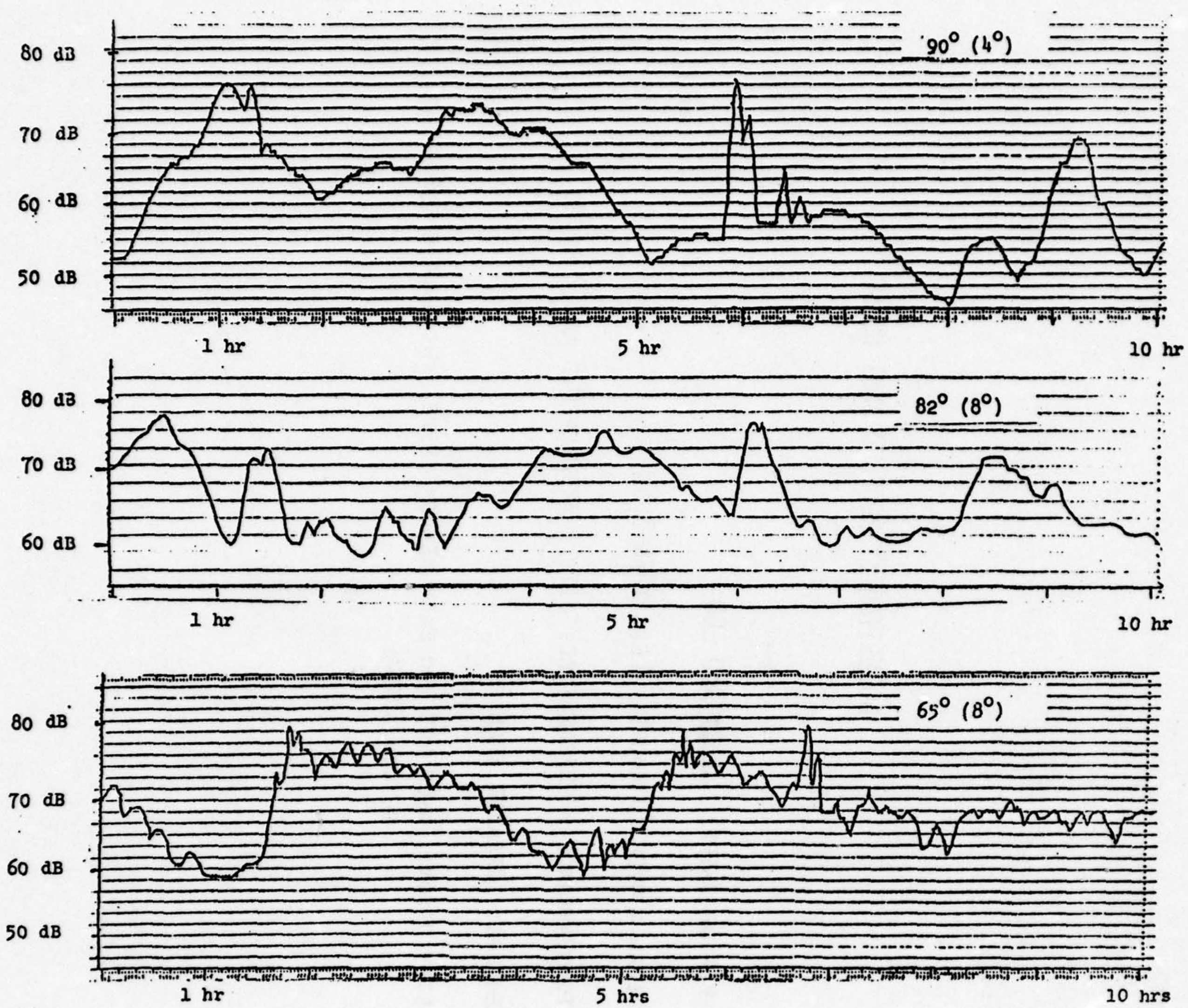

Beam Noise Time Series (Case 2)

Figure 17

BEAM-NOISE FLUCTUATIONS

<u>Acoustically Modeled Data</u>

- <u>Moments</u>:
  - as beamwidth decreases, variance increases, skewness decreases toward zero
- <u>Distribution</u>:
  - Consistent with chi-square theory
  - But nearby ships can result in bimodal distribution
- <u>Autocovariance</u>:
  - Fit well with decaying exponentials, 0.5 hrs $< \tau <$ 2 hrs
  - Long-term trends dominate (ships nearly tangential)
  - TL fluctuations can be important when radial speeds increase

<u>Stochastically Modeled Data</u>

- Although distribution shape depends on beam width, the Jump model was in reasonable agreement

Figure 18

SIGNAL-TO-NOISE RATIO (SNR)

$$SNR(\tau) = SL - TL(R(\tau)) + AG(\phi(\tau)) - N(\tau)$$

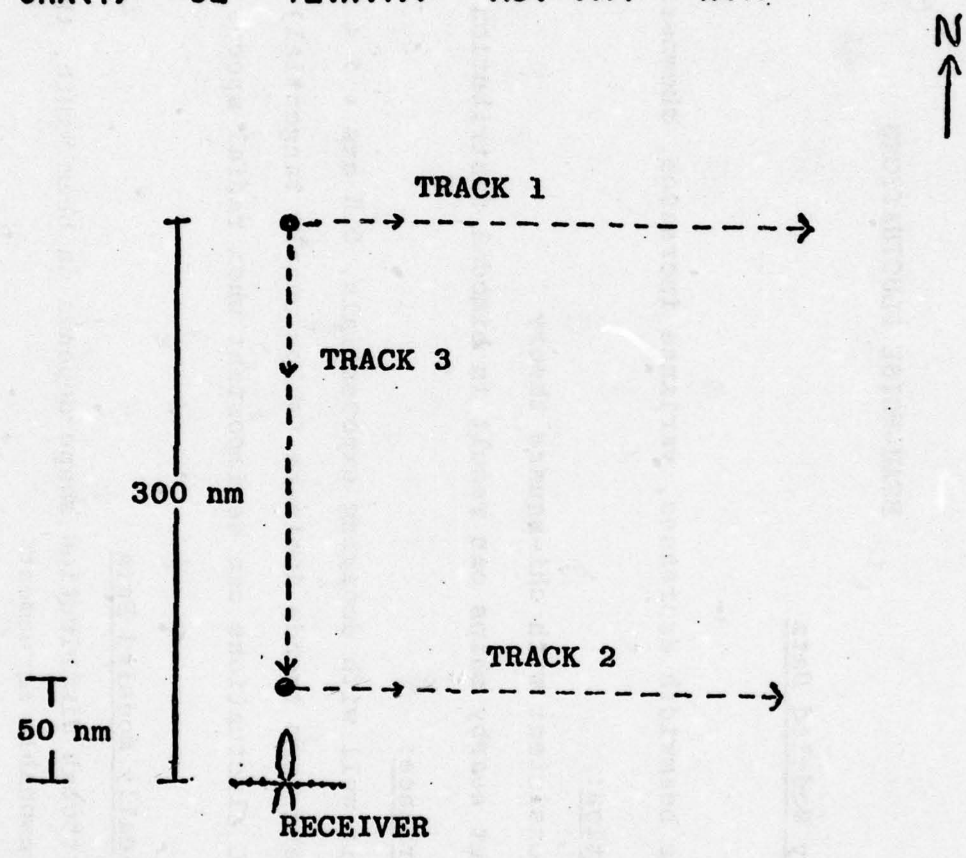

TARGET TRACKS

Figure 19

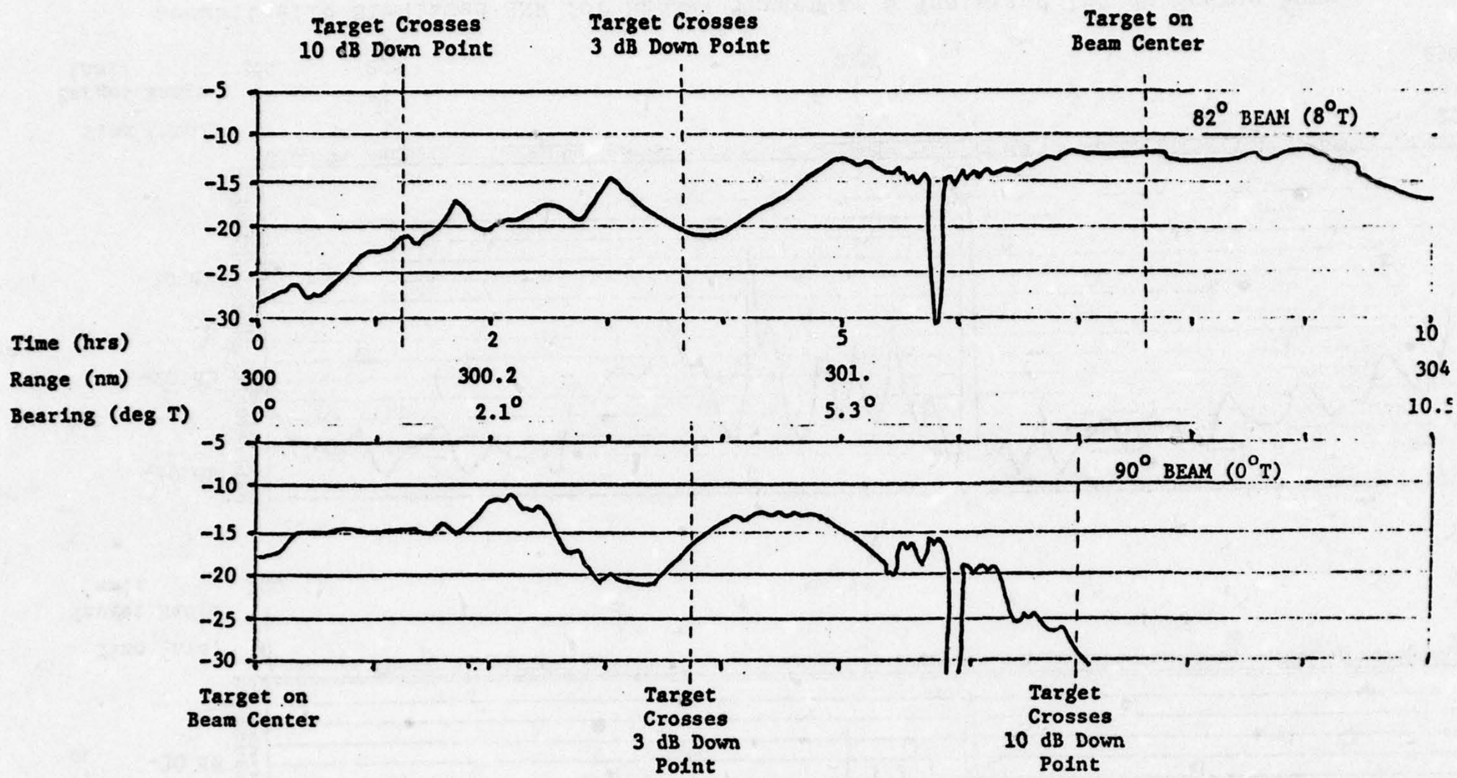

Acoustically Simulated SNR for 5-knot Tangential Target at 300 nm

Figure 20

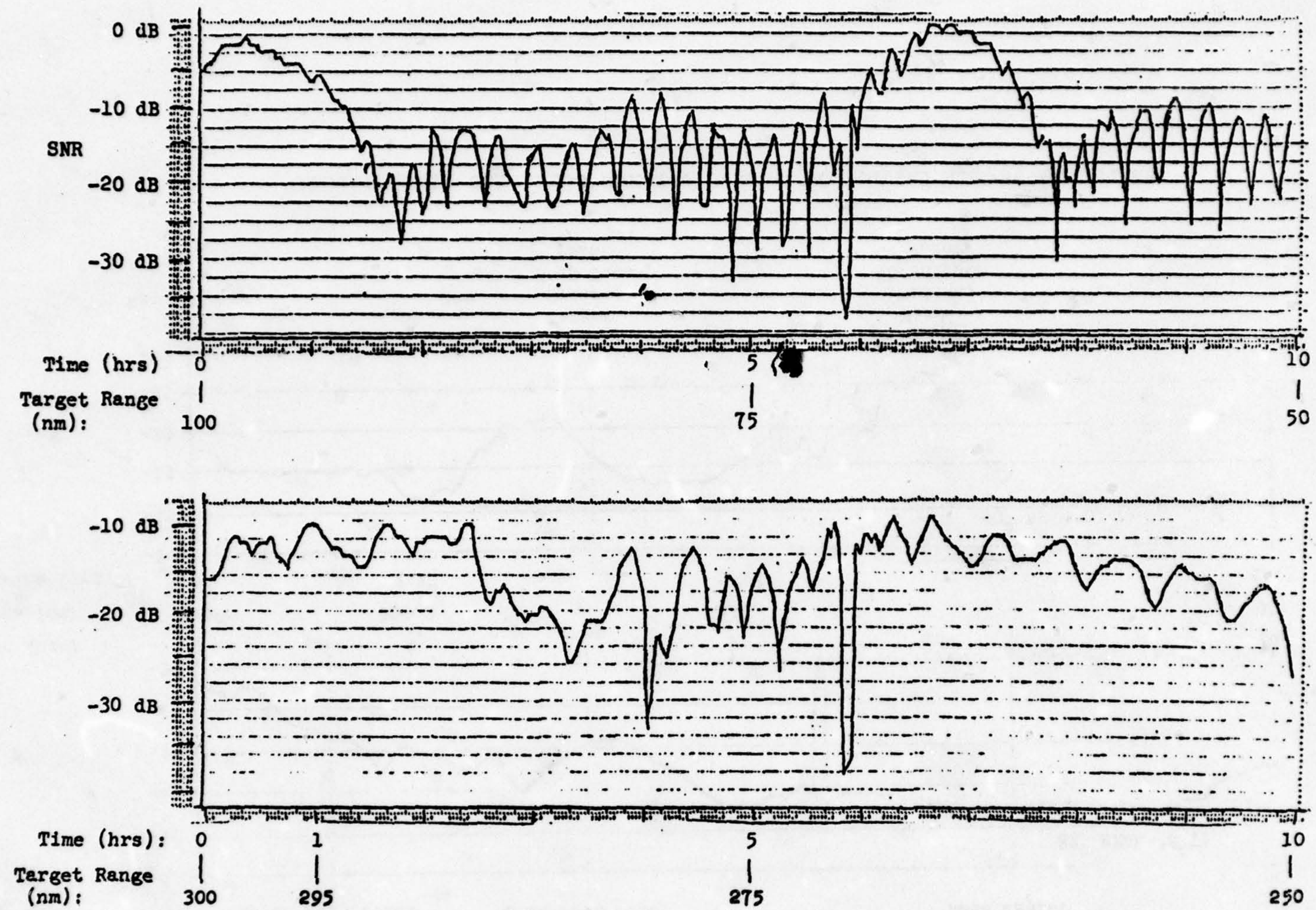

Acoustically Simulated SNR for Radial Target at 5 Knots and 155 dB Source Level
Array Steering = 90° (0°T), Target Bearing = 0°T

Figure 21

Property	Simulation	$R_D \simeq -11$ dB ($\overline{SE} \simeq -4$ dB)	$R_D \simeq -15$ dB ($\overline{SE} \simeq 0$ dB)	$R_D \simeq -19$ dB ($\overline{SE} \simeq +4$ dB)
P_D for 2-min. Detector	Stochastic	.16	.50	.84
	Acoustic	.15	.46	.83
P_D for 10-min. Dectector	Stochastic	.13	.43	.83
	Acoustic	.13	.42	.76
P_D for 30-min. Detector	Stochastic	.12	.30	.71
	Acoustic	.12	.35	.64
60-minute CP_D for 2-min. Detector	Stochastic	.36	.78	.95
	Acoustic	.28	.72	.93
Expected Waiting Time for Detection by 2-min. detector (minutes)	Stochastic	190	35	7
	Acoustic	210	40	4
Expected Waiting Time for Loss of Contact by 2-min. Detector (minutes)	Stochastic	7	35	190
	Acoustic	7	25	65

*Values labeled "Acoustic Simulation" are derived from averages over 50 ten-hour replications of the acoustic noise model.

*Values labeled "Stochastic Simulation" are averages over many sample paths for the Gauss-Jump model of noise using the acoustically-derived parameters:

$(\mu, \sigma, \tau) = (67.1, 3.7, 36)$.

Comparison of Acoustically and Stochastically Modeled Detection Propertie for Tangential Target on Broadside Beam of 8° Width and at Range 300 nm

Figure 22

Property	Simulation	$R_D \simeq -6$ dB	$R_D \simeq -12$ dB	$R_D \simeq -18$ dB
P_D for 2-min. Detector	Stochastic	.27	.46	.71
	Acoustic	.21/.26/.31	.41/.46/.50	.69/.71/.77
P_D for 10-min. Detector	Stochastic	.14	.29	.53
	Acoustic	.13/.15/.23	.27/.28/.32	.41/.49/.50
P_D for 30-min. Detector	Stochastic	.04	.16	.30
	Acoustic	.06/.09/.16	.16/.19/.23	.25/.31/.35
60-minute CP_D for 2-min. Detector	Stochastic	.63	.90	1.0
	Acoustic	.42/.50/.55	.72/.80/.83	.97/.99/1.0
Expected Waiting Time for Detection by 2-min. Detector (minutes)	Stochastic	49	15	4
	Acoustic	76/84/100	20/27/40	2/4/7
Expected Waiting Time for Loss of Contact by 2-min. Detector (minutes)	Stochastic	5	12	25
	Acoustic	4/5/11	12/14/18	21/25/28

*Values labeled "Acoustic Simulation" are 20th, 50th, 80th percentiles over 10 ten-hour replications of the acoustic noise and signal.

*Values labeled "Stochastic Simulation" are averages over many sample paths of SNR, using the:

-Gauss-Jump model for noise with $(\mu, \sigma, \tau) = (67.1, 3.7, 36)$

-Gauss-Jump + 2-mile average TL for signal

Comparison of Acoustically and Stochastically Modeled Detection Properties*
for 5-knot Radial Target on Broadside Beam of Width 8°, at Ranges 100-50 nm

Figure 23

Property	Simulation	$R_D \simeq -6$ dB	$R_D \simeq -12$ dB	$R_D \simeq -18$ dB
P_D for 2-min. Detector	Stochastic	.04	.28	.70
	Acoustic	.00/.05/.12	.21/.32/.48	.70/.75/.84
P_D for 10-min. Detector	Stochastic	.00	.19	.58
	Acoustic	.00/.02/.04	.11/.22/.44	.58/.65/.71
P_D for 30-min. Detector	Stochastic	.00	.11	.44
	Acoustic	.00/.00/.00	.00/.20/.29	.39/.53/.55
60-minute CP_D for 2-min. Detector	Stochastic	.26	.58	.96
	Acoustic	.00/.17/.35	.48/.65/.72	.87/.97/1.0
Expected Waiting Time for Detection by 2-min. detector (minutes)	Stochastic	130	60	7
	Acoustic	132/206/600	38/46/98	2/6/15
Expected Waiting Time for Loss of Contact by 2-min. Detector (minutes)	Stochastic	0	7	46
	Acoustic	0/0/2	3/10/24	40/48/70

*Values labeled "Acoustic Simulation" are 20th, 50th, 80th percentiles over 10 ten-hour replications of the acoustic noise and signal.

*Values labeled "Stochastic Simulation" are averages over many sample paths of SNR, using the:

-Gauss-Jump model for noise with $(\mu, \sigma, \tau) = (67.1, 3.7, 36)$

-Gauss-Jump + 2-mile average TL for signal

Comparison of Acoustically and Stochastically Modeled Detection Properties*
For 5-knot Radial Target on Broadside Beam of Width 8^{o}, at Range 300-250 nm

Figure 24

BEAM OUTPUT FLUCTUATIONS ON TWO TOWED ARRAYS

Andrew G. Fabula

(See Volume 2)

FLUCTUATIONS DUE TO RANGE RATE

Ira Dyer
Massachusetts Institute of Technology
Cambridge, Massachusetts

(Editorial Note: A full text of this paper has not been received. The following editorial summary is provided to give guidance to the reader.)

The purpose of this research is to determine the effects of platform motion on the received signal. Assume source/receiver are in relative motion V and a signal at single frequency ω_o is transmitted. Let the ocean be hypothesized "frozen." It is then required to find the frequency shift ω_a as a function of cross-over angle θ_o, and velocity V. Evidently, θ_o depends on the sound speed profile of the channel. Choose a convenient profile and with it the energy $E(\theta_o)$ of the ray at cross-over angle θ_o. The N normalized autocorrelation $\gamma(\tau)$ of the sinusoid at delay τ is then calculated. From this one derives an expression for the N normalized power spectrum $F(\omega)$ of the fluctuation of the received signal due to range rate as a function of the energy of a ray traversing the sound speed profiles selected. From $F(\omega)$ one can obtain mean, variance of this fluctuation. Three types of channel analyzed are (1) isospeed, (2) bilinear, (3) Munk. The conclusion is that the range rate spectrum is not sensitive to static background model of the sound speed profile. Next, a comparison is made between fluctuation due to range rate and that due to internal waves. From this comparison a critical range-rate is found which provides a frequency shift just equal to that of internal waves.

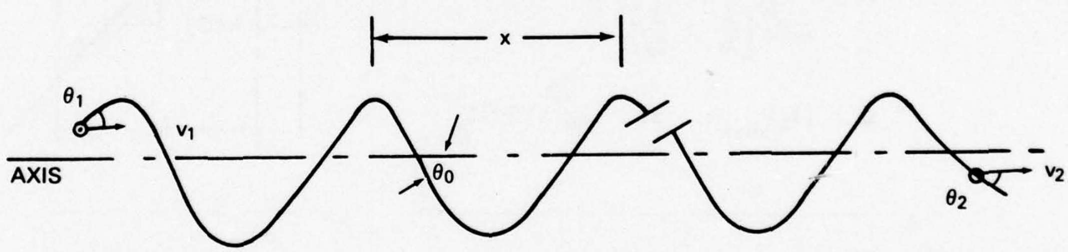

$$\omega_i = \omega_0 + \frac{d\beta}{dt} = \omega_0 \left[1 + \frac{V\cos\theta_0}{C_0}\right]; \qquad V = v_1 - v_2$$

$$\omega_d \equiv \omega_0 \left[1 + \frac{V}{C_0}\right]$$

$$\omega_a = \omega_i - \omega_d = -k_0 V(1 - \cos\theta_0)$$

$$\gamma(\tau) = \frac{1}{N}\int_{-\theta_\ell}^{\theta_\ell} E(\theta_2)\cos\omega_a\tau\, d\theta_2 \, ; \qquad N = \int_{-\theta_\ell}^{\theta_\ell} E(\theta_2)\, d\theta_2$$

$$E(\theta_2) = \frac{2D_s(\theta_1)\exp(-Q)}{RX(\theta_2)\tan|\theta_1|}$$

$$F(\omega) = \int_{-\infty}^{\infty} \gamma(\tau)e^{-i\omega\tau}\,d\tau\ ; \qquad \gamma(\tau) = \frac{1}{2\pi}\int_{-\infty}^{\infty} F(\omega)e^{i\omega\tau}\,d\omega$$

$$\boxed{F(\omega) = \frac{\pi}{N}\int_{-\theta_\ell}^{\theta_\ell} E(\theta_2)\left[\delta(\omega+\omega_a) + \delta(\omega-\omega_a)\right]d\theta_2}$$

BILINEAR CHANNEL

$$E(\theta_2) = \frac{e^{-\alpha R}}{RC_0\left(\frac{1}{g_1}+\frac{1}{g_2}\right)\tan|\theta_0|\tan|\theta_1|}$$

$$\boxed{\Delta C_2 >> \Delta C_1}$$

$$N = \frac{e^{-\alpha R}}{RC_0\left(\frac{1}{g_1}+\frac{1}{g_2}\right)}\ \frac{\Phi_b}{\psi}$$

$$\psi = (\theta_0)_{max}\ ; \qquad \Omega = k_0|V|\psi^2/2$$

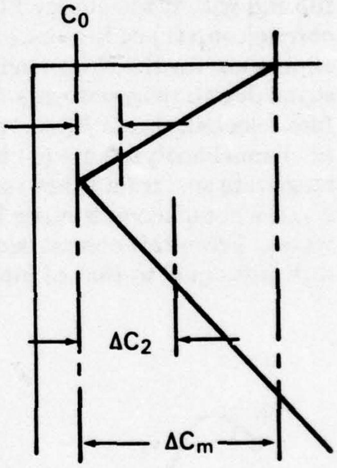

$$\boxed{\Omega F(\omega) = \begin{cases} 0 & 0 \leqslant \frac{|\omega|}{\Omega} < \frac{\Delta C_2}{\Delta C_m} \\[2ex] \frac{\pi}{2\Phi_b}\ \dfrac{1}{\frac{|\omega|}{\Omega}\sqrt{\frac{|\omega|}{\Omega} - \frac{\Delta C_2}{\Delta C_m}}} & \frac{\Delta C_2}{\Delta C_m} \leqslant \frac{|\omega|}{\Omega} \leqslant 1 \\[2ex] 0 & \frac{|\omega|}{\Omega} > 1 \end{cases}}$$

$$\left\langle \frac{|\omega|}{\Omega} \right\rangle = \frac{\Delta C_2}{\Delta C_m} \frac{\sqrt{\dfrac{1 - \Delta C_2/\Delta C_m}{\Delta C_2/\Delta C_m}}}{\tan^{-1}\sqrt{\dfrac{1 - \Delta C_2/\Delta C_m}{\Delta C_2/\Delta C_m}}} \; ; \qquad \left\langle \left(\frac{\omega}{\Omega}\right)^2 \right\rangle = \left(\frac{1}{3} + \frac{2\Delta C_2}{3\Delta C_m}\right) \left\langle \frac{|\omega|}{\Omega} \right\rangle$$

$$\boxed{\frac{\Delta C_2}{\Delta C_m} > \frac{2}{3}} \qquad \boxed{\gamma(\tau) = \cos\left(\frac{\Delta C_2}{\Delta C_m}\,\Omega\tau\right)\frac{C(u)}{u} - \sin\left(\frac{\Delta C_2}{\Delta C_m}\,\Omega\tau\right)\frac{S(u)}{u}}$$

$$u^2 \equiv \frac{2}{\pi}\,\Omega\tau\left(1 - \frac{\Delta C_2}{\Delta C_m}\right) \qquad \Omega\tau_{1/2} = \frac{\pi}{3}\,\frac{\Delta C_m}{\Delta C_2}$$

ISOSPEED CHANNEL

$$\left.\begin{aligned} E(\theta_0) &\approx \frac{1}{RD}\, e^{-\alpha R} e^{-\theta_0^2/\theta_\ell^2} \\ N &= \frac{\sqrt{\pi}\,\theta_\ell}{RD}\, e^{-\alpha R} \end{aligned}\right\} \text{small angles}$$

$$\boxed{\Omega F(\omega) = \begin{cases} \dfrac{\sqrt{\pi}\, e^{-\frac{|\omega|}{\Omega}}}{\sqrt{\dfrac{|\omega|}{\Omega}}} & 0 \leqslant \dfrac{|\omega|}{\Omega} \leqslant \left(\dfrac{\pi}{2\theta_\ell}\right)^2 \\ 0 & \dfrac{|\omega|}{\Omega} > \left(\dfrac{\pi}{2\theta_\ell}\right)^2 \end{cases}}$$

$$\Omega \equiv k_0 |V| \psi^2/2 \qquad \psi = \theta_\ell \qquad \text{for isospeed}$$

$$\left\langle \frac{|\omega|}{\Omega} \right\rangle = \frac{1}{2} \qquad \left\langle \frac{\omega^2}{\Omega^2} \right\rangle = \frac{3}{4}$$

$$\boxed{\gamma(\tau) = \frac{1}{\sqrt{2}}\left[\frac{1}{1 + (\Omega\tau)^2} + \frac{1}{\sqrt{1 + (\Omega\tau)^2}}\right]^{1/2}}$$

$$\Omega\tau_{1/2} = 2.54$$

MUNK CHANNEL

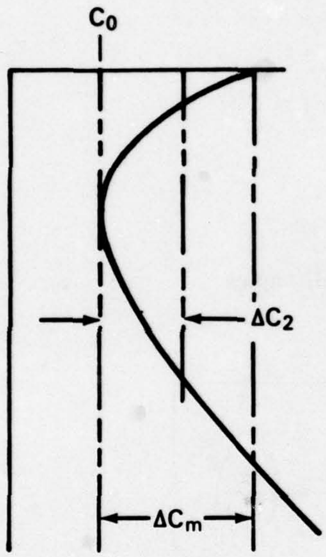

$$E(\theta_2) = \frac{2e^{-\alpha R}}{RB\pi\epsilon^{-1/2}(1 + 0.29\theta_0^2 + \ldots)\tan|\theta_1|}$$

$$\boxed{0.29 = \frac{\psi^2}{24\epsilon}}$$

$$N = \frac{4e^{-\alpha R}}{RB\pi\epsilon^{-1/2}}\Phi_m$$

$$\boxed{\Omega F(\omega) = \begin{cases} 0 & 0 \leq \dfrac{|\omega|}{\Omega} < \dfrac{\Delta C_2}{\Delta C_m} \\[2ex] \dfrac{\pi}{2\Phi_m}\,\dfrac{1}{\left(1 + 0.29\,\dfrac{|\omega|}{\Omega}\right)\sqrt{\dfrac{|\omega|}{\Omega}}\,\sqrt{\dfrac{|\omega|}{\Omega} - \dfrac{\Delta C_2}{\Delta C_m}}}, & \dfrac{\Delta C_2}{\Delta C_m} \leq \dfrac{|\omega|}{\Omega} \leq 1 \\[2ex] 0 & \dfrac{|\omega|}{\Omega} > 1 \end{cases}}$$

$$\boxed{\frac{\Delta C_2}{\Delta C_m} << 1} \qquad \left\langle \frac{|\omega|}{\Omega} \right\rangle \approx \frac{0.71}{\ell n \dfrac{\Delta C_m}{\Delta C_2} - 0.29}$$

$$\left\langle \left(\frac{\omega}{\Omega}\right)^2 \right\rangle \approx 0.57 \left\langle \frac{|\omega|}{\Omega} \right\rangle$$

COMPARISON WITH INTERNAL WAVE PHASE RATE

(1) ***in each path*, for internal wave perturbations:**

$$\nu_{rms} \approx 5.7 \times 10^{-8}\, \omega_0 \sqrt{R}_{km}\,, \qquad \text{rad/sec}$$

(2) ***over all paths*, for frozen ocean range-rate:**

$$\omega_{rms} = a\Omega = ak_0 |V| \psi^2/2 \qquad a \leqslant 1$$

(3) can define a critical range-rate, V_c, from:

$$\omega_{rms} = \nu_{rms}$$

$$\boxed{V_c = \frac{2C_0}{a\psi^2} \frac{\nu_{rms}}{\omega_0}}$$

(4) for $a = \frac{1}{2}, \quad \psi^2 = 6 \times 10^{-2}\ (\psi = 14°)\,, \quad R = 10^3$ **km**

$$V_c \sim 0.2 \text{ m/sec} \sim 0.4 \text{ knot}$$

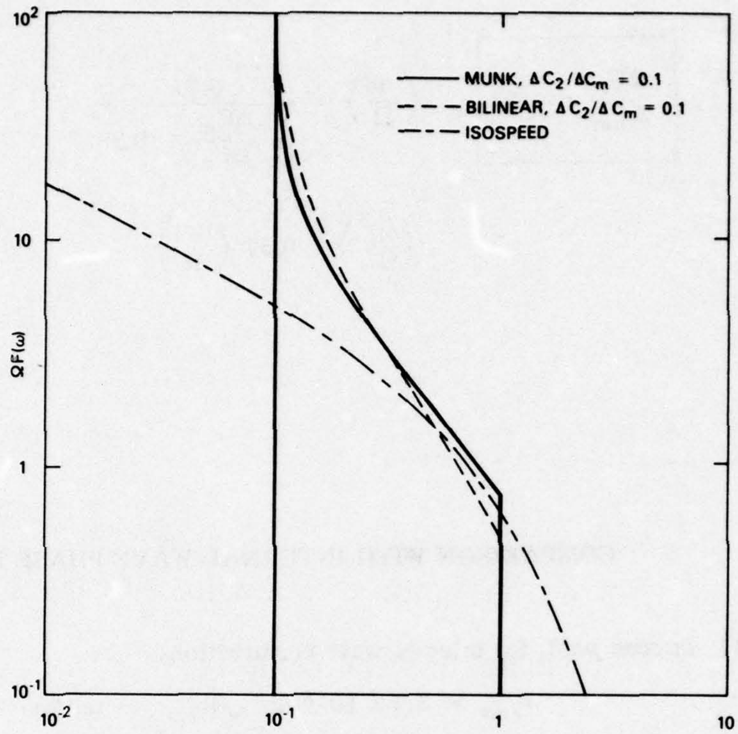

MUNK, $\Delta C_2/\Delta C_m = 0.1$
BILINEAR, $\Delta C_2/\Delta C_m = 0.1$
ISOSPEED
10^2
10
1
10^{-1}
$\Omega F(\omega)$
10^{-2}
10^{-1}
1
10
ω/Ω

THE IMPORTANCE OF SOURCE MOTION, RECEIVER ORIENTATION, AND THE OCEAN ENVIRONMENT

William Jobst
Institute of Acoustic Research
Miami, Florida

ABSTRACT

(U) When a signal transmitted from a moving source is observed at an array of sensors, the signal field fluctuates as functions of space, time, and frequency. The fluctuations may be characterized by the statistical moments of the received signal field—mean, variance, and joint second order moments typically called coherence. We examine coherence as a function of space, time and frequency using data from recent experiments in the Atlantic and Pacific. It is shown that the fluctuations in the received signal field are related to source motion, to receiver location and orientation, and to the ocean environment.

IMPACT OF SOURCE MOTIONAL FLUCTUATIONS

ON INTERARRAY SIGNAL COHERENCE

Albert A. Gerlach

(See Volume 2)

ACOUSTIC FLUCTUATIONS

The Woods Hole Oceanographic Institution and the Institute of Geophysics and Planetary Physics of the Scripps Institution of Oceanography

Robert C. Spindel
The Woods Hole Oceanographic Institution

The Woods Hole Oceanographic Institution and the Institute of Geophysics and Planetary Physics of the Scripps Institution of Oceanography are engaged in a cooperative research program to study the effects of oceanic variations on acoustic propagation. The objective of the joint program is to identify and quantify the role of ocean processes (internal wave induced temperature and current fluctuations, intrusive effects and finestructure, currents, mesoscale eddies, etc.) in determining the variability of sound transmission. The ultimate goals are to further our understanding of the fundamental limits on signal coherence in space and time and to develop techniques for monitoring the ocean acoustically. Scientists at both institutions have been active in acoustic fluctuation research for a number of years. Woods Hole has concentrated on low frequency (100–400 Hz), narrowband, long range (10–1500 km) transmissions whereas IGPP has focused on high frequency (2250 Hz), wideband, short range (25 km) propagation. The former studies have emphasized moored sources and receivers and have resulted in fluctuation data as a function of range, depth and frequency. The latter, conducted from drifting ships, have yielded amplitude and travel time data along selected single paths.

THE WOODS HOLE PROGRAM

The Woods Hole deep ocean experiments have used primarily moored sources and receivers to minimize interactions with the ocean boundaries. Acoustic transmissions have been narrowband so that acoustic travel time variations are manifest as phase (as well as amplitude) fluctuations in the received signal. A precision Doppler acoustic position-keeping system has been developed to permit coherent phase measurements over ranges of several hundreds of kilometers. Phase and amplitude fluctuations are measured using remote digital receivers that record continuous time series of up to 60 days duration. The receivers contain a digital Doppler tracking device for 0.1 meter position-keeping. The moored acoustic sources have a comparable lifetime and transmit continuous tones at a level of 176 dB re 1 μPa.

Relating observed fluctuations to ocean processes is complicated by the multipath field. The random superposition of a large number of multipaths results in phase (or travel time) fluctuations that obscure those due to ocean variations. Even the phase of a single (ray) path may fluctuate widly because the sound velocity finestructure can split the ray into a number of fluctuating raylets or micromultipaths. Thus a single transmitted pulse can be received as a cluster of fluctuating pulses corresponding to totally chaotic

interference. The particular region in range-acoustic frequency space where this occurs is known as the saturated scattering region and roughly corresponds to long ranges and high frequencies. For short ranges and low frequencies scattering is negligible and phase (travel time) variations are relatable to mesoscale ocean processes. A systematics of acoustic fluctuation regimes based on acoustic-internal wave interaction has been developed (Dashen, Flatte, Munk, Zachariasen) to predict those frequency, time and range conditions under which micromultipaths are expected to dominate the received signal, and those regimes where phase (travel time) measurements can be related directly to observable mesoscale phenomena.

The Woods Hole effort has been devoted to perfecting techniques to permit coherent phase and travel time measurements to be made from deep ocean moored systems. The analysis of Woods Hole continuous tone phase and phase rate fluctuation data has underscored the important role that internal waves play in acoustic variability with periods of several minutes to a day. Woods Hole experiments have been accompanied by environmental ocean measurements such as temperature and current in order to permit the correlation of acoustic data with observed ocean variations. In addition, WHOI experiments have been designed to delineate weak and strong ocean scattering regimes so that the parameters of an ocean acoustic monitoring system can be defined.

THE IGPP PROGRAM

IGPP has performed short range, high frequency, ship-to-ship experiments using broadband pulse compression codes to measure directly acoustic travel time fluctuations. Pulse transmissions have allowed observation of strong micromultipath regions (near surface paths) and weak scattering regions (deep paths). Reciprocal pulse transmissions have enabled discrimination between currents and variable finestructure. IGPP is now constructing an encapsulated version of their digital processing apparatus so that the 2250 Hz transceivers can be moored. This eliminates travel time variations due to ship drift.

SOME NUMBERS

It is the goal of the collaboration between IGPP and WHOI to demonstrate the feasibility of monitoring mesoscale ocean processes via acoustic methods. Direct travel time measurements of transmitted pulses (or regenerated pulses from wideband transmissions) is the preferred mode of operation since it avoids the problem of multipath interference and resulting phase discontinuities inherent in continuous tone systems. A typical mesoscale feature has a temperature variation of about 2°C, a fractional change in sound speed of $\delta c/c \approx 5 \times 10^{-3}$, and a spatial extent of about 100 km. This large temperature anomaly is confined, for the most part, to the upper 500 m. Within this scale there will be two upper turning points each extending for about 20 km within the upper 500 m. The net travel time variation is about

$$\tau = \frac{\delta c}{c} \times \frac{2 \times 20 \text{ km}}{c} \approx 10^{-1} \text{ sec}.$$

Thus we require a system capable of 0.1 sec *accuracy* in travel time in order to detect the mesoscale feature. Multipaths will arrive with a separation of about 0.1 sec (including

only early arrivals and excluding the closely spaced late arrivals) so that a time *resolution* of 0.1 sec is required to separate paths. This implies a signal bandwidth of 10 Hz or more.

Consider now the errors associated with the required travel time measurements. At short ranges, or low frequencies, micromultipathing will contribute negligible jitter to the received signal. Error in travel time measurement arises solely through additive ambient noise. The rms travel time error due to noise is approximately

$$\sigma_t \approx \frac{1}{B\omega} \cdot \frac{1}{\sqrt{SNR}} \approx 10^{-2}\ \text{sec}$$

for an SNR of 20 dB and a transmitted band of 10 Hz. If phase coherent processing is used this error can be reduced to

$$\sigma_t \approx \frac{1}{220} \cdot \frac{1}{\sqrt{SNR}} \approx 0.5 \times 10^{-3}\ \text{sec}$$

for a 220 Hz carrier and a SNR of 20 dB. In either case it is clear that the requisite accuracy and resolution of 10^{-1} sec can be achieved in each transmission.

At long ranges and higher frequencies where scattering is saturated, micromultipaths may cause significant travel time jitter. Experimental evidence at 206 Hz and 500 km (MIMI) indicates that time jitter due to micromultipaths will be small ($\approx 10^{-2}$ sec) implying an ocean bandwidth of about 100 Hz. Theoretical formulations (Flatte) predict a somewhat smaller bandwidth, ≈ 20 Hz, but still sufficiently wide to support a 10 Hz bandwidth transmission and a resolution of 10^{-1} sec. If we take the lower of the two bandwidths, resolution will be of order 5×10^{-2} sec. This can be improved through simple averaging over multiple transmissions. Since decorrelation times are of the order of 200 sec, both from CW measurements (WHOI) and theory (Flatte) the time bandwidth product of the ocean for 500 km ranges and frequencies of several hundred Hz is about 2×10^4 Hz-sec. A 10 day experiment with a 10 Hz transmitted band results in

$$N = \frac{10\ \text{days} \times B6.4 \times 10^4\ \text{sec/day} \times 10\ \text{Hz}}{2 \times 10^4\ \text{Hz-sec}} \approx 400$$

independent estimates of travel time so that the achievable accuracy will be

$$\frac{1}{B\omega} \times \frac{1}{\sqrt{N}} \approx 5 \times 10^{-3}\ \text{sec}\,.$$

These simple calculations indicate that it should be entirely feasible to measure oceanic mesoscale processes by acoustic methods.

WHOI-IGPP EXPERIMENTS

A preliminary test of these notions is to be conducted during the spring of 1978. A moored version of the IGPP computer controlled high frequency transceivers will be

deployed at 25 km spacing together with WHOI continuous wave and 10 Hz bandwidth sources and receivers. The WHOI 10 Hz band source has a carrier frequency of 220 Hz modulated by a coded sequence. Reception is via a microprocessor controlled moored receiving capsule at ranges of 25 and 125 km. In addition, reception is scheduled to occur at remote hydrophones some 1000 km distant. The experiment is to last 10 days. The range of acoustic frequencies and distances spans predicted oceanic scattering regimes from weak to full saturation. A rather complete environmental measuring program including current meter and CTD stations will complement the acoustic experiment.

In the summer of 1978 WHOI will conduct another experiment in conjunction with an intense physical oceanographic experiment known as the Polymode Local Dynamics Array. The goal of the oceanographic experiment is to monitor, in detail, mesoscale processes in the Atlantic. The WHOI acoustic experiment consists of a continuous tone source placed as near to the center of a mesoscale eddy as possible, with three receivers on a 100 km radius from the source. The intent is to measure travel time anomalies, through phase variations, of a mesoscale process.

RANGE INDEPENDENT FLUCTUATIONS AND PATTERN RECOGNITION OF VERTICAL ANGLE OF ARRIVAL STRUCTURE

Fred H. Fisher

(See Volume 2)

OMNIDIRECTIONAL AMBIENT NOISE AS A FUNCTION OF DEPTH AND FREQUENCY IN THE DEEP NORTHEAST PACIFIC

J. A. Shooter

(See Volume 2)

MEASUREMENT OF CHARACTERISTICS OF AN ACOUSTIC PROPAGATION CHANNEL BY INVERSE FILTER

Harry A. DeFerrari and Robert F. Tusting
University of Miami
Rosenthal School of Marine and Atmospheric Science
Miami, Florida 33149

Several characteristics of a propagation channel, such as Doppler spectrum, scattering function, or pulse response, can be conveniently and rapidly computed in real-time, employing a small computer and the Fast-Fourier algorithm by the method of inverse filtering. We have used the method with good success in several experiments, both with on-line processing and post-processing of analog tapes.

We report results and examples from three broad-band experiments. The first is for transmission over 60 km between a fixed bottom-mounted source and receiver (750 Hz) carrier. The second is for towed source transmission at a range of from 35 to 100 km at speeds of from 3 to 8 knots. And the third is for transmission from a moored source to a moored set of receivers in the water column at a range of 90 km and, simultaneously, to a second moored hydrophone at a range of 270 km.

Inverse filtering consists of dividing the spectrum of the received signal $R(\omega)$ by the spectrum of the transmitted signal $S(\omega)$ in order to compute the system response of $H(\omega)$ of the channel.

$$H(\omega) = R(\omega)/S(\omega), \quad S(\omega) \neq 0 .$$

The system response function of the channel can then be transformed over the bandwidth of the transmitted signal to give a pulse response.

$$p(t) = \int_{-\Delta\omega}^{+\Delta\omega} R(\omega)/S(\omega)\, d\omega .$$

The inverse filter is known to perform poorly to noise, since the lower values of the spectrum are contaminated. However, for many ocean acoustic measurements, high signal-to-noise is available and desirable since the objective is to measure the range of fluctuation.

Augmented-linear-maximal-pseudo-random sequences (recommended to us by Metzger and Birdsall, University of Michigan) have the necessary nonzero spectrum for the transmitted signal. The sequences have length $N = 2^n$. The convenience and computational speed of the method is achieved by storing complex demodulates from M successive sequences to form a time series of length L.

$$M = 2^m$$

$$L = 2^{m+n}.$$

Processing consists of first, performing a Fast-Fourier transform on the time series of length L, resulting in N × M spectral line (demodulates are also stored on magnetic tape for post-processing). Any desired characteristics of the propagation channel can then be computed from spectral lines.

Denoting the index of each spectral line by

$$S_i, \quad i = 1, 2, 3, \ldots, L,$$

we note that

1. i = 1 identifies CW carrier line assuming 0 Doppler.

2. The broad-band signal strength is computed by averaging the spectral lines

$$\frac{1}{N} \sum_{p=0}^{N} S_{(p \times m+1)} .$$

3. The pulse response at zero Doppler is obtained by performing an inverse filter on the set of lines given by

$$S_{p \times m+1}, \quad p = 0, 1, 2, \ldots, N.$$

4. The Doppler shifted pulse response may reside in any of the lines separated by an interval of M lines.

5. The scattering function is computed by inverse filtering *all* sets of lines separated by an interval of M lines.

Doppler shift is readily observable, since the set of lines containing the signal energy can be observed to shift to another set. Doppler compensation can be accomplished by adjusting the demodulating clock frequency. In experiments where the source-motion is measured by other means, such as bottom navigation systems, the effects can be removed from the spectral response by adjusting each of the spectral lines for a time-varying phase, computed from the motion.

Several examples of time history of pulse responses, scattering functions, Doppler compensation and the removal of measured source and receiver motions are given and discussed.

MEASUREMENT TOOLS

Dave Keir

(See Volume 2)

APPENDIX B

SYNOPSIS OF FLUCTUATION WORKSHOP PAPERS
NOT SUBMITTED FOR PUBLICATION

(See Volume 2)

Appendix C

A REVIEW OF SIGNIFICANT PAPERS AT 94th ASA MEETING

Sam Hanish

PREFACE

From the very beginning, the Invited Papers and Evening Workshop on Ocean Fluctuations of the 94th Meeting of the Acoustical Society held 14 December 1977 were so highly specialized that any brief review in retrospect of the major papers will prove of little advantage, except to the deeply entrenched expert. It seems more appropriate to dwell a bit on the key issues here, in order to bring them into some focus and thus provide a background for appreciation of Workshop accomplishments. However, to keep the main ideas within bounds only the three principal invited papers, namely by Flatté, Dashen and Ellinthorpe will receive attention here. They cover a good portion of fluctuation modeling and experiment based on physics now current in this country. If one adds to them the work of Beran and McCoy, a rather representative total of the fluctuation modeling in the ocean becomes available. Although McCoy made some remarks at the Workshop the effort of the Session was clearly directed toward review of the work of the three people quoted. We begin then with some general remarks on the subject.

SCHOOLS OF RESEARCH IN FLUCTUATIONS OF ACOUSTIC SIGNALS IN THE OCEAN

Several schools of research are currently playing a role in ocean acoustic fluctuations. Each professes to have a reasonably complete phenomenological theory of the physics. However, upon examination it is found that the completeness of the theory is *potential* rather than proven. In actual work only small portions of the theoretical models are adapted to numerical calculation and/or experimental verification. The distinction between schools therefore rests on proven parts of the models to date rather than on their potential completeness, which is about the same for all.

The first school is that of the JASON Group (Fatté, Dashen, Munk, Dyson, etc.). This group has exercised their model in the regime of point temporal statistics of fluctuations. This means they have used their model to predict (or explain) the temporal character of received signals at a field point, or temporal coherence between field points, mostly in the region of saturation, that is, at ranges where the fluctuating part of the received CW signal vector executes a random walk in time. They consider a sum of many such arrivals (= multipath arrivals) at a single hydrophone, and couch their results in terms of the natural log of the amplitude squared and in terms of the phase of the multipath sum. In experiment these entities are time series and their power spectra can be modeled. At long enough ranges the modeling is that of a *random walk*. In a recent paper Dyson et al JASA 59, 1121 (1976) have compared predicted power spectra versus frequency with project MIMI experimental data. They found reasonable agreement at frequencies above a parameter $\gamma^{-1} = \sqrt{\sigma_\phi{}^2}$, where $\sigma_\phi{}^2$ is the variance of the fluctuating time derivative of phase, but at very low frequencies the power spectra actually measured differed considerably from the random walk model.

The second school is that of Beran and McCoy. They have exercised their model in connection with experiments on spatial coherence of acoustic wave-fronts across antenna apertures of many wavelengths in isotropic and anistropic media. This means they compared the statistics of phase variation across a wavefront as a function of position, *averaging these over time*. They found good agreement with theory in experiments with long horizontal arrays in the ocean receiving low frequency waves. They are currently working on temporal coherence between field points in an anistropic medium.

Other schools currently working in ocean fluctuations in the USA use distinctly different approaches than the two noted above. These are (1) those that use the Dyson equation and the Bethe-Salpeter equation, or its variants in the form of perturbation series (2) those that use Monte Carlo methods (3) the optical school who use the concepts of optical propagation through a turbulent medium in which the statistics of medium randomness are described by Kolmogoroff spectra of velocity turbulence (4) those that use "phase screen" methods (or path integrals).

As noted above each approach can be *formally* generalized to a single all-embracing formalism. A typical example is the formalism of the *path integral* which leads to almost all known results by symbolic manipulation. However, the all-inclusiveness is primarily potential, actual numerical consequences being difficult to obtain except in those special cases for which other methods have supplied the needed algorithms. As to testing models, agreement with experiment over all ranges of parameters is not achievable with known models to date. What is at fault in the current failure to make a model that covers everything is the complexity of the ocean environment. This requires a special note which is discussed next.

REGIMES OF FLUCTUATION STATISTICS

The physical parameters of ocean fluctuation are so diverse and cover such large range of values that theoretical modeling must be piecemeal approximated to limited portions of the total. A first problem in modeling is to classify the regimes in which the statistics of models are thought to be valid. A convenient classification scheme adopted by the JASON Group is based on two parameters, Φ and Ω. The parameter Φ measures the severity of phase randomization of a wavefront caused by random changes of sound speed. The second parameter Ω measures interference of effects of a blob of inhomogenity in the path of a wavefront. It is essentially a statement of coherence of signals radiated from the extreme ends of a blob and crossing each other at some distant field point. A plot of Ω as ordinate and Φ as abscessa provides a 4-quadrant classification grid in Φ-Ω space (Fig. 1).

A typical line of demarcation is Φ-Ω which divides the regime of *saturation* (shown shaded here) from all other regimes. Indeed, if $\Omega/\Phi \ll 1$ the coherence (in time) is neglible relative to the randomizing effect of medium inhomogeneities taken to be strong in this case. The remaining quadrants cover regimes of partial saturation (Rytov approximation) and geometric acoustics (WKB, Born etc. approximations).

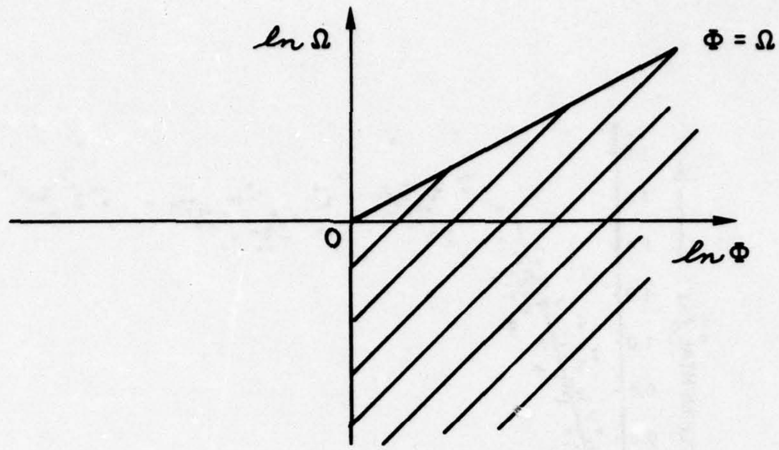

Figure 1

Let us examine the regime of saturation since it looms so large in the following discussion of the ASA Workshop. The term saturation is best understood in connection with early (circa 1965) experiments in the transmission of light through a random medium. A *plausible theory suggests* that the appropriate equation in the scalar electric field E is $\nabla^2 E + k^2 m^2 E = 0$. A Russian analyst Rytov (1937!) suggested solutions in the form $E = \exp(\psi) = Ae^{iS}$, $\psi = \chi + iS$ where $\chi = \ln A$. This is the origin of the famous log amplitude fluctuation parameter, and its physical counterpart, the variance σ^2 of fluctuation intensity I,

$$\sigma^2_{\ln I} \propto \langle \chi^2 \rangle$$

Later Tatarski (1961, 1967) used a Kolmogoroff spectrum for velocity turbulence to develop an explicit formula,

$$\sigma^2_{\ln I} = 1.23\, C^2_n\, k^{7/6}\, L^{11/6}$$

in which $k = \frac{w}{c} = \frac{2\pi}{\lambda}$, λ is the wavelength of light, L is the *range* at which the *fluctuation* of light intensity I is being measured, and C_n is a constant dependent on the chosen model. The object of experiment is to measure $\sigma^2_{\ln I}$ by measuring $\langle I^2 \rangle - \langle I \rangle^2$ of the received light, and plotting this number as ordinate against the theoretical expected value as abscissa. The result of this plotting showed that for small ranges L the theoretical formula and experiment were *linearly related* (Fig. 2). However, when the range became great enough this linear relation failed. In fact the variance of log amplitude squared no longer depended on range. It was then realized that the variance had become saturated (with range), and the statistics of the field resembled that of a random walk.

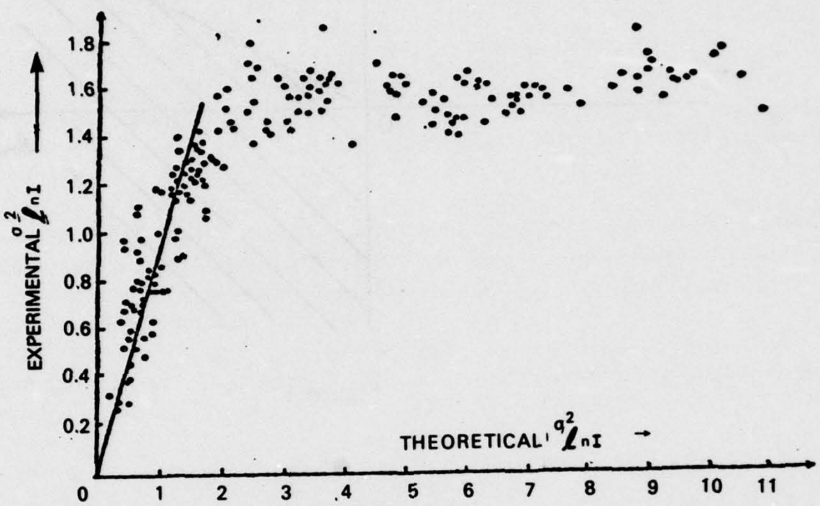

Figure 2

Experimental $\sigma^2_{\ln I}$ versus theoretical $\sigma^2_{\ln I}$ of Propagation of Light in a Turbulent Atmosphere

Saturation of the variance of acoustic intensity is an experimentally verified fact, as demonstrated by AFAR (See Ellinthorpe's conclusions below) and MIMI (Dyson's paper shows this to be true). A good portion of modeling-approaches now current attempt to explain its statistics.

With these remarks on some key issues we could go directly into discussion of the ASA papers. But it will be still valuable to try to outline the basic mathematics common to all the models, and so to allow an appreciation of the thread that ties them all together. We begin by noting that while mathematical models of the fluctuation of acoustic signals in the ocean are differentiated one from the other by what restrictions are placed on the source, on the medium and on the receiver, a single operator-type equation covers them all:

$$\mathcal{L}_b \{p\} = \mathcal{L}_f \{p\} + \mathcal{L}_q \{Q\} \qquad (1)$$

in which p is the acoustic pressure at the receiver, $\mathcal{L}_b$ is the background operator (that is, it describes the propagation of against a non-fluctuating background medium), $\mathcal{L}_f$ is fictitious source operator, $\mathcal{L}_q$ a true source operator, and Q is a true source.

The meaning of this equation may be clarified by the following. In most models the background operator $\mathcal{L}_b$ is taken to be a deterministic function of space and time, appearing as a collection of differential and integral forms, plus constants. Spatial variations of the medium are considered small over a distance of a wavelength of the acoustic signal, and temporal variations at a particular field point are taken to be slow over a period at the frequency of the acoustic signal. A typical example is the Helmholtz operator describing the propagation of sound in a homogenous isotropic medium $\mathcal{L}_b = \nabla^2 + \frac{\omega^2}{c^2}$. Another example is the parabolic operator which appears frequently in current models of fluctuating signals.

In contrast to $\mathcal{L}_b$ the operator $\mathcal{L}_f$ describing fictitious sources is taken to be random (or stochastic) when modeling fluctuations. Typical fictitious sources are signals reflected from rough ocean surfaces, or diffracted by inhomogeneous blobs in the ocean. In these cases the forms of $\mathcal{L}_f$ are typically algebraic, with space and time dependency that are statistical.

The true source operator $\mathcal{L}_q$ is taken to be deterministic if the source and receiver are fixed in space and communicate with each other with deterministic signals. It becomes a random operator if the source and receiver are in relative motion, and the motion is random. Specific forms are not treated in the following discussions since the ASA meeting was not concerned with source/receiver in motion.

The operator equation is father to a vast literature. The number and variety of solutions testify to a multitude of applications. A widely used solution takes the form of the Green's function G which is itself a solution of the differential equation in the operator $\mathcal{L}_b$,

$$\mathcal{L}_b \{ G \} = -\delta$$

in which δ is the unit amplitude delta function souce. By inversion of $\mathcal{L}_b$ one can write

$$G = \mathcal{L}_b^{-1} \{ \delta \}$$

A complete knowledge of G allows us to write the symbolic solution of Eq. (1)

$$p = G\,\mathcal{L}_f\{p\} + G\,\mathcal{L}_q\{Q\} \tag{2}$$

The two equations (1), (2) are the customary starting points for modeling acoustic fluctuations in the ocean. They are rewritten in a more suggestive form:

$$(\mathcal{L}_b + \mathcal{L}_f)\{p\} = \mathcal{L}_f\{Q\} \tag{3}$$

$$(\mathcal{I} + G\,\mathcal{L}_f)\{p\} = G\,\mathcal{L}_q\{Q\} \tag{4}$$

in which $\mathcal{I}$ is the identity operator. Except in special (trival) cases both equations must be solved by approximation.

It is to be appreciated that $\mathcal{L}_f$ and $\mathcal{L}_q$ are random operators. This makes the solutions p to be random variables which can be identified only through their moments $\langle p\rangle$, $\langle p(1)p^*(2)\rangle$, $\langle p(1)p^*(2)p(3)p^*(4)\rangle$ etc. in which 1, 2, 3, 4, etc. are location vectors in the field of p, and * signifies conjugate.

We now use Eqs. (1), (2), (3), (4) as convenient tools to review the principal papers of the ASA meeting.

Paper L1 Sound transmission through a fluctuating ocean. S.M. Flatté (UCLA).

Flatté considers a case of ocean fluctuations which is equivalent to Eq. (3) above. He takes Q = 0 (meaning there are no true sources in the volume of the ocean under analysis) *and by special approximation* (= parabolic approximation) derives the specific forms,

$$\mathcal{L}_b = -\left(\frac{1}{2k_0}\frac{\partial^2}{\partial z^2} + i\frac{\partial}{\partial r}\right)$$

$$\mathcal{L}_f = k_0\,\delta c/c,\ c = c(r,z,t),\ k_0 = \frac{\omega}{c_1},\ c_1 = \text{const.}$$

in which z is the depth coordinate, r is the range coordinate, δc is the random component of the sound speed, and c is the sound speed (total) taken as both depth and range dependent. The field $\Psi(r, z, t)$ is thus a solution of

$$\left(\frac{1}{2k_0}\frac{\partial^2}{\partial z^2} + i\frac{\partial}{\partial r}\right)\Psi = k_0\frac{\partial c}{c}\Psi,\quad \frac{\delta c}{c} \sim 10^{-4} \tag{5}$$

The fluctuations in sound speed (total) c is a slowly varying function of time. Various time scales have been observed. Of great interest is the time scale 1/3 h to 24 h. The primary cause of random fluctuations in c over this time scale is considered to be internal waves. The ratio $\delta c/c$ varies with space and time. In specific models of fluctuations the calculation of $\delta c/c$ must be accurately done because small deviations in the statistics of its value are important. The calculations of c is taken to be deterministic, while that of δc by definition, is statistical.

In the absence of values of c experimentally measured everywhere in the volume of the ocean under analysis it is convenient to choose a representative background sound speed profile. Flatté chooses the Munk "canonical" profile,

$$C_{c_p} = c_1 \left\{ 1 + \epsilon \left[e^{-\eta} - (1 - \eta) \right] \right\}, \quad \eta = 2(z - z_A)/B$$

Here z_A is the depth of the minimum value of c, labelled C_{cp}, B is an estimate of the depth thickness over which C_{cp} is substantially minimum, c_1 = const = 1500 ms^{-1}, and ϵ measures the order of magnitude of deviation from the minimum C_{cp}. A typical choice of parameters is:

$$z_A = 1000 \text{ m}, \quad B = 1000 \text{ m}, \quad \epsilon = 0.57 \times 10^{-2}$$

It is next required to calculate the random part δc caused by internal waves. In this type of wave motion ocean fluid particles move in elliptical paths in the vertical plane (as do ocean-surface waves) with velocity magnitudes that are functions of depth in the ocean and time. Internal waves must satisfy boundary conditions at the surface and bottom of the ocean (analogous to standing waves on finite strings). A single time harmonic component of these waves has the components of displacement, u, v, w. The vertical component is assumed to be separable in the coordinates,

$$w(x, y, z, t) = W(z)\, F(x, y)\, e^{-i\omega t}$$

The satisfaction of the boundary conditions restricts W to specific *modes*, W(j, k, z) in which j is the mode number, k is the "horizontal wave number" $\frac{2\pi}{\lambda_H}$, and λ_H is the horizontal wavelength of internal waves. The dimensions of k are cycles per kilometer. An example of W(z) is $W(3, 0.1, z)e^{i(kx - w\ (3,\ 0.1)t}$ where k = 1/10. This is shown in Fig. 3a. This pattern of displacement is moving to the right (x - direction), Fig. 3b: At any fixed distance x = const. The pattern of Fig. 3 oscillates with time-regulated phase ωt so that for odd multiples of π the displacement arrows shown reverse direction. These modes are key elements in the analysis. The basic premise is that $\delta c(z)$ can be expanded in modes W(j, k, z). The expansion coefficients are written as random variables A (j, k),

$$\delta c_{\text{ internal waves}} = \delta_{IW} = c_1 \frac{1}{\sqrt{2}} (\text{Re}\,\Delta + \mathfrak{Im}\,\Delta)$$

$$\Delta = \sum_{j,k} N^2(z)\, A(j, k)\, W(j, k, z) \exp\left[i\left(kx - \omega(j, k)t\right)\right]$$

Here it is assumed that the internal wave is traveling parallel to the sound wave (x-direction).

Attention is focused on amplitudes A. They are taken to be complex Gaussian random variables. For any mode j the power spectrum of internal waves is $\langle |A(j,k)|^2 \rangle$, and can be plotted as a function of horizontal wavenumber k of the internal wave. Models of internal wave spectra have been constructed on experimental bases. An oft-quoted model is that of Garrett and Munk: they take,

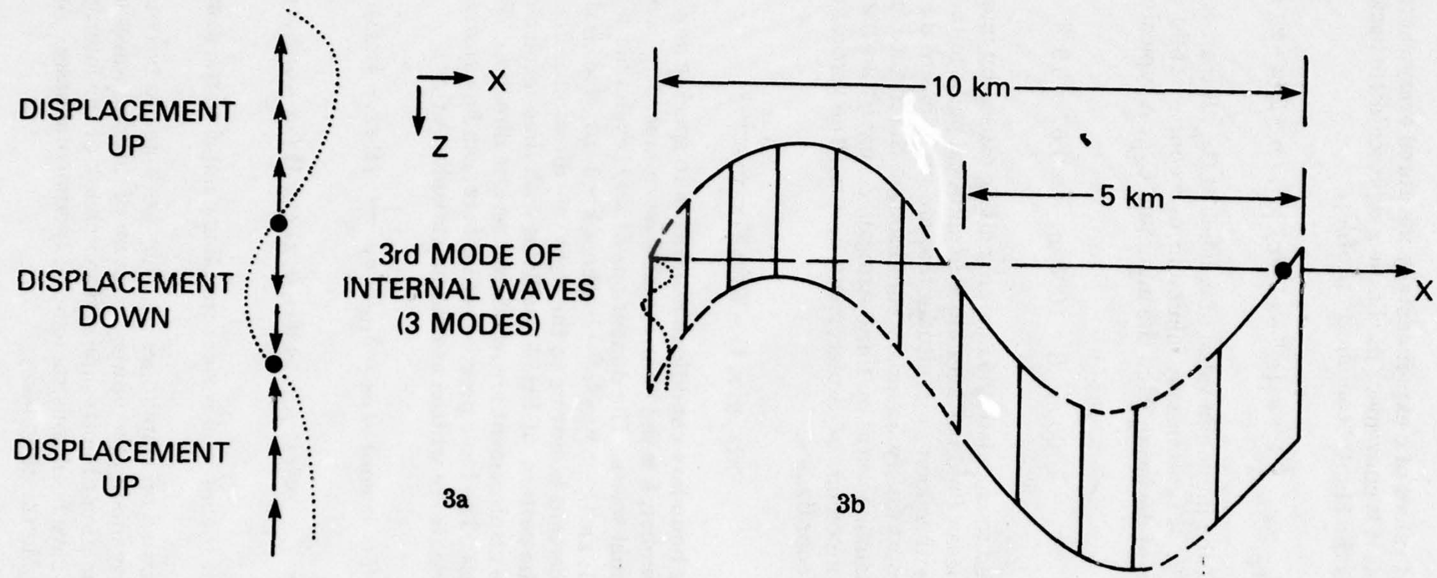

Figure 3

Sketch of 3rd mode of Internal Waves

$$<A> = 0, \quad <A(j, k)\, A^*(j', k')> = \delta_{jj'}, \delta_{kk'}, \beta^2\, H(j)\, B(j, k)$$

$$H(j) = \frac{6}{(\pi j)^2}\; ; \; B(j, k) = \frac{2}{\pi}\, \frac{k^2 l_j}{(k^2 + l_j^{\,2})^{1/2}}\; ; \; l_j = \frac{\pi}{B}\, \frac{\omega_i}{N_0}\, j'$$

in which $j = 0, 1, 2\ldots, N_0$ = const. = 3 cycles per hours, ω_i is the inertial frequency of the earth's rotation (Coriolis effect) and taken to be one cycle per day, and B = const = 1000 m. The spectrum is normalized such that

$$\sum_j \int_{\infty}^{\infty} H(j)\, B(j, k)\, dk = 1; \quad \int_{\infty}^{\infty} B(j, k)\, dk = 1$$

In numerical work, for each choice j, k the complex random expansion coefficient $|A(j, k)|e^{i\phi}$ is generated as follows: $|A|$ is a random number chosen from a population in which the probability of occurrence of magnitude lying between $|A|$ and $|A + dA|$ is Rayleigh distributed, and ϕ is a phase selected randomly from the range 0 to 2π with equal probability. A computer algorithm is available for calculating complex A according to this model. Typical curves are shown in Fig. 4. Once being calculated and available, the numbers δc_{IW} are added to C_{cp} to form the total c,

$$C(r, t) = C_{cp}(z) + \delta c_{IW}$$

$$\delta c/c = \epsilon\, [e^{-\eta} - (1 - \eta)] + \frac{\delta c_{IW}}{C_1}$$

Thus a randomized sound speed profile can be generated at any plane $|\vec{r}| = x$ = const, at any time t, as a function of depth z in any part of the ocean, recognizing that such a construction is a *model.*

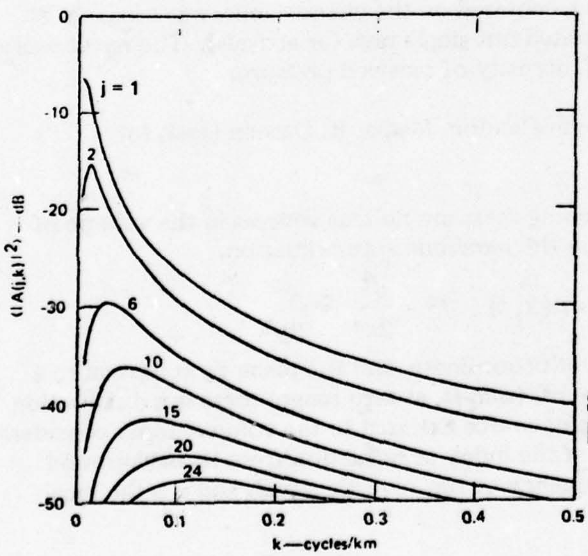

Figure 4

Squared-Magnitude Expansion Coefficients $|A|^2$ vs k with j = 1, 2 . . . as Parameter

Assume that *one* realization of a random sound speed profile caused by the entire spectrum of wavenumbers of the internal waves at a particular instant of time is made available by numerical computation as described. This quantity is next inserted into Eq. (5) (i.e., the parabolic equation). It is then directly found that the solution for the field p which can generate the form in Eq. (5), has itself a form,

$$p = \frac{\Psi}{\sqrt{r}} \exp i\,(k_o r - \omega t), \qquad k_o = \frac{\omega}{c_1},\ c_1 = \text{const.}$$

Thus the function $\Psi(r, z, t)$ also satisfies the parabolic equation and it is the entity to be determined from the differential equation. To solve for Ψ via Eq. (5) Tappert and Hardin use the "split-step-Fourier" method. This is a numerical "marching algorithm", meaning that given $\Psi(r, z)$ one is required to find $\Psi(r + dr, z)$. The rationale of their procedure is this: as a result of increasing range r by dr, a phase increment $\exp(-ik_o \frac{\delta c}{c} dr)$ occurs in the wavefront. The product of the field and phase increment, namely $\Psi(r, z) \exp(-ik_o \frac{\delta c}{c}\, dr)$ is then Fourier transformed with respect to z, using the transform pair $k_z z$, where k_z is the z-component of the field wavenumber. In "k_z space" the term $-\frac{1}{2k_o}\, \partial^2/\partial z^2$ adds its phase, namely $\exp i\,(kz^2/2k_o)dr$, which multiplies the previously obtained transform. This product is finally retransformed back into real space; the result is,

$$I(r + dr, z) = \mathcal{F}^{-1}\left\{ e^{i \frac{kz^2}{2k_o} dr} \left[e^{-i k_o \frac{\delta c}{c} dr}\, \Psi(r, z) \right] \right\}$$

In actual numerical work the field of a single point source at Z = 1000 m was used to give a starting value $\Psi(0, z)$. 512 increments in depth z were used to numerically evaluate the Fourier transforms (using FFT). The increment in range dr was 1/2 km. The time record allotted for calculation was 128 h during which $\delta c/c$ varied randomly according to the Garrett-Munk model.

Two types of receivers were used in the model calculation. In the first a single hydrophone received several acoustic rays simultaneously, resulting in a model of multipath interference. Fluctuations of a 100 Hz signal over a period of 128 hours showed 5 to 30 dB changes in the intensity of the received field. In the second type of receiver a vertical array of hydrophones 700 meters long, centered on the channel axis, was used. A beamformer in the signal processing separated out single rays (or arrivals). The result was a considerable reduction in fluctuations of intensity of received pressure.

Paper L2. Path Integrals for Waves in Random Media, R. Dashen (Inst. for Advanced Studies, Princeton).

Dashen takes Q = 0 in Eq. (1), meaning there are no true sources in the volume of ocean under consideration. He also makes the parabolic approximation,

$$\mathcal{L}_b = \frac{\nabla^2}{2k} + i\frac{\partial}{\partial z}; \quad \mathcal{L}_f = k\,\mu(\vec{x}, t)\,; \quad \nabla^2 = \frac{\partial^2}{2x^2} + \frac{\partial^2}{2y^2}$$

Here z is the range coordinate, x is the depth coordinate, and the plane xy is normal to z (direction of propagation). In the plane z = 0 (that is, at zero range) there is a distribution of field p(x, y, z = 0) due to some true point-source external to the volume under consideration. The quantity μ is the perturbation of the index of refraction from its background value, and $k = \omega/c$ where ω is the CW frequency of the acoustic signal, and c is the local sound speed.

The random variable μ has a characteristic length L, and a characteristic time T over which it is considered effectively fixed in value, and beyond which it is zero in magnitude and purely random in phase. L is analogous to the size of an inhomogeneous blob in the ocean, if spherical. If the blob has different sizes in different directions, L_v, L_h are used to designate characteristic sizes in the vertical and horizontal. T is analogous to the duration of a "blob" in time.

The acoustic size kL of a blob in the direction of propagation is taken to be much greater than unity. This means that the scattering (or diffraction) of a wave $\lambda = \frac{2\pi}{k}$ will be sharply in the forward direction. Similarly the time required for a wave of frequency ω and speed c to pass over a distance L is taken to be much smaller than T. This means the ocean is locally "frozen" during passage of the sound wave. Finally, in a range r = R over which the blobs follow each other closely there will be R/L of them. Assuming the angle of deflection of the normal of the acoustic wavefront is proportional to $<\mu^2>^{1/2}$ it is required that the rms multiple scattering angle (= $<\mu^2>^{1/2}$ R/L) be small. This is a basic assumption of Dashen's treatment of fluctuations.

Now as to approach. Dashen concentrates on the method of the path integral. By all accounts this is an intricate tool. As a first effort to elucidate it we use the simpler idea of a 2-dimensional "diffracting screen". Consider a 2-dimensional antenna lying in the plane z = 0, across which there is an "aperture function" $F(x_0, y_0)e^{iwt}$ (optical people call this "illumination"). In the Fraunhofer approximation the distance from an elementary area dx_0, dy_0 in the aperture to the far field point $P(x_1, y_1, z_1)$ is

$$|\vec{x}| \simeq z + \frac{1}{2z}\left\{(x_0 - x_1)^2 + (y_0 - y_1)^2\right\}$$

Thus the field itself is,

$$p(x_1,y_1,z_1) = \frac{i}{\lambda(z - z_0)}\, e^{ik(z_1 - z_0)} \iint_{-\infty}^{\infty} dx_0 dy_0\, F(x_0,y_0)\, e^{\frac{ik}{-2z_1}[(x_0-x_1)^2 + (y_0-y_1)^2]}$$

To make the notation symbolic let the location vector in the xy plane be

$$r_i = x_i\,\hat{e}_x + y_i\,\hat{e}_y,$$

$\hat{e}_x$, $\hat{e}_y$ are unit vectors in which i = 0, 1, 2. . . ., and i designates the range planes z = 0, z = 1. . . . . . .Then, given the aperture function in plane z = 0, one can write symbolically,

$$p(r_1, z_1 | r_0, z_0) = \frac{ike^{ik(z_1 - z_0)}}{2\pi(z_1 - z_0)} \int F(\vec{r_0})\, G(\vec{r_1}|\vec{r_0})\, d\vec{r_0}$$

in which $G(\vec{r}_1|\vec{r}_0)$ is a symbolic representation of the phase factor in the Fraunhofer approximation. In a similar way the field at plane z_2 can be determined by diffraction from plane $z = z_1$. The result (again symbolically written) is

$$p(r_2, z_2) = \frac{ik}{2\pi}\, \frac{e^{ik((z_2 - z_1) + (z_1 - z_0))}}{(z_1 - z_0)(z_2 - z_1)} \iint d\vec{r_0}\, d\vec{r_1}\, F(\vec{r_0}) \times G(\vec{r_2}|\vec{r_1})\, G(\vec{r_1}|\vec{r_0})$$

Let us carry this out to N (equal) increments of range: then, symbolically,

$$p(r_n, z_n) = \int \ldots\ldots \int d\vec{r}_0\, d\vec{r}_1 \ldots\ldots dr_{n-1}\; J(\vec{r}_0, \vec{r}_1, \ldots\ldots \vec{r}_{n-1})$$

In the limit as the number of diffracting apertures (or screens) in a given range increase to infinity one arrives at the infinite dimensional integral,

$$p(r, z) = \int D\,[r(x, y)]\;\; J(r(x, y)) \tag{6}$$

in which the symbol D specifies an infinite dimensional integration, namely a sum over all individual screens integrated completely over x, y in each screen. Eq. (6) is called the *path integral* and represents a *single* sweep over the volume between planes $z = 0$ and $z = Z_n$. A sketch of source (S) and receiver (R) situation calculated by a path integral is shown in Fig. 5.

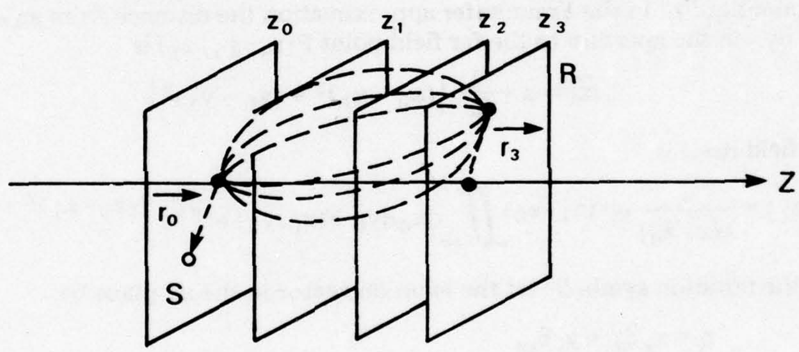

Figure 5

Path Integral Explained as a Sequence of Phase Screens

It is thus seen that if the source is at $(\vec{r}_0, z_0)$ and the receiver at $(\vec{r}_3, r_3)$ *every* point on every conceivable trajectory between planes z_0, z_3 is in the volume of integration. Thus Eq. (6), originally a functional integral because of the dependence r(x, y), is also a path integral.

The particular form of symbol J depends on the particular form of $\mathcal{L}_b$, $\mathcal{L}_f$ of Eq. (1). In the parabolic approximation treated by Dashen the diffraction screen is taken to have a complex amplitude distribution as an aperture function (that is, $F(x_0, y_0)$ is complex), and the propagation function is taken to be the phase (and amplitude) associated with the Fraunhofer approximation. In a homogeneous medium (meaning the index of refraction of the background is constant and the fluctuations are dependent only on distance $|\vec{x}_1 - \vec{x}_0|$) the phase at the end of the N increments of range (or N screens) is

$$\exp\left\{-ik\frac{R}{N}\sum_{j=i}^{N}\left\{\frac{N^2}{2}\left(\frac{r_j - r_{j-1}}{R}\right)^2 - \mu\,(r_j + \hat{e}_z\, z_j, t)\right\}\right\}$$

in which R is the total range, and $R/N = \Delta z$ the increment of range. Note that this is a sum of N increments of phase caused by Fraunhofer diffraction of a finite aperture with aperture function $F(x_0, y_0)$ and *also* caused by the random index of refraction μ. In the continuing limit as the number of screens between source and receiver becomes infinite the phase function becomes

$$\exp\left\{-ik\left[\int_o^R \frac{1}{2}\left(\frac{d\vec{r}}{dz}\right)^2 - \mu\,(r(z) + \hat{e}_z z)\,t\right]\right\}$$

Then field is then,

$$p(\vec{r}, \vec{r}_0, R, t) = \frac{-1}{2k}\int D\,(\vec{r}(z))\exp\left[-ik\int_o^R dz\left[\frac{1}{2}\left(\frac{dr}{dz}\right)^2 - \mu\,(r(z), t)\right]\right.$$

$$= \int d\vec{r}_0\;F(\vec{r}_0)\int D_1\,(r(z))\exp\int_o^R dz\left(\frac{d\vec{r}}{dz}\right)^2 - \mu(r(z), t)\Big]$$

where by definition,

$$\lim_{N\to\infty}\int D_1\,(\vec{r}(z)) \equiv \int \ldots\ldots \int d\vec{r}_1\; d\vec{r}_2\; \ldots\ldots\; d\vec{r}_{n-1}$$

The field p is stochastic. The amplitude of the moments of this random variable are defined as

$$\langle A^{2n}\rangle = \langle (pp^*)^n\rangle$$

For example, the mean value of field p in a homogeneous medium is

$$\langle p\rangle = \langle pp^*\rangle^{1/2}$$

$$= \int d\vec{r}_0\;F(\vec{r}_0)\int D_1\,(\vec{r}(z))\exp\left[\frac{ik}{2}\int_o^R\left(\frac{dr}{dz}\right)^2 - \frac{k^2}{2}\int_o^R\int_o^R\right.$$

$$\rho(|z - z'|)\, dz\, dz' \int D(\vec{r}(z)) \quad \exp\left[\frac{ik}{2}\int_o^R \left(\frac{dr}{dz}\right)^2 dz\right]$$

$$= \mathcal{E}_0 \exp\left[-\frac{1}{2}\Phi^2\right]$$

where

$$\Phi^2 = k^2 < \left(\int_o^R \mu(\hat{e}_z\, z, t)\, dz\right)^2 > \cong k^2 R \int_{-\infty}^{\infty} \rho(|z|, 0)\, dz$$

and $\mathcal{E}_0$ is the field of a homogeneous medium without fluctuations μ. Note that *in this approximation* any vector connecting r(z) and r(z′) (that is, connecting points at two range planes) is considered to have a magnitude $|r(z) - r(z') + (z - z')^2|$ not much different from $|z - z'|^2$. This once more is the parabolic approximation which assumes normals to the wavefronts point in directions *always* close to the z-axis (axis of propagation).

The symbol Φ is the same that appeared earlier in this review. It is a measure of the strength of fluctuations caused by random index of refraction μ. By itself the parameter Φ does not account for an additional deflection of the normals to the wavefront caused by diffraction of these fronts around blobs of inhomogeneities (in μ). This is treated by a second parameter Ω, or the squared ratio of scale size L of the inhomogeneous blob to the extent of the Fresnel zone ($\sqrt{\lambda R}$) as measured at range R,

$$\Omega = 6kL^2/R$$

From its definition it is seen that when Ω is large the angle of diffraction of a wave caused by the blob is very small, that is, geometrical acoustics applies. Small Ω therefore corresponds to large diffraction effects. The reciprocal $\Lambda = \Omega^{-1}$ is sometimes used to express the same effects, namely small Λ means small diffraction effects. The ratio Ω/Φ (called α) is thus a measure of both fluctuation strength and diffraction. For example if $\alpha << 1$ the fluctuations fo the field p are very nearly purely random. The field is then said to *saturate*, that is, the field is determined by the statistics of a random walk and is independent of range. However, when Φ is less than unity and Ω/Φ is greater than unity the vector representing the complex field retains its orientation in vector space, making only small random deviations about its orientation. The field is then partially saturated or unsaturated.

The parameter α is very important in discussing the higher moments of p. To see its significance we again examine $<p>$. In the phase integral method there is only one volume of integration between initial and final planes transverse to the direction of propagation (Fig. 5). The actual *rays* from $\vec{r}_0$ to r_1, are limited by the small scattering angle assumption to the angle $\sim\lambda/L$ relative to the geometric acoustic ray. The points along all paths that contribute to p will extend at the outermost a transverse distance $\theta R = \lambda R/L$ from the geometric path. But $\lambda R/L = \sqrt{\lambda R}\ \sqrt{\lambda R/L}$, and by assumption $\sqrt{\lambda R/L} << 1$. Hence only a very small volume of paths (= rays) actually contribute. If we take Φ to be large the mean field $<p>$ will be exponentially small as the range increases. Similarly the average intensity, $<pp^*>$ will also be small for the same reasons.

A more important second moment of the fluctuating field is the mutual coherence function, $\langle p(\vec{r}_1, \vec{r}_{01}, t_1) p^*(\vec{r}_2, \vec{r}_{02}, t_2)\rangle$. The path integral formulation of this quantity is

$$\langle p(1)\, p^*(2)\rangle = \frac{1}{4k^2} \iint D(r_1(z))\, D(\vec{r}_2(z)) \exp\left[\frac{ik}{2}\int_o^R (\vec{r}_1{}'^2(z) - \vec{r}_2(z)^2)dz - V\right]$$

in which $\vec{r}\,' = \frac{dr}{dz}$. The symbol V expresses a sum of three quantities: the self correlation of field along path 1, self-correlation along path 2, and cross-correlation between path 1 and path 2. To define the word "path" we present Fig. 6.

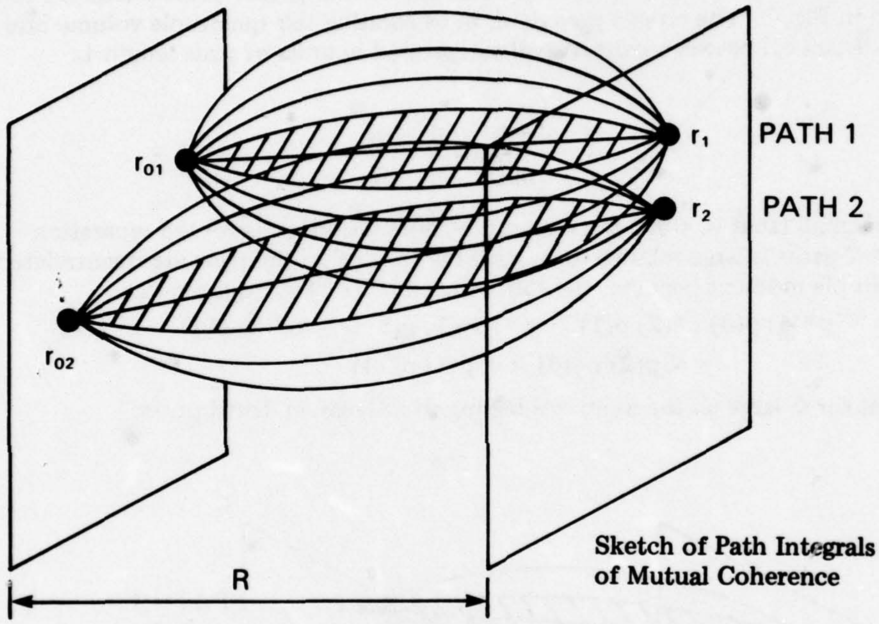

Figure 6

Sketch of Path Integrals in Propagation of Mutual Coherence

The figure shows that the path integral formulation of $\langle p(1)\, p^*(2)\rangle$ requires a double volume integration over the same range between the initial and final plane. The actual calculation depends on the type of field equation used. Assuming for example the parabolic approximation one arrives at the result

$$\langle p(1)\, p^*(2)\rangle = p^*_0(2) \exp\left[-\frac{D(1,2)}{2}\right]$$

in which $p_0(1)$, $p_0(2)$ are solutions for the field in a homogeneous deterministic medium, and D (1, 2) is the *structure function*, where for large Φ,

$$D(1,2) = \Phi^2 \left[\frac{(\vec{r}_1 - \vec{r}_2)^2 + (\vec{r}_{01} - \vec{r}_{02})^2 + (\vec{r}_1 - \vec{r}_2)(\vec{r}_{01} - \vec{r}_{02})}{3L^2} + \frac{t^2}{T^2} + \dots\right]$$

It is seen that only when $\vec{r}_1 \sim \vec{r}_2, \vec{r}_{01} \sim \vec{r}_{02}$ the mutual coherence has significant magnitude. Thus the value of the double volume integral is significant only when the paths are close together.

The fourth moment of the random field is also important,

$$< p^*(4)\, p(3)\, p^*(2)\, p(1) > = (2\pi)^{-4} \int D(r_1(z))\, D(r_2(z))\, D(r_3(z))\, D(r_4(z))$$

$$\exp\left[\frac{-ik}{2} \sum_{j=1}^{n} (-1)^j \int_o^R \frac{dr_j}{d_z}^2 dz - M \right]$$

in which M is a matrix of all self and cross correlations of four paths. A sketch of the four paths is shown in Fig. 7. The crucial parameter in calculating this quadruple volume integration is the distance d between pairs of paths expressed in units of scale length L. Roughly

$$\frac{d}{L} \sim \frac{\Phi R}{6kL^2} = \frac{1}{\alpha} = \frac{\Phi}{\Omega}$$

Thus when α is small (that is, when the strength of fluctuations is large) the separation between pairs of paths is large relative to L, with the result that the pairs are uncorrelated. Thus the quadruple moment becomes the sum of products of second moments,

$$< p^*(4)\, p(3)\, p^*(2)\, p(1) > \cong < p^*(1)\, p(3) > < p^*(2)\, p(4) >$$
$$+ < p(2)\, p^*(3) > < p(1)\, p^*(4) >$$

This shows that for Φ large all the moments belong to a Gaussian distribution.

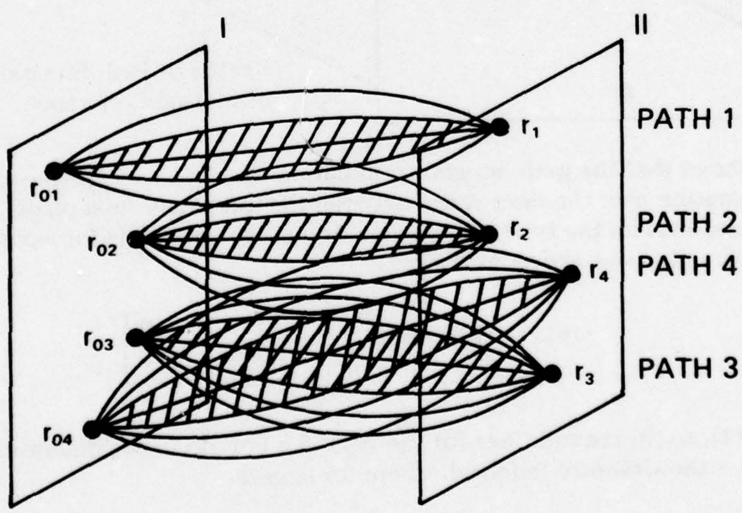

Figure 7
Sketch of 4th Order Moment (or Mutual Integrity)
Calculated by Path Integrals

CLASSIFICATION OF REGIONS IN $\Omega\Phi$ SPACE

By definition the correlation for index of refraction in a homogeneous medium is

$$<\mu(\vec{x}, t)\, \mu(\vec{x}, 't)> = \rho(|\vec{x} - \vec{x}'|, t - t')$$

Let $\widetilde{\rho}$ (q) be the dimensional fourier transform of ρ, that is, $\widetilde{\rho}$(q) is the power spectrum of μ in the wavenumber q. Assume that $\widetilde{\rho}$(q) goes as $|q|^{-2-p}$ where for large q, $4 < p < 1$. To account for time variations suppose that the medium μ is time-dependent so that plane waves propagating through it have a dispersion relation $\omega \sim k^\delta$. Then the Fourier transform of the second derivative of is,

$$\ddot{\rho}(|q|) = \text{const} \times |q|^{-(2+p-\delta)}$$

Four parameters are now available for classifying signal statistics, Φ, Ω, p and δ. They will be applied to collections of paths that connect source to receiver. Any group of paths that satisfy a perturbed ray equation of the form

$$\frac{d^2 \vec{r}(z)}{dz^2} + \left(\frac{\partial^2}{\partial x^2} + \frac{\partial^2}{\partial y^2}\right) \mu\, [\vec{r}(z) + \hat{e}_z z] = 0$$

will be called *Fermat paths*, or nearly geometric paths. If in a given space and time varying medium there are meaningful multiple Fermat paths all lying within a correlation length L of each other, the regime of fluctuations of the field p in the $\Phi\Omega$ plane will be called *partially saturated*. If the Fermat paths are spaced more than L units apart the regime will be called fully saturated. The exact location of regimes in the $\Phi\Omega$ plane depends on the magnitude of p. The following table lays out the regime for the case when temporal changes in ρ can be neglected.

Case	Partially Saturated	Fully Saturated
$2 < p < 4$	$\Phi > 1,\ \Phi^{4/p}/\Omega > 1,\ \Phi/\Omega < 1$	$\Phi > 1,\ \Phi/\Omega > 1$
$1 < p < 2$	$\Phi > 1, \Phi^{4/p}/\Omega > 1, \Phi^{2/p}/\Omega < 1$	$\Phi > 1,\ \Phi^{2/p}/\Omega > 1$

Now let us suppose that the medium has significant time-varying μ, and choose $p < 2$ for the partially saturated region. Then the statistics of acoustic pressure p_a are given by the table:

		Variation of Signal with			
	Intensity of p_a	Space	Time		Frequency
			$p - \delta < 0$	$p - \delta > 0$	
Statistics of p_a	Rayleigh	Gaussian	Gaussian	Phase Wrapping	Phase times a Guassian

The meaning is: (1) as long as $p < 2$ the intensity I of field p_a is Rayleigh distributed, that is the probability distribution is

$$P(I) = \frac{1}{<I>} \exp\left| - \frac{I}{<I>} \right|$$

$$<I^n> = n! <I>^n$$

(2) if the Fourier power spectrum of ρ falls of as $|q|^{-\xi}$ where $\xi < 4$, then the signal variation with random spatial variations of ρ is Gaussian. (3) if $\rho \sim |q|^{-\xi}$, $\xi < 4$, then if p is varying in time such that plane waves are dispersed in frequency as $\omega \sim k^{\delta}$, and if $p - \delta < 0$, the track of the tip of the vector p_a representing the complex signal will have a Gaussian distribution in angle (that is, all angles can occur with equal probability). The tip then executes a path that looks like a random walk. (4) if condition (3) holds, except that $p - \delta > 0$, the track tip will wrap around the origin, changing only slightly in amplitude. Random walk and phase wrapping of the complex vector of the field as shown in Fig. 8.

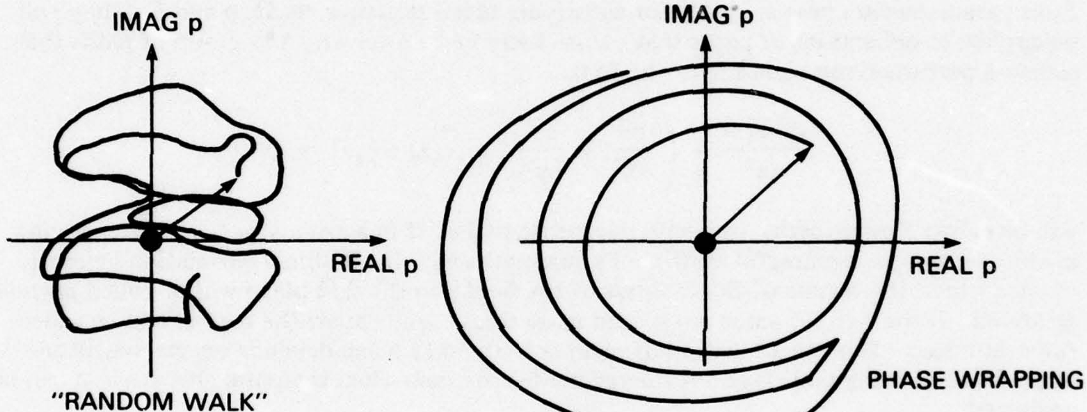

Figure 8

Sketches of Random Walk and Phase Wrapping of Phase Angle of a Propagating Wave

(5) When the field p_a varies in frequency the statistics of correspond to

$$p_a(w) = p_0(w)\, e^{i\omega\psi}\, X(\omega)$$

in which ψ is a real Gaussian random variable with $<\psi> = 0$ and $<\psi^2> = R\hat{\rho}(0) \times C^{-2}$, X is an independent complex Gaussian random variable with zero mean, and

$$< X^*(w)\, X(w') > = \Lambda\,(w' - w)$$

Thus in the partially saturated regime,

$$\frac{<p^*(w)\, p(w')>}{p_0(w)\, p_0(w')} = \exp\left[-\frac{1}{2} (\omega - \omega')^2 \; R\,\hat{\rho}\, c^{-2} \right] \Lambda\,(\omega' - \omega)$$

The quantity $\hat{\rho}$ will be explained later. This explains why, in the table, one finds the entry that the statistics of p_a for *variable frequency* correspond to that of a field of phase (i.e. $\exp i\omega\psi$) multiplied by a Gaussian (namely $X(\omega)$).

So much for the partially saturated regime. In the fully saturated regime ($\Phi > 1, \alpha \rightarrow 0$) the exponential ψ factor leads to factors of unity in higher order statistics of p_a. Thus in the second order moment of p_a,

$$\frac{< p_a^*(\omega)\, p_a(\omega') >}{p_0^*(\omega)\, p_0(\omega')} \rightarrow \Lambda(\omega' - \omega)$$

The absence of the phase factor (see in the above table in the entry under variation of the signal with frequency) constitutes the principal difference between partially saturated and fully saturated regions.

INHOMOGENEOUS AND ANISOTROPIC MEDIA

The random index of refraction μ in the case of inhomogeneous media is considered to have a mean $<\mu>$ which is a function of range and depth. In addition the covariance $\rho (= <\mu(\vec{x}_1, t)\, \mu(\vec{x}_2, t)> - <\mu(x_1, t)><\mu(\vec{x}_2, t')$ depends on $\vec{x} = 1/2\,(\vec{x}_1 + \vec{x}_2)$ as well as on the shorter length vector $\vec{x}_1 - \vec{x}_2$. Finally, in anisotropic media ρ depends on the orientation of $\vec{x}_1 - \vec{x}_2$.

We begin with an inhomogeneous medium. To obtain tractable path integrals one requires (1) variations in ρ over lengths of order $L\Phi/\Omega$ to be negligible (2) variations in $<\mu>$ over $L\Phi/\Omega$ to be also negligible (3) the parabolic equation is valid. With these assumptions the statistics of the field p_a in an inhomogeneous medium are,

$$<p> = p_0\, e^{-1/2\Phi^2}; \quad <p^*(2)\, p(1)> = p_0(2)\, p_0(1)\, e^{-1/2D}$$

Evidently, the form of these equations is the same as for a homogeneous medium but the explicit forms of Φ and D are different,

$$\Phi^2 = k^2 \int_o^R \hat{\rho}(\vec{0}, 0; z)\,dz; \quad D = 2 \int_o^R d(\vec{w}(z), t_1 - t_2; z)\,dz$$

in which

$$d(\vec{w}, t; z) \equiv k^2\, [\hat{\rho}(\hat{0}, 0; z) - \hat{\rho}(\vec{w}, t; z)]$$

All formulas depend on the quantity $\hat{\rho}$. For a homogeneous medium $\hat{\rho}$ is the transverse correlation function in the Markov approximation, i.e.

$$\rho(\vec{x}, t) = \delta(z)\, \hat{\rho}(|\vec{r}|, t)$$

In an inhomogeneous medium $\hat{\rho}$ is more complicated but retains the same basic definition. Explicit forms for special choices of $\mu(\vec{x}, t)$ are available.

Next one considers anisotropic media. As a measure of anisotropy one adopts the angle θ_0 which is the ratio of the small dimension of an inhomogeneous blob to the large dimension. The most important case is propagation in a channel wherein the unperturbed ray makes loops and wherein the long axis of the inhomogeneities is parallel to the channel axis. This is shown in the figure. (Figure 9)

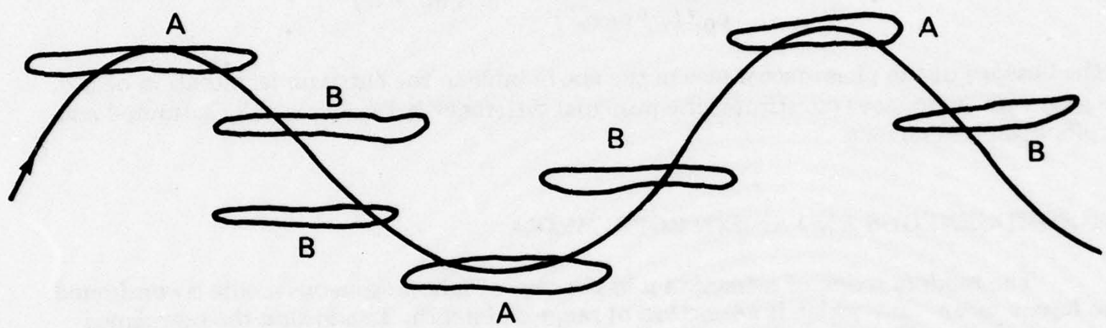

Figure 9

Sketch of the Propagation of a Ray in Anisotropic Media

The scattering of the wave is strongest at the "turning points" of the ray path A, and weakest in between, B. To understand the *cumulative* effects of scattering we consider Fig. 10. in which we show a wavefront WF passing through a homogeneous random medium from z_1, to z_2. We assume μ is well correlated in the plane z = const. However, in the direction of propagation the correlation is a delta function $\delta(z - z')$: this means there is no "memory" of previous states of μ with change in the z-coordinate. The wavefront itself moves nearly unaffected. Hence the coupling between random field p_a and random index of refraction is the same as that of two statistically independent entities viz $\langle p_a \mu \rangle = \langle p_a \rangle \langle \mu \rangle$. A medium which is thus delta function correlated in the direction of propagation generates a field p which is *Markov approximated*. In isotropic media the scattering does not depend on angle of the normal of the wave front relative to some reference. In the Markov approximation (still considering isotropic media) the multiple scattering angle (i.e. its total accumulation) is small. The picture is that of a wave moving nearly in the same direction, whose normals bob back and forth randomly, making small angles to the direction of propagation. In anisotropic media scattering of the field p_a is highly dependent on angle of incidence as soon as the angle is of order θ_0. Hence the scattering is reinforced in special directions and the wavefront normals "remember" previous history. Hence the Markov approximation fails at a shorter range than for isotropic media. But suppose the medium is anisotropic and at the same time inhomogeneous (as pictured in Fig. 9). The scattering effectively occurs only at the turning points (points A). At each turning point we assume the Markov approximation holds. Generally, the turning points are separated by more than a coherence length. Hence the effect of previous scatterings will be equivalent to a *random* modulation. Thus the Markov approximation will be valid at long ranges.

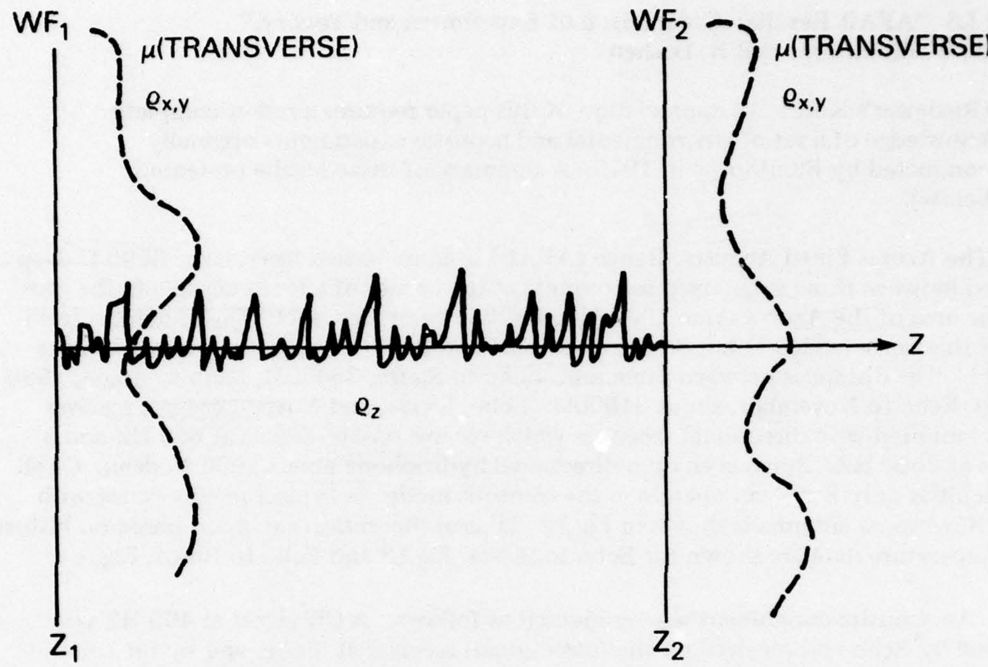

Figure 10

Sketch of Cumulative Effects of Scattering

To this point it has been shown that formulas for $\langle p_a \rangle$ in *inhomogeneous anisotropic* media have the same form as those of homogeneous insotropic media, but requiring only change in the definition of Φ and D. In the same manner it can be shown that by redefining Ω and Φ the table of statistical regimes of the field p_a in the partially saturated regime have the same *form* but that the statistics of p_a in the saturated regime where frequency changes are in question is Gaussian with the added phase described before. The great importance of the parameter Ω is once again brought out by this redefinition. It is this: Ω measures the rate at which the phase of the oscillating factor in the path integral formulation of the field p_a varies as the rays of the path move away from the unperturbed ray. In different terms, Ω is a measure of the phase change required to move a ray a distance L away from the unperturbed ray. A specific form of Ω for the case of anisotropic inhomogeneous media has been derived. Together with the similarly modified form of Λ $(\omega - \omega')$ it can be shown that the statistics of the fully saturated regime are completely Gaussian.

Paper L3 "AFAR Results: Comparison of Experiment and Theory."
A. W. Ellinthorpe and R. Dashen

(Reviewer's Note: An appreciation of this paper requires a rather complete knowledge of a set of environmental and acoustic experiments originally conducted by Ellinthorpe in 1975. A summary of these results presented below).

The Azores Fixed Acoustic Range (AFAR) is an underseas basin some 8500 ft deep located between three submerged sea mounts at the corner of a loose triangle in the geographic area of the Azores some 1800 ft to 2500 ft below sea level. The underseas facilities of this range (called Echo, Sierra, November and Bravo) are located on this mounts (Fig.11). The distances between them are: Echo to Sierra, 35000M; Echo to Bravo, 2990 meters; Echo to November, about 34000M. Echo, Sierra, and November have receiver masts mounted with directional receivers which receive on 30° beams at 600 HZ and 8° beams at 3500 HZ. Bravo is an omnidirectional hydrophone about 1000 ft. deep. Of all the facilities only Echo can operate in the transmit mode. A typical receiver mast with three directional antenna is shown in Fig.12. Typical *theoretical* ray paths based on historical temperature data are shown for Echo to Sierra, Fig.13 and Echo to Bravo, Fig. 14.

An acoustic experiment was conducted as follows: A CW signal at 400 HZ was radiated by Echo and received by the (directional) receiver at Sierra, and by the (omnidirectional) receiver at Bravo. A 5-HR record of reception is shown in Fig.15. The received signal at Sierra is a recognizable sinusoid, that is, a rotating vector whose relative amplitude on dB shows slow variations of up to 40 dB over the 5 hour period. The phase of this vector as measured against a local clock changed by some 0.009 - 0.001 = 0.008 sec at 400 Hz (or 6.4 π radians). The same CW signal at Bravo shows very rapid amplitude fluctuations of some 1 dB superimposed on a slow fluctuation of some 5 dB. The phase change at Bravo relative to a local clock was about 0.0088 - 0.0048 = 0.004 sec. or 3 π radians.

A second experiment repeated the first at 4400 Hz. A 5 hour record is shown in Fig.16. This time the signal amplitude received at Sierra showed very rapid fluctuations of from 0 dB to 40 dB while the phase varied by about 0.004 sec or 35.2 π rad.) relative to a local clock. The received amplitude at Bravo showed rapid severe fluctuations of some 5 to 30 dB over the period and a phase change of 0.004 sec or 35.2 π radians relative to a local clock.

In order to explain these received signals a set of environmental data was taken, which was then reduced to statistics of sound speed profiles as functions of space and time in the AFAR basin, as well as data on buoyance frequency. Typical calculations in the signal processing were: (1) the variation of sound speed along a horizontal track of 10 miles was Fourier transformed to a spatial power spectrum versus wavenumber "k" in units of cycles per meter. A typical plot is shown in Fig.17 in which the noticeable feature is the breakpoint between two regimes. (2) the spatial power spectrum for a 90 mi track is shown in Fig.18. Note the three breakpoints. (3) the coherence in time of two instruments measuring sound speed in the horizontal plane separated by 1100 meters versus wavenumbers k was measured and is shown in Fig.19. Also the coherence of two instruments in the vertical plane, Fig. 20. (4) Typical sound speed profiles are shown in Fig. 21. (5) The

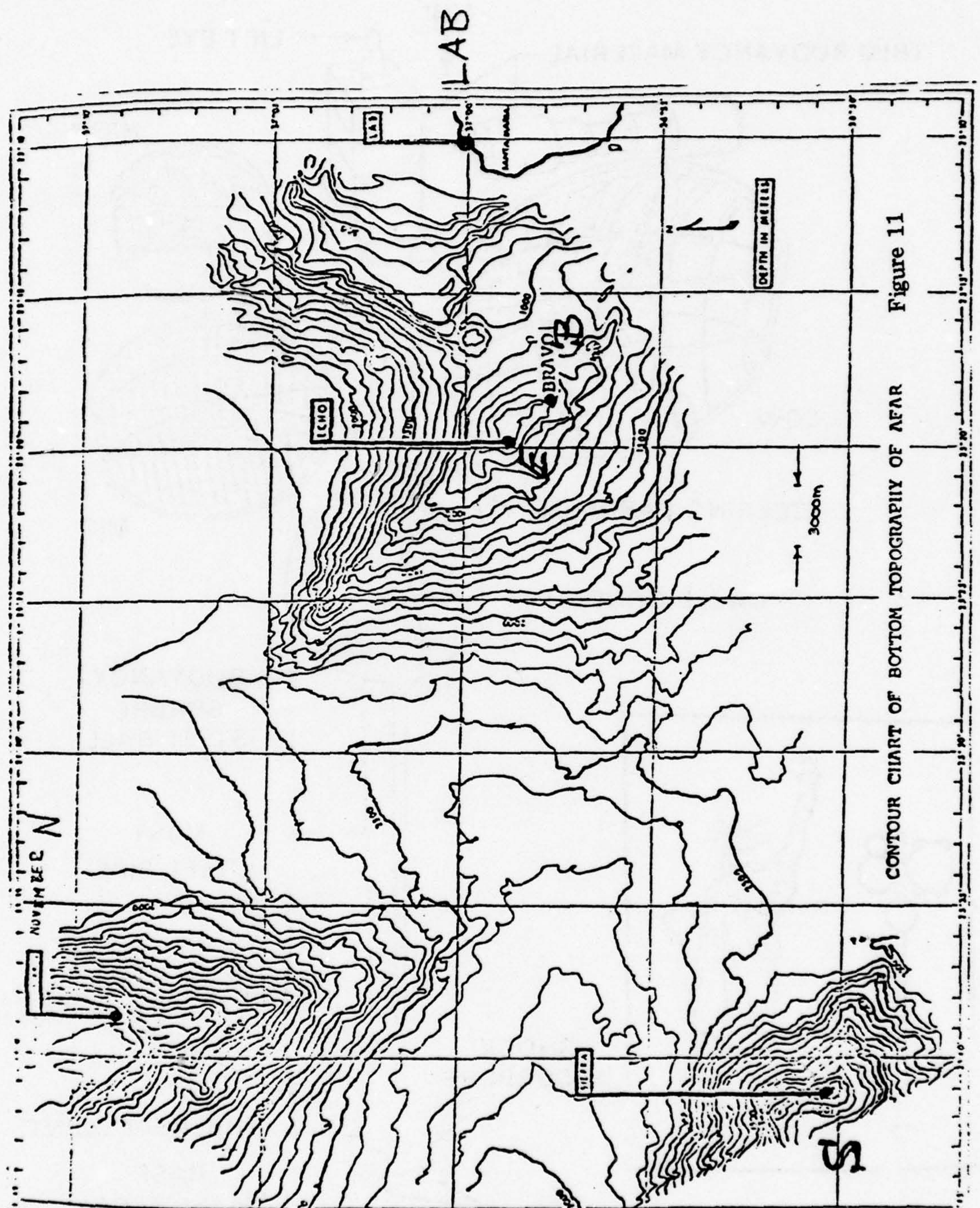

CONTOUR CHART OF BOTTOM TOPOGRAPHY OF AFAR

Figure 11

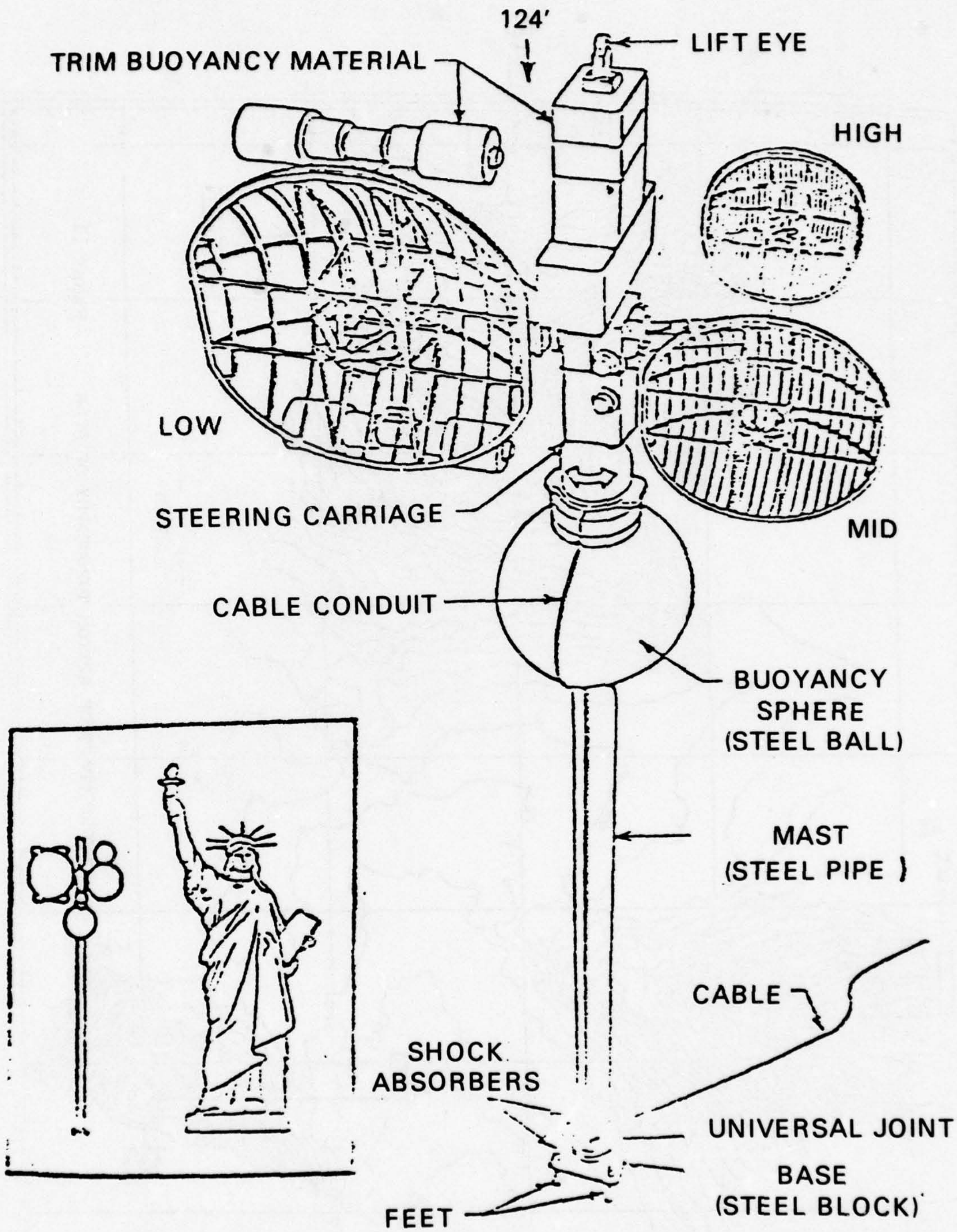

Fig. 12 —Physical Size and Proportions of AFAR MAST

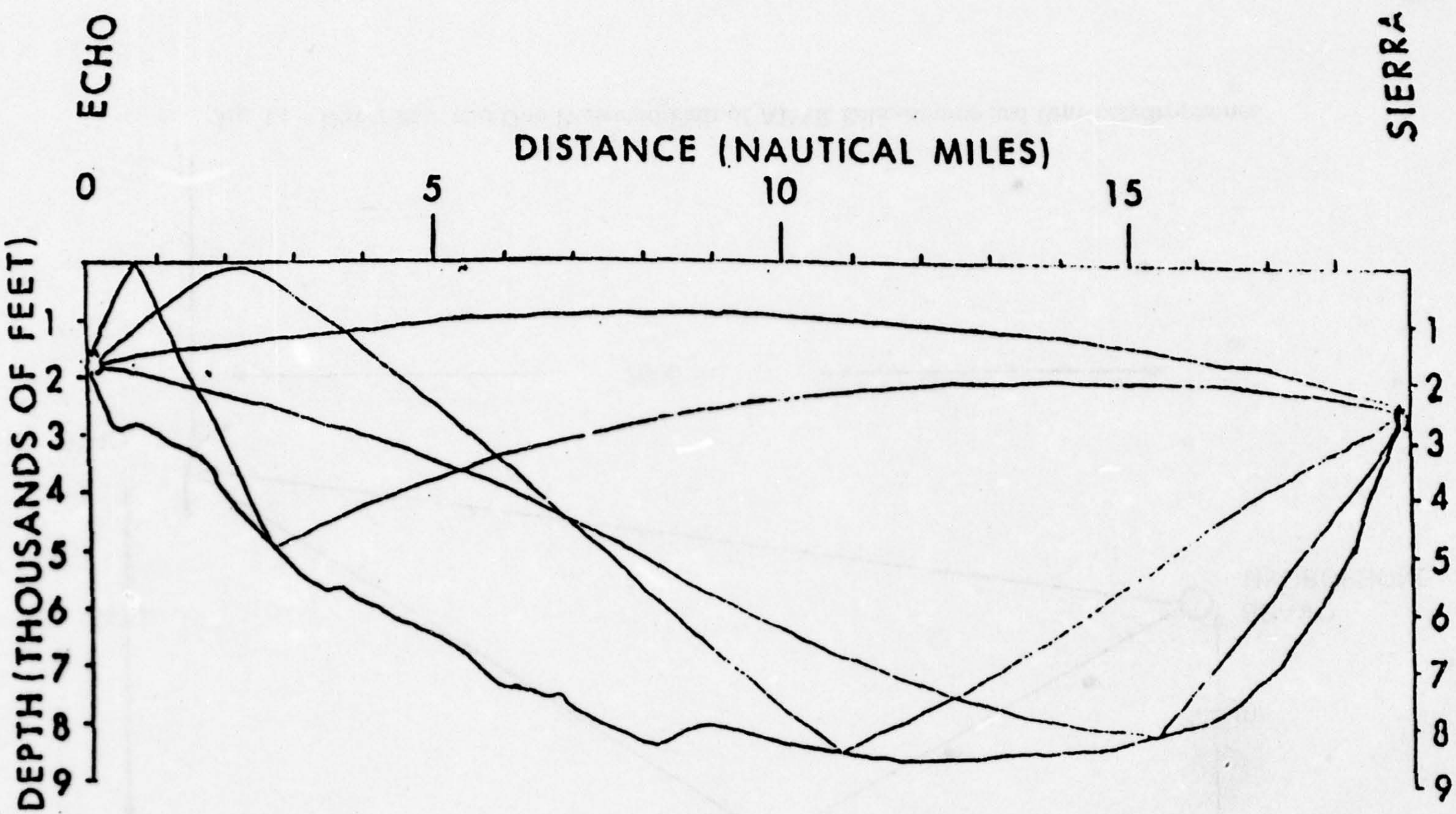

Fig. 13 —AFAR Simplified Ray Diagram

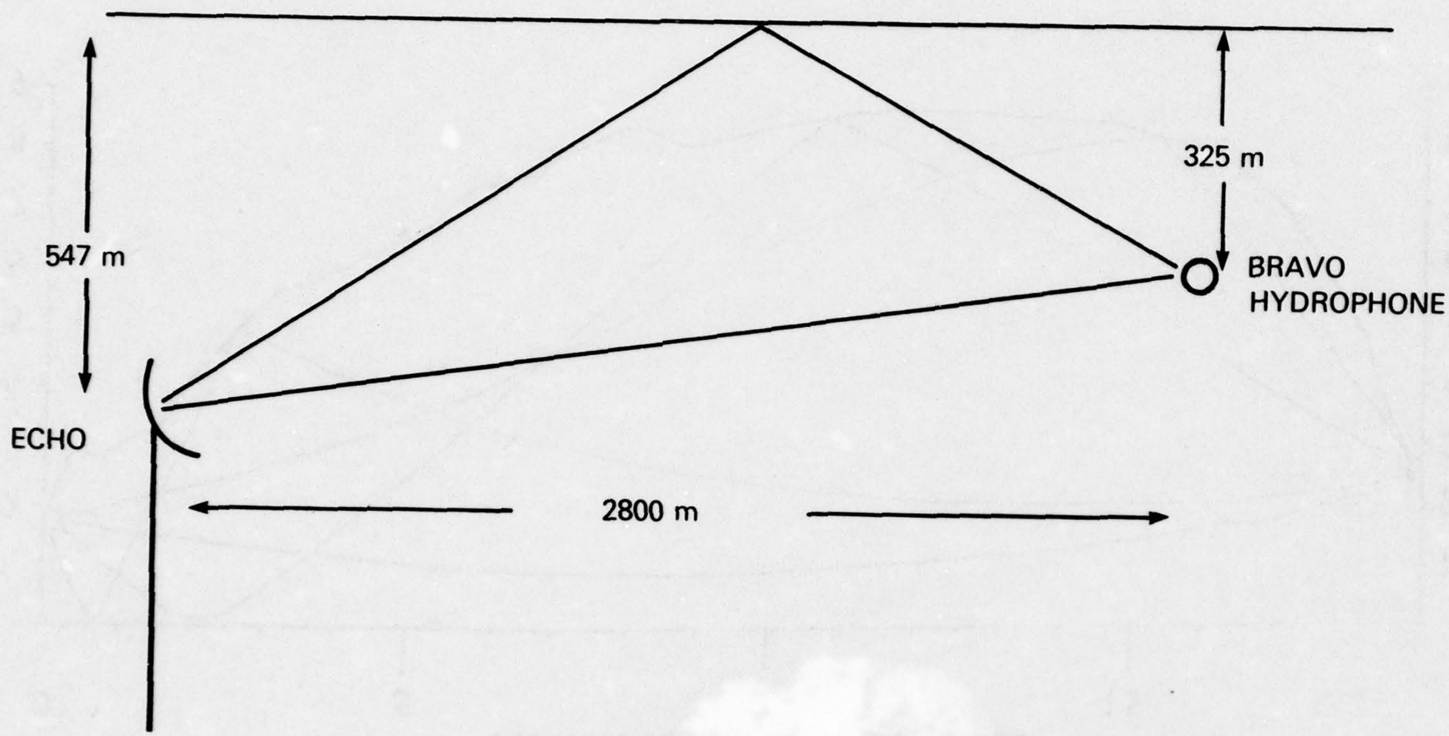

Fig. 14 —Direct Path and One Reflected Path of AFAR Echo-Source and Bravo Hydrophones

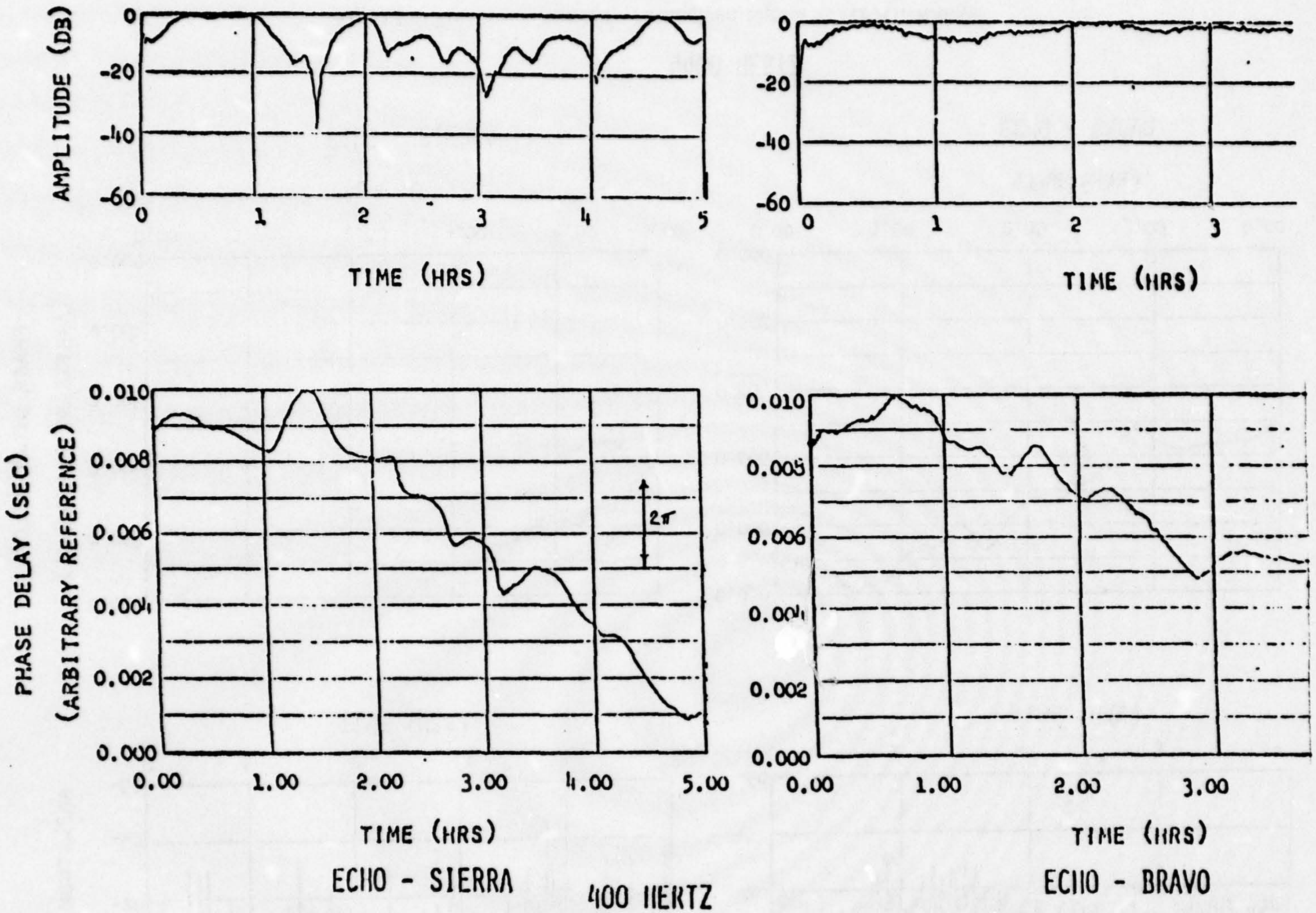

Fig. 15 — Five-hour Record of Received Signals at AFAR Range

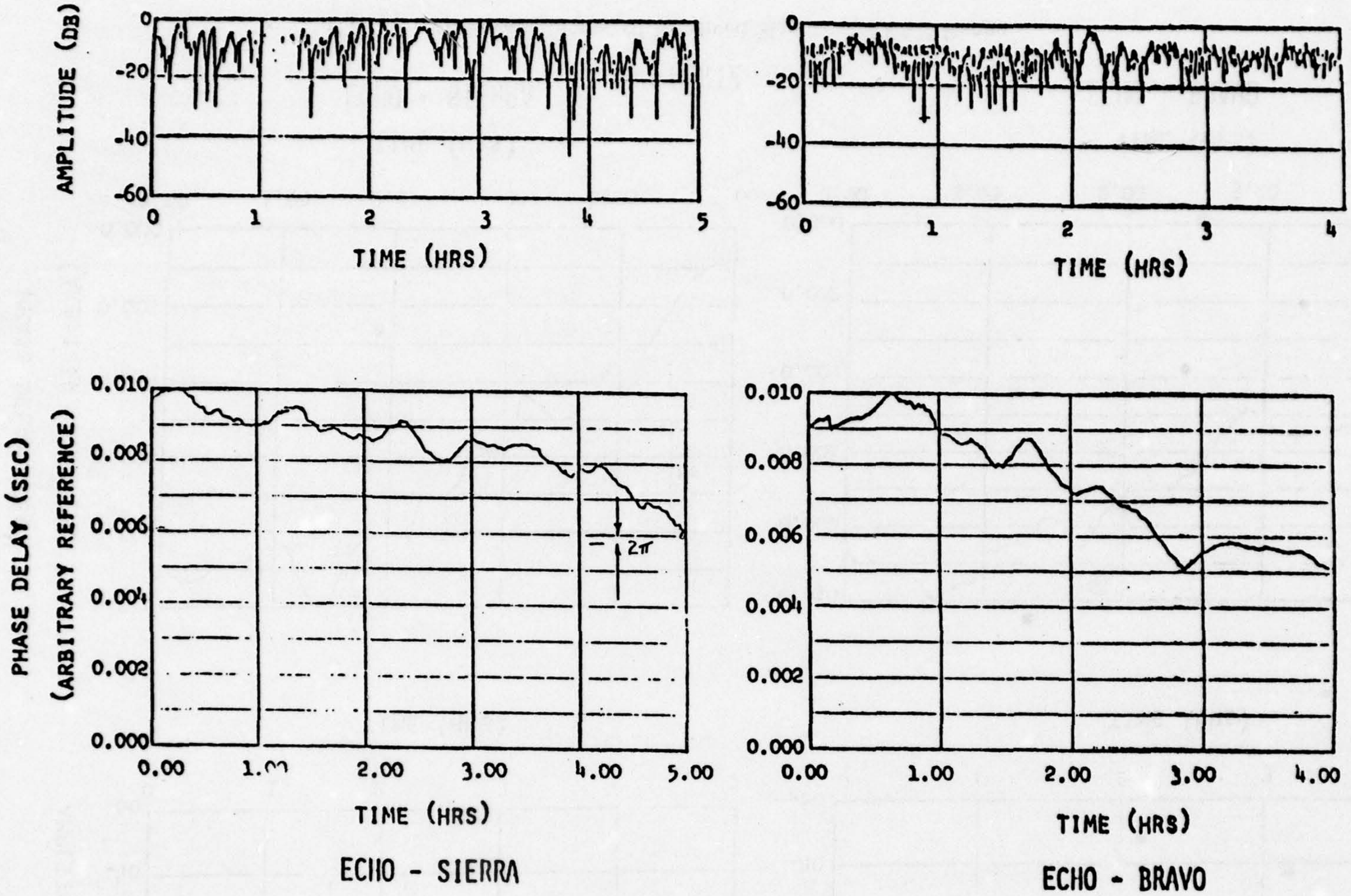

4400 HERTZ

Fig. 16 —Five-hour Record of Received Signal at AFAR Range

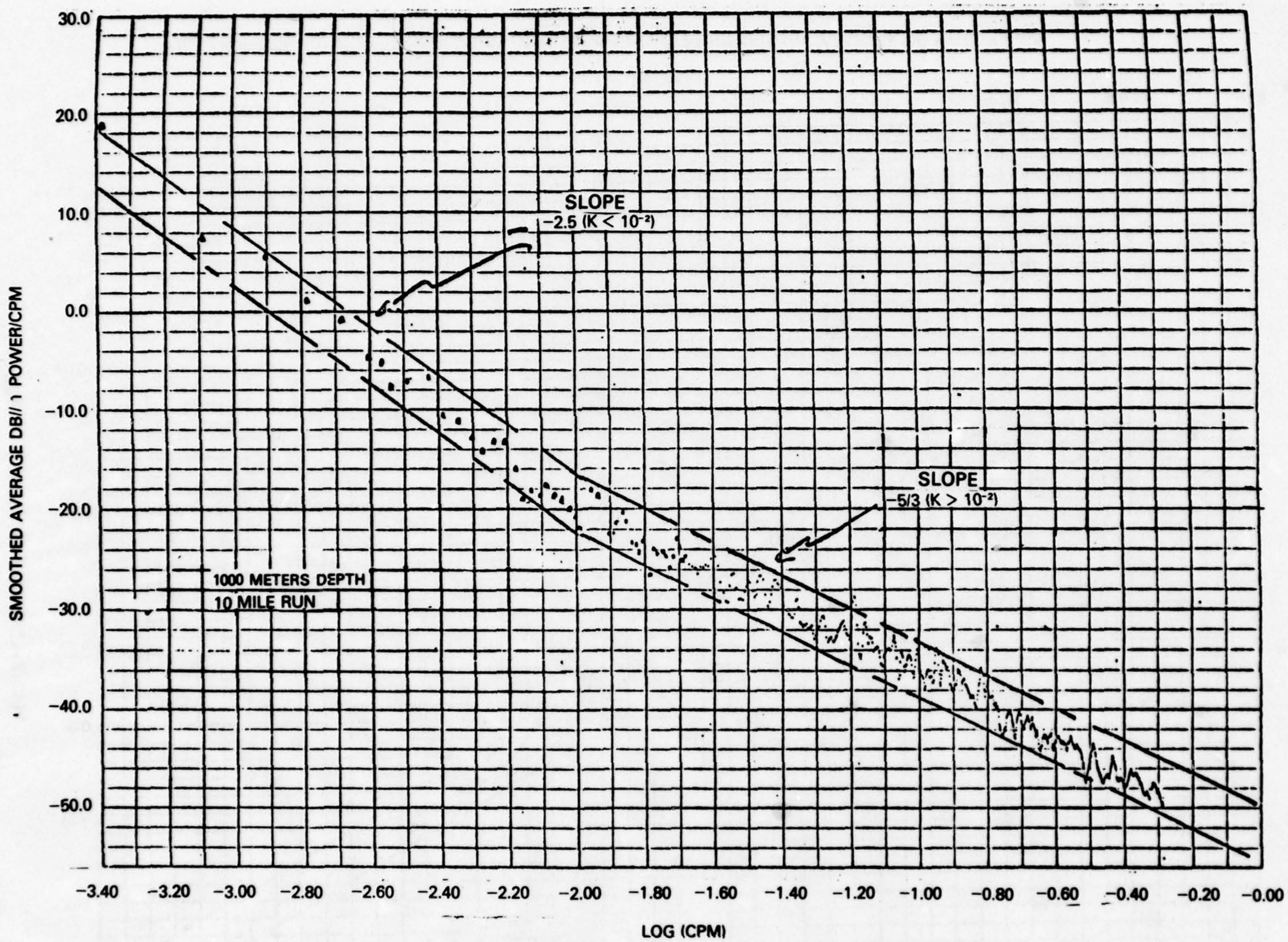

Fig. 17 —Spatial Power Spectrum of Sound Speed Fluctuations

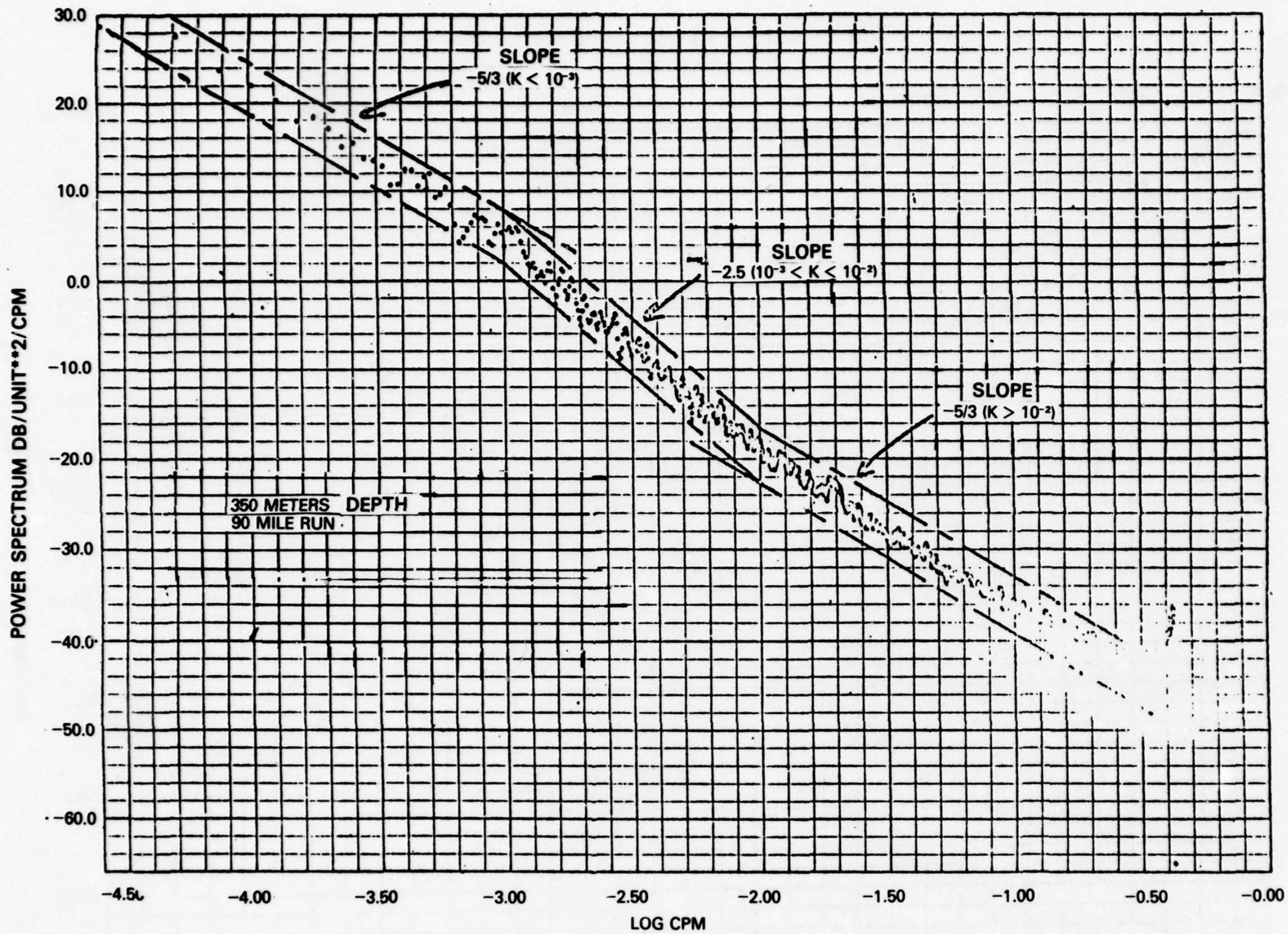

Fig. 18 —Spatial Power Spectrum of Sound Speed Fluctuations Along a 90 mile Track

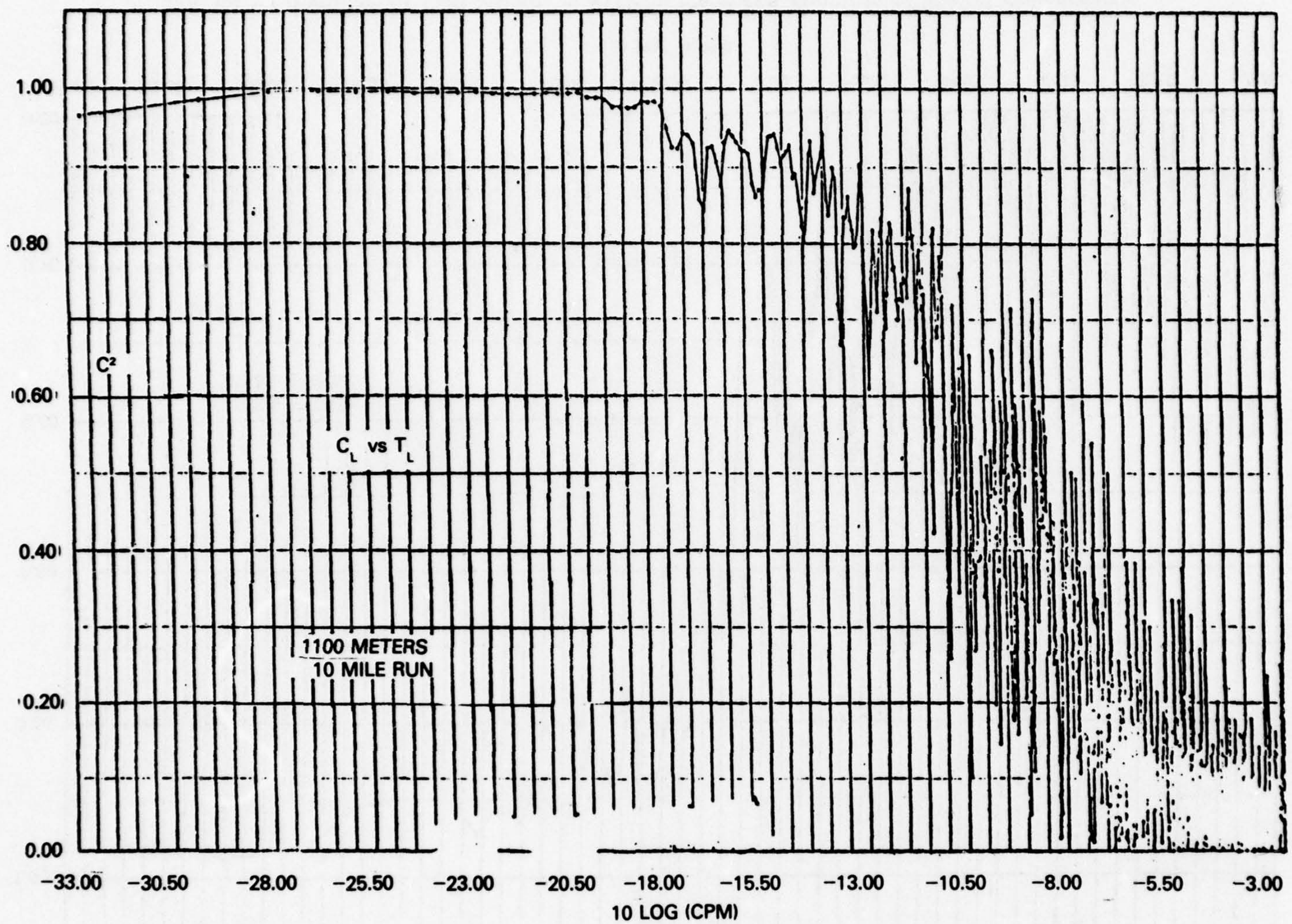

Fig. 19 — Temporal Coherence of Sound Speed Fluctuations as a Function of Spatial Wavenumber

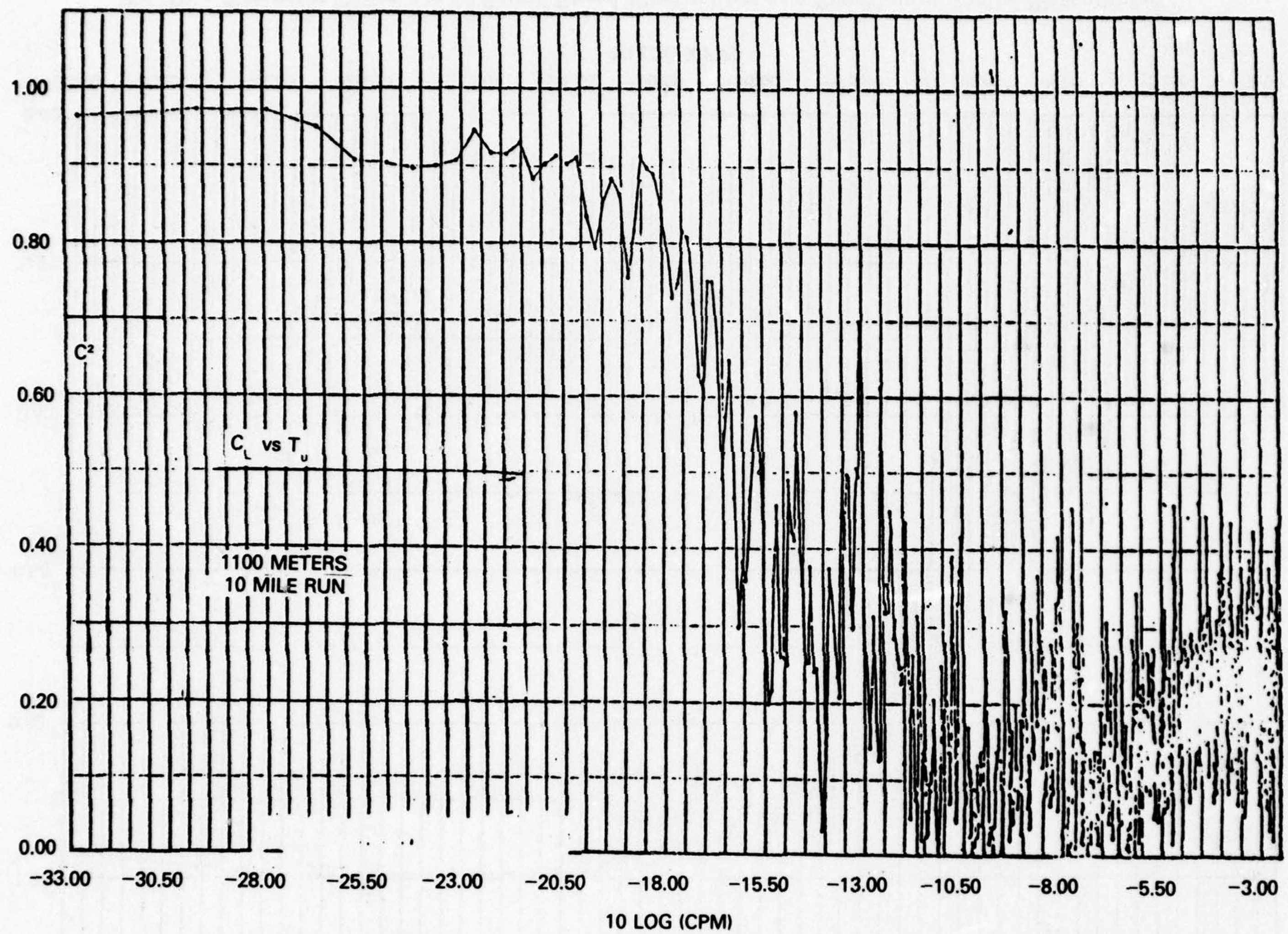

Fig. 20 — Coherence of Two Sensors in Vertical Plane as a Function of Spatial Wavenumber

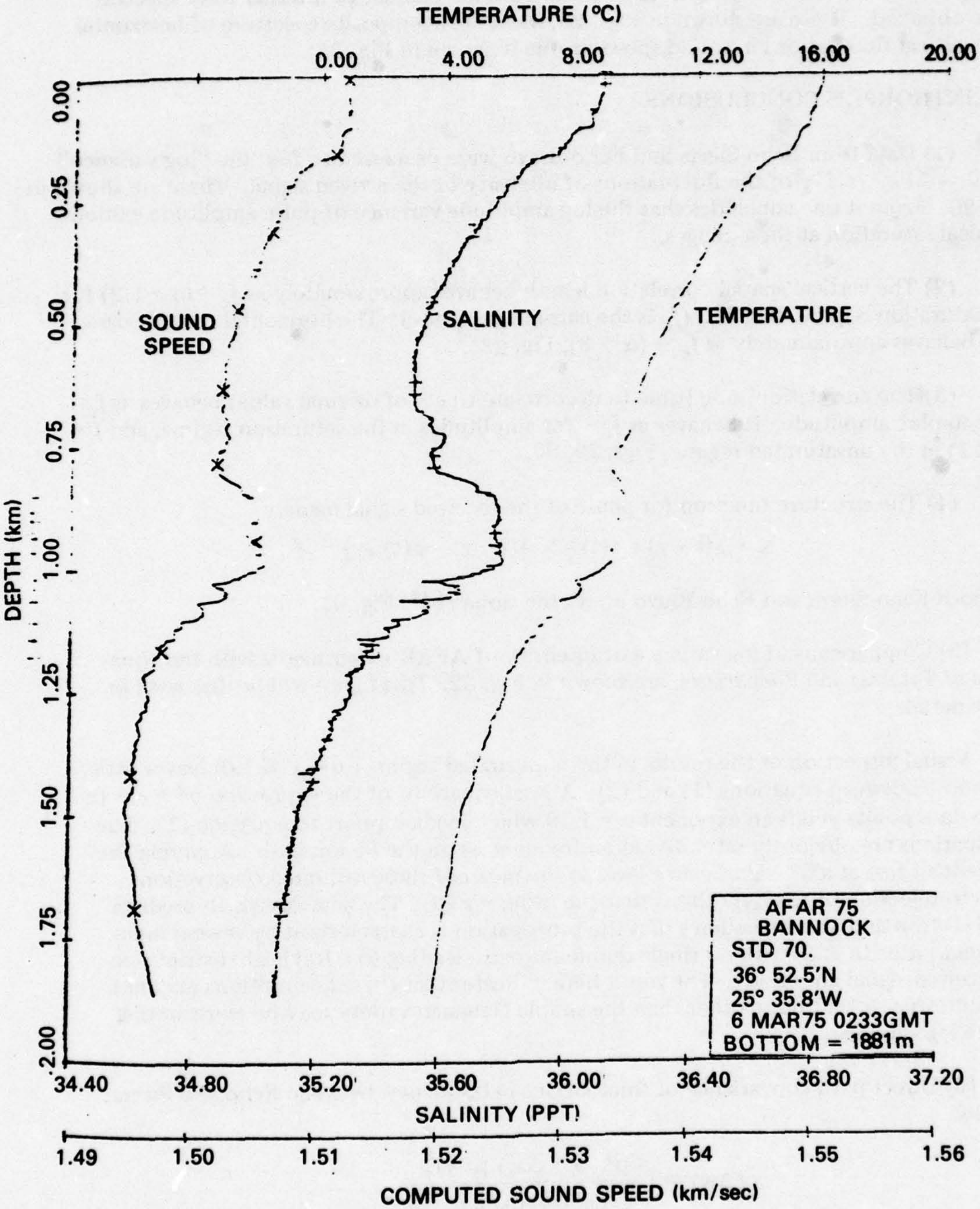

Fig. 21 — Typical Sound Speed Profiles on AFAR Range

power spectrum of random variations in vertical sound speed profile with mean removed is shown in Fig. 22. (6) Power spectra of water currents (similar to internal wave spectra) were obtained. These are shown in Figs. 23, 24. (7) A composite spectrum of horizontal and vertical fluctuations in sound speed profile is shown in Fig. 25.

ELLINTHORPE'S CONCLUSIONS

(1) Data from Echo-Sierra and Echo-Bravo were processed to find the "log variance" $<I^2> - <I>^2 / <I>^2$ of the fluctuations of intensity of the arrived signal. These are shown in Fig. 26. From it one concludes that the log amplitude variance of pulse amplitude exhibits classical saturation at these ranges.

(2) The vertical spatial correlation length behaves approximately as $f_c^{-\alpha}$ ($\alpha \sim 1/2$) for the saturation regime, Fig. 27. (f_c is the carrier frequency). The horizontal spatial correlation behaves approximately as $f_c^{-\alpha}$ ($\alpha \sim 3$), Fig. 28.

(3) The correlation time (time to decorrelate to e^{-1} of original value) behaves as f_c^{-1} for complex amplitude. It behaves as f_c^{-1} for amplitudes in the saturation regime, and $f^{-\alpha}$ ($\alpha < 1$) in the unsaturated regime, Figs. 29, 30.

(4) The structure function for phase of the received signal namely

$$< \left\{ \phi(t+\tau) - \phi(t) - < \phi(t+\tau) - \phi(t) > \right\}^2 >$$

for both Echo-Sierra and Echo-Bravo obeys the slope $\tau^{5/3}$, Fig. 31.

(5) Comparisons of log variance of intensity of AFAR experiments with the equations of Tatarski and Zachariasen are shown in Fig. 32. This figure will be discussed in some detail.

Visual inspection of the results in the unsaturated regime ($\sigma^2_{\ln I} \leqslant 1.0$) leaves little to choose between equations (1) and (2). A least square fit of the expression $\sigma^2 = cf^\alpha$ to these data points yeilds an exponent $\alpha = 1.19$ which lends support to equation (1). The fluctuations are obviously saturated at all frequencies on the 35 km path. Applying the Student's t test at a 5% significance level to the mean of these saturated observations leads to rejection of the hypothesis that the mean = $\pi^2/6$. The analysis which predicts $\pi^2/6$ (Dyson and Munk) assumes that the propagation is characterized by several independent paths ($n \geqslant 3$) with no single dominant path, leading to a Rayleigh distribution of received signal amplitude. The result here indicates that these assumptions may not be quite true or that noise other than the simple Gaussian variety may be contributing to the log variance.

(6) Direct path convariance of fluctuations in frequency between Echo and Sierra, namely

$$c(\Delta w) = \frac{<p^*(w + \Delta w)\, p(w)>}{p_0^*(w)\, p_0(w)}$$

has been measured and appears in Fig. 33.

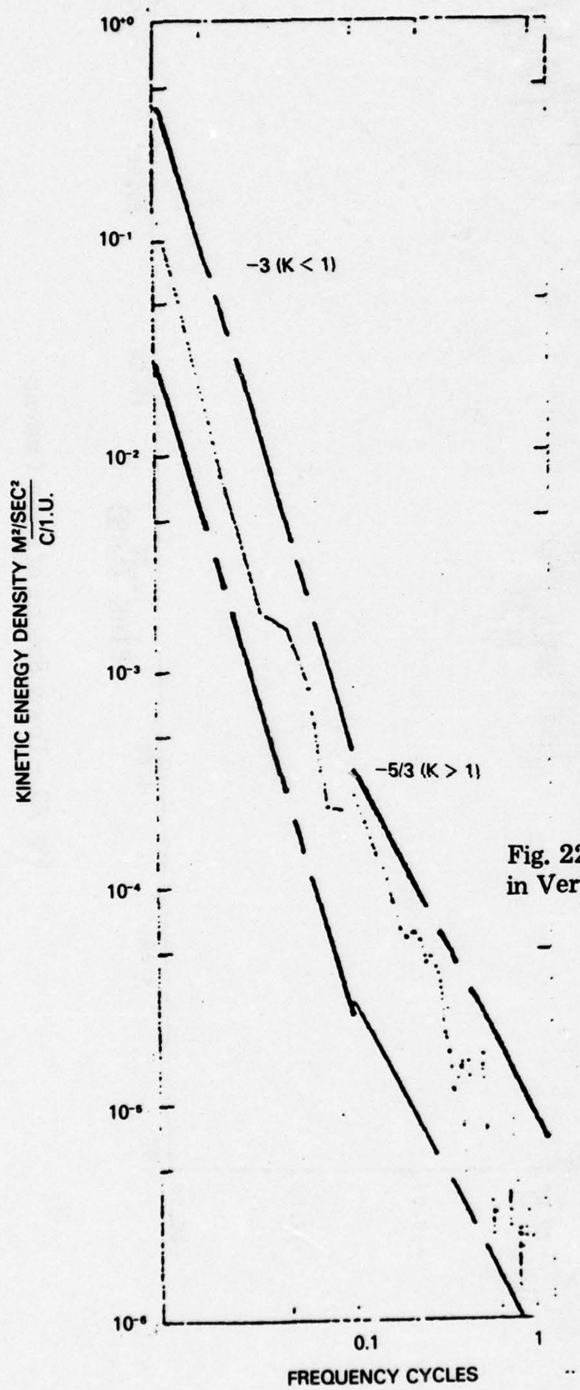

Fig. 22 — Power Spectrum of Random Variations in Vertical Sound Speed Profile

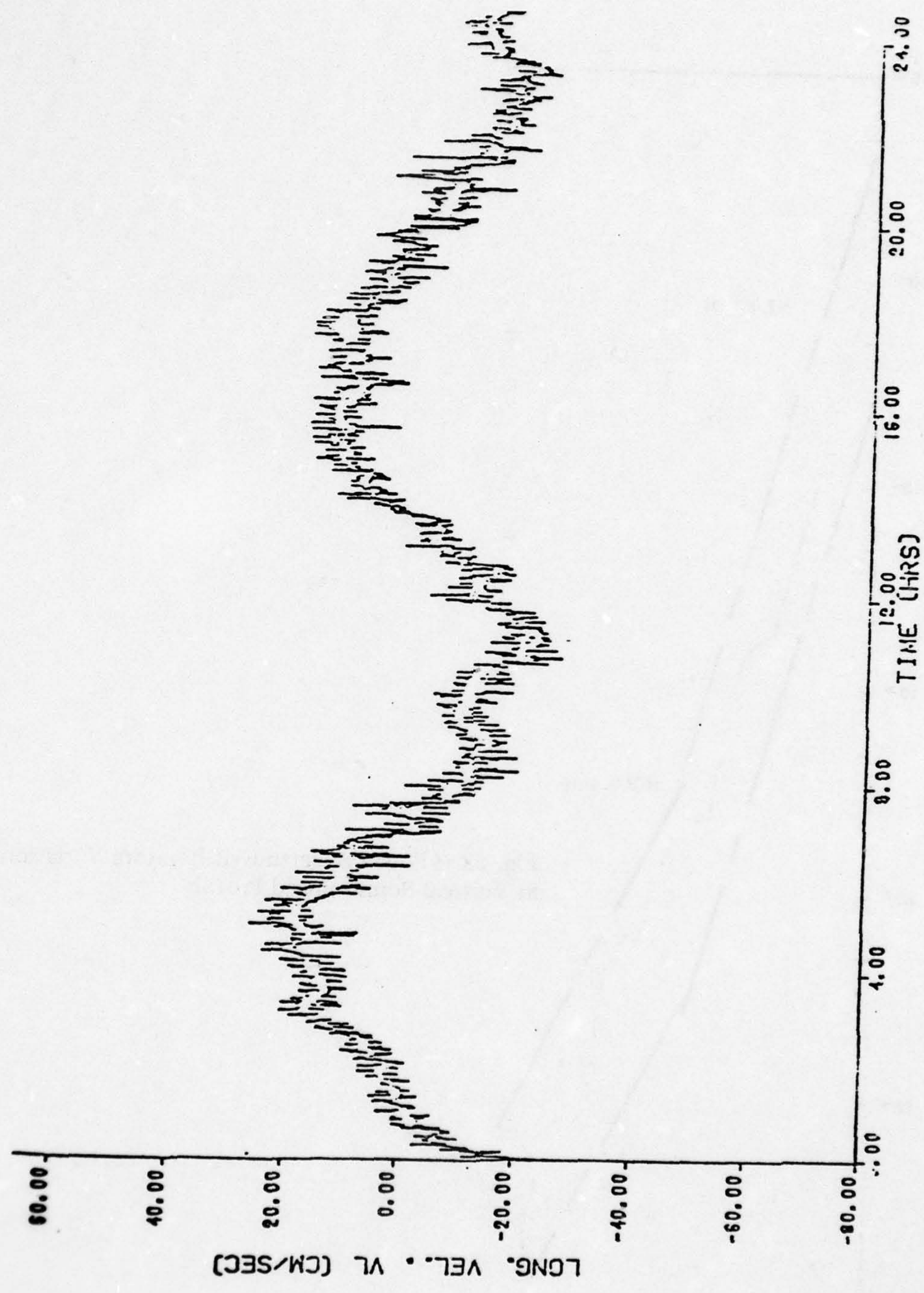

Fig. 23 — Power Spectra of Water Currents

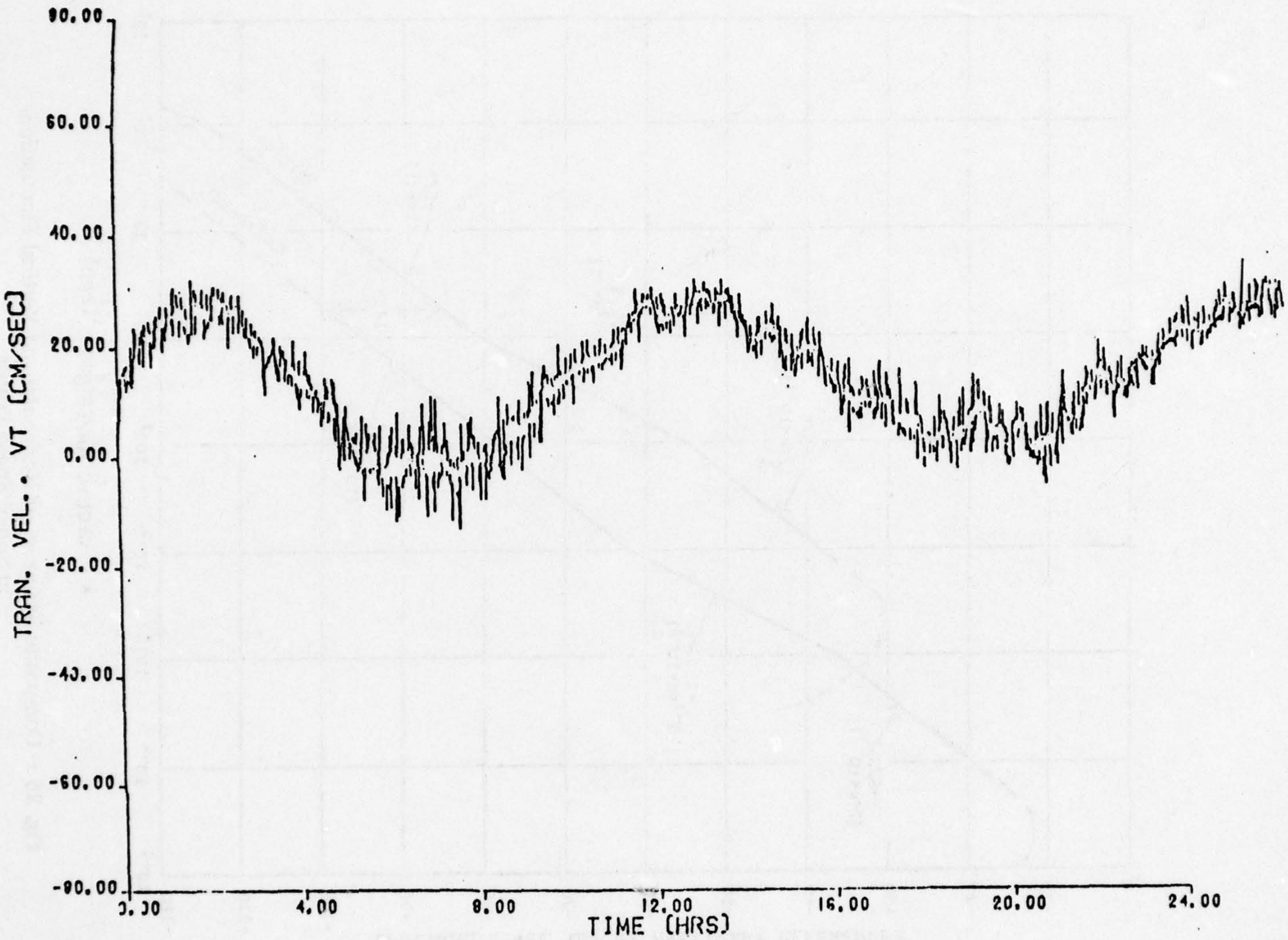

Fig. 24 — Power Spectra of Water Currents

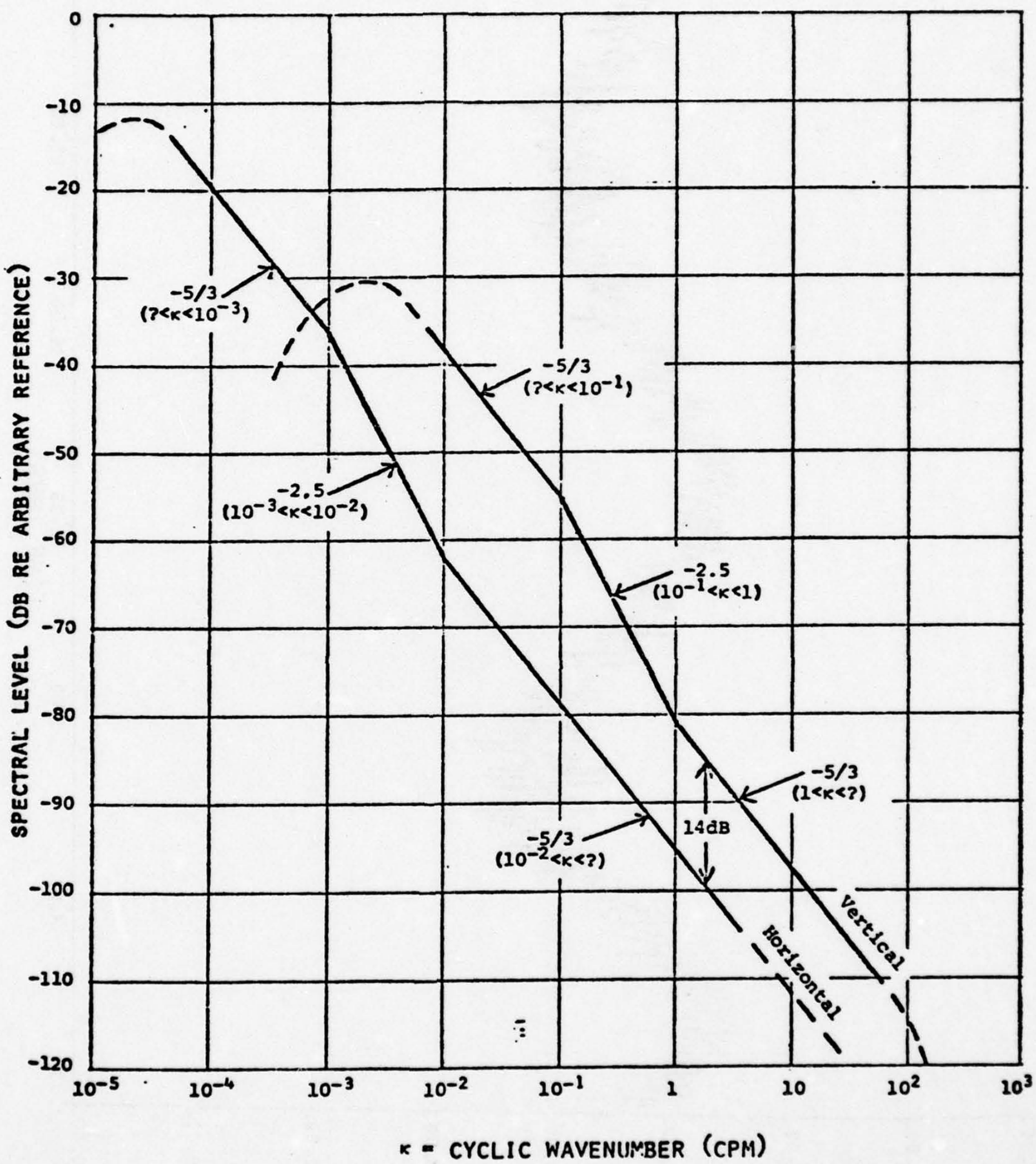

Fig. 25 — Composite Spectrum of Horizontal and Vertical Fluctuations in Sound Speed Profile

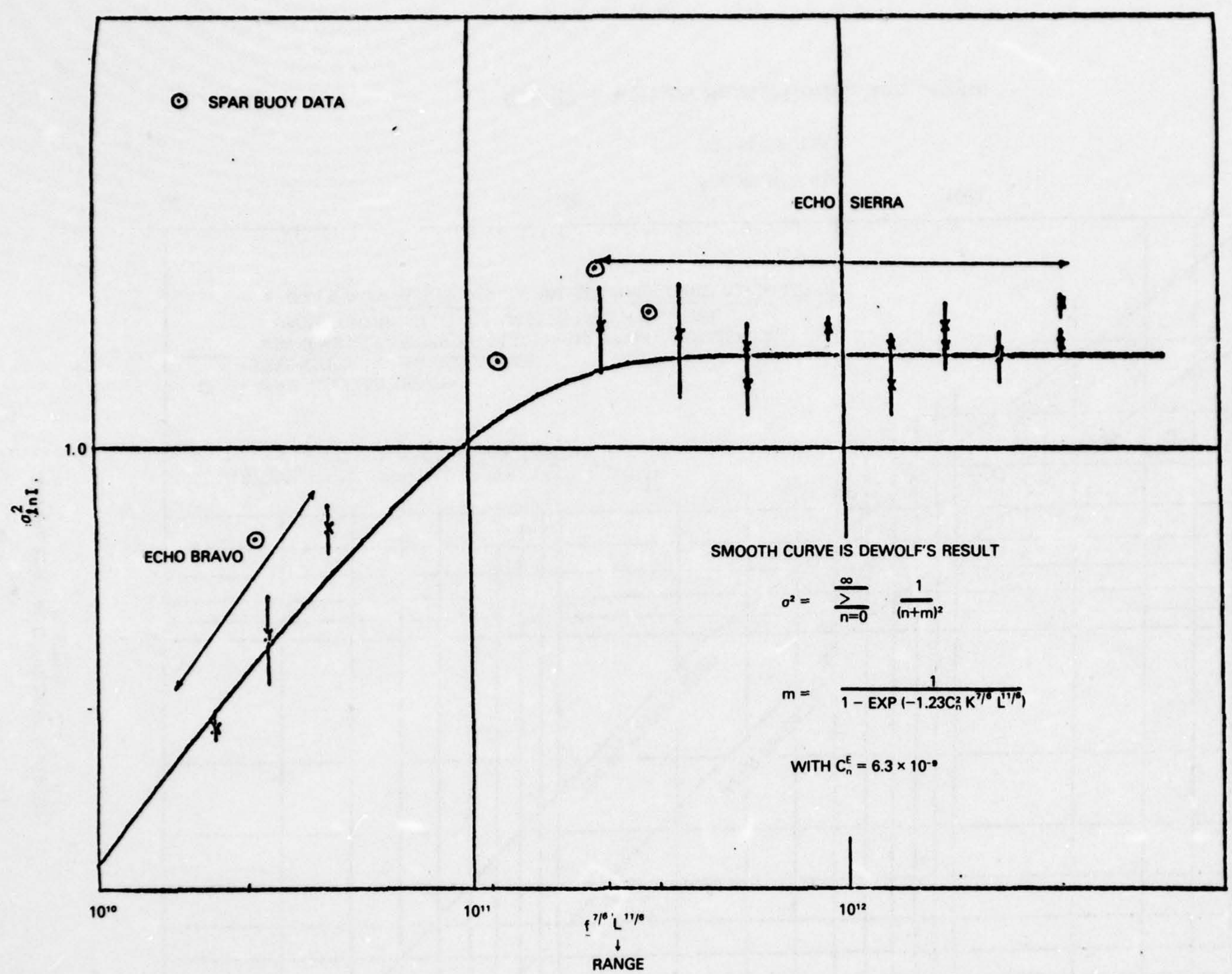

Fig. 26 — Log-variance Plot of Fluctuations of Intensity of Arrived Signal

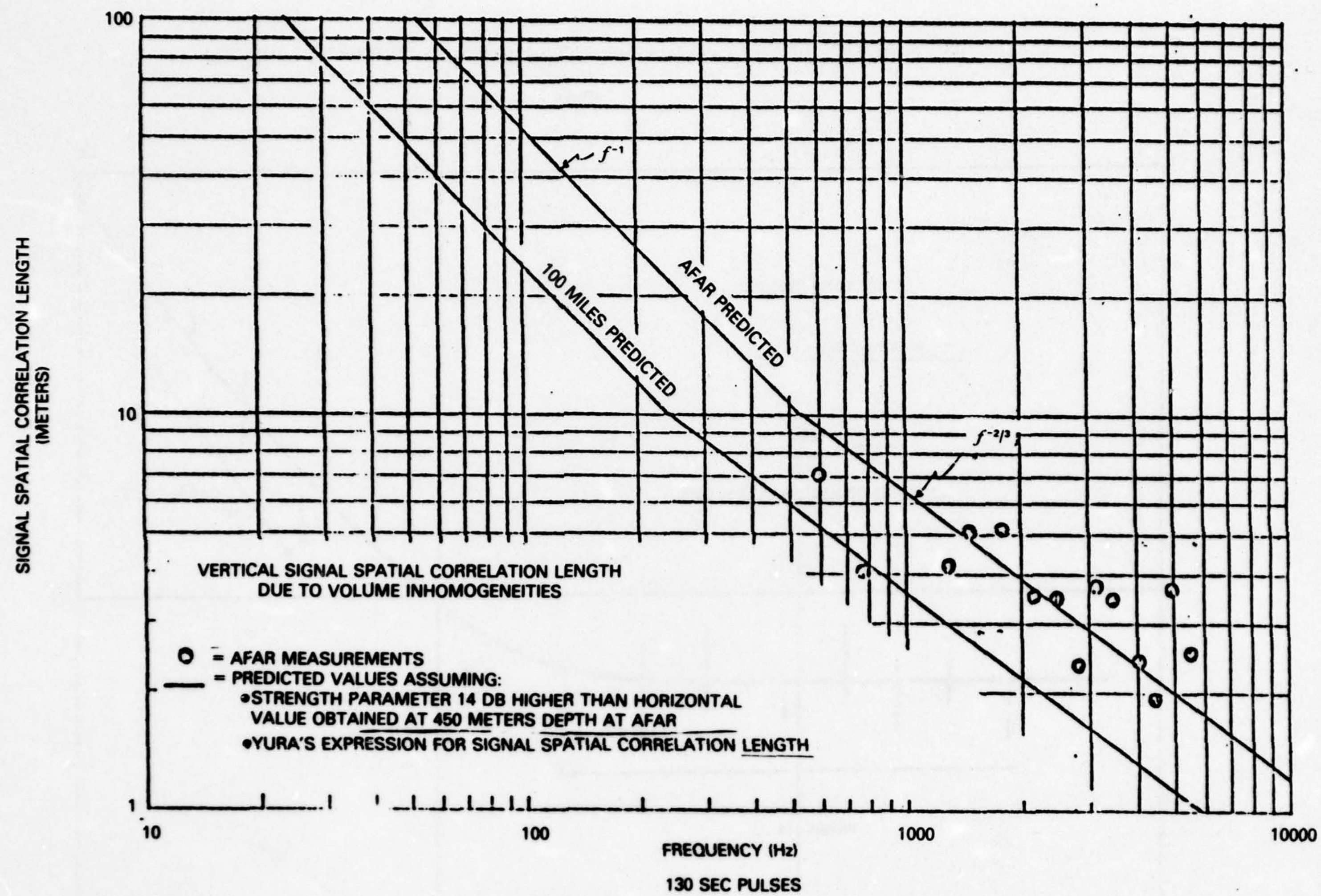

Fig. 27 — Vertical Spatial Correlation Length

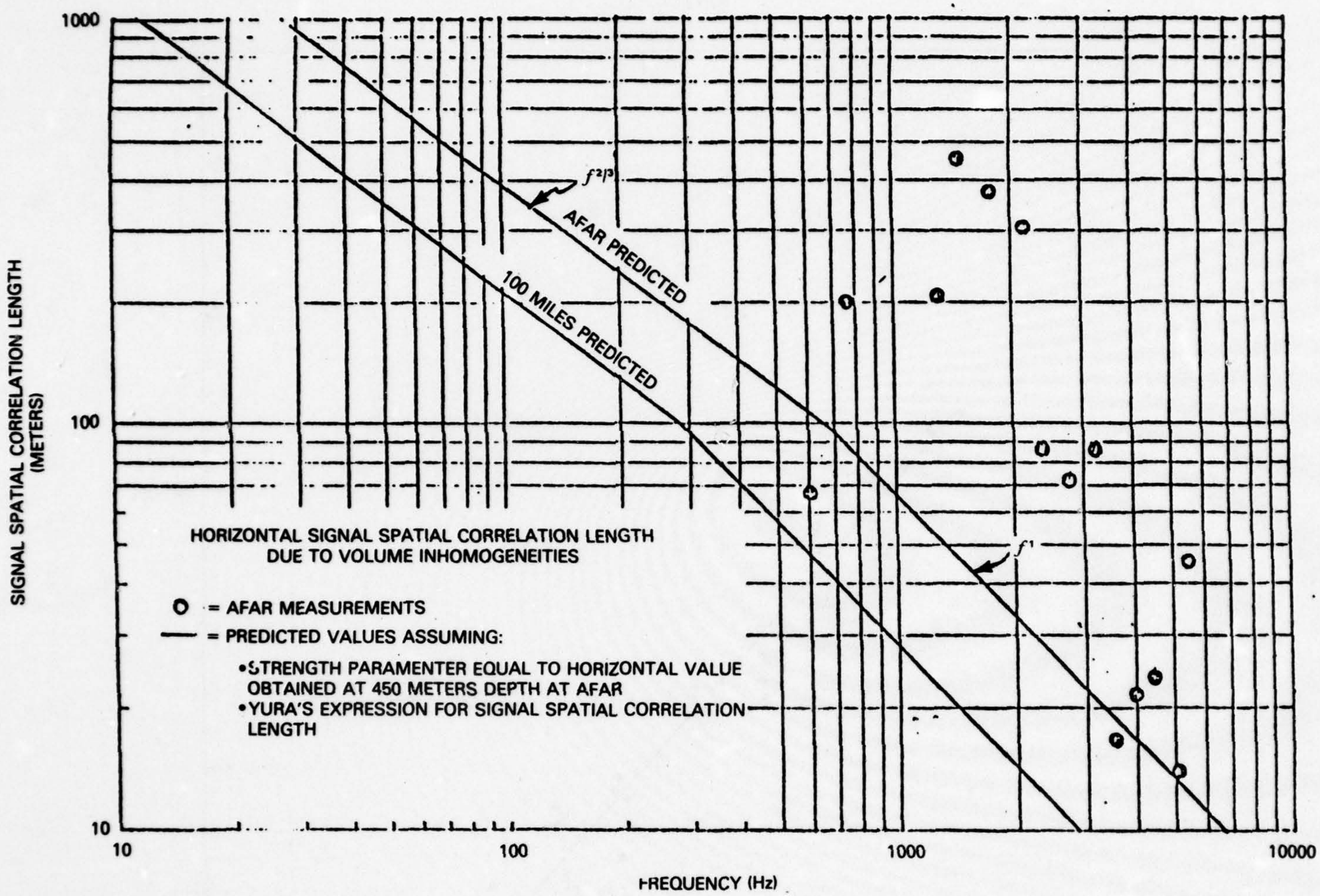

Fig. 28 — Horizontal Spatial Correlation Length

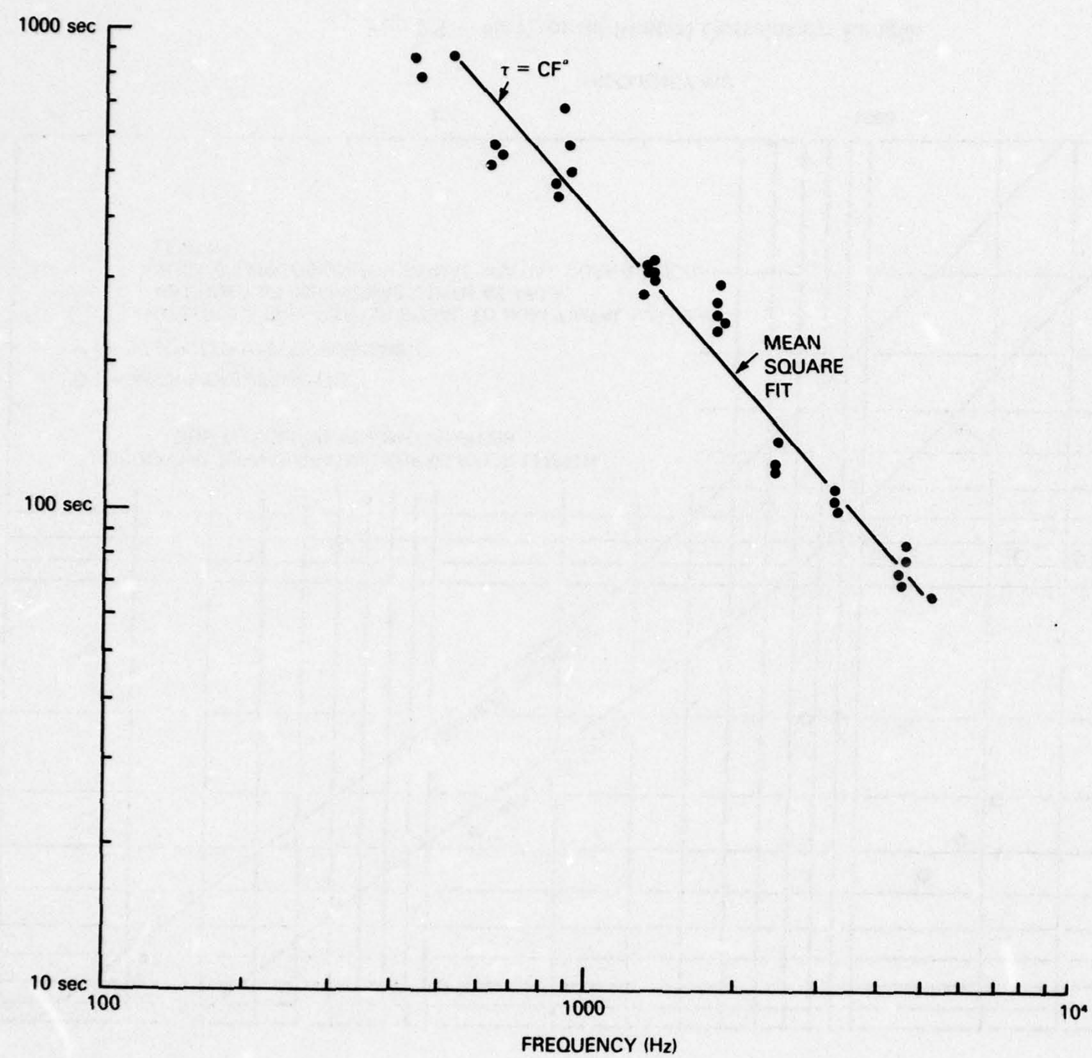

Fig. 29 — Correlation Time versus Frequency

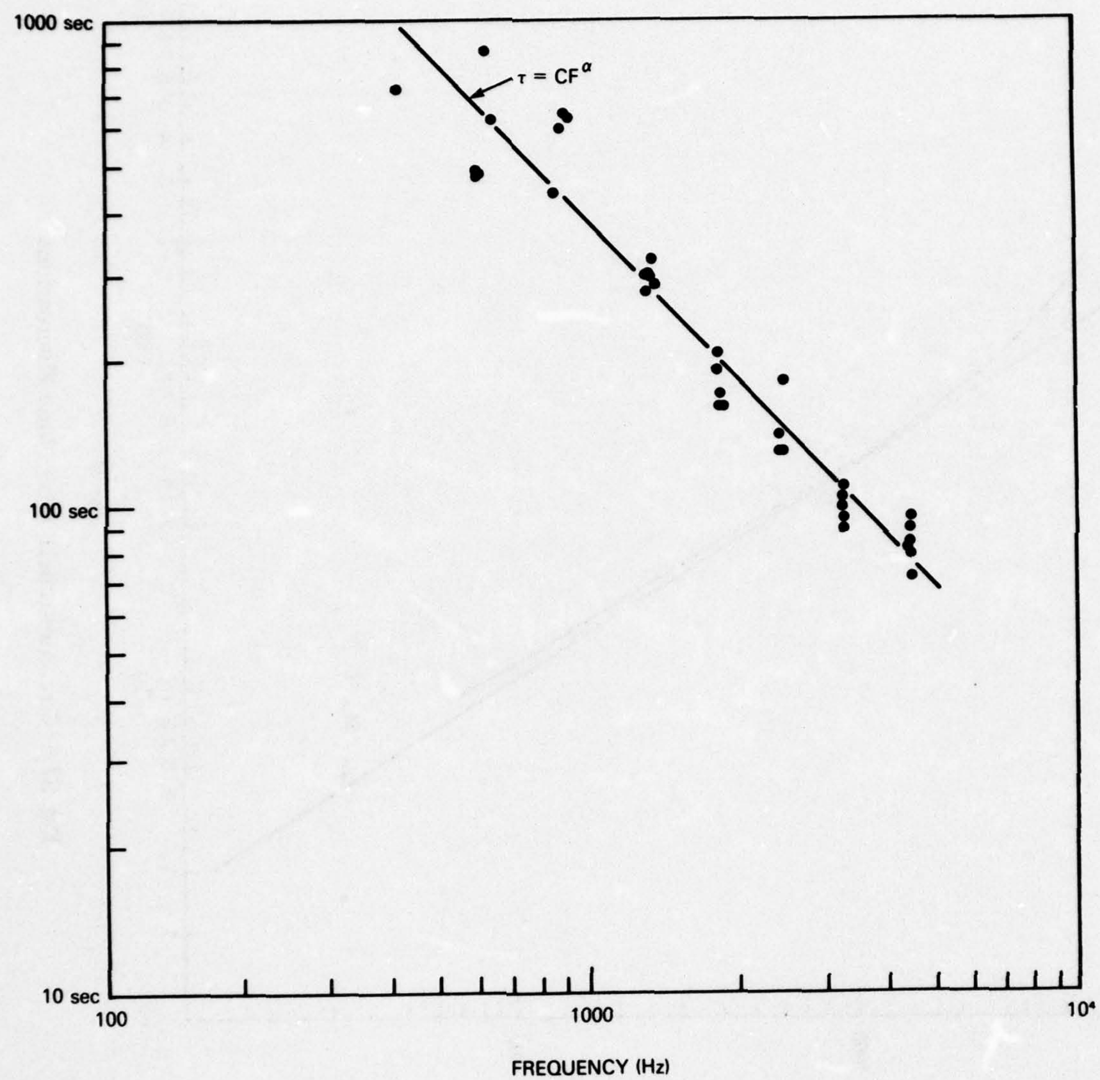

Fig. 30 — Correlation Time versus Frequency

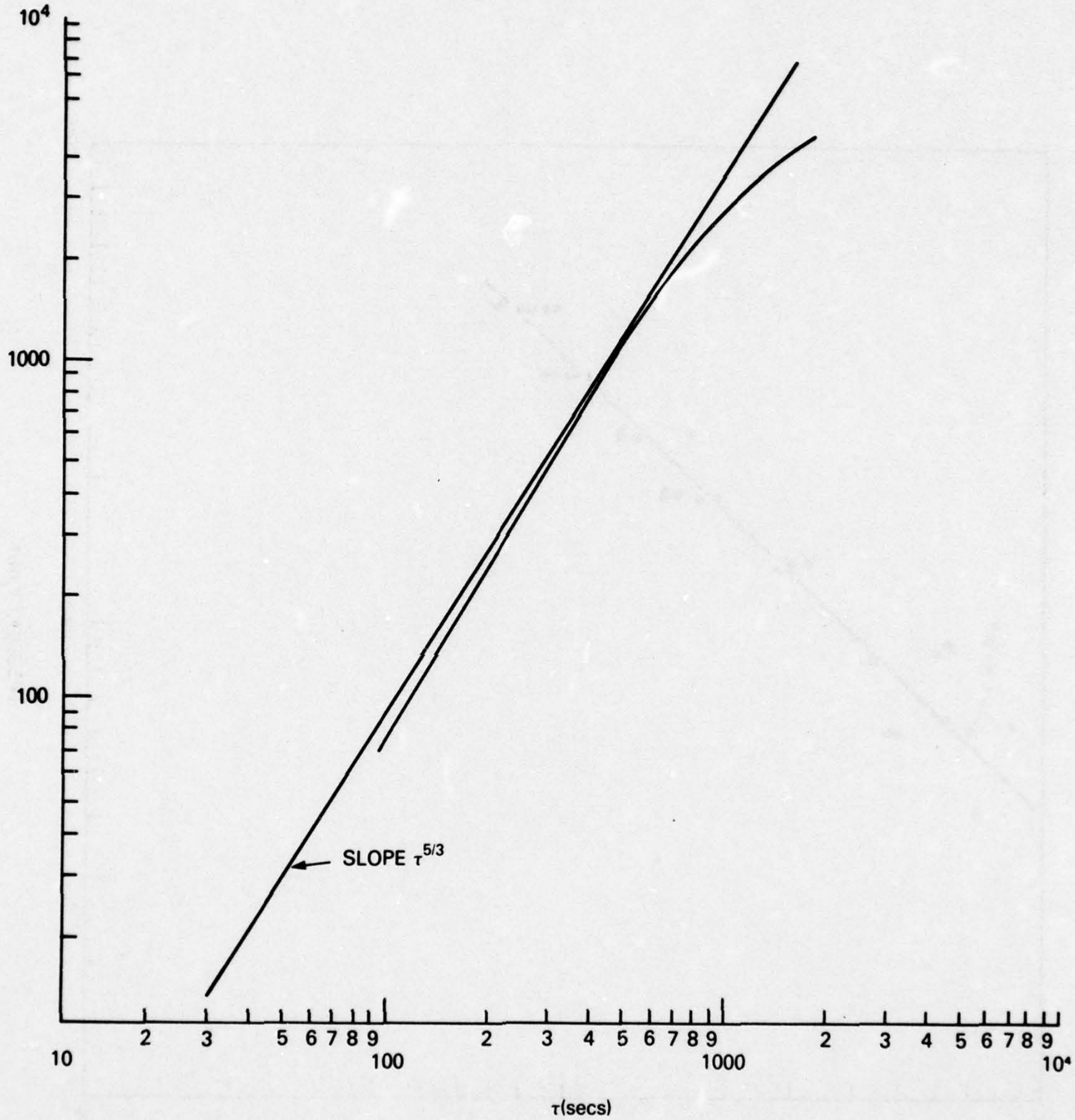

Fig. 31 — Structure-function for Phase Fluctuations

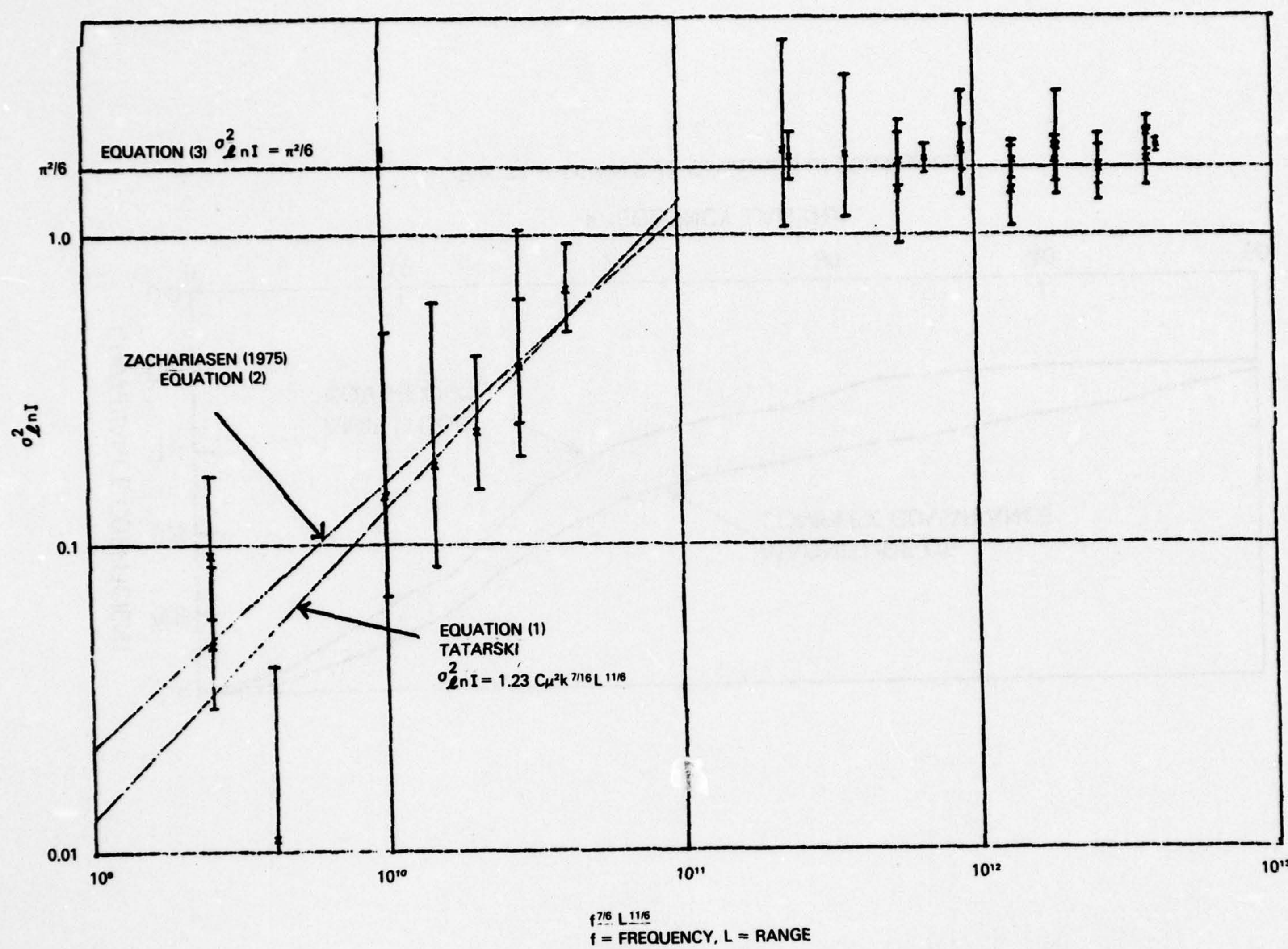

Fig. 32 — Comparisons of Theoretical Log-variances with Experimental Data

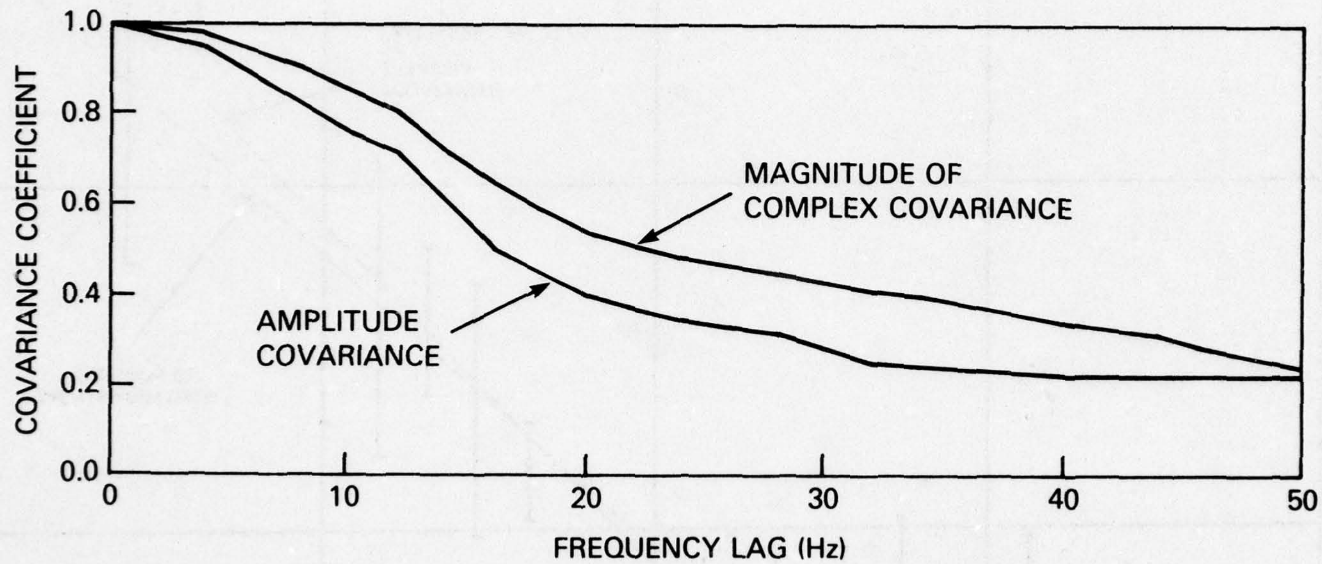

Fig. 33 — Direct Path Covariance of Fluctuations

COMPARISON OF JASON THEORY WITH AFAR EXPERIMENTAL DATA

At the completion of the expositions of Flatté, Ellinthorpe and Dashen, the final portion of the invited papers was reached. In it Dashen presented a detailed comparison between predictions of the Jason Group and actual measurements at the AFAR facility. A summary of these comparisons is presented below.

A single, fully-refracted path of the Echo to Sierra stations over the 35 km range was used to check theory. The first task was to obtain a sound speed profile which was the sum of a background profile plus fluctuations. Profiles of sound-speed measurements were made between depths of 240 m to 840 m. Upon averaging these to obtain a background profile, it was found that the average did not agree with the canonical model of Munk. The experimental profile was then fitted to a sixth-order polynomial, and the result was used in the analysis as the deterministic background sound speed profile.

A second task was to obtain the fluctuating part of the sound speed, $\langle\mu^2(z)\rangle$. It was assumed, to start, that this part was caused by internal waves. To calculate it from the internal wave model required measurements of the buoyancy frequency m(z) as a function of depth. Actually, temperature and salinity measurements were first made, and then from these a profile of buoyancy frequency versus depth was constructed. It roughly approximates the form $N_o e^{-z/B}$. Furthermore, in addition to m(z) one needs the gradient of the sound speed, $\partial C_p/\partial z = \frac{\partial c}{\partial z} + C_1\gamma_A$, where C is the background sound speed profile, C_1 = $1500 ms^{-1}$ and γ_A is a stochastic variable from the theory. These quantities were all assembled from the constructed background profile and from the internal wave model, and the prediction was made that

$$<\mu^2(z)> = \text{const.} \times n(z)\left(\frac{\partial C_p}{\partial_z}\right)^2$$

Measurement of sound speed fluctuations were compared with this prediction for the purpose of testing it for depth variation. It was found that the internal wave model holds well in the depth region between 240m and 790m.

Thus there was on hand an experimentally certified model of the random sound speed profile. One was then prepared for comparison of the *acoustic* experiments with theory.

First the CW experiments. Pulses centered at several frequencies with widths of 130 msec were used to simulate CW transmission. The received signal was a CW sinusoid modulated by the random properties of the medium. A first question was, how severely did the random sound speed affect the phase and amplitude of the received signal, visualized as a rotating phasor, $Ae^{i\phi}$? The answer required calculation of the two parameters, Φ and $\Omega^{-1}(=\Lambda)$, as explained earlier in the expository discussions written above. The calculation of Φ depends on the numerical evaluation of an integral of $\langle\mu^2(s)\rangle f_1(s)$ along the refracted path, where $f_1(s)$ is a theoretical quantity known from the theory of Munk and Zachariasen. The result of the integration was

$$\Phi = \frac{\sigma}{40}, \text{ (HZ)}$$

in which σ was the acoustic frequency. The calculation of $\Omega^{-1} = \Lambda$ was made from the simple formula $\Lambda = R/6kL_V{}^2$, in which R is the range, $K = \omega/c$, and L_V is the vertical correlation length of the random inhomogeneities in index of refraction in the ocean. The result was

$$\Lambda = \frac{25}{\sigma}; \text{ HZ}, \; L_y = 240 \text{ M}$$

Thus the all-important product, $\Phi\Lambda$, had the value 0.63, and the product $\Lambda\Phi^2$ was $\frac{\sigma}{64}$ Hz. At the frequencies in question (412 to 4672 HZ) this combination in the $\Lambda\Phi$ plane indicated that the regime of statistics of $Ae^{i\phi}$ was *partially saturated.*

Upon certification of this regime it was then predicted that the amplitude statistics of $Ae^{i\phi}$ would be approximated Rayleigh distributed (rather than log normal). This was experimentally verified, Fig. 34. In addition it was predicted that the variance of log-intensity distribution would follow the classical plot, that is, increase with $\Lambda\Phi$ up to an asymptotic value, calculated in this model to be $\pi^2/_6$. This prediction was verified, Fig. 35. A separate issue was how well the *higher* moments of received intensity agreed with the *modified* Rayleigh distribution derived by Dashen, namely

$$< I^n > = n! \; < I >^n \; (1 + \frac{1}{2} n (n-1) \gamma$$

This prediction was verified at the frequency 4671 Hz, but no verification was possible with data at the lower frequencies because of insufficiently long experiment-time-records.

Another group of comparisons between theory and experiment was concerned with temporal fluctuations of the two-point correlations of the field ψ. Dashen's theory predicts that

$$< \psi (t + \Delta t) \, \psi^*(t) > \propto e^{-\frac{D}{2} (\Delta t)}$$

and that for small Δt time separations one should have $D \simeq \dot{\Phi}^2 (\Delta t)^2$. Thus one requires an environmental parameter $\Phi / \dot{\Phi}$ to be constructed. Actually $\dot{\Phi}$ was obtained from the internal wave model, and Φ itself was calculated in the manner discussed above. A set of predictions of the various 2-point temporal statistics of ψ is shown in Fig. 36. The experimental points verify the predictions very well, incidentially certifying that the regime *is* partially saturated, as predicted by other parameters. In particular the time variation of the phase of ψ shows phase wrapping as predicted.

A final group of comparisons was concerned with the temporal statistics of arriving trains of short pulses. These pulses were centered at 3200Hz and were 1.28 ms wide. As they traveled through the medium they were randomly dispersed in frequency so that the intensity on arrival varied randomly with time. The first order statistic of intensity, namely the mean value $<I(\tau)>$ was measured, and then compared with predictions based on the AFAR model of the sound channel. The agreement with experiment is good over the time interval 0 to 40 msec, Fig. 37. Two theoretical models are used to compare intensity distribution experimentally obtained. In one, the quantity $<I>$ is considered proportioned to $\exp(-\sigma/\Phi)\, Q(\alpha)$, in which σ is the acoustic frequency; $\alpha = \Delta\tau/\eta_0$ is a parameter describing the frequency spread $\Delta\sigma$ relative to a reference bandwidth η_0 (= 40HZ) provided by the model; and $Q(\alpha)$ is a factor derived from an internal wave model. In the other model, $<I>$ is proportional only to exp $(-\sigma/\Phi)$. Fig. 37 shows that the inclusion of $Q(\alpha)$ brings experiment and theory much

closer to agreement on the variation of $<I>$ with time. The second statistic checked is the auto correlation (in time) of the received intensity $<I(t+\tau)I(t)>$. Theory predicts that the Fourier transform of this quantity should be proportional to the Fourier transform of $|Q(\alpha)|^2$ obtainable from the internal wave model. Comparison with experiment shows good agreement, Fig. 38.

The success in these comparisons is commendable. However, it is recognized that the isolation of a single path in these AFAR experiments excludes the serious difficulty of multipath interference. This problem is still under investigation.

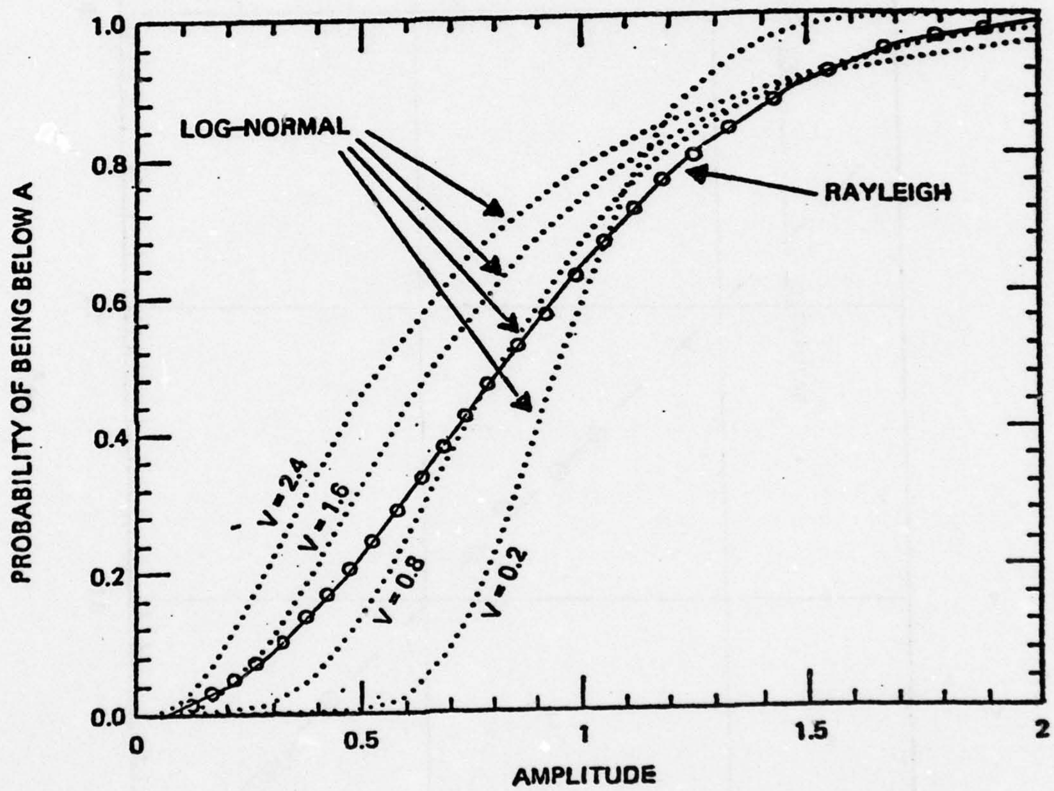

Fig. 34 — Experimental Verification that Amplitude Statistics are Rayleigh Distributed

AD-A072 309 NAVAL RESEARCH LAB WASHINGTON DC F/G 20/1
ACOUSTIC FLUCTUATION WORKSHOP, HELD AT NAVAL RESEARCH LABORATOR--ETC(U)
JUL 78 S HANISH, C R ROLLINS, J CYBULSKI
UNCLASSIFIED NRL-MR-3884-VOL-1 NL

3 OF 3
AD
A072309



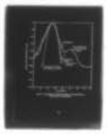
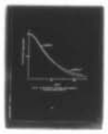


END
DATE
FILMED
9-79
DDC

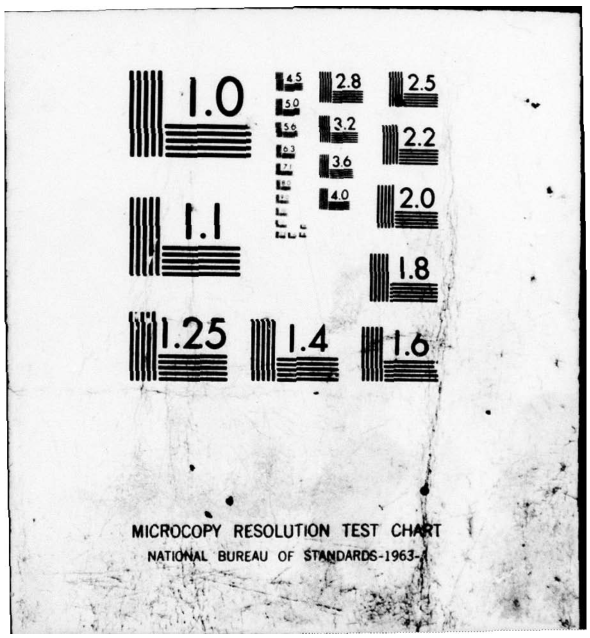
1.0
1.1
1.25
1.4
1.6
1.8
2.0
2.2
2.5
2.8
3.2
3.6
4.0
4.5
5.0
5.6
6.3
7.1
MICROCOPY RESOLUTION TEST CHART
NATIONAL BUREAU OF STANDARDS-1963-A

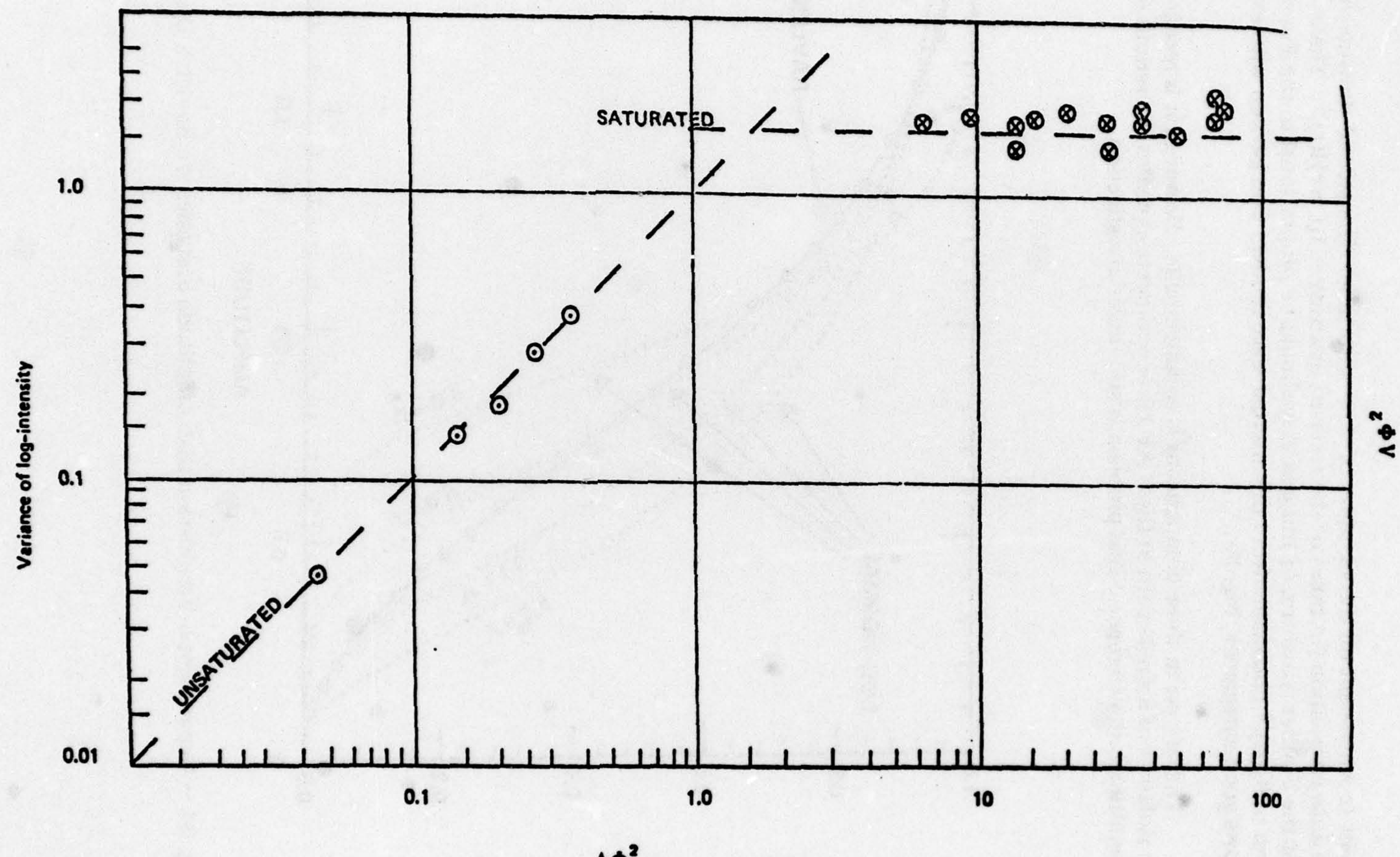

Fig. 35 — Experimental Vertification that the Variance of the Log-Intensity Agrees with Classical Plot

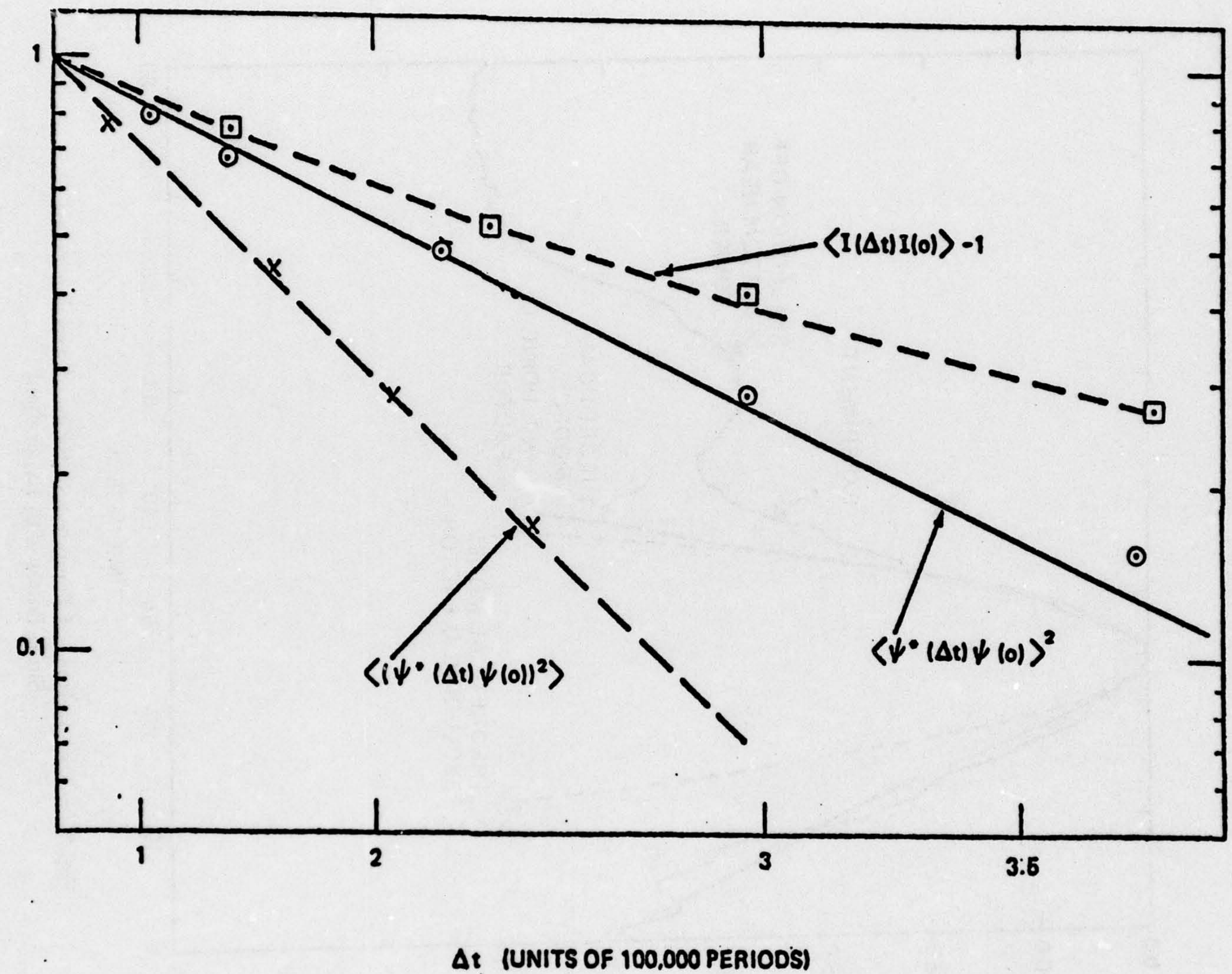

Fig. 36 — Predictions of Two-point Temporal Statistics and Experimental Measurements

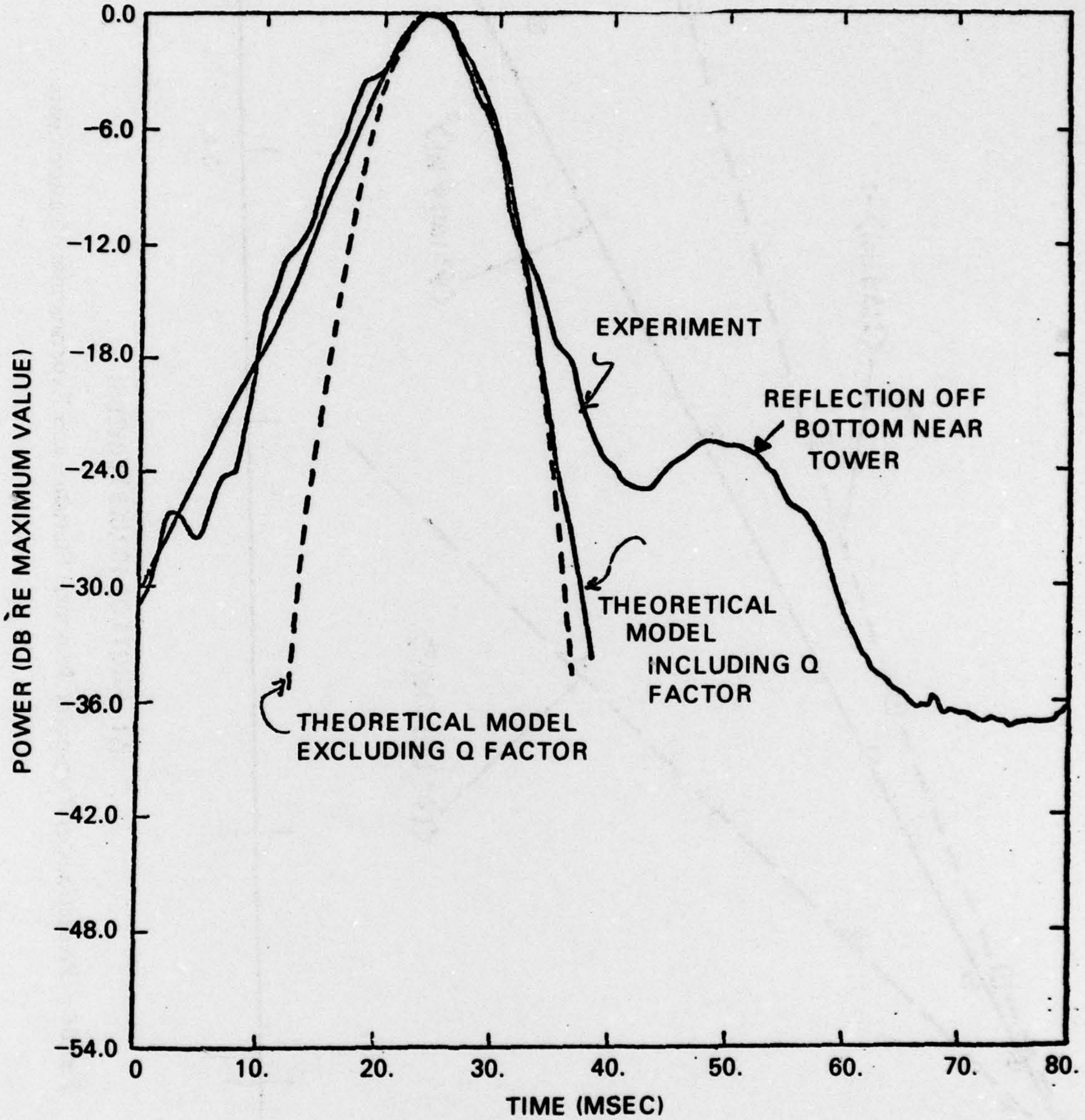

Fig. 37 — Comparisons of Temporal Statistics of Arriving Trains of Short Pulses with Experiment

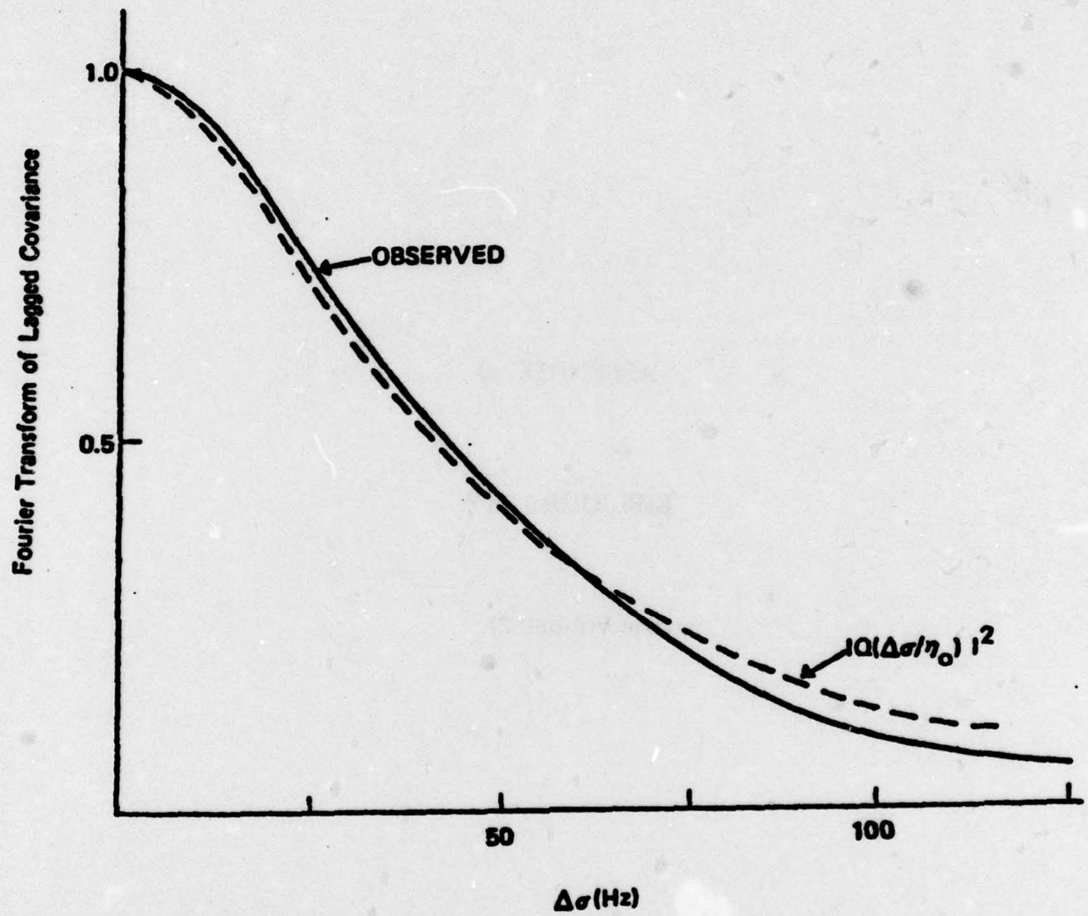

Fig. 38 — Fourier Transform of Temporal Autocorrelation of Intensity Compared to $|Q(\alpha)|^2$

APPENDIX D

BIBLIOGRAPHY

(See Volume 2)

*U.S. GOVERNMENT PRINTING OFFICE : 1979 O-281-484/57